DISTRIBUTION OF VERY FAST FRONTED SURGES IN TRANSFORMER WINDINGS

by

IMAD R. SUKAR

A Thesis submitted to

THE UNIVERSITY OF MANCHESTER

for the degree of

DOCTOR OF PHILOSOPHY

in the Faculty of Technology

Department of Electrical Engineering and Electronics

University of Manchester

Institute of Science and Technology

(UMIST)

1991

To My Parents

DECLARATION

No portion of the work referred to in this thesis has been submitted in support of an application for another degree or qualification of this or any other university or institution of learning.

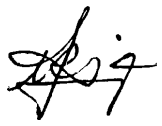

IMAD R. SUKAR

CONTENTS

ABSTRACT

The increasing usage of Gas Insulated Substations (GIS) has led to anamolous failures of GIS components and connected plant. Such failures are thought to be the results of very fast fronted surges generated by switching operations performed within GIS. Transformers are especially considered at risk as they are increasingly used at higher voltages.

The problem of very fast fronted surge distribution in transformer winding is basically that both GIS and transformers interact. Thus, adequate representation of all components is of utmost importance in order to investigate the characteristics (in particular, wavefront nature) of the surges impinging on transformer windings and the way they distribute themselves inside such windings. In this thesis, the latter aspect of the problem is addressed through the development of a computer model of the sections in the line-end region of the winding.

The model is based on multiconductor transmission line theory together with modal analysis (including two-port network representation) and considers the individual turn as the basic element. The electrical parameters of the coil under study are obtained in a rather simple way. The capacitances matrices are calculated by approximating the walls of the different turns to parallel plate capacitors and the inductance matrices are calculated from the relation between the inverse capacitance matrices in air, velocity of light and loss factor. The series losses are due to skin effect.

The model accurately predicted the surge distribution in the top four sections of the HV winding, where insulation failure is most likely to occur, in the first few hundred nanoseconds after surge arrival. The validity of the model was demonstrated through comparison with experimental results obtained from measurements on the real HV winding. Such accuracy

also justified the derivation of the electrical parameters.

A sensitivity analysis of various parameters illustrated the ability of the developed model to accurately predict insulation status of different transformers under different operating conditions.

The computer model developed in this thesis could be used to adequately represent transformer windings in future studies allocated to the investigation of the wavefront characteristics of the surges created by switching operations in GIS. As a result, the exact nature of the surges reaching the transformer will be obtained together with the way they distribute themselves inside the windings leading to an accurate assessment of the transformer insulation status.

ACKNOWLEDGEMENTS

The author wishes to express his gratitude to his supervisor in this project, Mr. K. J. CORNICK, whose help and encouragement were the key factors in completing the thesis.

The author also wishes to thank the Hariri Foundation for providing the financial support for the whole period of the Ph.D studies.

CHAPTER 1

INTRODUCTION

The technology of Gas Insulated Substations (GIS) has been brought more and more into service[1] on power systems in the past twenty years. Although GIS are more reliable than open air substations[1], there is concern that switching operations performed within GIS at voltage levels higher than 300 Kv[1,2] may have resulted in so-called anamolous failures within GIS and of connected plant. This is attributed to the generation of very fast transients[1,2] during switching operations of loadbreak switches, circuit breakers and, especially, disconnectors in GIS. In fact, reported failures[2] are insulation failures in GIS, bushing failures, insulation faults in transformers and malfunctionning of electronic devices, i.e., relays. Transformers are especially considered at risk as they are increasingly used at higher voltages, thus subjecting their insulation to switching surges of ever increasing severity.

The created very fast fronted surges are characterized by a very steep front with a risetime[2,3,4] less than 10 nsec at the disconnector itself. However, before such transients do reach connected equipment such as transformers, they naturally have to propagate through other substation equipment. During such propagation, attenuation[1] of the initial surges will occur due to the multiple reflections and refractions at all the encountered impedance discontinuities leading in turn to what is known as very fast transient overvoltages.

On reaching transformer windings, the impinging very fast transients will distribute themselves inside the transformer winding causing the overstressing of insulation between parts of the winding itself and between parts of the winding and ground. This in turn could lead to insulation failure. The cause[1] for such insulation stress could be either the

initial distribution of the very fast front of the transients and the following oscillations in the line-end region of the transformer winding or part-winding resonnance caused by the oscillatory nature of the very fast transients.

From the above, it is clear that GIS and transformers interact. There is no use examining the characteristics of very fast switching transients in GIS without adequately representing the transformer winding in order to include its effects on the nature of these transients. Similarly, there is no use examining the distribution of " assumed " GIS generated fast fronted transients in transformer windings. In fact, when dealing with the problem of very fast fronted transients and their distribution in transformer windings, all components of GIS together with connected equipment should be adequatly represented by especially taking into account the fact that the risetime of such fronted transients is comparable with the travel time of these transients through many of the components, for instance, bushings and transformers.

Hence a first step on the way to solving the above mentioned problem is to find an adequate representation of the transformer winding itself. The Ph.D thesis addresses this aspect of the problem. It deals with the distribution of very fast fronted surges in transformer windings. In particular, it predicts the surge voltage distribution in the line-end and adjacent discs resulting from very steep transients with different risetimes similar to those encountered on the power system itself[2,5]. This is achieved through the development of a computer model for the coils in the line-end region, by using the multiconductor transmission line theory[56] together with modal analysis, including two-port network representation, which adopts the turn itself as the basic element.

The structure of the Ph.D thesis can be summarised as follows :

Chapter 2 gives a thourough background on the origin of very fast transients in GIS, their propagation through GIS and to connected equipment

and their effects on GIS and connected equipment, i.e., transformers. This chapter also gives a review of the previous work on the distribution of surges in transformer windings.

Chapter 3 explains the multiconductor transmission line theory together with the modal analysis, which form the basis for the computer model and also decribes the application of this theory to transformer windings. A brief explanation of the application of the above theory to A.C. machine windings is also provided. Finally, this chapter also gives in detail the steps followed for the calculation of the transformer winding parameters.

Chapter 4 deals with the accuracy of the computer model by comparing the computational results obtained from the computer model with the experimental results obtained from actual measurements performed on the actual HV winding which has been modelled on the computer and which already existed in the HV laboratory. It also contains the discussion and analysis of all obtained results.

Chapter 5 presents a sensitivity analysis by modifying various parameters and monitoring their effects on the behaviour of transformer windings.

Chapter 6 contains the conclusions obtained from the research project.

CHAPTER 2

BACKGROUND WORK

During the last two decades, Gas Insulated substations up to 765 Kv level have been more and more installed in power networks with reliabilities at least good if not better than open air substations. However, at the higher voltage levels (above 300 Kv)[1], fast fronted transients generated in SF6 substations by switching operations were thought to cause anamolous failures within GIS and of connected plant. In particular transformer windings are considered at risk as transformers are increasingly used at higher voltages and thus their insulation is subjected to switching surges of ever increasing severity. In order to prevent such insulation damage, the nature of the fast transients (risetime and waveshape) and the way they distribute themselves inside transformer windings must be accurately investigated.

As far as the nature of switching fast transients is concerned, there is a general agreement[2,3,4] that the precise risetime of these transients is below 10 nsec at the source (disconnector). However, these transients have to propagate through the substation equipment, namely, spacers, busbar chambers, bushings, overhead lines and/or cables before reaching transformer windings. During propagation, distortion of the initial switching wave (at the source) will occur. Hence, a close observation of the effect of substation equipment on the nature of the fast fronted transients during propagation is necessary in order to accurately estimate the risetime (most important) and waveshape of resultant switching transients incident to transformer windings.

On reaching transformer windings, these fast fronted transients (surges) will propagate through the windings and the manner they distribute themselves inside must be accurately known. Consequently, interturn and

intercoil insulation stresses can be deduced for different transformer parameters and risetime of surges. Subsequently the correct insulation design to withstand such very fast fronted transients impinging on transformer windings can be determined.

From what has preceded, we conclude that both aspects of the problem, namely, the nature of steep fronted surges and how they distribute themselves inside transformer windings, have to be deeply understood and investigated. As a result, a relevant background on both aspects is thus required.

2.1 GENERATION OF VERY FAST FRONTED TRANSIENTS IN GIS

Very fast fronted transients (surges) in SF6 GIS are generated during disconnector, breaker or grounding switch operation or by earth fault during on site testing or in service. However, almost all anomalous failures of electrical plant connected to GIS are reported[5] to be caused by disconnector operation. This is due to the occurence of transient overvoltages with steeper voltage rises and higher frequencies[6] in comparison with conventional switchgear as a consequence of the specific design and speed of operation of the isolator itself, the voltage across the disconnector at the instant of operation (trapped charge from previous switching), the characteristics of breakdowns in electronegative gases (e.g. SF6) and the short overall length of the GIS which includes different impedance discontinuities (e.g. spacers, bendings, bushings) encountered by the generated switching surges during propagation, stressing the equipment in GIS as well as adjacent and secondary equipment. Reported failures[2] during disconnector switching in GIS are insulation failures in GIS, bushing failures, malfunction of electronic devices (e.g. protective relays) and resonnances in connected transformers with consecutive insulation faults.

Disconnectors are installed in several locations in SF6 GIS[6] (fig 2.1) and, depending on their function, are known as busbar or line

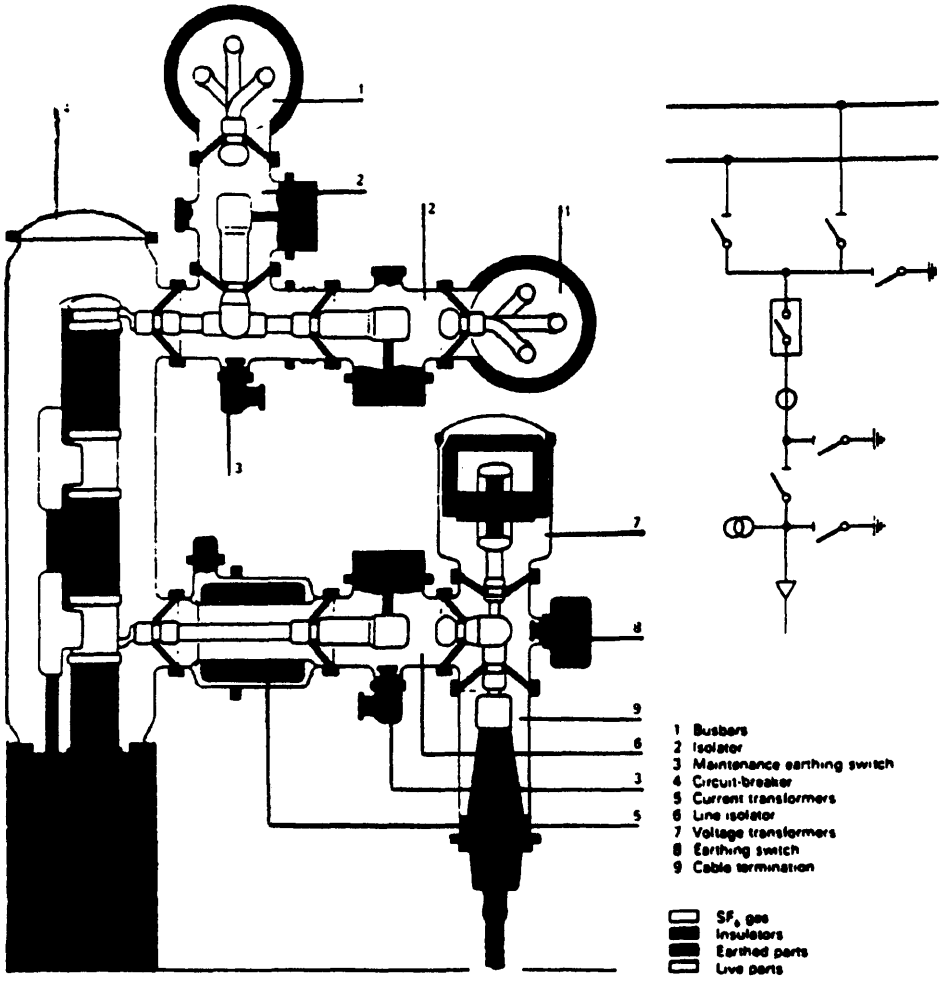

Fig 2.1 Cross-sectional view of an SF6-Gas insulated switchgear installation[6]

disconnectors. Fig 2.2 shows a cross section through such a disconnector, in which both the open and closed switching positions are simultaneously shown. Disconnectors are mainly used either to isolate two networks (or one network and a supply generator) connected together via an open circuit breaker (fig 2.3.a) or, more frequently, to connect or disconnect unloaded parts of the electrical plant (fig 2.3.b).

In the 420 Kv gas insulated substation KUPFERZELL[2] (fig 2.4) and during the closure of disconnector A, overvoltages with magnitudes of about 1.7 p.u.and frequencies of about 10-20 MHz were measured at a distance of 3m from the top of the bushing (point 1) of an indirectly connected transformer. Another field measurements at different points in the 420 Kv gas insulated substation WIEN SUED[7] (fig 2.5) were carried out during switching of disconnectors and circuit breakers. A maximum overvoltage of 1.7 p.u., occuring in the KHz range, was recorded at point 3 (2.3m away from the transformer busing) when the circuit breaker III was closed with disconnector II closed and busbar energised, with a front being roughly 1 p.u. in 500 nsec. In contrast, a voltage transient with a front time of only 13 nsec to the first peak of 0.5 p.u was recorded at point 3 when disconnector II was closed to energise the busbar from the transformer. In addition, on switching disconnector II,an exceptionally high frequency of 200 MHz was measured at point 2. This exceptionally high frequency oscillations decreased very quickly in amplitude with increasing distance away from the disconnector.

Before we precede with looking into the origin of very fast fronted transients, their nature and their mechanism, it would be very helpful to investigate the effect of such transients on the equipment within GIS and connected plant, for instance, transformers.

2.1.1 EFFECT OF VERY FAST FRONTED TRANSIENTS ON EQUIPMENTS

2.1.1.1.EFFECT ON TRANSFORMERS

Transformers are connected to GIS[1] either directly through SF6-oil

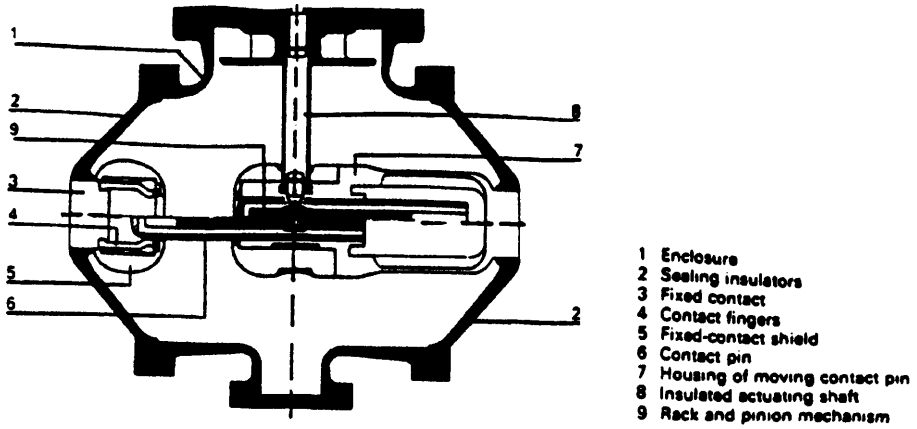

Fig 2.2 Section through an isolator[6]

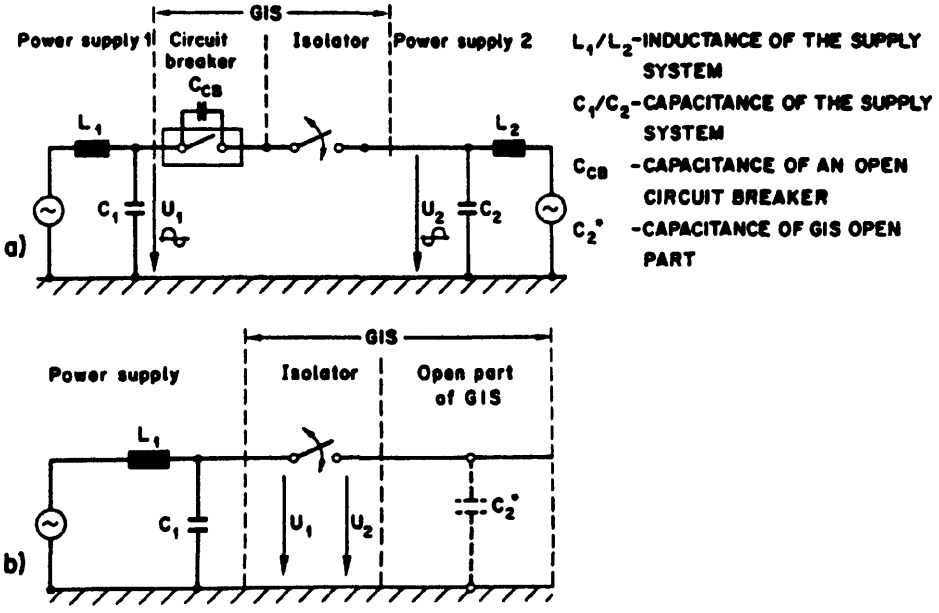

Fig 2.3 a) Isolator switching in phase opposition[6]
b) Isolator switching of an open GIS-section[6]

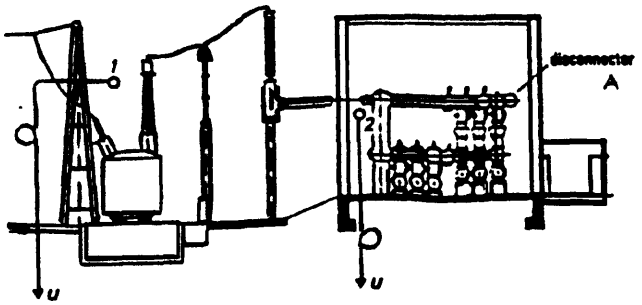

Fig 2.4 SF6-switchgear KUPFERZELL[2]

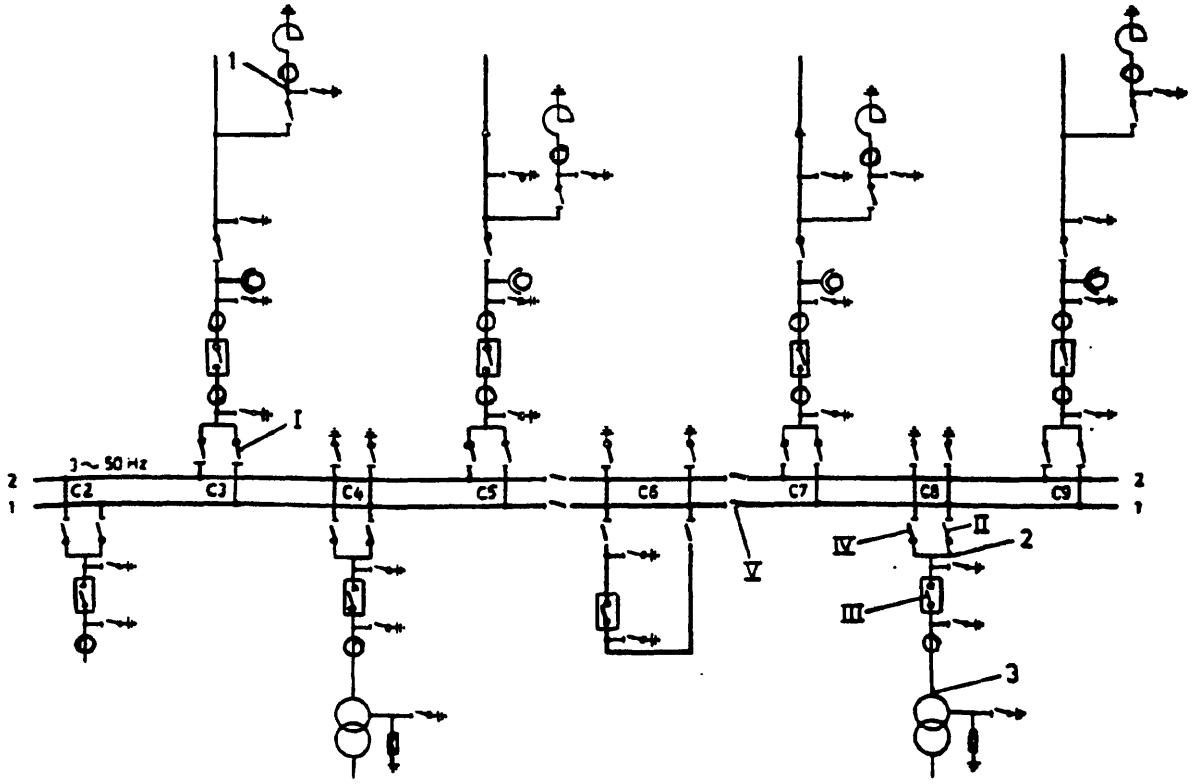

Fig 2.5 Single line diagram of GIS WIEN SUED[7]

bushings or indirectly through SF6-air bushings, overhead lines and air-oil bushings. However, in both cases, two different effects have been observed on transformer windings as a result of fast fronted switching transients generated in nearby GIS and impinging on such windings.

The first effect is the creation of an extremely non linear initial voltage distribution[8-13,15,41] along the high voltage winding especially the first few coils connected to the HV line end. Such an effect could be explained by the simple fact that when the initial rate of rise of a transient surge impinging on a transformer winding is sufficiently steep, then negligible current will flow in the inductive elements (fig 2.6.a[14]) of the winding since the inductance paths would have high impedance at the initial instant of time and, consequently, the voltage distribution will initially be governed entirely by the distribution of capacitances within the winding. This initial voltage distribution will therefore depend on the relative values of series interturn and intercoil capacitances and shunt capacitances to ground. Normally, because the ground capacitance is significant compared with the series capacitance, a large part of the applied voltage is developed across the series capacitance elements near the line end and the initial voltage distribution is far from linear. In fact the gradient of the initial voltage distribution curve is related to a parameter $\alpha = (C_g/C_s)^{1/2}$ where C_g and C_s are the total ground capacitance and series capacitance of the transformer winding, respectively. Various initial voltage distribution curves (grounded neutral) are shown in fig 2.6.b[14] for different values of α. For values of α greater than 5 (in practice, typical values of α for power transformers are 20 to 30), the maximum voltage gradient which occurs at the line terminal is approximately numerically equal to α times the average gradient[10,11]. For example, measurements carried out on a transformer HV winding[5] subjected to an impulse wave with 0.2 μsec front showed a maximum voltage of 50% (of the applied voltage) across the first coil made of ten turns with a maximum

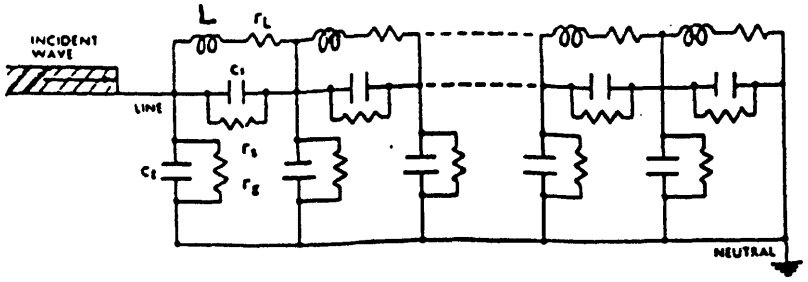

The Circuit Parameters, uniformly distributed, are:

- L = Inductance
- Cs = Series (Turn-to-Turn) Capacitance
- Cg = Shunt (Turn-to-Earth) Capacitance
- r_L = Loss Component of Inductance (Winding Resistance)
- r_s = Loss Component of Series Capacitance
- r_g = Loss Component of Shunt Capacitance

a)

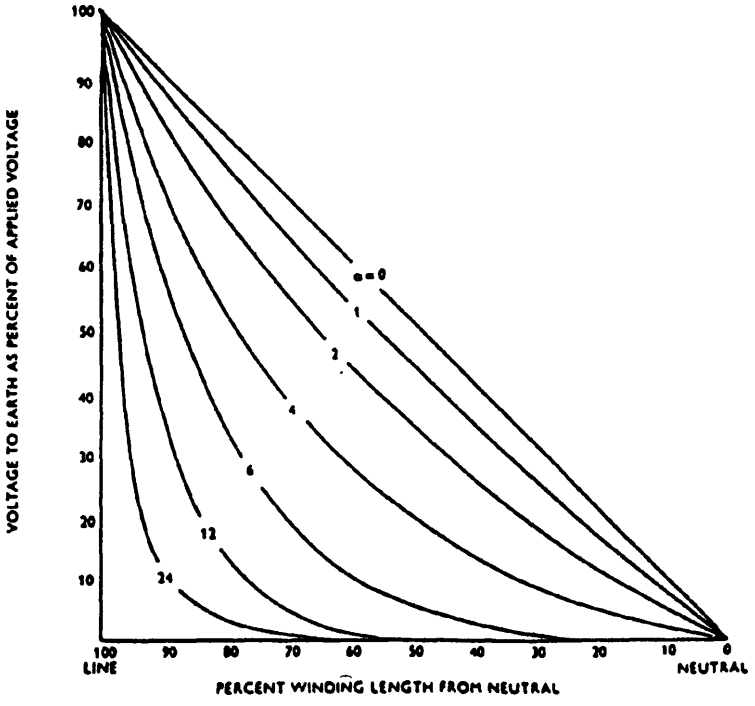

b)

Fig 2.6 a) Equivalent circuit of transformer for simple uniform winding[14]
b) Initial voltage distributions for different values of α[14]

voltage of 9% across each of turns 7 and 8 within the first coil itself. Moreover, the initial voltage distribution together with the following oscillations which occur in the transition stage with the L-C circuit of fig 2.6.a in order to reach the uniform power frequency distribution (final distribution) cause insulation stresses between parts of the winding itself and between parts of the winding and ground. Nontheless, for indirectly connected transformers, the front of incident very fast fronted transients is less steep as a result of attenuation and degradation caused mainly by overhead transmission lines and hence the above described effect is less pronounced (less resulting stresses) but still occuring.

However and in order to improve the initial voltage distribution in the line-end coils and subsequently decrease the following oscillations in the transitional (intermediate) stage, different approaches have been suggested :

1) Reinforcement of the line end coils [8,11,15] (graded insulation) : As it can be seen from fig 2.7.a[11], the line end discs are insulated to a greater extent than the rest of the winding with a graded transition from the reinforced to the normal insulation. However, since to some extent the additional insulation reduces the series capacitance of the line end coils leading to a higher voltage gradient in the line end region, care must be taken to ensure that the increase in insulation strength is greater than the increrase in voltage concentration.

This method has been criticised from the point of view that although it improves the intitial voltage distribution in the reinforced coils, it only shifts the dangereous region into the inner part of the winding[9,12]. It also affects the progress of free oscillations[12,15] in the winding due to the change in inductance.

2) Use of static rings[11,12,15] : The static ring consists of a continueous conducting surface with rounded edges with almost the same shape and dimensions as those of the line end coils. Such a ring is

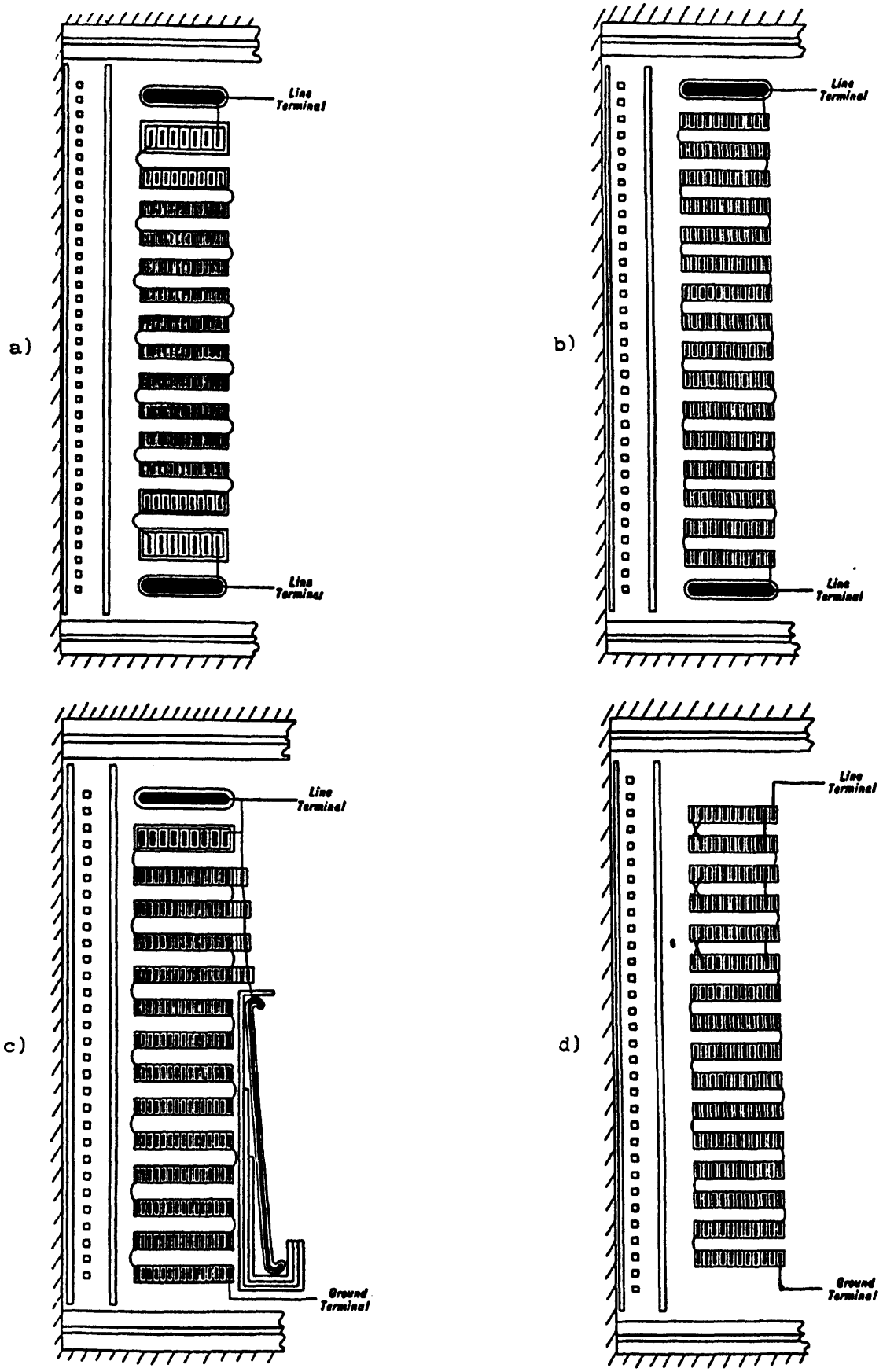

Fig 2.7 a) HV winding with graded insulation and static ring[11]
b) HV winding with static ring[11]
c) HV winding with graduated shield[11]
d) HV interleaved winding

usually placed adjacent to the line-end coil and electrically connected to the line as shown in fig 2.7.b[11]. As a result, the ring charges capacitively the turns of the line-end coil and thus produces a virtually linear voltage distribution along its turns.

Considerable care must be taken when using a static ring in that it could, as in the case of graded insulation, shift the dangereous region towards the inside of the winding.

It should be noted here that a static plate could be used with a graded insulation type winding as shown in fig 2.7.a.

3) Shielding[8,11,12,14,41] : As explained above it is the significant value of the capacitance to ground which yields the undesirable initial voltage distibution (especially at the line end coils) together with the following oscillations in the transitional stage. Hence, neutralising the effect of the ground capacitance is highly desirable in order to avoid the effect described above. This result of neutralising the gound capacitance is achieved in the so called " shielded winding " shown in fig 2.7.c[11]. The basic principle of the shielded winding is that, under all operating and abnormal conditions, no electrostatic charging current will be flowing in the turns in any part of the winding. This is accomplished by earthing the neutral and enveloping the whole winding with a metal shield insulated form both winding and ground. Furthermore, this metal shield is spaced so that, at any point along the coil stack, the electrostatic charging current flowing from the shield to the HV winding is equal to the electrostatic charging current flowing from the HV winding to the LV winding, core and tank.

Different types of shields have been used for different types of transformer windings (layer and disc types) with remarquable improvements in the initial voltage distribution[8,14]and the following oscillations, leading to less stress on insulation.

4) Interleaving of windings[8,9,12,16,17] : Rather than neutralising

the effect of ground capacitance by use of shields and the difficulties encountered both at the design and manufacture stages, a new type of winding which has a simple design and is very easy to build and which has a very much improved initial voltage distribution has been recommended. Such winding is known as the " interleaved (transposed) winding " and is shown in fig 2.7.d. In such a winding, two consecutive electrical turns are separated physically by a turn which is electrically much further down the winding. By doing so, the series capacitance of the winding is increased[8,9,12,16,17,18], leading to a higher ratio of the effective series capacitance to the capacitance to ground and consequently to an improved initial voltage distribution. Hence, the coil to coil stresses would be limited (especially in the line end region) and adequate axial insulation could be provided without excessive insulation in any part. This is so since the voltage gradient across turns is highly comparable to the voltage gradient across coils whereas in the conventional winding the intercoil voltages could be as ten times high as the interturn voltages.

Although there is a general agreement towards the much improved behaviour of transposed windings under surge conditions, the high series capacitance theory of such windings has been criticised from the point of view that an increased series capacitance as a result of interleaving is incompatible[19] with the concept of pure initial voltage distribution. The theory proposed instead[19] suggests that interleaving of turns result in the coils being surge impedances through which heavy curents flowing into the winding would charge the distributed earth capacitances during the initial period. Such theory has been illustrated with the derivation of formulas for the initial voltage distribution and the maximum voltage gradient.

The second effect is the development of an extremely high part-winding resonnance[1,20,23,25] in the regions of winding entrance and tap winding as a result of transient oscillations up to 10 MHz[1,26] within GIS. For

indirectly connected transformers, transient oscillations up to only 1 MHz[1] can reach transformer windings. In fact, transformer failures[22] on the American Electric Power system occured due to flashovers in the tap region as a consequence of internal part-winding resonnances which have been excited by transient overevoltages impinging on the transformer terminals. It is such transients with steeper fronts and longer tails[1,22,24], compared with standard lightning and switching impulses, which excite the natural frequencies in internal parts of the winding leading to excessive stresses with consequent failures. This is so because transient overvoltages and especially oscillatory ones (although of lesser magnitudes than aperiodic overvoltages) can inject more energy at the natural frequencies of the winding than in the case of standard impulses. One important feature in the protection of transformer windings against such transient overvoltages is the damping[23,24] in the winding which could very much suppress the amplitude of the resulting resonnant overvoltages.

Part-winding resonnance in the region of the winding entrance was observed when a winding consisting of two branches with 570 turns and 30 coils each was excited with its natural frequencies which had been calculated by modern computer programs[26]. The voltages were related to the exciting sine wave amplitude (k factor) and to the amplitude assuming a linear voltage distribution (q factor). As it can be seen from fig 2.8.a[26], the distribution is sinusoidal at natural frequencies of lower order with k factors of 2 to 3 whereas the amplitudes at the natural frequency of order $\lambda = 29$ are very high with steep fronts in the region of the winding entrance. Hence, local high gradients were to be expected in the entrance region and as it can be seen from fig 2.8.b[26], the high q factor at 726 KHz (natural frequency of order 29) indicates the high overstressing of insulation between the middle points of discs 1 and 2.

Part-winding resonnance in the tap region[1] is illustrated in fig 2.9

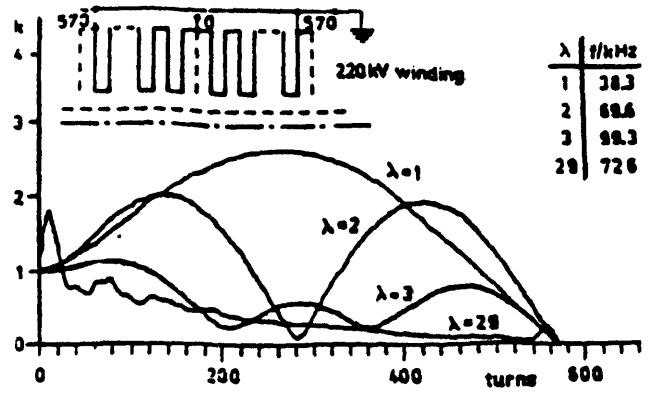

a)

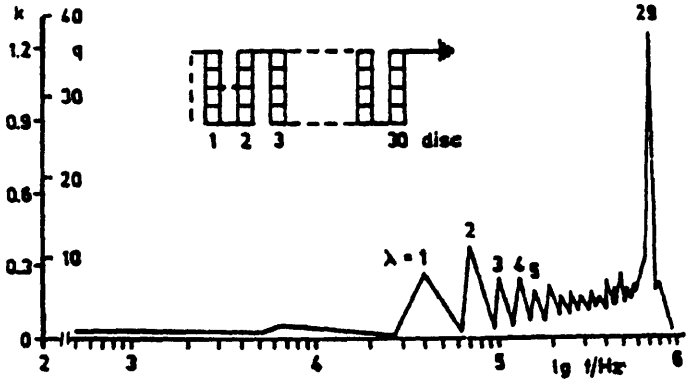

b)

Fig 2.8 a) Spatial voltage distribution for periodical excitations with various natural frequencies F(λ)[28]

b) Frequency response of the voltage difference between middle of discs 1 and 2 [28]

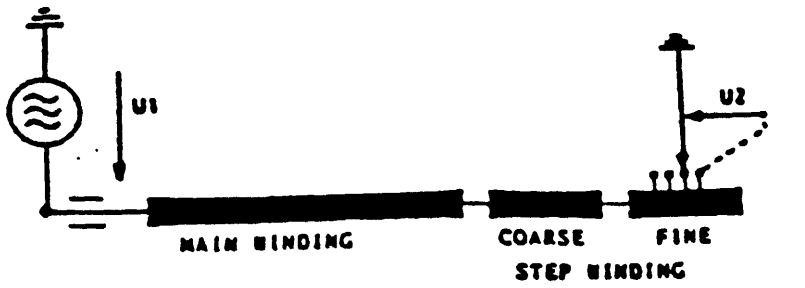

$$\left(\frac{U2}{U1}\right)_{50\ Hz} \approx 0.0105 \; ; \; q \approx \frac{U2}{U1} \Big/ \left(\frac{U2}{U1}\right)_{50\ Hz}$$

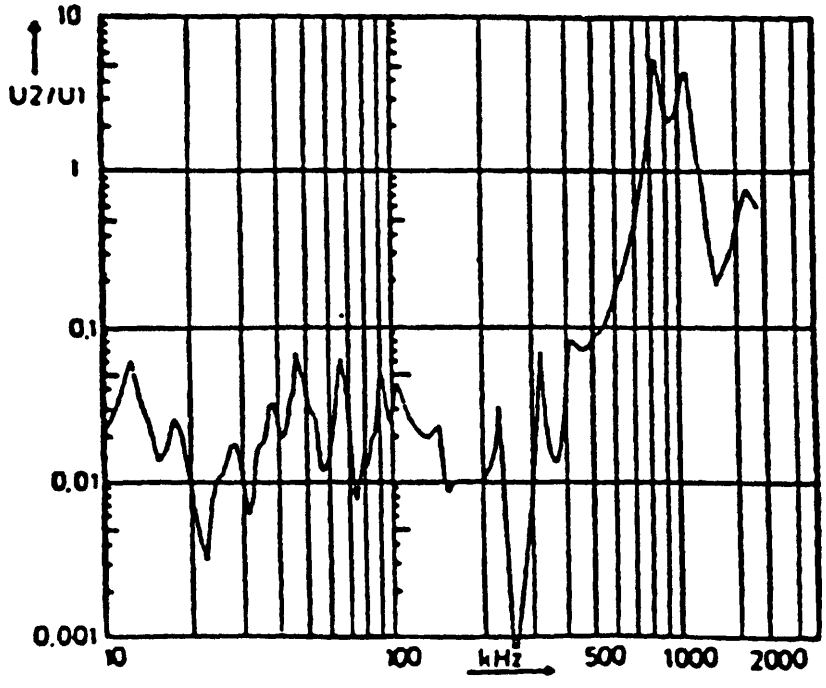

Fig 2.9 Voltage ratio between one step of trapped winding and HV side versus frequency[1]

which shows the voltage ratio between one step of the tapped winding and the high voltage side of a 420 Kv transformer directly connected to a GIS as a fuction of frequency. Again, extremely high values developed in the MHz range with the peak transient voltage amounting to 200 times the corresponding power frequency voltage with all that due to the transient potential rise of the neutral point[1].

Part-winding resonnance in both the entrance and tap regions has been observed through measurements carried out on another HV winding[27].

2.1.1.2.EFFECT_ON_DISCONNECTORS_AND_BREAKERS

Testing of the dielectric of switching equipment, according to IEC standards, have to be performed with specified impulse or a.c. withstand voltages while the contact system is either in the open or in the closed state[1]. In fact, striking occurs in the intermediate state which has not been included in the tests. Consequently, the dielectric stress in the intermediate positions may indeed cause a development of a discharge towards the earthed enclosure leading to an internal arc and breakdown. The dielectric stress depends on the design parameters[1] of the switching equipment, i.e, electrode geometry, gap distance, gas pressure and service voltage.

Since the contact system in circuit breakers and loadbreak switches operates in gaseous atmosphere with comparatively high overpressure, the striking distances between the contacts are very small compared to the distance between the contacts and enclosure and the resulting dielectric stress is too small to cause a discharge propagation towards the enclosure[1]. In fact, no earth faults have been caused by self generated very fast transients by such equipment. In addition, the insulation of circuit breakers and loadbreak switches has not been endangered by very fast transient overvoltages generated in adjacent GIS components especially disconnectors[1].

During disconnector operations, earth faults caused by self generated

very fast transient overvoltages have been observed[1]. This is mainly due to the design of the disconnector which necessitates a change in the electric field when a restrike occurs[1,28,29,30]. Actually, before a restrike takes place, the equipotential lines in the contact gap are mainly perpendicular to the axis of the disconnector and hence the field lines run mainly axially between the electrodes as shown in fig 2.10.a[1]. As soon as the leader type discharge bridges the disconnector gap and the arc is formed, the field lines will show a radial pattern (fig 2.10.b[1]) and it is such distribution of the electric field together with self generated very fast transient overvoltages[1,28,29,30] which could very well enhance the breakdown to earth, or, in other words, the "breaking out" of the arc by simply pushing at least one branch of the leader radially towards the enclosure (fig 2.10.c[1]) . This is the case since the behaviour of a radial branch depends on the intensity of the electric field at its tip and the voltage applied to the branch itself[30] which has to be above a "critical voltage" in order for the propagation towards the enclosure to proceed. The usual time for the "breaking out" of the arc is about 500 nsec[29] after the first ionisation in the contact gap has occured. In order to avoid such breakdowns, an optimised disconnector design was obtained after an extensive test series on disconnectors was carried out for the highest system voltages[28]. Such optimised designs have proved to be reliable[1,28].

2.1.1.3 EFFECT ON SF6 INSULATION

In a pure GIS insulation, the upper curve B (fig 2.11[1]) represents the lightning impulse[1,31,32] voltage-time characteristic. This is a very well known characteristic with increasing withstand values for increasing front steepness, which is mainly caused by the formative time lag in the breakdown channel. Measurements have shown that the breakdown voltages for very fast fronted transients are above the lightning impulse withstand level[1,31,32] (LIWL) in area A in fig 2.11. Furthermore, due to the longer

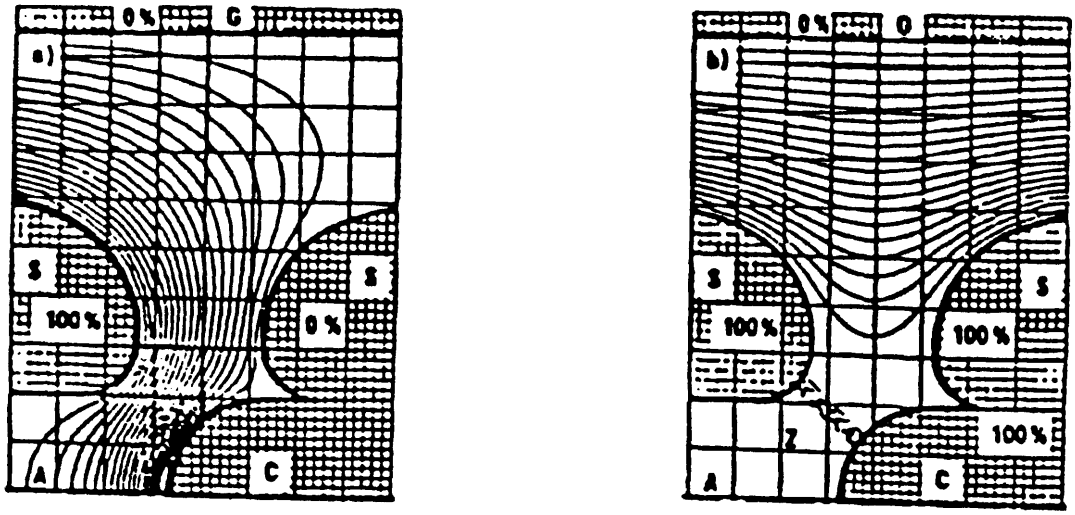

a)

b)

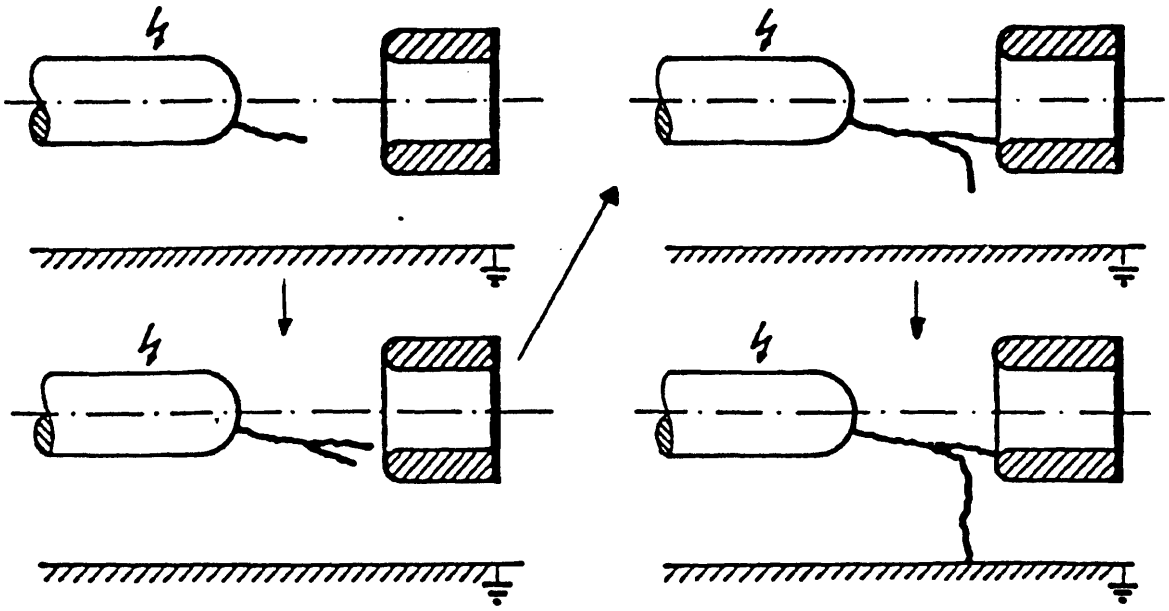

c)

Fig 2.10 a) Electric field distribution of a disconnector before striking[1]

b) Electric field distribution of a disconnector after striking[1]

c) Development of an earth fault by branching of the leader discharge[1]

formative time lag, the negative polarity very fast transient overvoltage breakdowns occured delayed for some hundred nanoseconds in the oscillatory tail (fig 2.12.b[1]) and at higher values in comparison with positive breakdowns in the initial front or close to the primary peak (fig 2.12.a[1], all that making the positive polarity breakdown values decisive for the very fast transients[31]. However, when spacers are included, both polarities should be taken into consideration for very fast transients[32]. Measurements have also shown the big scatter for both polarities but all breakdown values with or without spacers are close together within the area A above the LIWL. All this leads to the conclusion that a very fast transient overvoltage breakdown is unlikely in a correct GIS insulation during normal operation.

If any irregularities are to be found in the GIS insulation, extensive investigations[31] have shown the downturning trend of the corresponding lightning impluse voltage-time curves D (fig 2.11) with increasing front steepness. The marked area C in fig 2.11 represents the breakdown voltages during switching operations and very high frequency oscillations if protrusive irregularities exist. The breakdowns occured late on the oscillating tail as shown in fig 2.12.c[1] with a big scatter[31]. Again, the positive polarity breakdowns are decisive in the case of high frequency switching transients[31]. The lower range of area C is the service voltage phase to ground and that explains the failure to ground during switching operations in adjacent bus duct sections[31]. It should be emphasised that with such irregularities, the main cause for the breakdowns is the very high frequency oscillations (even if they have low amplitudes[31]) which are evident in the shape of very fast transient due to the multiple reflections at the different GIS discontinuities. It is these oscillations which provide the displacement current which together with the current caused by the corona discharge ahead of the leader tip make the leader current necessary for the gas thermalization at leader tip, which is vital

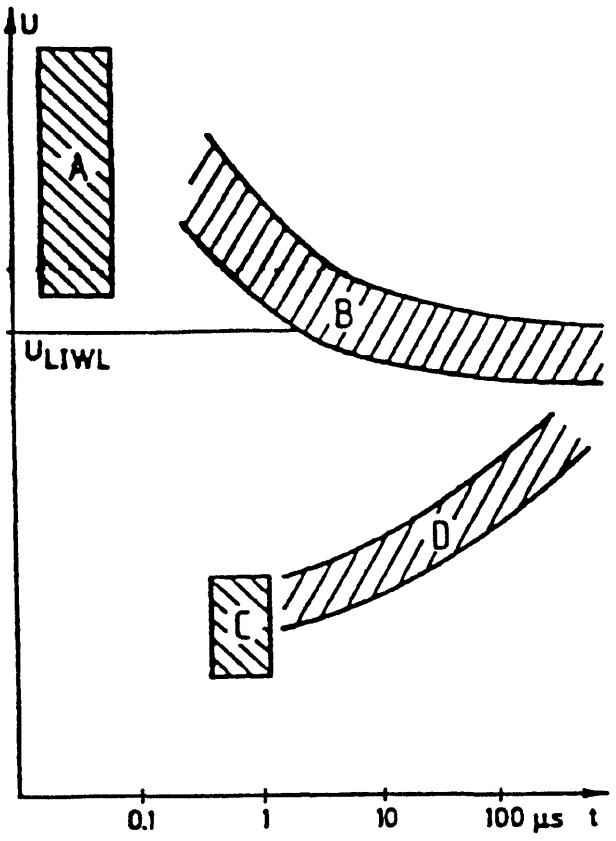

Fig 2.11 Principal voltage-time characteristics[1]

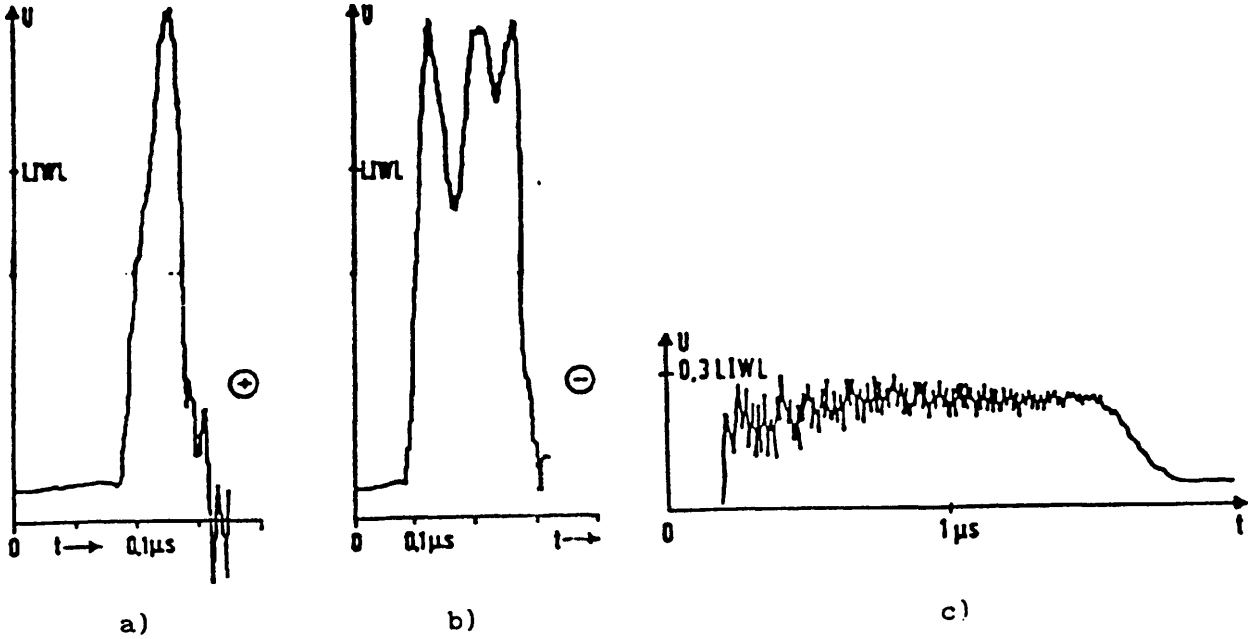

Fig 2.12 a) Positive breakdown in pure GIS insulation[1]
b) Negative breakdown in pure GIS isulation[1]
c) Breakdown in GIS insulation with irregularities[1]

for leader inception and propagation[31]. The abscence of dangereous irregularities can be proved by lightning impulse voltage tests which in this case have to be added to a.c. or switching impulses[31].

2.1.1.4 EFFECT ON OTHER SUBSTATION EQUIPMENT[1]

During switching of disconnectors in GIS, the rise in the transient enclosure voltage (TEV) causes sparking across the insulating flanges which provide high frequency continuity in the enclosure and limit the magnitude of the TEV coupled onto the enclosure to about 10 Kv whereas no such continuity exists (near SF6 to air connections), the transient ground potential rises up to 100 Kv. Such sparking could puncture the insulation of the enclosure which limits the circulation of currents within the enclosure due to the flow of current in the main conductor, leading to damaging effects in the case of a short-circuit at any point in the electrical network. TEV, though intermittent and of short duration, may very well lead to the malfunctionning of any secondary equipment, i.e, relays, meters, etc., by rising the potential of its housing which could be connected directly or via cable shields to the enclosure, or by inducing currents and voltages in the equipment through radiation. No effects on capacively graded bushings has been observed, except for the case where failure due originally to a bad contact design may have been accelerated by very fast transients.

Potentially damaging problems can be avoided by the following means :

1) The design of a substation map to which all the earthing points are effectively attached through earthing straps with minimal surge impedance and electrical length. The more the earthing connections are the less the TEV will be. This could well be supplemented by the introduction of voltage limiting varistors with suitable ratings where insulated spacers must be employed.

2) the use of shielding to prevent the very fast transients generated internally from reaching the outside of the enclosure.

3) The appropriate connections of cables, the mounting of control cables closely along all grounded structures and the grounding of cable shields in order to minimize, and eliminate if possible, the influence on related equipment. In the secondary equipment, voltage limiting devices have to be added.

2.1.2 ORIGIN OF VERY FAST TRANSIENTS

2.1.2.1. VOLTAGE COLLAPSE TIME DURING SF6 BREAKDOWN

During disconnector operations, any line to earth fault leads to a voltage collapse at the fault location in a similar way as in the disconnector gap during striking. Such breakdown phenomena in the compressed gas insulation of GIS, wether across the contacts of a disconnector or a line to earth fault, generate very fast fronted surges which propagate in either direction from the disturbance source throughout GIS and to other connected equipment.

The risetime of the very fast fronted voltage surges can be obtained knowing that the properties of a spark gap are almost similar to those of an ideal switch[33]. With the voltage applied between the electrodes less than the sparking voltage, an infinitely high insulating resistance exists between them. The value of this resistance decreases rapidly as soon as the voltage between the electrodes increases above the sparking voltage, giving way to an arcing voltage of 100 V across the gap. The switching process of a spark gap can be divided into three different phases. These are illustrated in fig 2.13[33] for the case of a spark gap triggered through an impulse voltage of amplitude U_0 which is higher than the statistical breaking voltage U_{stat}.

1) the first phase, so called dispersing time T_σ, depends on the number of available electrons at the start of the process. The dispersing time can be considerably reduced by triggering the spark gap through application of higher overvoltage, ultraviolet radiations very closely below the sparking voltage or secondary discharge with the help of a laser beam.

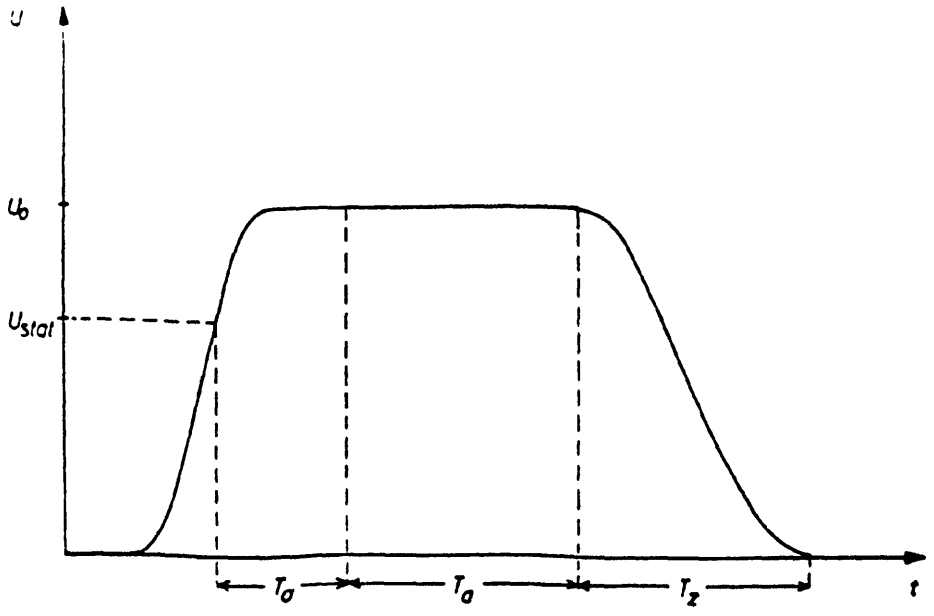

Fig 2.13 Three phases of a switching process in a spark gap[33]

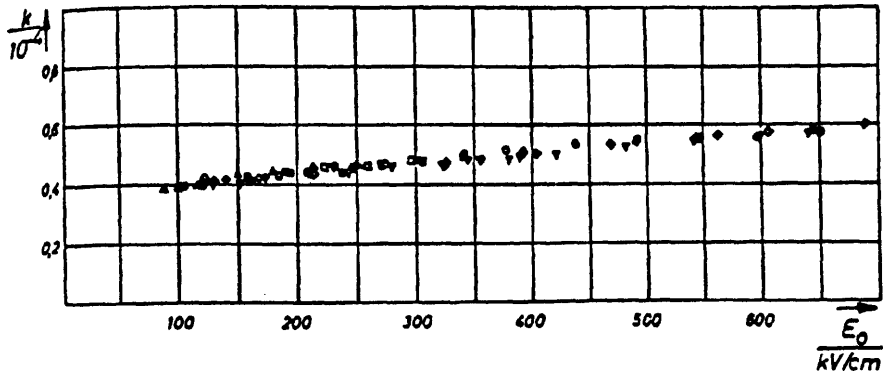

Fig 2.14 Toepler constant as a function of spark gap field strength[33]

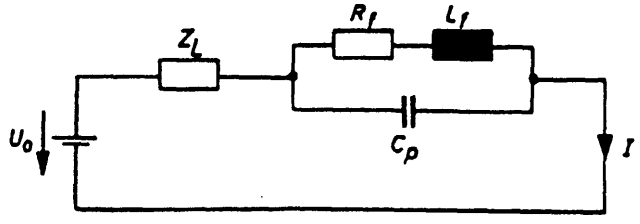

Fig 2.15 Equivalent circuit for discharge of conductor over a spark gap[33]

2) During the build up time T_a, a weak conducting spark channel is formed and on which, practically, the full voltage U_0 applies and the switch is still off. In case of high pressure gas with spark path of small striking distance, this process always happens in the form of single electron avalanche. The amount of bulid up time depends on the quotient of mean field strength E_0 and pressure P, E_0/P.

3) During the collapse time T_z, the conductance of the pre-spark channel rises very rapidly. This process could be calculated via three different[34] approaches. The simplest overview with satisfactory results is from the toepler law[33]:

If we neglect the loss of charge carriers through recombination, then the electron concentration changes as follows

$$dn_e = n_e Q_{wi} dx \qquad \ldots(2.1)$$

where Q_{wi} is the number of generated pairs of charge carriers, in the elementary length dx. But

$$dx = v_e dt \qquad \ldots(2.2)$$

$$v_e = b_e E \qquad \ldots(2.3)$$

$$E = U / s \qquad \ldots(2.4)$$

where

v_e is the electron velocity

b_e is the electron mobility

s is the striking distance

E is the field strength along the spark gap

By substituting (2.2) and (2.3) in (2.1), we get

$$dn = n_e Q_{wi} b_e e dt \qquad \ldots(2.5)$$

By the relevant brief changes , only the electrons contribute to the current so as to yield the following current density j

$$j = n_e b_e e E \qquad \ldots(2.6)$$

By substituting (2.6) in (2.5), we get

$$dn = \frac{Q_{wi}}{e} j dt \qquad \ldots(2.7)$$

At time t after the begining of the transformation of the pre-discharge channel, the electron concentration will be

$$n(t) = \frac{Q_{wi}}{e} \int_o^t j \, dt \qquad \ldots(2.8)$$

If we assume that the current density over the cross section of the spark channel and the field strength along the channel are constant, and if in addition the cross section of the spark channel is assumed as time independent, then the toepler spark law is

$$R(t) = \frac{u}{i} = \frac{k\,s}{\int_0^t i \, dt} \qquad \ldots(2.9)$$

where R (t) is the spark channel resistance

$$k \text{ is the toepler constant} = \frac{1}{b_e Q_{wi}} = 0.5*10^{-4} \text{ vs/cm} \qquad \ldots(2.10)$$

k has a small dependence on the spark field strength E as shown in fig 2.14.

With the knowledge of k and using toepler law, The collapse time of a spark channel can be calculated. A complete solution can only be obtained for a relatively simple discharge circuit. As an example for that is the discharge of a conductor charged up to a voltage U_0 with characteristic impedance Z_L over a discharge channel. The equivalent circuit diagram is shown in fig 2.15[33].

By neglecting the spark inductance L_f and electrode capacitance C_p, we get the following current

$$i(t) = \frac{U_0}{R_f(t) + Z_L} \qquad \ldots(2.11)$$

By substituting $R_f(t)$ and relating the spark discharge current to its maximum value

$$y = \frac{i}{I_{max}} \qquad \ldots(2.12)$$

$$I_{max} = \frac{U_0}{Z_L} \qquad \ldots(2.13)$$

we get

$$\int_0^t y \, dt = \frac{k\,y}{E_0\,(1-y)} \qquad \ldots(2.14)$$

By differentiating (2.14), we get

$$y = \frac{k}{E_0} \frac{dy/dt}{(1-y^2)} \qquad \ldots(2.15)$$

By separation of variables and partial factorisation

$$dt = \frac{k}{E_0} \left[\frac{1}{y} + \frac{1}{1-y} + \frac{1}{(1-y)^2} \right] \qquad \ldots(2.16)$$

And by integration the resulting discharge time will be

$$t = \frac{k}{E_0} \left[\ln \frac{y}{1-y} + \frac{1}{1-y} + c \right] \qquad \ldots(2.17)$$

and with $y = 0.01$, $c = 3.58$, the risetime of the discharge current is

$$T_z = 13.3 \frac{k}{E_0} \qquad \ldots(2.18)$$

And as a pure ohmic discharge circuit exists, the same expression is also valid for the collapse time for the voltage, which is the risetime of the generated fast fronted surges in a pure GIS insulation system with almost homogeneous field distribution and is

$$T_r = 13.3 \frac{k}{\Delta u/s}$$ [1,33,34]

Hence, in an insulation without any impurities and a system without any design defects, the lower limit $T_{r_{min}}$ of the expected risetimes can be gained by

$$T_{r_{min}} = (1, \ldots\ldots, 1.5) \frac{1}{P} \quad [\text{ nsec, MPa }]^{(1)} \qquad \ldots(2.19)$$

Risetimes increase with increasingly inhomogeneous fields. Extraordinarily long risetimes up to 200 nsec[31] are obtained for extremely inhomogeneous fields, caused for instance by long needles shaped protrusions in case of very fast breakdowns where $\Delta u/s$ is considerably reduced.

2.1.2.2 DISCONNECTOR AND CIRCUIT BREAKER OR LOAD BREAK SWITCH OPERATIONS

GIS disconnector transients are generated by the propagation of fast fronted surges[1,4,5,6] created by the voltage collapse across SF6 insulated electrodes as a consequence of restrikes (or line to earth fault) during operation. The very fast transient overvoltage shape is formed by the multiple reflections and refractions of travelling waves at impedance discontinuities inside GIS[1,4,5,6]. Consequently, the frequency of the transients is determined by the length of GIS segments and connected lines,

or in other words, GIS configuration[1,4,5]. Moreover, both the risetime and magnitude of the initial fast fronted surges are instrumental in giving the transient its particular form and peak value[1]. The risetime of the created surges limits the highest frequency component of the transient and is a key factor in the determination of its peak value[1]. The magnitude of the created surges, determined by the actual conditions prevailing on each side[1,4,5,6] of the disconnector at the instant of striking, is the other important parameter which determines the overall crest value of the fast fronted transient.

In order to understand the general switching behaviour of a disconnector, consider the case where a disconnector is used to connect the floating section of a switchgear (load side) to an energised gas insulated system (fig 2.3.b)[1,4].

As the contacts approach, the static breakdown voltage for the cold gas will decrease whereas the electric field between the disconnector contacts will increase. The breakdown voltage is determined by the contact gap, electrode geometry and the properties of the cold insulating gas[4,6]. As soon as the voltage across the gap of the disconnector ($U_2 - U_1$) exceeds the instantaneous breakdown voltage for the cold gas, or in other words, the instantaneous dielectric strength of the gaseous medium between the contacts, a breakdown and thus a first strike occurs. Due to the relatively low speed of disconnectors, the first strike usually occurs at the peak of power frequency voltage. Both electrodes are thereby electrically connected by a conducting spark through which a transient current will flow to charge the capacitive load to the source voltage. As it does so, the potential difference across the contacts falls leading to the interruption of the transient current and eventual extinguishing of the spark itself (fig 2.16.a[4]). Subsequently, the voltage on the load side remains constant with time while the voltage on the source side follows the power frequency, thus falling from the peak value. Consequently, the voltage across the

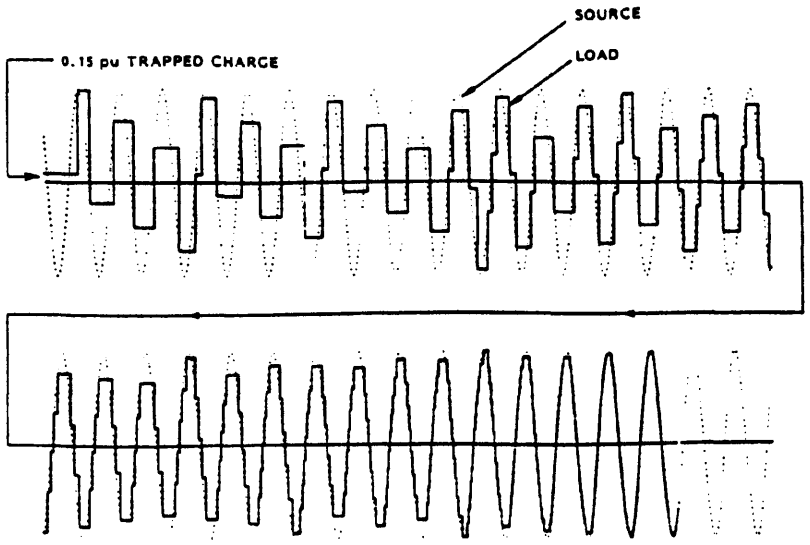

a)

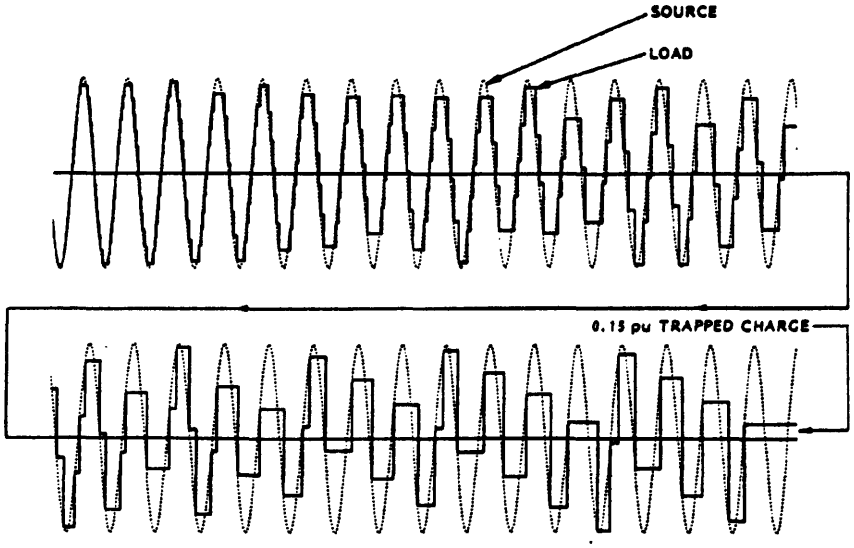

b)

Fig 2.16 a) General switching behaviour of a disconnector when closing into a capacitive load[4]

b) General switching behaviour of a disconnector when opening on a capacitive load[4]

disconnector will rise again in the opposite polarity and as soon as this voltage exceeds the instantaneous dielectric strength of the gaseous medium between the contacts, a restrike will take place.

It should be mentioned , however, that due to the asymmetry of the electric field distributions at the two electrodes[1,4], the intercontact breakdown voltage is always higher in one polarity than inthe other (negative breakdown voltage is approximately 15% higher than positive breakdown voltage) and the first strike will often occur[1] when the moving contact has a negative polarity. As a result, the second strike will take place for a greater potential difference across the contacts than the first strike and will occur when the source voltage has crossed zero[1].

As the contacts continue to approach, the instantaneous dielectric strength of the intercontact gap steadily reduces which causes a steady increase in the number of restrikes per cycle and the amplitude of the individual voltage steps (fast fronted surges) becomes smaller and smaller as shown in fig 2.16.a. As mentioned above, since the amplitude and risetime of the generated fast fronted surges is an important factor in determining the peak value of the corresponding transients, the severity of such transients decreases rapidly as closing precedes. Hence, the largest and steepest surges are generated by those breakdowns at the largest contact gap[4].

When a disconnector is used to separate the source and load sides, the behaviour is a complete reversal of the above description[1,4,6] (fig 2.16.b[4]). Moreover, it is very important to note that the asymmetry in the breakdown voltage leads to a falling pattern near the end of the operation which continues until the voltage across the disconnector gap cannot cause neither positive nor negative breakdowns[4]. This will leave a trapped charge on the floating section of the switchgear. The higher the trapped charge is, the higher the voltage across the contacts at the first strike will be, leading to the steepest surges having higher magnitudes.

It should be mentioned that in practice, during each restrike, capacitive currents above few amperes may sustain continuous arcing for substantial periods of time longer than those predicted for charging the load through the surge impedance of the GIS bus[1,4,6]. This is due to the high frequency nature of such currents which keep the arc burning until they are damped out[1]. In fact, a time of around 50 microseconds was measured during disconnector switching[4].

The precise number and amplitude distributions of steps during disconnector switching will depend[1] firstly on the specific disconnector design and operating speed, secondly on the behaviour of GIS after each restrike spark extinction and thirdly on specific GIS functional procedure. With relation to the specific disconnector design and operating speed, low speed disconnectors of conventional design[1,4] (with mean breakdown asymmetry of 15%), the trapped charge left when opening on a pure capacitive load gives remaining voltages of 0.1 to 0.5 pu peaking around 0.3 pu leading to a voltage of around 1.3 pu across the contacts at first strike[4]. On the other hand, fast operating switches[1] can leave trapped charge corresponding to 1.0 pu in a non negligible number of cases, leading to a voltage of 2.0 pu across the contacts at first strike. This is the case as well when a specific GIS operational mode, though rarely adopted and involving the opening of a circuit breaker, can leave a floating busbar generated to a level near maximum of 1.0 pu[1].

It is important to mention that, independently of the actual disconnector design, after the extinction of an intercontact arc, the source and load sides of the disconnector can oscillate at the corresponding natural frequencies[1,4] (few tens to several thousands Hz). This can create conditions under which the phase differences between the two sides of the opening disconnector can trigger the final restrikes with a voltage of 2.0 pu across the contacts. A practical example of this would be the opening of a GIS bus containing a saturable magnetic voltage

transformer[35].

Each of the created very fast fronted surges will propagate in either direction from the disturbance source through the GIS bus to other connected equipment. During such propagation, The waveshape of the travelling waves will vary as a result of distortion and attenuation as it will be explained in the following section.

2.1.3 PROPAGATION OF VERY FAST TRANSIENTS

As described above, fast fronted travelling waves generated by voltage collapse during switching operations of disconnectors, will travel in either direction from the disturbance source through GIS and to connected equipment. These fast fronted travelling waves have a risetime of less than 10 nsec[2,3,4] at the disturbance source. During propagation, such travelling waves will be reflected and refracted at all points which represent impedance discontinuities inside GIS and at connected equipment. As a result, the original travelling waves created at the source will be distorted in magnitude and waveshape before they impinge on connected equipment. The degree of distortion will depend mainly on the GIS configuration and the means of connection between GIS and connected equipment.

2.1.3.1 TRANSIENTS INTERNAL TO GIS

Initial fast fronted travelling waves, when propagating through the GIS bus duct, will encounter different impedance discontinuities such as spacers, bendings, shields, open/closed circuit breakers, etc... Consequently, Such waves will be transmitted with magnitudes[1,6] according to basic transmission line theory. It is the superposition of such reflections and refractions[1,3,5,6] which will lead to the formation of very fast fronted overvoltages which overstress the insulation. Because of this travelling wave nature, the very fast transient shape can be significantly different at points within GIS separeted by only few meters[36]. Hence, in order to conveniently analyse the effect of the

different GIS components on the risetime (most important) and waveshape of initial travelling waves, these components have to be precisely modelled.

In order to obtain the correct models for GIS components, low voltage pulse propagation measurements[36-39] have been carried out. Low voltages have been injected with conical, constant impedance coupling devices, or by the use of mercury switches, enabling distortioneless measurements of nanosecond pulses using standard instrumentation. Such measurements were supplemented by calculations using the EMTP (electromagnetic transients program). By obtaining the best agreement between calculated and measured results, the exact component models were obtained.

By using the above models, different simulations of transients in different GIS configurations[35,36,38,39] were obtained and in good agreement with the corresponding measurements. A comparison of a computer simulation[39] and actual measurement of a disconnector transients is given in fig 2.17.b[39]. The GIS configuration illustrating the operated disconnector and the measurement point is shown in fig 2.17.a[39]. The simulation of fig 2.17.b neglects the presence of propagation losses (skin effect, etc...) resulting in less damping of high frequency details of the waveform. In addition, the effects of spacers, flanges, elbows, corona shields and other connection hardware were included by adjusting the propagation velocity along the coaxial bus duct in the gaseous medium to 0.95 the velocity of light. In other configurations, such velocity was adjusted to 0.9 the velocity of light[38]. All this emphasises the fact that GIS is in fact a network of interconnected transmission lines with individual lengths, impedances and velocities of propagation.

As far as the risetime of the front of the initial travelling waves is concerned, no degradation of the rate of rise has been seen during propagation inside GIS. Indeed, the magnitude of such front is only affected by transmission (according to basic transmission line theory). It has been acknowleged that when a travelling wave encounters a 'T'

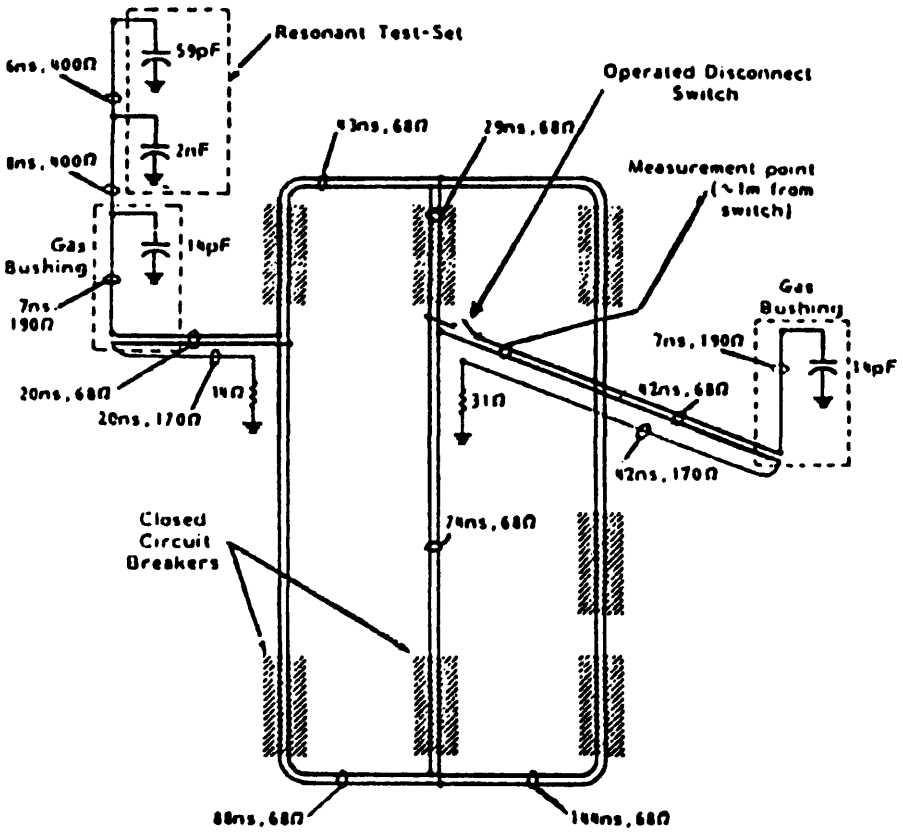

a)

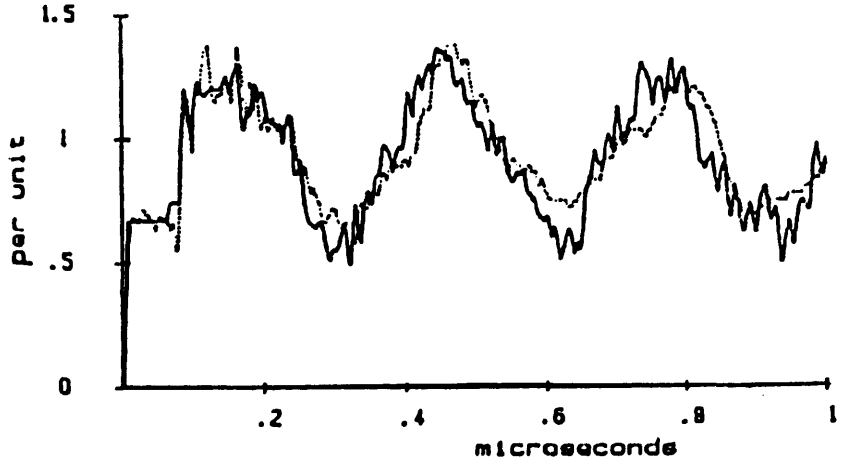

b)

Fig 2.17 a) GIS configuration illustrating operated disconnector and measurement point[39]

b) Comparison of predictive simulation (solid line) and actual measurements (dotted line) of disconnector transients[39]

section, the front with the same rate of rise is reduced by 33% in magnitude[5]. The waveshape of the fast transients is dependent[1,3,4,35,38,39] on the conditions prevailing at the disconnector contacts prior to striking, the GIS layout, the disconnector location and functional procedures. With relation to the maximum peak, for normal switching conditions of most disconnector designs, a voltage collapse of 1.5 pu is not exceeded resulting in maximum overvoltage values of up to 1.7 pu for most configurations and 2.0 pu for very specific cases with maximum value reached at the second or even later peaks[3]. On the other hand, the main frequency of the very fast transient is given by the total length of the GIS bus switched by the disconnector. Due to damping and refraction effects, the very high frequency components steadily decay leading to mainly monofrequent oscillation in the range of 1 to 40 MHz normally after some few microseconds. It should be noticed that sometimes, close to the disconnector, frequencies of up to 100 MHz[3,35] are observed created by reflections at adjacent internal GIS components in short distance or within the disconnector itself.

2.1.3.2 EXTERNAL VERY FAST TRANSIENTS

The initial travelling waves, having propagated through GIS would normally encounter the GIS bushing, before going on to other connected apparatus. Two types of bushing are normally used, i e, gas filled bushings and capacitively graded bushings. As the travelling waves encounter the impedance discontinuity at the bushing, a part will be reflected onto the enclosure leading to the creation of the transient enclosure voltage[1,2,40] and the remaining part will propagate along the transmission line and stress connected equipment. The effect of capacitively graded bushings[5] on the incident travelling waves is to cause a slight risetime degradation (to about 10-20 nsec) of the front with reduction in its magnitude (to about 75%). Such waveform distortion is mainly due to phase shifts caused by the passage through the grading

layers though dielectric losses contribute to a lesser extent to such distortion. Such conclusions have been reached through calculations verified by measurements. In all the calculations, the capacitively graded bushing was modelled as a distributed parameter (since the travelling wave has a front risetime comparable to the travel time of the bushing) using concentric transmission lines which represented the grading layers. Representing the capacitively graded bushing by an equivalent capacitance would yield to erroneous results[5] when the rate of rise of the transient is of utmost importance. For this reason it has been suggested that the equivalent transmission line model is prefered when the grading layer model cannot be implemented[5]. Another model for the capacitively graded bushing was also checked by measurements and based on coaxial transmission lines[37].

Before preceeding further into the connected equipment to GIS, it is worthwhile mentioning the transient enclosure voltage (TEV). This is the voltage which appears[1,2,40] on the external of the earthed GIS enclosure as a consequence of coupling of internal transients of the enclosure at enclosure discontinuities, and the bushing is the most significant source of TEV[1]. The TEV occurs because the normal earthing connections are too inductive to provide effective grounding for the very fast fronted transients. This TEV has a short risetime and a short duration. It has two components. The first component is dependent on GIS layout and earthing conditions and is characterised by a short risetime and oscillations in the 5-10 MHz range whereas the second component is of lower frequency (hundreds of KHz) and is often associated with the discharge of large capacitive devices. Both components are damped very quickly and the TEV persists only for few microseconds. The magnitude of the transient varies along the enclosure with values generally between 0.1-0.25 pu but can reach higher values near SF6 to air terminations.

During surge propagation from the GIS bushing to connected equipment,

i.e. transformers, the length of the overhead transmission line has a very pronounced effect[5]. If the overhead connections are relatively short, they will cause a magnitude reduction of the initial fast front of the transient impinging on the transformer or other station equipment to about 20%-40% of the incident magnitude with risetimes in the 10-20 nsec range. In contrast, long overhead lines (around 1 Km) cause severe risetime degradation to the propagating transients. The change in voltage rate-of-rise is attributed to losses to the high frequency components of the waveform during surge propagation. As a consequence, computer simulations for the case of directly connected apparatus involving a gas to oil bushing indicated a risetime of 10 nsec and no reduction in the amplitude of the front especially.

External very fast fronted transients have two characteristics[1,5]:

1) Fast fronted portion with a risetime of 20 nsec and a magnitude of 20%-40% of the incident magnitude.

2) The overall transients which are dictated by lumped circuit parameters of the whole system consisting of the GIS and the transformer, with an overall risetime in the range of a few hundred nanoseconds and frequencies in the range 20-100 Hz

When such very fast fronted transients impinge on transformer HV windings, they will propagate into the inside of the windings, stressing the insulation. Previous work on transformer response to impinging surges is illustrated in the following section.

2.2 DISTRIBUTION OF SURGES IN TRANSFORMER WINDINGS

Early work on surge distribution was based on the standing wave theory advocated by Blume[11] in which the initial and final distributions are considered (fig 2.18.a) (earthed neutral). A unit function is applied to the transformer windings having uniformly distributed inductance and capacitance. The initial distribution, mentioned in section 2.1.1.1, consists of two components. One is the uniform voltage distribution (final

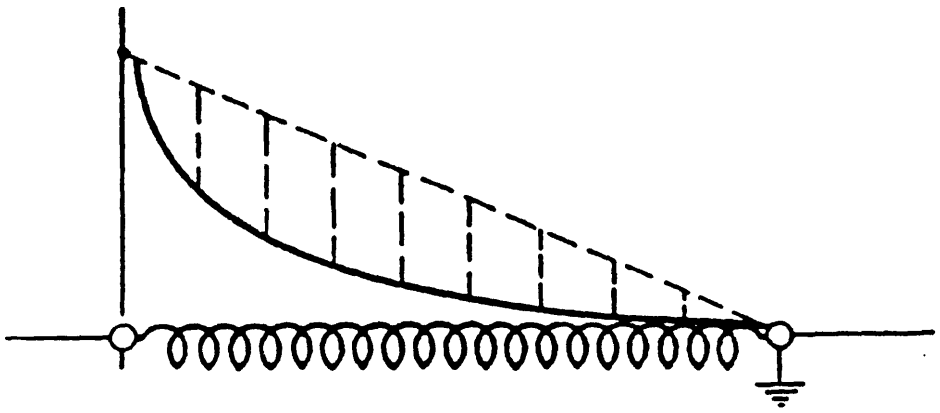

a)

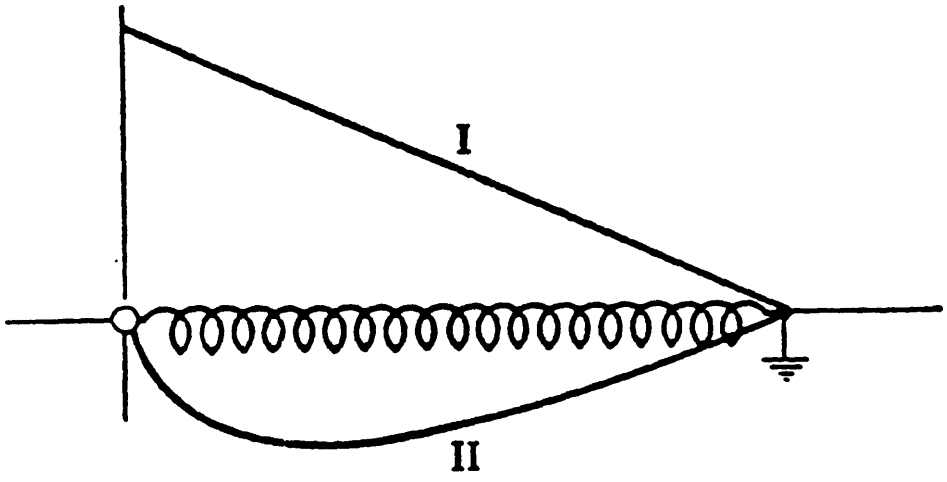

b)

Fig 2.18 a) Solid curve, initial voltage distribution; Dotted straight line, final distribution[11]

b) Curve I, steady state component; Curve II, transient component[11]

distribution) called for the inductive network, and the other is the difference between this and the actual initial distribution, represented by the shaded part in fig 2.18.a. These two components are shown in fig 2.18.b as (I) and (II). It will be seen then if (I) and (II) are combined algebraically, the result will be the initial voltage distribution in fig.2.18.a. the lower curve (II) in the condition of the transient oscillation, at the begining of the readjustment period (after the initial period), which takes place above and below the component (I) as the axis of oscillation. As curve (II) represents a distribution of voltages, with no currents anywhere, it follows that at this instant the oscillation is at its maximum voltage zero-current phase. Hence, when (II) is resolved into its harmonics, these are the natural modes of oscillation characteristic of the particular winding. This method is an unsatisfactory method for the voltage to be predicted accurately.

Rudenberg[42] used the travelling wave theory. In his work, the effect of the mutual inductances between the elements was taken into consideration by increasing the self inductance of the element itself. Capacitances to ground of elements and capacitances between elements were also taken into consideration. Thus the follwing differential equations can be developed

$$-\frac{\delta i}{\delta x} = C\frac{\delta e}{\delta t} - K w^2 \frac{\delta^3 e}{\delta t\, \delta x^2} \qquad \ldots(2.20)$$

$$-\frac{\delta e}{\delta x} = L\frac{\delta i}{\delta t} \qquad \ldots(2.21)$$

where

i is the mean current within the element

e is the mean voltage of the element

C is the capacitance to ground of each element per unit length

K is the capacitance between any two elements per unit length

w is the wire length of the element

L is the total self inductance of the winding per unit length

The element itself could be a turn in a cylindrical single layer coil, a layer in a coil made up of several layers or a coil in a winding

consisting of several coils.

Equations (2.20) and (2.21) are valid to a good degree of approximation if the number of elements is relatively large. Furthermore, it should be noted that the term with K in equation (2.20) forms the sole difference in comparison with the well known differential equations of smooth transmission lines.

If we eliminate the current i from equations (2.20) and (2.21), we get

$$\frac{\delta^2 e}{\delta x^2} - L\,C\,\frac{\delta^2 e}{\delta t^2} + L\,K\,w^2\,\frac{\delta^4 e}{\delta t^2\,\delta x^2} = 0 \qquad \ldots(2.22)$$

The simplest solution for the above equation is

$$e = E \exp j\,(\,\omega t + \alpha x\,) \qquad \ldots(2.23)$$

according to which a voltage with maximum amplitude E oscillates sinusoidally in time and also in space along the extension x of the conductor. ω is the angular frequency in 2π seconds, and α is the wave density along the wire of the coil expressed as the number of wavelengths in 2π cm of wire.

Instead of equation (2.23), which represents standing waves within the coil, another solution which represents travelling waves within the coil is given by

$$e = E \exp j\,(\,\omega t - x/v\,) \qquad \ldots(2.24)$$

according to which such waves oscillate in time with the frequency ω, but propagate along the coil with a velocity v given by

$$v = \left(\,\frac{1}{C\,L} - \frac{K}{C}\,w^2\omega^2\,\right)^{1/2} \qquad \ldots(2.25)$$

As it can be seen, as the frequency ω increases, the velocity of propagation decreases and becomes zero at a certain value of the frequency known as the "critical frequency" given by

$$\omega_c = \frac{1}{\omega\sqrt{K\,L}} \qquad \ldots(2.26)$$

For subcritical frequencies we can have either travelling waves with velocities given by (2.25) with only waves with indeed very low frequencies travelling at almost the velocity of light $v_0 = \frac{1}{\sqrt{C\,L}}$ or standing waves

with wave density α. For frequencies above the critical frequency, known as supercritical frequencies, there no longer exist any standing or travelling waves within the winding, but only an exponential attenuation of the voltage from the terminals towards the interior.

Hence, when analysing impulse wave which consists of a continuous spectrum of frequencies, the voltage at time t and at any point inside the winding will be the sum of voltages of different travelling waves (or standing waves) of subcritical frequencies and the voltages obtained by exponential attenuation for subcritical frequencies. This technique is not very accurate because the effect of mutual coupling is approximated by modifying the self inductance and moreover it is not applicable when the number of elements is small.

In the work done by Lewis[43], the transformer winding is represented as a ladder type network subdivided into a finite number of sections with uniformely distributed capacitances and inductances. A step unit function voltage is applied to the ladder type network. His method was proved not to be very successful as it was found that capacitance and inductance distributions are not uniform and the application of a step unit function voltage is far from the practical surge waveform. In Lewis's work, the coil was the basic unit of the model and hence no attempt was made to analyse voltage distribution inside the coil itself. This method was the begining of the equivalent circuit technique which was improved with the use of modern computing facilities.

Dent and Hartill[44] modified Lewis's model by taking into account any non-uniformities existing in the winding. Furthermore, their equivalent circuit allows for the correct representation of all the winding parameters, i.e, individual self-inductance of each section, mutual inductances with other sections, ground capacitance of each section, series capacitance to adjacent sections and series capacitance between turns. Winding losses are neglected. Moreover, a standard impulse wave is used

instead of a unit step function and the effect caused by the chopped wave can also be represented simply by employing a negative wave which is delayed for a certain time equal to the chop time in order to cancel the positive wave. The general ladder network used by Dent and Hartill[44] is shown in fig 2.19. The way of solving the network is based on mesh current analysis. Mesh currents i_0, i_k, i'_k, are defined as shown in fig 2.19, where i_0 is the current through the voltage source, i_k is the current in the lower mesh of division k and i'_k is the current in the upper mesh of division k. Hence, for each section, two differential equations can be set up, one for the upper mesh and the other for the lower mesh. If the network has n divisions, there are altogether 2n simultaneous equations which can be integrated by runge-cutta method. The analysis of transformer surge distribution using this method can be laid out systematically and is very suitable for computer programming.

Krondl and Schleich[45] used kirchoff's current law in order to obtain the integro-differential equations of the transient voltages in transformer windings. As nodes they regarded those winding section ends or terminals which are connected together operationally. Connected to those nodes are the equivalent distributed ground and series capacitances of the winding, the conductances (representing the damping effect due to iron, copper, dielectric losses and ohmic resistance of the winding) and the inductances (representing the electromagnetic couplings between the sections of the winding). Consequently and as it can be seen from fig 2.20, the node currents consist of capacitive, ohmic and inductive currents. According to kirchoff's current law, we have

$$[I] = [I_C] + [I_R] + [I_L] = [0] \qquad \ldots(2.27)$$

Calculating the three components of the node currents, equation (2.27) becomes

$$[I] = \left(p\,[C] + [G] + \frac{1}{p}\,[H] \right) [U] = [0] \qquad \ldots(2.28)$$

where

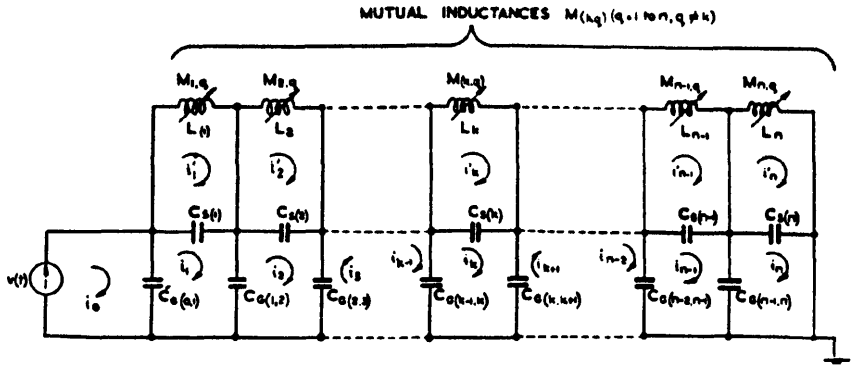

Fig 2.19 General equivalent circuit of a transformer winding divided into n sections[44]

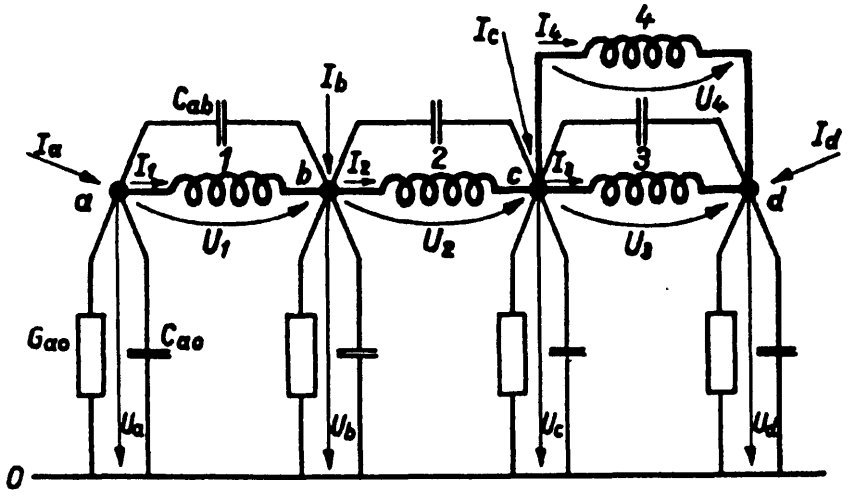

Fig 2.20 Magnetically linked windings with equivalent winding capacitances and damping conductances[45]

[C] is the capacitance matrix (according to the connection diagram)

[G] is the damping conductances matrix

[H] is the matrix of the inverse winding inductances

$p = j\,\omega$

The above equation (2.28) describes the dynamical behaviour of the transformer.

An additional equation for the impulse generator is required in order to determine the transient process during an impulse test. Hence, the following equation is obtained by Krondl and schleich[45]

$$[I] = \left(p\,[C] + [G] + \frac{1}{p}\,[H] \right) [U] - p\,C_{s0}\,U_{s0} = [0] \qquad \ldots(2.29)$$

where $C_{s0}\ U_{s0}$ is the initial condition representing the charge of the impulse generator C_{s0} at the moment of breakdown (t = 0).

The methods used for solving the integro-differential equation (2.29) which describes the transient voltages are

- Measurements on the equivalent circuit
- Computation using an electronic analogue computer
- Calculation using an electronic digital computer
- Calculation using a digital differential analyser

Dugan et al[46] used kirchoff's current law as well in order to obtain the different nodes transient voltages in transformer windings. The transformer model is shown in fig 2.21.a[46]. It consists of a number of tightly-coupled inductors with the capacitor network superimposed. Resistances are added in parallel with each inductor to represent losses since it is thought that impulses are influenced more by eddy current phenomena than by skin-effect phenomena.

The solution for the above described model was obtained by writing a RLC program for a PC (personel computer) environment rather than using general-purpose electromagnetic transient programs. The circuit of fig 2.21.a was separated into parallel subnetworks of resistance, inductance and capacitance with the corresponding matrices fed into the RLC program in

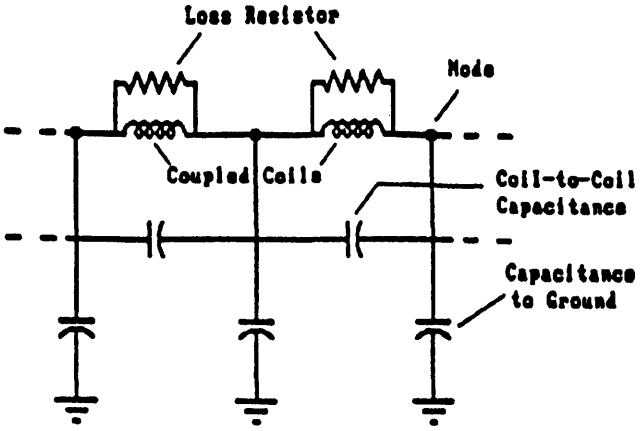

a)

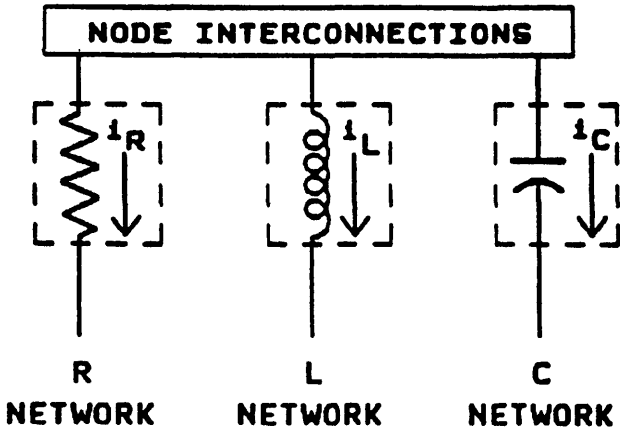

b)

Fig 2.21 a) Basic transformer model for simple series connected-coils[46]
b) Simplified one-line diagram of the circuit solved by the RLC program[46]

nodal admittance form where they are combined essentially simply by adding (hence, the parallel representation shown in fig 2.21.b[46]). The solution of the circuit was obtained by using the trapezoidal rule in order to discretize the differential equations representing the kirchoff constraint

$$[I_C] + [I_R] + [I_L] = [0] \qquad \ldots(2.30)$$

over a number of time steps. In other words, the complete solution was obtained by computing all node voltages at the end of each time step.
The wave applied to the model is a unit step wave and calculations of transient voltages at crossovers compared well with measurements. However, this model was only applicable to layer windings and , moreover, two or three coils were lumped into one element in the equivalent circuit thus further limiting its accuracy to a specified frequency range.

Fergestad and Henriksen[47] used the state-space approach in order to calculate voltage oscillations in transformer windings when subjected to impulses. The proposed equivalent network for multi-windings transformers consists of a number of sections, each containing lumped inductance, series and ground capacitance and loss resistances as shown in fig 2.22. The inductive elements are all mutually coupled to each other.
The differential equations for the equivalent network are formulated in matrix form as follows

$$\dot{[X(t)]} = [A][X(t)] + [B]\, v(t) \qquad (2.31)$$

$$[U(t)] = [S][X(t)] + [D]\, v(t) \qquad (2.32)$$

where

X(t) is the state vector

U(t) is the output vector of node voltages

v(t) is the applied impulse voltage (scalar)

A, S are matrices of constant coefficients

B, D are coulomn matrices of constant coefficients

The input voltage is assumed to be standard full wave which is given by

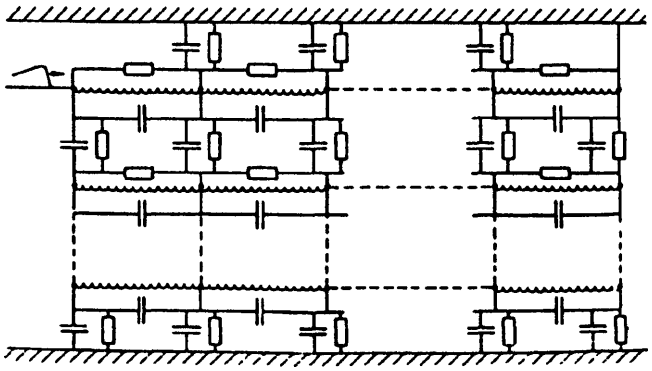

Fig 2.22 Equivalent circuit of multi-winding transformer[47]

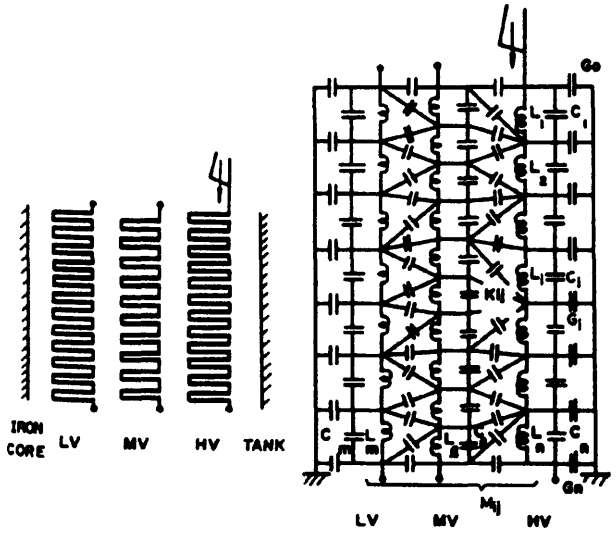

Fig 2.23 Equivalent circuit of multi-winding transformer[48]

$$v(t) = v_0 \left(\exp(-\beta t) - \exp(-\delta t) \right) \qquad (2.33)$$

It was found that the best method for solving equation (2.31) is based on eigenvalues and eigenvectors. Networks with up to 60 nodes have been handled successfully. The calculated maximum values and frequencies of impulse voltage responses lie in general within 10% of the measurements.

Miki, Hosaya and Okuyama[48] carried out a detailed and more precise calculation for impulse voltage distribution in transformer windings. An equivalent network for multi-windings transformers was proposed in order to calculate voltage distribution in impulsed winding and transferred voltage to non-impulsed windings. The inductance in the network represents one pair of disc coils and any node in the network was joined with any other node by a capacitance between windings as shown in fig 2.23[48].

Equations for a multi-winding equivalent network are obtained in matrix form as

$$[A]\, V(t) - [B][V] = [M] \frac{d}{dt} [I] \qquad \ldots(2.34)$$

$$[B]^t[I] = -[E] \frac{d}{dt} V(t) + [F] \frac{d}{dt} [V] \qquad \ldots(2.35)$$

where

[V] is the nodal voltage vector

[I] is the current vector through an inductance element

[A], [B] are the transformation matrices determined by network conditions

[M] is the inductance matrix

[E], [F] are the capacitance matrices

V(t) is the applied voltage

Eliminating [I] from (2.34) and (2.35), we obtain

$$\frac{d^2}{dt^2} [V] = \left([P] \frac{d^2}{dt^2} + [Q] \right) V(t) - [R][V] \qquad \ldots(2.36)$$

Where

$$[P] = [F]^{-1}[E]$$

$$[Q] = [F]^{-1}[B]^t[M]^{-1}[A]$$

$$[R] = [F]^{-1}[B]^t[M]^{-1}[B]$$

Equation (2.36) was solved using Milne's method which is an iterative technique based on numerical integration method. The calculated peak values of impulse voltage responses in various types of transformers were found to agree with the measured ones within ± 15%.

Burrage, Veverka and McConell[13] adopted a test program[49] to evaluate key apparatus and insulations which was specified as a result of an extensive litterature search[49] of steep front short duration sources, their characteristics and effect on power system equipment. They used such a program in order to study the low voltage SFSD impulse response of conventional oil insulated shell form and core form distribution transformers. They proposed that from the test data on the transformers, it is possible to calculate the projected winding voltage distribution based on the magnitude of the incident wave which the overvoltage protective device will pass to the transformer winding. This in turn can be used to forecast the maximum allowable incoming voltage transient that can enter the winding with the expectation that the insulation system will survive.

2.3 DISCUSSION OF BACKGROUND WORK

From what it has been said so far, we can conclude that when investigating the nature of the very fast front transients impinging on transformer windings as a result of switching operations in GIS and consequently the way they distribute themselves inside the windings (overstressing the insulation), the formulation of the problem should always be based on the fact that GIS and transformers interact.

1) There is no use examining the generation and propagation of GIS created surges and most importantly their characteristics unless the transformer winding is adequately represented. Such adequate representation of the transformer winding has not materialised whenever the transformer was included in the studies. Transformers were represented by lumped capacitances[38], or, lumped elements[39] by admitting that lumped capacitance representation is inadequate for very fast transients but with

no mention whatsoever made about the nature of such lumped elements.

A better idea of transformer representation was advocated by Konig[50] who acknowledged that the interaction of a transformer with the grid can be more or less easily described with the help of transformers equivalent circuits with different resonnant frequencies and based on modal analysis. However his representation only dealt with frequencies up to few hundreds of KHz. Hence, as the steep fronted surges created by disconnector operations in GIS include frequencies up to 100 MHz, such equivalent circuits, in our mind, would include a large number of resonnant branches and, consequently, the best way forward is to represent the transformer through its input impedance which is frequency sensitive and which will have different values over all the frequency spectrum of the studies.

It should be stressed again that transformers could not be ignored when studying the nature of the fast fronted surges, especially the transformer windings could have a flattening effect[51] on the fast front itself and of course would play a prominent part on the oscillations of the overvoltages. However, representing the transformer by its input impedance would not lead to the prediction of the stresses inside the winding when the fast fronted surge impinges on its terminals. Consequently, the transformer winding could be represented by an equivalent circuit with distributed parameters using modal analysis and as a part of the whole circuit including all components of GIS and connected equipment. This would lead to an accurate prediction of the surges impinging on the transformer terminals and the way they distribute themselves inside the winding.

More, due to the very short rise time of such surges which is comparable with the transient time of many GIS components and connected equipment, most components must be accurately represented as distributed parameters. For instance, bushings are modelled using concentric transmission line models[5] which clearly predicted the effect of such bushings on the fast front of the transients. In fact, it was demonstrated

that a lumped[5] capacitance representation of the bushing gave erroneous result as it dramatically increased the risetime of the front. Unfortunately, the capacitance representation of the bushing was used[3] during some investigations of very fast transients in GIS.

2) With relation to the distribution of fast fronted surges inside transformer windings, the standing wave theory is unsatisfactory for the voltages to be predicted accurately. Similarly, the travelling wave technique was applied to transformers with uniformely distributed capacitances and inductances and again it is not very accurate since the effect of mutual coupling is approximated by modifying the self inductance and, moreover, such technique is not applicable when the number of elements is small. Both techniques did not represent satisfactorily the magnetic circuit and no mention whatsoever was made on the difference a lightning surge would have on the magnetic core in comparison with the switching surge. The mathematical model advocated by Dent and Hartill[44] is a good technique to evaluate surge voltage distribution since it involves all parameters and non uniformities and uses a standard impulse voltage instead of a unit step function.

It should be strongly emphasised that all above mentioned work was in relation with lightning waves reaching the transformer. This, of course, would be totaly inaccurate to predict the response of transformer windings when GIS (disconnector) created surges which have fast fronts with risetimes of about 20 nsec (compared with 1.2 μsec for the lightning wave) impinge on the transformer terminals. Therefore, due to the fact that the travel time of such fast fronted surges through the coils of the transformer windings is comparable to the risetime of the front itself, the transformer winding should be represented by a network of distributed capacitances and inductances by taking the turn itself as the basic element. Such network should be able to give accurate prediction for the interturn and intercoil voltages and therefore the stresses endured by the

insulation under GIS disconnector switching operations.

2.4 BRIEF EXPLANATION OF THE RESEARCH WORK

The purpose of the Ph.D research is to develop a computer model for the coils in the line-end region of transformer HV winding, in order to predict very fast fronted surge distribution and resulting interturn and intercoil voltages which could lead to insulation overstress and failure. The model is based on the the multiconductor transmission line theory[56] together with modal analysis and adopts the turn itself as the basic element. In this model, series propagation along the winding as well as capacitive links between the different turns, within the same coil and of different coils, are both taken into consideration, i.e. series and parallel propagation are due to take place simultaneously. The model will be validated by experimental measurements taken on the transformer HV winding which already exists in the HV laboratory.

It should be noted that such theory has already been applied to a.c.machine windings[52,53,54,55] and was successful in predicting the interturn voltages within the coils.

Such a computer model of the transformer winding could be implemented in future computational studies of the nature of the GIS fast fronted surges, in which the transformer has to be adequately represented as explained above. At the same time, insulation stresses inside the transformer itself would be obtained.

CHAPTER 3

COMPUTER MODEL

The following sections describe the most important steps included in the development of the computer model for the transformer winding, which is used to carry out the computational studies. Such a computer model is based on multiconductor transmission line theory[56] together with modal analysis. An illustration of the application of the multiconductor transmission line theory to a.c.machine windings[53,54,55] is also provided.

The first section deals with the mathematical representation of the terminal coils taken on a turn by turn basis. It explains the multiconductor transmission line theory[56] together with the modal analysis (including two-port network equations), which form the basis of the multiconductor transmission line model of the transformer winding. The model itself represents the whole coil under study as a two-port network with the individual turn as the basic element.

Before proceeding into transformer windings, The second section briefly explains how the multiconductor transmission line theory was applied to a.c. machine windings[53,54,55] in order to predict the interturn voltages within the individual coils and consequently the insulation stresses.

The third section deals with the application of the multiconductor transmission line theory to transformer windings by explaining the concepts of single-section and multiple-section models of the coil and illustrates a technique to solve the two-port network equations of the model itself. This section also describes the types of transformer windings on which the computational studies were carried out. By considering each type of winding at once, it deals with the calculation of its parameters by showing the equivalent circuit of the coil model itself and describing the procedure used to calculate its admittance and impedance matrices.

Finally, before proceeding to our computational studies, the excitation functions used in such studies are given.

3.1 MULTICONDUCTOR TRANSMISSION LINE THEORY[58]

Consider an homogeneous transmission line containing n conductors. At a distance x from one end of the line and due to current i_j flowing in the j^{th} conductor, the voltage developed in length Δx of the k^{th} conductor (where k goes from 1 to n to include all conductors) is given by :

$$\Delta v_k = -\sum z_{kj}\, i_j\, \Delta x$$

where z_{kj} is the mutual impedance per unit length of the k^{th} conductor for current in the j^{th} conductor. Similarly, with the application of potential v_j to the j^{th} conductor, a displacement current in length Δx of the k^{th} conductor does occur and is given by :

$$\Delta i_k = \left(-y_{kk}\, v_k + \sum_{j=1\neq k}^{n} y_{kj}\, v_j \right) \Delta x$$

where y_{kk} is the self admittance per unit length of the k^{th} conductor and y_{kj} is the mutual admittance per unit length of the k^{th} conductor for a voltage applied to the j^{th} conductor. Dividing Δv_k and Δi_k each by Δx and for $\Delta x \to 0$, the following set of differential equations (in matrix form) is appropriate

$$\frac{d}{dx}[V] = -[Z][I] \qquad \ldots(3.1)$$

$$\frac{d}{dx}[I] = -[Y][V] \qquad \ldots(3.2)$$

where :

[Z] is the series impedance matrix per unit length

[Y] is the shunt admittance matrix per unit length

[V] is the voltage vector at point x

[I] is the current vector at point x

By differentiating equation (3.1) with respect to x and substituting $\frac{d}{dx}[I]$ (from equation (3.2)) in the resultant derivative, equation (3.1) becomes :

$$\frac{d^2}{dx^2}[V] = [Z][Y][V] = [\Psi]^2[V] \qquad \ldots(3.3)$$

In the same way equation (3.2) becomes :

$$\frac{d^2}{dx^2}[I] = [Y][Z][I] = [\Psi_t]^2[I] \qquad \ldots(3.4)$$

where $[\Psi] = ([Z][Y])^{1/2}$ is the propagation constant matrix and $[\Psi_t] = ([Z][Y])^{1/2}$ its transpose, since both [Z] and [Y] are symmetrical, but in general $[\Psi] \neq [\Psi_t]$.

The solutions to equations (3.3) and (3.4) are :

$$[V_x] = \exp(-[\Psi]x)[V_i] + \exp([\Psi]x)[V_r] \qquad \ldots(3.5)$$

$$[I_x] = \exp(-[\Psi_t]x)[I_i] + \exp([\Psi_t]x)[I_r] \qquad \ldots(3.6)$$

for a point at a distance x along the line.

Equations (3.5) and (3.6) may be interpreted on the basis of forward and reverse travelling waves. In practice, the suffixes i and r refer to incident and reflected values. $[V_i]$, $[V_r]$, $[I_i]$ and $[I_r]$ are vectors required to satisfy conditions at the boundaries.

By differentiating equation (3.5) with respect to x and substituting the derivative in equation (3.1), equation (3.6) can be rewritten in a more convenient form as :

$$[I_x] = [Y_0](\exp(-[\Psi]x)[V_i] - \exp([\Psi]x)[V_r]) \qquad \ldots(3.7)$$

where $[Y_0] = [Z]^{-1}[\Psi]$ is the characteristic admittance matrix

So a general solution to the multiconductor wave equation is given by equations (3.5) and (3.7).

For an homogeneous multiconductor line of length l, equations (3.5) and (3.7) can be combined as such that the general solution to the multiconductor wave equation has the form of two-port network equations, which is especially useful when terminal conditions in one end of the line are known. By putting x = 0 and x = l in equations (3.5) and (3.7) respectively, in order to satisfy conditions at the ports, we get :

$$[V_S] = [V_i] + [V_r] \qquad \ldots(3.8)$$

$$[V_R] = \exp(-[\Psi]l)[V_i] + \exp([\Psi]l)[V_r] \qquad \ldots(3.9)$$

$$[I_S] = [Y_0]([V_i] - [V_r]) \qquad \ldots(3.10)$$

$$[I_R] = [Y_0](\exp(-[\Psi]1)[V_i] - \exp([\Psi]1)[V_r]) \qquad \ldots(3.11)$$

where :

$[V_S]$ and $[I_S]$ are the voltage and current vectors at the sending end, respectively.

$[V_R]$ and $[I_R]$ are the voltage and current vectors at the receiving end, respectively. By finding the values of $[V_i]$ and $[V_r]$ in terms of $[V_S]$ and $[V_R]$ from equations (3.8) and (3.9) and subsequently substituting them in equations (3.10) and (3.11), we get the two-port network form of the general solution to the multiconductor wave equation , which is given by :

$$\begin{bmatrix} [I_S] \\ [I_R] \end{bmatrix} = \begin{bmatrix} [A] & -[B] \\ -[B] & [A] \end{bmatrix} \begin{bmatrix} [V_S] \\ [V_R] \end{bmatrix} \qquad \ldots(3.12)$$

where [A] and [B] are the two port-network parameters with :

$$[A] = [Y_0]\coth([\Psi]1) \quad ; \quad [B] = [Y_0]\mathrm{cosech}([\Psi]1)$$

So far, the equations obtained were in terms of phase variables. By using the concept of natural modes of propagation which is of benefit very often in clearly understanding the nature of wave propagation on complex transmission systems and by taking $[\gamma]$ as the diagonal eigenvalue matrix of $[\Psi]$, we have :

$$[\Psi] = [Q][\gamma][Q]^{-1}$$

where [Q] is the modal transformation matrix which consists of the eigenvectors (coulomns) corresponding to the eigenvalues γ_k (k = 1,..,n) of $[\Psi]$. Furthermore, we have :

$$[V_m] = [Q]^{-1}[V]$$

where [V] and $[V_m]$ are the voltage matrices in the real (phase) domain and modal domain respectively.

As far as the two port-network equations given in equation (3.12) are concerned, they will remain the same but rewritten in modal form, i.e., :

$$\begin{bmatrix} [I_S] \\ [I_R] \end{bmatrix} = \begin{bmatrix} [A_m] & -[B_m] \\ -[B_m] & [A_m] \end{bmatrix} \begin{bmatrix} [V_S] \\ [V_R] \end{bmatrix} \quad \ldots(3.13)$$

with [A] and [B] defined in the modal domain respectively as :

$$[A_m] = [Y][Q][\gamma]^{-1}\coth([\gamma]l)[Q]^{-1}; \quad [B_m] = [Y][Q][\gamma]^{-1}\mathrm{cosech}([\gamma]l)[Q]^{-1}$$

It is clear from above equations that given the impedance and admittance matrices for any multiconductor transmission line section, the $[A_m]$ and $[B_m]$ matrices can be easily calculated and therefore, the terminal conditions of such a section are given by equation (3.13).

3.2 APPLICATION OF MULTICONDUCTOR TRANSMISSION LINE THEORY TO MOTOR WINDINGS

The multiconductor transmission line theory[56] together with the modal analysis (including two-port network equations) has already been used[53,54,55] to develop a mathematical model for the line-end and adjacent coils for large a.c. motors under transient conditions. In doing so, the basic unit of the developed model was a single turn, which allowed the prediction of surge voltage distribution at the different turns inside the coil itself together with the interturn voltage distribution.

3.2.1 SINGLE COIL MODEL[54,55]

The multiconductor transmission line model for electric motor windings divide the coil into two distinct regions, namely, slot and overhang as shown in fig 3.1.a. Accordingly, each coil was divided into five sections which are treated separetely and interconnected as shown in fig 3.1.b.

The turns of each coil section are taken as a multiconductor transmission line in that all turns (all of the same length) run in parallel for one turn. More, each turn is closely coupled to its neighbours. Each coil section was modelled as a two-port network, with the parameters $[A_m]$ and $[B_m]$ of equation (3.13) derived from the electrical characteristics and parameters of the individual turns within that section and the region they are passing through (slot or overhang).

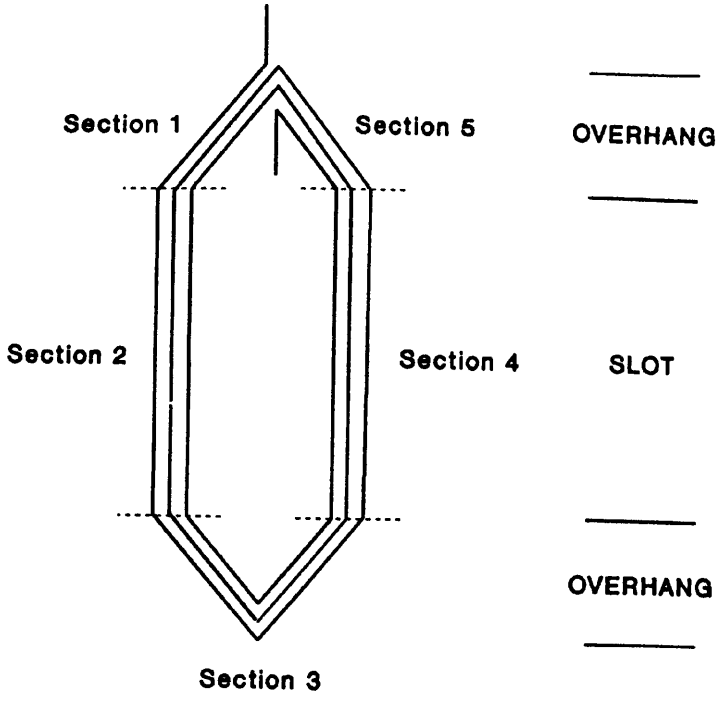

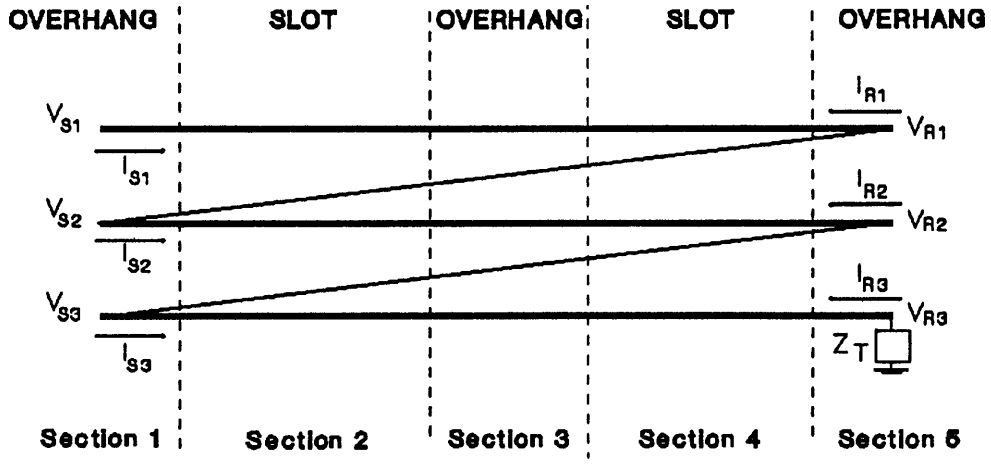

Fig 3.1 a) Sectionalised three-turn coil
b) Single-coil model

By cascade two-port netwok theory, the five two-port representations of the five coil sections connected in cascade were resolved into a single two-port network representation of the coil with constants [A'],[B'],[C']and [D']. Using these constants in equation (3.13), the multiconductor transmission line representation of the coil is obtained.

By applying the modified equation (3.13) to the three turn coil of fig 3.1.a which is terminated by the termination impedance Z_T, the two port network equation for the coil can be obtained as

$$\begin{bmatrix} I_{S1} \\ I_{S2} \\ I_{S3} \\ I_{S4} \\ I_{S5} \\ I_{S6} \end{bmatrix} = \begin{bmatrix} [A'] & -[B'] \\ -[C'] & [D'] \end{bmatrix} \begin{bmatrix} V_{S1} \\ V_{S2} \\ V_{S3} \\ V_{S4} \\ V_{S5} \\ V_{S6} \end{bmatrix} \qquad \ldots(3.14)$$

From inspection of the boundary conditions of fig 3.1.a and by using matrix manipulation and simplification it is possible to arrange the equation to yield

$$\begin{bmatrix} I_{S1} \\ V_{S2} \\ V_{S3} \\ V_{S4} \end{bmatrix} \begin{bmatrix} Y \end{bmatrix} \begin{bmatrix} V_{S1} \\ 0 \\ 0 \\ 0 \end{bmatrix} \qquad \ldots(3.15)$$

From this, the termination voltages for the different turns were obtained by means of a simple multiplication of the excitation function V_{S1} and the first coulomn of matrix [Y].

3.2.2 MULTIPLE COIL MODEL[53,54]

In machine windings, the coils are arranged or distributed in the slots in such a way that the upper half of a slot would contain one section of the coil under study, say coil 1, whereas the lower half of the same slot would contain a section of another coil which could be eight coils electrically down the winding as shown in fig 3.2. Hence, there is no

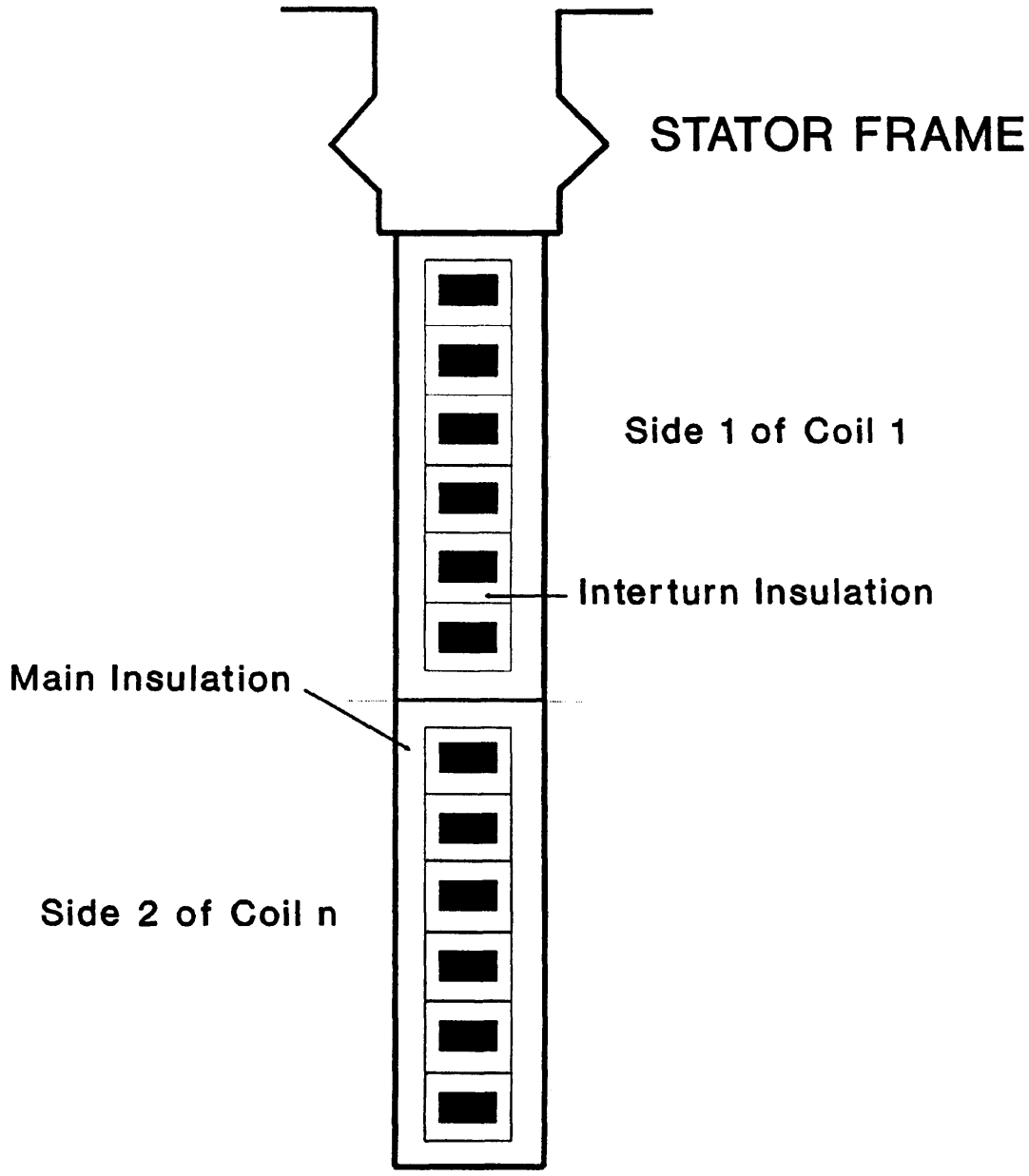

Fig 3.2 Stator slot of an a.c. machine containing different sides of non-consecutive coils

coupling between sections of two consecutive coils and moreover, the couplings between the sections of the different coils in the same slot are very weak. Consequently, each coil could be separated from the others due to the above reasons and the winding itself was considered to be a cascade connection of two-port networks (each corresponding to one coil).

As mentioned in the preceding section, the coil was terminated with a termination impedance which represents the characteristic impedance of the remaining series connected coils. However, although this approach led to certain simplifications in the analysis, there was some doubt as to wether the correct value of the termination impedance had been chosen and if not, the effect that an incorrect value would have had on the turn voltages. This doubt was overcome by including the second coil (after the line-end coil) in the analysis and terminated with the impedance Z_T. By doing so, the turn and interturn voltages of the second coil were obtained together with its input admittance Y_{inp} given by the matrix element Y_{11} in equation (3.15). Susequently the line-end coil was terminated by the input admittance Y_{inp} of the second coil, which would give more accurate results than the single coil model. The accuracy of the model itself could be further improved by repeating the above procedure with a recursive algorithm to include the third, fourth and other coils in the winding.

3.1.3 CALCULATION OF COIL PARAMETERS[52,54,55]

In order to calculate the volatge distribution by means of the technique mentioned above, it was necessary to determine the electrical parameters of the coil sections.

The capacitance matrices were calculated by approximating the sides of the turns to parallel plate capacitors. The values of the capacitive elements were calculated from the coil dimensions and the relative permittivity for the interturn and main insulation.

The inductance matrices were obtained by assuming that the magnetic flux did not penetrate the iron laminations at all and that the iron acts

as a boundary within which the flux is constrained. By using the fact that, for a multiconductor transmission line in an homogeneous medium, the wave velocity is constant, the inductance matrix was calculated from the capacitance matrix by

$$[L1] = \frac{\varepsilon_r}{v_0^2} [C]^{-1} \qquad \ldots(3.16)$$

where

v_0 is the velocity of light in free space

ε_r is the relative permittivity of the insulation

The resistance matrices were calculated in a similar manner to that used for overhead transmission lines, as the sum of losses in the forward and return paths. It was assumed that the losses in the return path are equal to those in forward path since no technique was available to calculate the resistance of the return path.

The accuracy of the computer model was verified through comparaison of computational and experimental results. The experimental measurements were carried out on one section of a phase winding consisting of ten coils in series and located in the machine frame. The machine[54,55] is a 1640 Kw, 6.6 Kv induction motor. Steep fronted waves of approximately 350 nsec and 50 V crest were applied from a recurrent surge generator.

3.3 APPLICATION OF MULTICONDUCTOR TRANSMISSION LINE THEORY TO TRANSFORMER WINDINGS

Before preceeding further, it should be noted that the multiconductor transmission line theory[56] together with modal analysis has already been applied[69] to develop a mathematical model for the line-end disc and adjacent discs of the transformer winding. The aim was to predict turn to ground voltage distributions and interturn voltages due to very steep fronted surges with risetimes in the range 10-100 nsec impinging on the transformer HV winding, with the observation time being 0.5 μsec. Each turn was considered as a single conductor transmission line with three discs in

the line-end region represented as a single two-port network therefore taking into account the various interturn and interdisc couplings. The network was terminated by a single resistance which represented the remaining cascade-connected discs which were not included in the studies.

3.3.1. SINGLE-SECTION MODEL

The simplest computer model would be that of a single section of the HV winding, which in our case is a disc type winding. Each individual turn of the section is regarded as a single conductor transmission line of the same length l and is closely coupled to its neighbours. In other words, the turns of the section constitute a multiconductor transmission line of length l (mean length of the turn) with all the turns running in parallel for one turn. However, at the the end of each turn, the " end " of one turn becomes the " start " of the next turn as shown in fig 3.3. The computer model is a single two port-network representation of the section, on a turn by turn basis, with the $[A_m]$ and $[B_m]$ parameters of the two-port network derived from the electrical parameters of the section under study. The single-section model is a very simple representation as it only includes the couplings between the turns within the same section, with the other cascade-connected sections represented by a termination impedance Z_T, as shown in fig 3.3. As the transformer is a very complex structure with the sections of the winding connected in cascade having strong couplings between them especially consecutive ones and indeed, on a finer basis, between the turns of the different sections, the inclusion of a single section in the computer model would yield errouneous results as the couplings between the turns of this section and those of the remaining sections simply would not be included in the study. As a consequence, it is of the utmost importance to include more than one section in the model, which gives rise to the concept of multiple-section model.

3.3.2. MULTIPLE-SECTION MODEL

In the multiple-section model, all the sections included in the study

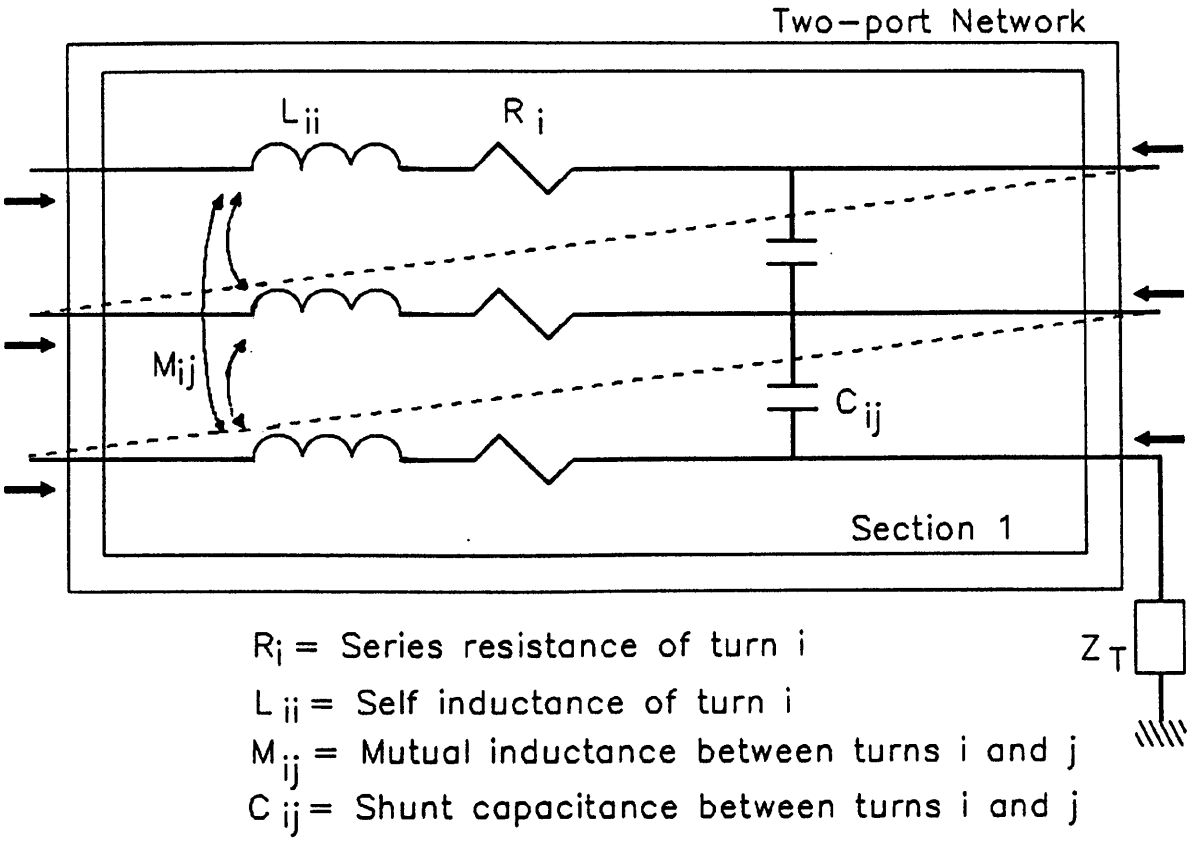

Fig 3.3 Single-section model

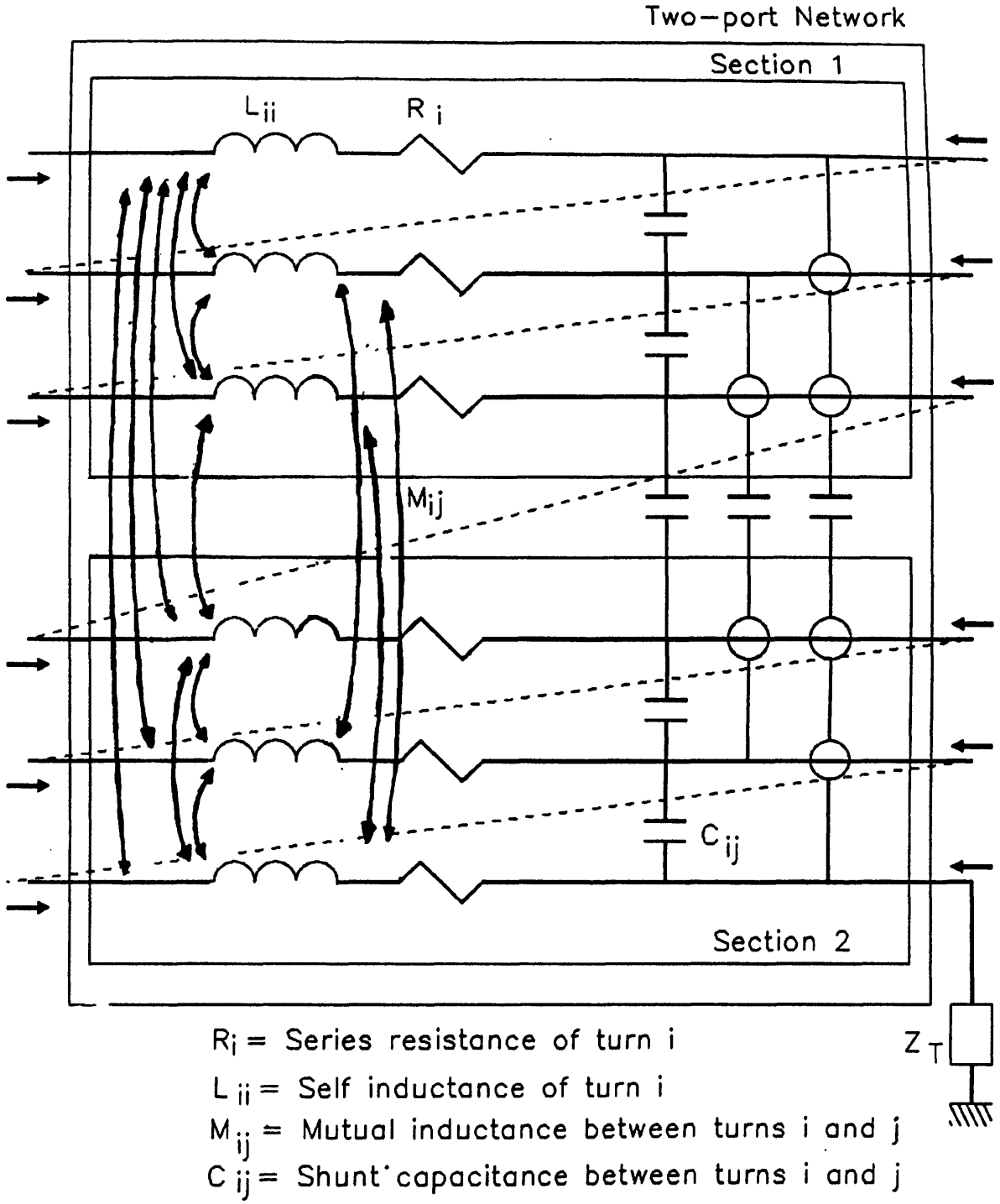

Fig 3.4 Double-section model

are taken to constitute one coil which is represented as a single two-port network on a turn by turn basis as shown in fig 3.4. The $[A_m]$ and $[B_m]$ parameters of the two-port network are derived from the electrical parameters of the coil under study. In this multiple-section model, the parameters will represent all the couplings between the turns within the same section as well as with the turns of other sections, as shown in fig 3.4. Again, the model is terminated by a termination impedance Z_T which is chosen to represent the characteristic impedance of the remaining cascade-connected sections, further down the winding and which have not been included in the model ,of the transformer winding.

The technique used to solve the model equations, given by equation (3.13) , is as follows :

As an example and for simplicity, let us consider the case of an eight turn coil (n = 8), constituted from two sections of the winding, as shown in fig 3.5 with the coil being terminated by an impedance Z_T.

Equation (3.13) can be written in detailed form as follows :

$$\begin{bmatrix} I_{S1} \\ I_{S2} \\ I_{S3} \\ I_{S4} \\ I_{S5} \\ I_{S6} \\ I_{S7} \\ I_{S8} \\ I_{R1} \\ I_{R2} \\ I_{R3} \\ I_{R4} \\ I_{R5} \\ I_{R6} \\ I_{R7} \\ I_{R8} \end{bmatrix} = \begin{bmatrix} & & & & & & & & & & & & & & & \\ & & & & & & & & & & & & & & & \\ & & & & & & & & & & & & & & & \\ & & & & & & & & & & & & & & & \\ & & & & & & & & & & & & & & & \\ & & & & & & & & & & & & & & & \\ & & & & & & & & & & & & & & & \\ & & & & & & & & & & & & & & & \\ & & & & & & & & & & & & & & & \\ & & & & & & & & & & & & & & & \\ & & & & & & & & & & & & & & & \\ & & & & & & & & & & & & & & & \\ & & & & & & & & & & & & & & & \\ & & & & & & & & & & & & & & & \\ & & & & & & & & & & & & & & & \\ & & & & & & & & & & & & & & & \end{bmatrix} \quad M \quad \begin{bmatrix} V_{S1} \\ V_{S2} \\ V_{S3} \\ V_{S4} \\ V_{S5} \\ V_{S6} \\ V_{S7} \\ V_{S8} \\ V_{R1} \\ V_{R2} \\ V_{R3} \\ V_{R4} \\ V_{R5} \\ V_{R6} \\ V_{R7} \\ V_{R8} \end{bmatrix} \quad .(3.16)$$

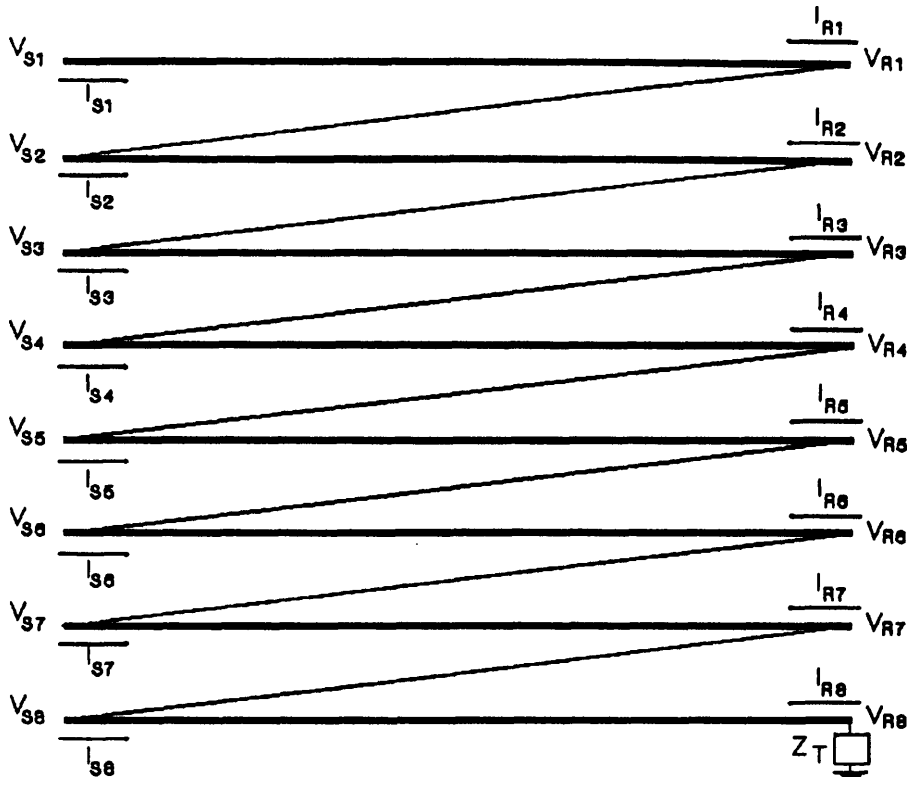

Fig 3.5 Double-section model of conventionally wound coil

where $[M] = \begin{bmatrix} [A_m] & -[B_m] \\ -[B_m] & [A_m] \end{bmatrix}$ from equation (3.13) and is of order (2n×2n).

It is evident from fig 3.5 the validity of the following equations :

$$V_{R1} = V_{S2} \quad \ldots(3.17)$$

$$V_{R2} = V_{S3} \quad \ldots(3.18)$$

$$V_{R3} = V_{S4} \quad \ldots(3.19)$$

$$V_{R4} = V_{S5} \quad \ldots(3.20)$$

$$V_{R5} = V_{S6} \quad \ldots(3.21)$$

$$V_{R6} = V_{S7} \quad \ldots(3.22)$$

$$V_{R7} = V_{S8} \quad \ldots(3.23)$$

$$I_{R1} = -I_{S2} \quad \ldots(3.24)$$

$$I_{R2} = -I_{S3} \quad \ldots(3.25)$$

$$I_{R3} = -I_{S4} \quad \ldots(3.26)$$

$$I_{R4} = -I_{S5} \quad \ldots(3.27)$$

$$I_{R5} = -I_{S6} \quad \ldots(3.28)$$

$$I_{R6} = -I_{S7} \quad \ldots(3.29)$$

$$I_{R7} = -I_{S8} \quad \ldots(3.30)$$

In order to simplify equation (3.16), equations (3.17) to (3.23) are substituted in equation (3.16). This is achieved by adding coulomns nine to two, ten to three, eleven to four, twelve to five, thirteen to six, fourteen to seven and fifteen to eight in order to give :

$$\begin{bmatrix} I_{S1} \\ I_{S2} \\ I_{S3} \\ I_{S4} \\ I_{S5} \\ I_{S6} \\ I_{S7} \\ I_{S8} \\ I_{R1} \\ I_{R2} \\ I_{R3} \\ I_{R4} \\ I_{R5} \\ I_{R6} \\ I_{R7} \\ I_{R8} \end{bmatrix} = \begin{bmatrix} & & \\ & M' & \\ & & \end{bmatrix} \begin{bmatrix} V_{S1} \\ V_{S2} \\ V_{S3} \\ V_{S4} \\ V_{S5} \\ V_{S6} \\ V_{S7} \\ V_{S8} \\ V_{R8} \end{bmatrix} \qquad \ldots(3.31)$$

The formulation given by equation (3.31) can be further simplified by the substitution of equations (3.24) to (3.30) in equation (3.31) itself. This is achieved by adding rows nine to two, ten to three, eleven to four, twelve to five, thirteen to six, fourteen to seven and fifteen to eight and by subsequently omitting rows nine to fifteen, whose information will have been by then redundant. Hence, the model equations will be reduced to

$$\begin{bmatrix} I_{S1} \\ 0 \\ 0 \\ 0 \\ 0 \\ 0 \\ 0 \\ 0 \\ I_{R8} \end{bmatrix} = \begin{bmatrix} & & \\ & M'' & \\ & & \end{bmatrix} \begin{bmatrix} V_{S1} \\ V_{S2} \\ V_{S3} \\ V_{S4} \\ V_{S5} \\ V_{S6} \\ V_{S7} \\ V_{S8} \\ V_{R8} \end{bmatrix} \qquad \ldots(3.32)$$

with given terminal conditions at the receiving end, the receiving end current is :

$$I_{R8} = \frac{-V_{R8}}{Z_T} \qquad \ldots(3.33)$$

and by adding the above quantity to row nine of equation (3.32), we obtain

$$\begin{bmatrix} I_{S1} \\ 0 \\ 0 \\ 0 \\ 0 \\ 0 \\ 0 \\ 0 \\ 0 \end{bmatrix} = \begin{bmatrix} & & & & & & & & \\ & & & & & & & & \\ & & & & & & & & \\ & & & & & & & & \\ & & & & N & & & & \\ & & & & & & & & \\ & & & & & & & & \\ & & & & & & & & \\ & & & & & & & & \end{bmatrix} \begin{bmatrix} V_{S1} \\ V_{S2} \\ V_{S3} \\ V_{S4} \\ V_{S5} \\ V_{S6} \\ V_{S7} \\ V_{S8} \\ V_{R8} \end{bmatrix} \qquad \ldots(3.34)$$

where [N] is the same matrix as [M''] but with

$$N(9,9) = M''(9,9) + \frac{1}{Z_T}$$

V_{S1} is the input excitation function and is thus known. As a result, we are left with nine linear equations with nine unknowns. The technique which has been used in our calculations to solve the linear equations, given by equation (3.34), in order to obtain the voltages in the different turns of the coil is as follows :

Equation (3.34) can be expressed in the following form :

$$\begin{bmatrix} V_{S1} \\ V_{S2} \\ V_{S3} \\ V_{S4} \\ V_{S5} \\ V_{S6} \\ V_{S7} \\ V_{S8} \\ V_{R8} \end{bmatrix} = \begin{bmatrix} & & & & & & & & \\ & & & & & & & & \\ & & & & & & & & \\ & & & & & & & & \\ & & & & N & & & & \\ & & & & & & & & \\ & & & & & & & & \\ & & & & & & & & \\ & & & & & & & & \end{bmatrix}^{-1} \begin{bmatrix} I_{S1} \\ 0 \\ 0 \\ 0 \\ 0 \\ 0 \\ 0 \\ 0 \\ 0 \end{bmatrix} \qquad \ldots(3.35)$$

Since V_{S1} is known , whereas I_{S1} is not and by using partial inversion technique, equation (3.35) becomes :

$$\begin{bmatrix} I_{S1} \\ V_{S2} \\ V_{S3} \\ V_{S4} \\ V_{S5} \\ V_{S6} \\ V_{S7} \\ V_{S8} \\ V_{R8} \end{bmatrix} = \begin{bmatrix} & & & & & & & & \\ & & & & D & & & & \\ & & & & & & & & \end{bmatrix} \begin{bmatrix} V_{S1} \\ 0 \\ 0 \\ 0 \\ 0 \\ 0 \\ 0 \\ 0 \\ 0 \end{bmatrix} \qquad \ldots(3.36)$$

where [D] is the resulting matrix from the partial inversion of matrix $[N]^{-1}$. [D] is of order (n+1)x(n+1)

As it can be seen, the final formulation (equation (3.36)) enables us to calculate the terminal voltages for the different turns of the coil by direct multiplication of the corresponding element in the first coulomn of matrix [D] by V_{S1}, or in other words

$$V_{Sj} = D(j,1).V_{S1} \qquad \ldots(3.37)$$

It is worthwhile to mention here the concept of coil admittance. Element D(1,1) in equation (3.36) is no other than the input admittance to the whole section under study since $I_{S1} = D(1,1).V_{S1}$ or $I_{S1} = Y_{inp}.V_{S1}$. Consequently, the whole section can be represented by a single element ,which is very useful since this element was repeatedly calculated in order to obtain the best possible value of Z_T.

As mentioned earlier, in order to calculate two-port network parameters $[A_m]$ and $[B_m]$ of the coil model, the admittance and impedance matrices of the coil itself must be calculated.

3.3.3 CALCUATION OF COIL PARAMETERS

The first type of transformer winding used to carry out our computational studies is a conventional disc type winding, as shown in fig 3.6.a, in which consecutive turns are wound radially one over the other to form a disc. In the other type, namely ,interleaved disc type winding, turns which are electrically further down in the winding are interleaved

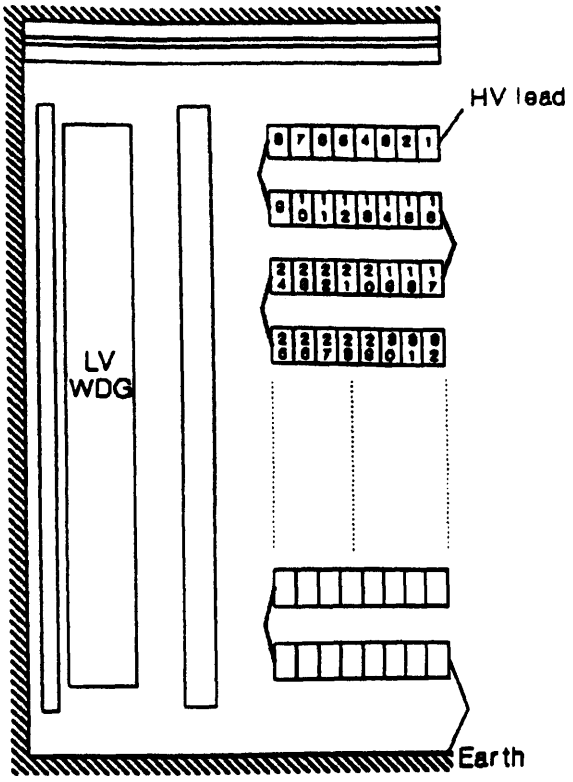

(a)

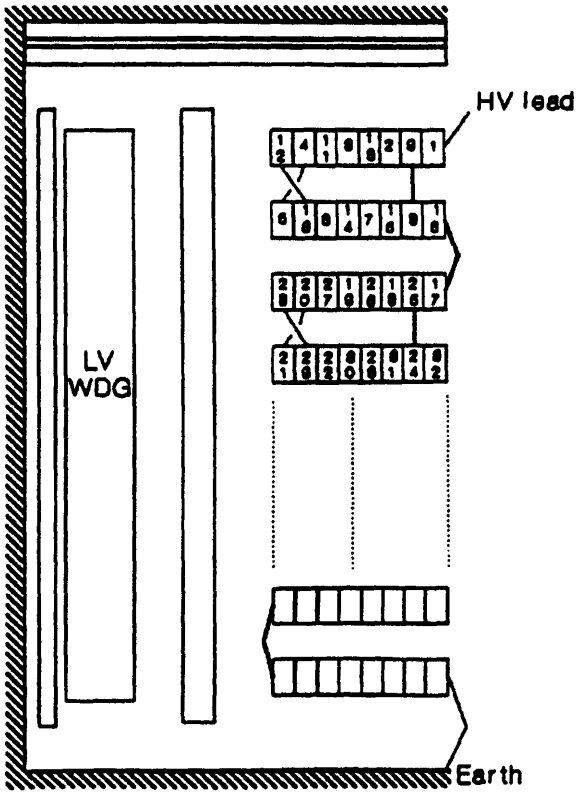

(b)

Fig 3.6 One phase of a transformer winding illustrating LV winding and

a) HV conventional disc winding

b) HV interleaved disc winding

between consecutive turns (fig 3.6.b). It should be noticed, however, that a single coil could be made of cascade connections of single section discs in the case of conventional winding whereas in the interleaved (sometimes known as transposed) winding a single coil is made of cascade connections of double-section discs.

In order to apply the mathematical model developed in the first section to transformer coils, it is necessary calculate the electrical parameters of such a coil. This will be carried out for each type of transformer winding mentioned above.

3.3.3.1 CONVENTIONAL DISC TYPE WINDING

The high voltage conventional disc type winding actually exists in the HV laboratory and is placed in open air. The HV winding is shown in fig 3.6.a which is a half section through one phase of a typical 3-phase core type transformer with a low voltage winding adjacent to the core. In our transformer in the HV lab, only one phase was built. Moreover, a close examination of the HV winding revealed that each disc consisted of eight turns wound by using two conductors in parallel. The electrical characteristics of the HV winding (used in the studies) are given in appendix A.

The whole coil under study is represented as a single two-port network on a turn by turn basis as stated in the first section. Considering the coil turns as a collection of multiconductor transmission lines, the equivalent model of the coil model is shown in fig 3.4 in which all parameters included in the study are illustrated (all parameters are on per unit length basis).

Losses can be divided into two categories :

a) Copper losses in the coil turns, which are visualised as resistances in series with each multiconductor transmission line (turn).

b) Dielectric losses in the insulation, which are represented by very low conductance shunt elements connected between turns and earth.

In our analysis, however, the dielectric losses were omitted because of lack of information about the loss tangent for the insulation materials , and more important, according to Mcleay[52], this omission (of dielectric losses) had a negligible effect on the computed results (error less than 1%).

In order to mathematically represent a coil, the admittance and impedance matrices have to be found.

3.3.3.1.1 ADMITTANCE MATRIX

The general equation which defines the admittance matrix for multiconductor transmission lines is :

$$[Y] = [G] + j\omega[C] \qquad ...(3.38)$$

where :

[G] is the conductance matrix

[C] is the capacitance matrix

ω is the frequency

As mentioned earlier, the dielectric losses were omitted from the calculations, and as a consequence, the conductance matrix was not included in the study. Hence, the admittance matrix was calculated by means of the following equation :

$$[Y] = j\omega[C] \qquad ...(3.39)$$

From the above equation, it is clear that in order to calculate [Y], [C] must be first obtained. This could be achieved by a close examination of the transformer coils. For simplicity, let us consider an eight turn coil consisting of two 4-turn discs and terminated by an impedance Z_T (with LV winding short-circuited and at earth potential,as it has been throughout the computational studies). Each element of the capacitance matrix [C] can be accurately determined by well known methods of field analysis or by using the several formulae given in appendix B. However , in our study and for simplicity of the computer model, the different elements of the capacitance matrix were calculated by considering that the walls of

the different turns formed the plane surfaces of parallel plate capacitors which do exist axially and radially between the neighbouring turns. Fig 3.7 shows the detailed capacitance equivalent circuit for the coil under analysis where CIT is the interturn capacitance, CS is the capacitance of the interdisc paper-insulation per turn and CID is the capacitance of the interdisc air-insulation per turn, CDL is the ground capacitance to core per disc, CDR is the ground capacitance to tank per disc, CT is the capacitance to ground of each turn of the top disc and CB is the capacitance to ground of each turn of the bottom disc (all capacitances are per unit length).

The values for the different capacitances were calculated by means of the basic formula :

$$C = \frac{\varepsilon_0 \varepsilon_r A}{D} \quad [57] \qquad \ldots(3.40)$$

where :

ε_0 is the permittivity of the free space

ε_r is the relative permittivity of the insulating material

A is the area normal to the electric field

D is the thickness of the insulation

The values of the capacitances CS, CID and CIT were obtained by a direct application of the above formula.

The value for capacitance CDL was obtained by assuming that the inside of the winding and the core form a cylindrical capacitor[57] or by using the above formula on a turn basis. However, due to the fact that the disc edge is thin and the separation to the core is relatively large, the fringing effect is dominant[46] and the assumption that the edges of each disc extend half way into the barrier on either side of the disc would yield a good approximation to CDL as seen by the impulse phenomena[46]. In fact, due to the complexity of the transformer construction (due to the presence of wraps and ducts) between the HV and LV voltage winding (

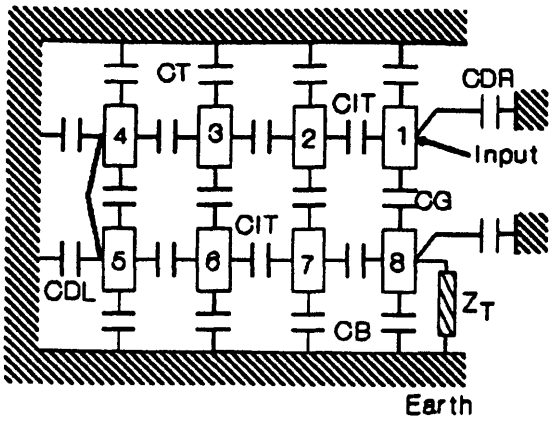

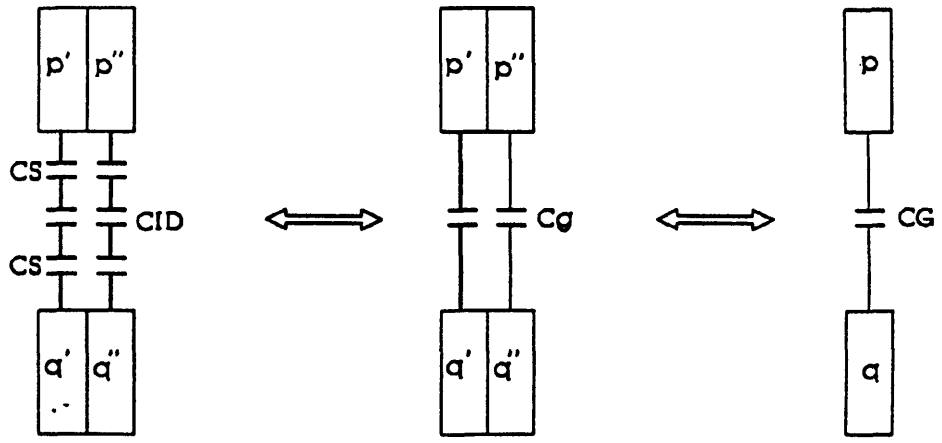

p & q are two axially adjacent turns made of two conductors in parallel

Fig 3.7 Capacitance equivalent circuit of a conventional coil

assumed to be at core potential , i.e ground potential), the calculation of CDL is itself a complex one.

The values of the capacitances obtained using the above procedures matched exactly those obtained by the formulae in appendix B[58].

The value of the capacitance CDR was found by using finite differences[58].

The value of the capacitance CT caused a lot of difficulties since it consisted of different components, namely, capacitance to core, tank and ground plane situated at a certain distance from the top of the line-end disc, all of which are dominated by fringing effects. However, the obtained approximated value was reasonable due to the close agreement between computed and experimental results.

CB was given a negligible value since the bottom disc of the model is too far from the transformer frame.

C_g is the interdisc capacitance per turn unit length and is given by :

$$C_g = \frac{CS.CID}{CS + 2.CID} \qquad \ldots(3.41)$$

The capacitance matrix [C] is then formed as follows :

For any turn "a" of the coil, C(a,a) is equal to the sum of the values of all equivalent capacitances connected to turn "a", while C(a,k) is the opposite value of the capacitance connected between turns "a" and "k" (it should be mentioned that all capacitances between non-neighbouring turns, both radially and axially, were neglected). The capacitance [C] is then formed by varying "a" to include all the turns of the coil. Since each turn in our transformer HV winding is made from two conductors in parallel, the interdisc capacitance per turn per unit length is actually twice the value of C_g (and it will be denoted as CG) with all the other capacitances retaining their original values. Subsequently, the admittance matrix [Y] is formed using equation (3.39).

From what has been explained so far, the capacitance matrix for a

conventional disc type coil consisting of two 4-turn discs is :

$$[C_c] = \begin{bmatrix} C_{11} & C_{12} & - & - & - & - & - & C_{18} \\ C_{21} & C_{22} & C_{23} & - & - & - & C_{27} & - \\ - & C_{32} & C_{33} & C_{34} & - & C_{36} & - & - \\ - & - & C_{43} & C_{44} & C_{45} & - & - & - \\ - & - & - & C_{54} & C_{55} & C_{56} & - & - \\ - & - & C_{63} & - & C_{65} & C_{66} & C_{67} & - \\ - & C_{72} & - & - & - & C_{76} & C_{77} & C_{78} \\ C_{81} & - & - & - & - & - & C_{87} & C_{88} \end{bmatrix}$$

The nul elements are in places of radial and axial non-neighbouring capacitances which have been neglected.

3.3.3.1.2. IMPEDANCE MATRIX

The general equation which defines the impedance matrix for multiconductor transmission lines is :

$$[Z] = [R] + j\omega[L] \qquad \ldots(3.42)$$

Where :

[R] is the resistance matrix

[L] is the inductance matrix

ω is the frequency

An accurate obtention of the impedance matrix is not an easy task due to the proximity of the iron core and the range of frequencies (0.5 MHz up to around 100 MHz) involved in the analysis. Hence, in order to construct the resistance and inductance matrices, some assumptions have been made.

As stated earlier, copper losses can be represented by the inclusion of resistances in series with multiconductor transmission line. Such losses are due mainly to the skin effect, though proximity effect[57] is another reason for the incurring of these losses.

According to Mcleay[52], a perfect evaluation of the proximity effect is almost impossible because such effect is frequency dependent, and more important, because the influence of adjacent conductors will depend on

conductor and insulation geometry. As a consequence, this effect was excluded from our studies.

From what preceded, the copper losses have been taken to be mainly due to skin effect caused by the conductor surge current. These losses can be easily calculated for each single frequency by using the resistance of the forward path of each turn (like in overhead transmission lines) which is given by[58]:

$$R_{fw} = \frac{h}{a\ S} \qquad \ldots(3.43)$$

With

$$S = \sqrt{\frac{2}{\omega\ \mu\ \sigma}} \qquad \ldots(3.44)$$

Where :

ω is the frequency

μ is the copper permeability

σ is the copper conductivity

h is the length of the turn

a is the cross-section of the turn

Since no technique is available to calculate the resistance of the return path, it has been assumed that the copper losses due to the forward and return pathes are the same. Accordingly, the total series resistance of the turn was taken as :

$$R_t = R_{fw} + R_{rt} = 2 * R_{fw} = \frac{2h}{aS} \qquad \ldots(3.45)$$

And hence the reistance matrix for the section is a diagonal matrix whose elments are given by equation (3.45).

An accurate calculation of the inductance matrix is possible by solving the magnetic field equation for the relevant range of frequencies. In their study, Mclaren and Oraee[53] describe how the PED2 finite-elements field package is used, which produces field distributions from which self and mutual inductances of the transmission line model (of the coil) can be calculated. However, such analysis is time consuming and the accuracy

requirements in our work do not require the usage of such package. Therefore, for the simplicity of the computer model, the inductance matrix was calculated from the capacitance matrix. However, in contrast to the a.c. machine windings where all the insulation is homogeneous leading to the electromagnetic waves travelling with a propagation velocity[52,53,54] which depends on the electrical characteristics of the insulation, the isulation in transformer windings is not homogeneous and hence equation (3.16) could not be used to obtain the inductance matrix for such windings. This is the case because, in transformers, the insulation between the turns (for instance, nomex) is different from the insulation between the coils themselves (for instance, air). Subsequently, Knowing that self and mutual inductances of a conductor array are invariant parameters of the dielectric permittivity, the inductance matrix for the computer model of the transformer was obtained from[61] :

$$[L^*] = \frac{1}{v_0^2} [C^*]^{-1} \qquad \ldots(3.46)$$

where :

v_0 is the velocity of light in the free space

$[C^*]$ is capacitance matrix with all insulation removed, i.e in air

However, at the very high frequencies included in the studies (0.5 MHz up to 100 MHz), the iron core acts as a barrier to magnetic flux (no flux penetrates in the iron core)[12,52,53,54] as the space constant for the flux has extremely low values[54,57] at such high frequencies. This effect is due to the presence of eddy currents in the core[60]. As a result the inductance, when calculated, should be that with an air core.

More importantly, experiments[62,63] on the inductance in transformers revealed that at high frequencies the inductance could indeed be lower than the air inductance itself. That was attributed to various losses[63] caused by unknown factors. The inductance decreased in exponential form[62] with the rapid decrease occuring in the frequency range up to 50 KHz. Hence, a

loss factor K_{loss} which is frequency dependent had to be included in the evaluation of the inductance[62].In fact, experimental measurements of the coil inductance in a.c. machine windings[55] up to 300 KHz confirmed the exponential trend mentioned above with the inductance converging to an asymptotic (almost constant) value towards the upper range of the frequency. Such asymptotic value (at 300 KHz) was almost 50% of the value of inductance in air (around 50 KHz[62]). Consequentlty, from what has preceded and since the coil in the transformer could be looked at as being within a slot of big dimensions, and due to the very high frequencies included in the studies, the loss factor K_{loss} was assumed to be constant with a value of 0.5. As a result, the inductance matrix for the transformer was calculated from :

$$[L1] = K_{loss} \left(\frac{1}{v_0^2} [C^*]^{-1} \right) = 0.5 \left(\frac{1}{v_0^2} [C^*]^{-1} \right) \qquad \ldots(3.47)$$

Where :

[L1] is the inductance matrix per unit of length

It is important not to forget that due to the skin effect at the very high frequencies included in our studies , an increase in the internal inductance of the turns do occur, which is given by :

$$[L2] = \frac{h}{a\ S} \qquad \ldots(3.48)$$

As a result, in our study, the impedance matrix of the coil was calculated from :

$$[Z] = [R_t] + j\omega([L1] + [L2]) \qquad \ldots(3.49)$$

The above desribed way and assumptions made in obtaining the different electrical parameters for the section of the transformer winding under study was justified by the close agreement between the computed and experimental results of surge distribution inside the transformer winding in the line-end region.

3.3.3.2 INTERLEAVED DISC TYPE WINDING

As far as the solution of equation (3.13) is concerned, it is the same

for both types of winding on which our computational studies were carried out. This is because the unknown quantities (voltages of the different turns of the coil) are identical with the same conditions at the boundaries. This could be more clearly seen by comparing fig 3.5 and fig 3.8, which also illustrates the difference in coil construction between the two types leading to different coil parameters as it will be explained next.

Hence, the technique illustrated in section 3.2.1.1 is also applicable to interleaved (transposed) disc type winding.

The high voltage interleaved disc type winding did not exist in the HV lab. It was studied computationally in order to compare the results with those of the conventional winding under the same conditions and consequently to monitor the effect of interleaving of turns on the general behaviour of windings. Accordingly, we assumed the transposed winding (fig 3.6.b) had exactly the same electrical dimensions and characteristics as the conventional one.

3.3.3.2.1. ADMITTANCE MATRIX

The admittance matrix for interleaved disc type coil was calculated by using the same procedure used to calculate that of the conventional disc type coil, i.e :

1) The dielectric losses were omitted from the calculations, and as a result, the admittance matrix was calculated using the equation $[Y] = j\omega[C]$ (equation (3.39)).

2) The different elements of the capacitance matrix [C] were calculated by considering that the walls of the different turns formed the plane surfaces of parallel plate capacitors which do exist axially and radially between the neighbouring turns. The values for the different capacitances were calculated by means of the formula $C = \frac{\varepsilon_o \varepsilon_r A}{D}$ (equation (3.40)).

3) The capacitance matrix [C] was then formed as follows :

For any turn "a" of the coil, C(a,a) is equal to the sum of the values of

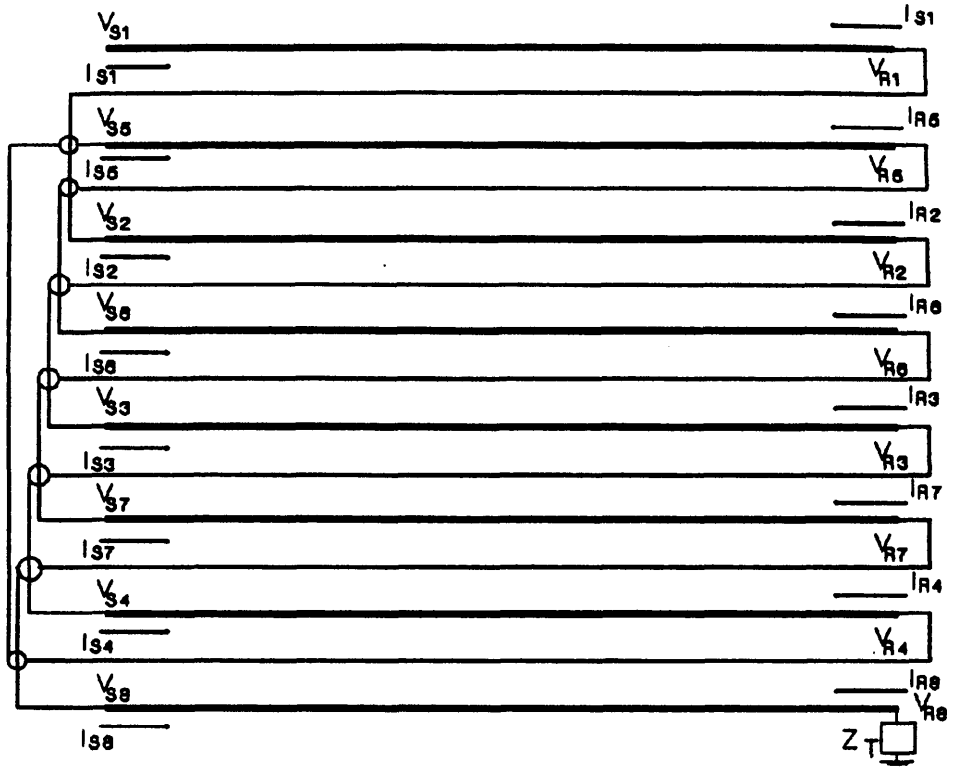

Fig 3.8 Double-section of an interleaved coil

all equivalent capacitances connected to turn "a", while C(a,k) is the opposite value of the capacitance connected betwwen "a" and "k". Again , all capacitances between non-neighbouring turns both radially and axially were neglected. The capacitance [C] is then formed by varying "a" to include all the turns of the coil under study.

Having said that the procedure to calculate the capacitance matrix for both types of winding is the same, their capacitance matrices however are not. This is due to interleaving of turns which are electrically further down the coil between consecutive turns in the transposed winding, which does not exist in the conventional one, or, in other words, due to coil construction. In order to make things clearer and for simplicity, consider an eight-turn interleaved coil consisting of one double section interleaved disc. Fig 3.9 shows the detailed capacitance equivalent circuit for the coil under study. It should be noted that all capacitances quoted in those figures, namely, CIT, CT, CDL, CDR, CB AND CG, are identical in both meaning and value to those in the capacitance equivalent circuit of the conventional winding. From what has been said so far, the capacitance matrix for an interleaved disc type coil made from an eight-turn double section disc is :

$$[C_I] = \begin{bmatrix} C_{11} & - & - & - & C_{15} & - & - & - \\ - & C_{22} & - & - & C_{25} & C_{26} & C_{27} & - \\ - & - & C_{33} & - & - & C_{36} & C_{37} & - \\ - & - & - & C_{44} & C_{45} & - & C_{47} & C_{48} \\ C_{51} & C_{52} & - & C_{54} & C_{55} & - & - & - \\ - & C_{62} & C_{63} & - & - & C_{66} & - & - \\ - & C_{72} & C_{73} & C_{74} & - & - & C_{77} & - \\ C_{81} & - & - & C_{84} & - & - & - & C_{88} \end{bmatrix}$$

The nul elements are in places of radial and axial non-neighbouring capacitances which have been neglected.

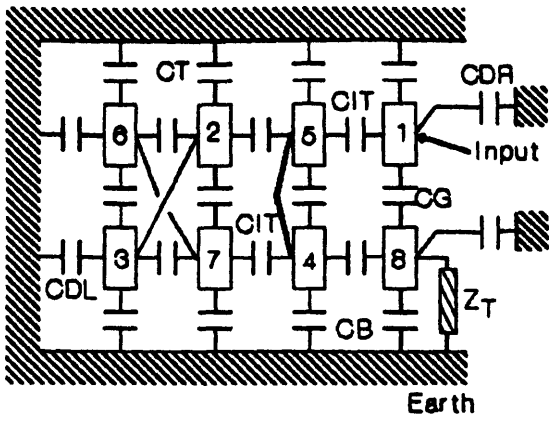

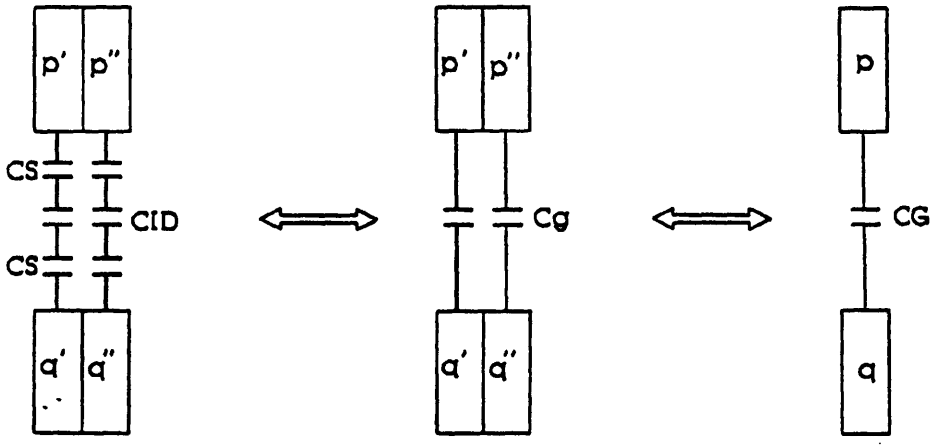

p & q are two axially adjacent turns made of two conductors in parallel

Fig 3.9 capacitance equivalent circuit of an interleaved coil

3.3.3.2.2 IMPEDANCE MATRIX

The impedance matrix for the interleaved disc type winding was obtained in the same way as for the conventional one, i.e :

1) The impedance matrix was calculated using the equation $[Z] = [R] + j\omega[L]$ (equation (3.42))

2) The matrix [R] is a diagonal matrix whose elements represent the copper losses in the turns of the coil. These elements are no more than resistances inserted in series with each turn. Copper losses have been taken to be mainly due to skin effect caused by the conductor surge current with the proximity effect being dropped because of the impossibility of a perfect evaluation of such effect. The total series resistance of the turn was obtained using $R_t = \frac{2h}{aS}$ (equation (3.45)).

2) For the simplicity of the computer model the inductance matrix was obtained from the capacitance matrix, calculated in the preceeding section, using the relation $[L1] = K_{loss} \left(\frac{1}{v_0^2} [C^*]^{-1} \right)$ (equation (3.47)). Moreover, due to the high frequencies involved in our studies and the skin effect, an increase in the internal inductance of the coil occurs and is given by $[L2] = \frac{h}{a\,S}$ (equation (3.48)). Hence, the total inductance matrix $[L] = [L1] + [L2]$.

From what has been said so far and finally, we can summarize by quoting that the procedure to calculate the different turn voltages of the coil model is the same for both types of winding. However, the parameters are not the same due to different capacitance matrices which in turn lead to different impendance matrices and consequently to different $[A_m]$ and $[B_m]$ (equation (3.13)) for each type of winding. More simply, to switch from one type of winding to the other , it only requires the modification of the capacitance matrix in the computer program which will be explained in the next chapter.

3.4 EXCITATION FUNCTION TO THE MODEL

The model developed in the above sections has been used to calculate the response of coils of transformers to discrete frequencies. In our studies and in order to calculate the response (turn to ground voltages of the coil turns) in the time domin to the input excitation function (also defined in the time domain), the convolution[84] of functions was carried out as explained in appendix C.

The input excitation functions to the computer model were the very steep fronted waves injected into the transformer HV winding in the laboratory for validation purposes. These very steep fronted waves were produced by a recurrent surge generator.

The recurrent surge generator (fig 3.10) operation principles basically consist in that the capacitor C_s is alternatively charged through the transformer and diode and then discharged into the circuit under test through the contacts of a relay. With the transformer winding under test connected to the recurrent surge generator terminals and by varying C_s, C_x, R_f and R_t, the front and tail of the applied wave can be modified. Accordingly, by a suitable choice of the values of the above mentioned parameters at once, very steep fronted waves with 30 , 60 , 120 and 240 nsec wavefronts and very long tails were obtained. These are shown in fig 3.11 to 3.14. The very steep fronted wave with almost 30 nsec is similar to surges impinging on transformer terminals during switching operations of disconnectors in GIS[5]and together with the other produced waves were suitable to check the validity of the computer model under different operating conditions encountered by directly and indirectly connected transformers in GIS[5].

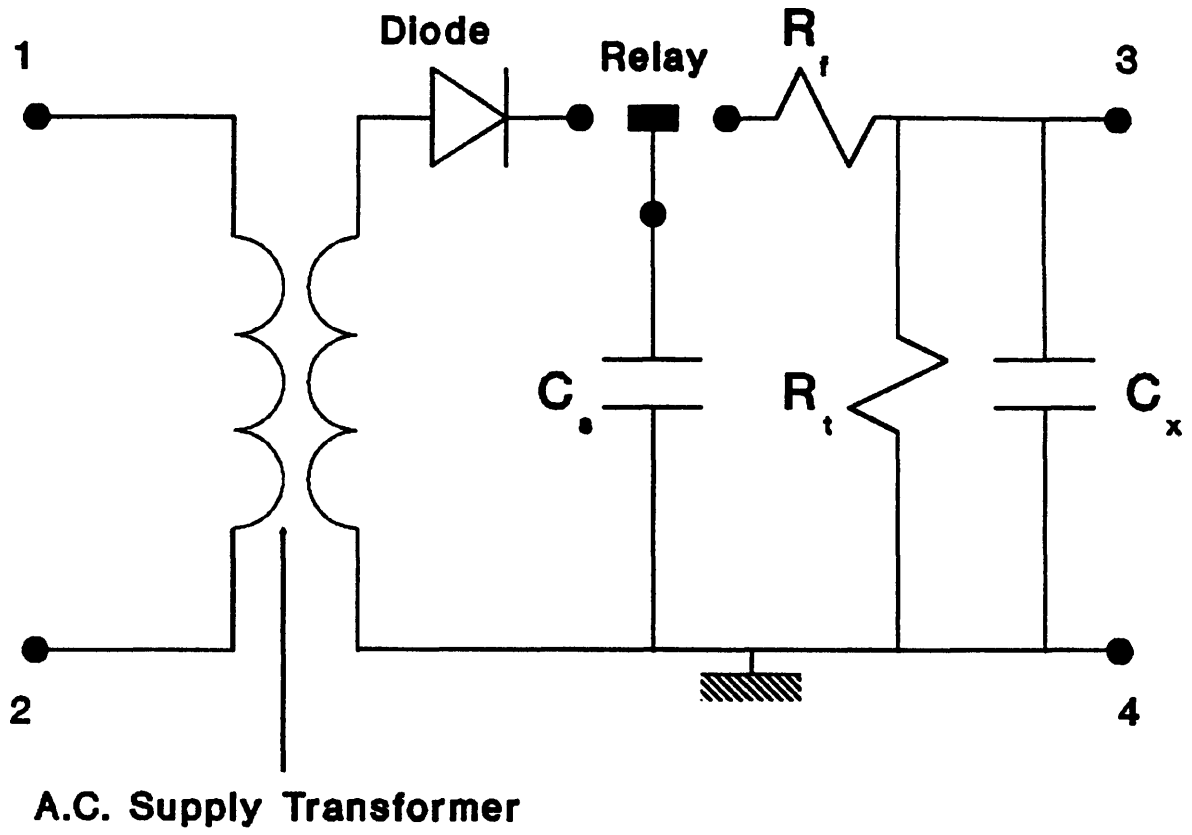

A.C. Supply is connected to terminals 1 and 2

Circuit under test is connected to terminals 3 and 4

Fig 3.10 Recurrent surge generator

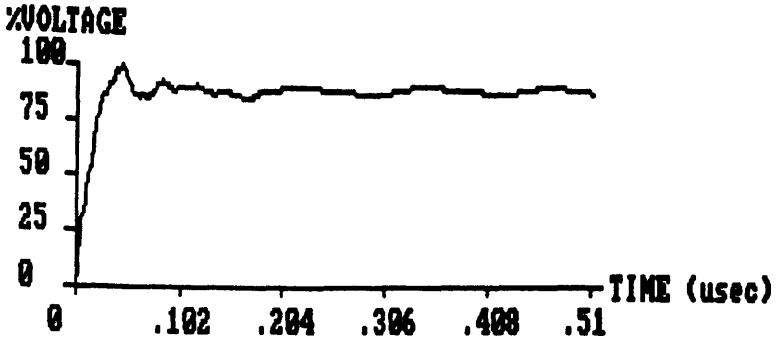

FIg 3.11 Excitation function with 30 nanoseconds risetime and long tail

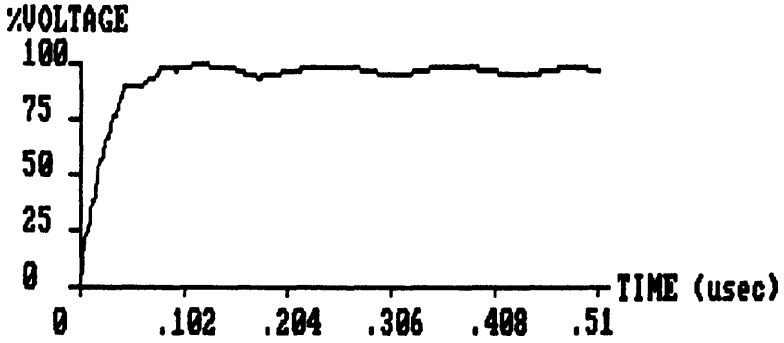

Fig 3.12 Excitation function with 60 nanoseconds risetime and long tail

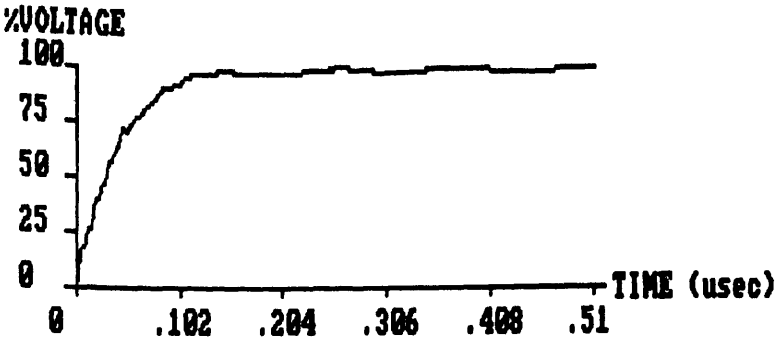

Fig 3.13 Excitation function with 120 nanoseconds risetime and long tail

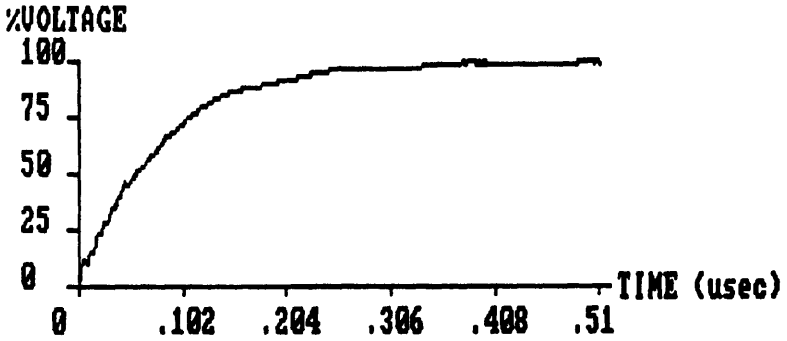

Fig 3.14 Excitation function with 240 nanoseconds risetime and long tail

CHAPTER 4

ACCURACY OF THE COMPUTER MODEL

This chapter presents the results obtained from the computational studies carried out by applying the coil model described in the previous chapter to transformer coils. It also shows the best way, in terms of both computer resources and accuracy, to obtain such results. Most important, It investigates the accuracy of the computer model by comparing the computational results with experimental results obtained from measurements performed on the transformer HV winding which already existed in the HV laboratory. Throughout the chapter, results obtained from the studies are analysed and discussed.

First of all, the main steps of the computer program, of which the computer model is a main part, which have been followed in order to calculate the voltages of the different turns of the coil, are briefly explained. Second , the different points in the transformer coil whose voltages have been predicted are illustrated together with the concepts of interturn and interdisc voltages. Next, the effects of accuracy parameters (number of discs and number of frequency samples) on both the output results and computer resources are found out. Following is an explanation of the method which has been adopted in order to obtain a fairly good estimation of the termination impedance Z_T of the model as a function of frequency. After all this , the computational results of the model are presented and, subsequently, the accuracy of the computer model is checked through comparison of the computational results obtained from the model and experimental results obtained from measurements on the modelled transformer coil which already existed in the HV laboratory. All obtained results are directly analysed and discussed throughout the chapter. Finally, a

discussion the performance of the computer model is given.

4.1 BRIEF EXPLANATION OF THE COMPUTER PROGRAM

The main intention of the computer program is to calculate the response of the transformer coil, modelled as a single two-port network on a turn by turn basis, to any arbitrary excitation function.

By the response of the transformer coil is meant the voltage predictions at the end of all turns of the coil model as a result of the excitation function being applied to the input of the model itself.

Such a response is obtained in the time domain, through a convolution[64] between the excitation function and the impulse response of the model, both of which are in the time domain. Hence, the computer program used to carry out the computational studies can be divided into three consequent main parts :

The computer model which is able to calculate the transfer function of the coil of the transformer to discrete frequencies. The discrete frequencies, f_n (n = 1, 2, 3,....., N, where N is the number of frequency samples which is also the number of time intervals $T_0 = \frac{2T}{N}$ into which twice the observation time 2T was divided), were taken as multiples of the fundamental frequency $f_0 = \frac{1}{4T}$ [68] , with $f_n = \frac{2n-1}{4T}$. After reading the data related to the transformer winding and for each frequency sample, the coil was mathematically modelled as explained in section 3.3.2 and its capacitance matrix together with its other parameters were calculated as explained in section 3.3.3, before its response at such frequency to the input function, which is the direct fourier transform of a unit impulse applied at time t = 0, was calculated. However, a unit impulse is rather difficult to simulate in the computer program because of its own characteristics[64,65], namely, infinite amplitude, zero duration and finite area. Nevertheless, good results are obtained when the unit impulse is represented by a unit pulse of width T_0 which is the time interval[66,66]. The set of frequency responses, at all the frequency

samples considered, for each point under consideration in the coil, represent the transfer function of that point and consequently all the transfer functions of the different points in the coil where voltages are to be predicted represent what is known as the transfer function of the coil itself.

After calculating the responses of the coil for the N samples and in the second part, these responses were transferred back to the time domain by using the fast fourier transform procedure[67]. In this way, and for a unit impulse incident to the coil model, the voltage in each turn of the coil was found in the time domain. In other words, the impulse response (which forms a fourier pair with the transfer function[66]) of the two-port netwok model of the coil is obtained.

Finally, in the third part, each of these turn voltages was convoluted, as explained in appendix C, with the excitation function (section 3.4) in order to calculate the coil final response. Subsequently, the turn voltages were plotted out together with the interturn and interdisc voltages whose concepts will be explained in the following section. All voltages are plotted on a three dimensional basis in order to obtain a clearer insight into their magnitudes and waveshapes and to clearly observe any phenomena occuring in the winding.

It is worth mentioning that each part of the computer program explained above was itself run as an independent program so that due to the huge computer resources required to run part 1, instead of computing the response for all the frequency samples together (in the frequency domain), it could be decided on how many samples can be taken at once (the bigger the model the less is the number of samples for each run) and at the end, all the data (of all frequency samples) could be read by part 2 whose data in turn is read by part 3 and convoluted before being plotted out.

A flow chart of the computer program is shown in fig 4.1.

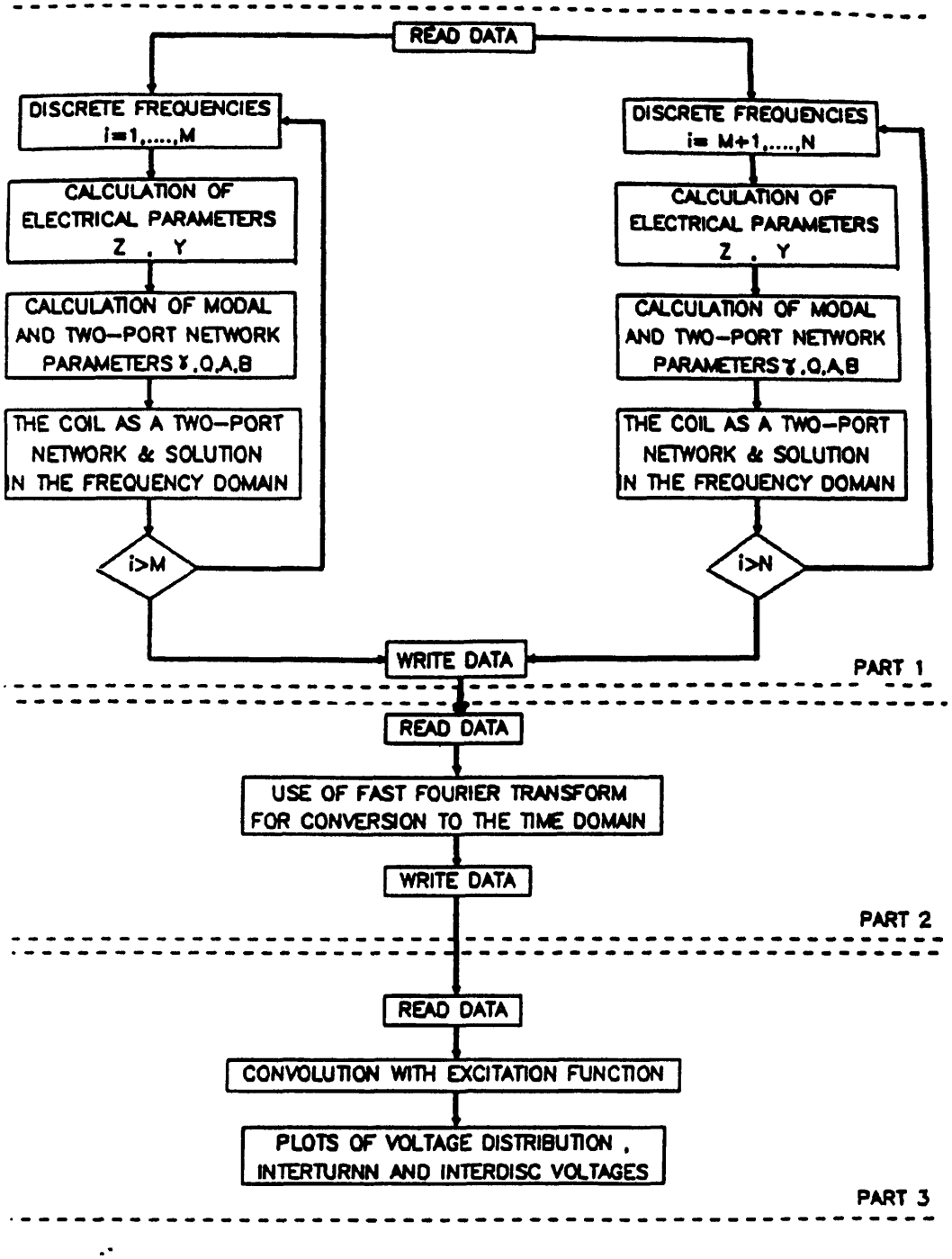

Fig 4.1 Flow chart of the computer program

4.2 LOCATION OF COMPUTATIONAL PREDICTIONS AND OTHER CONCEPTS

Before we precede with our computational studies, it is important to both illustrate the different points in the coil where voltages have been computed and explain the concepts of interturn and interdisc voltages.

The excitation function (input voltage pulse) was always applied at the begining of the first turn of the line-end disc of the coil and the responses to the applied excitation function were predicted at the end of each turn. In order to make things clearer and by refering to fig 4.2, the excitation function was applied to point 0, and the turn voltages were calculated at points 1, 2, 3, 4, ... ,N, where N is the number of turns of the coil under study.

The interturn voltage is defined as the difference of voltages between radially adjacent turns. For the coil shown in fig 4.2, the interturn voltages would be the difference of voltages between points 0-1, 1-2, 2-3 ,....., etc.

The interdisc voltages, however, are the differences of voltages between axially adjacent turns. By refering to fig 4.2, these voltages would be the differences between ppoints 0-16, 1-15, 2-14,..., etc.

The plotting procedure (third part of the computer program) was as follows :

First, the different turn voltages were plotted out with each plot showing the voltage distribution in each disc separetely. The excitation function was plotted within the voltage distribution of the first disc, as this function was considered to be the voltage at the end of turn 0.

Second, the interturn voltages in each disc were plotted separetely. In addition, the maximum interturn voltages in all discs included in the study were plotted on the same scale in order to see the trend of such voltages while going down the winding.

Finally, the interdisc voltages for each pair of adjacent discs were plotted separetly. Similarly to the interturn voltages , the maximum

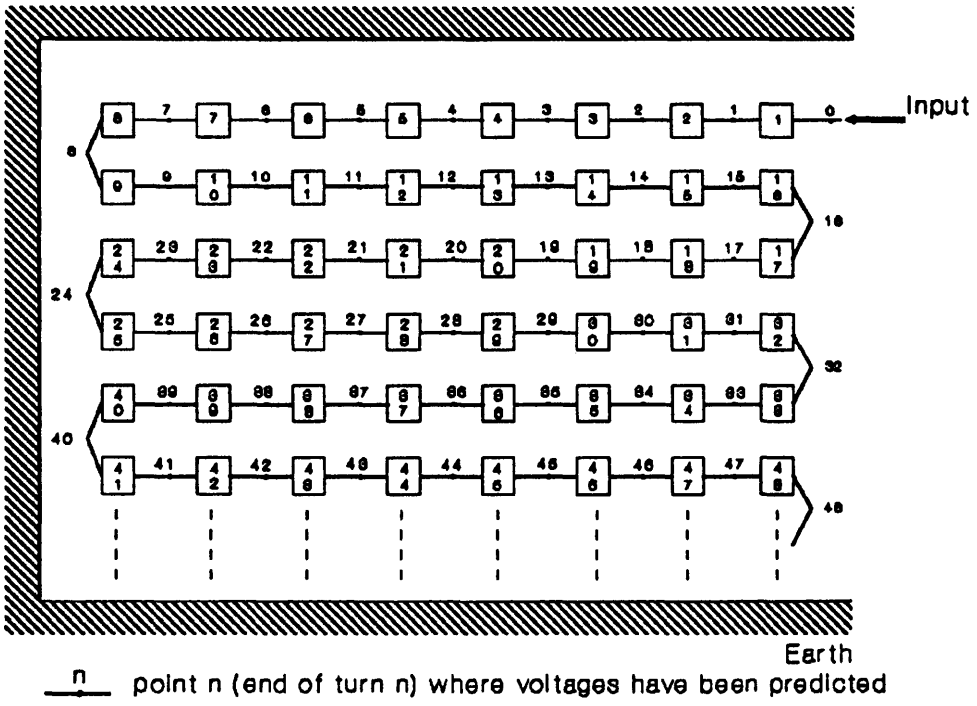

Fig 4.2 Location of computational predictions

interdisc voltages were plotted out.

All plots are on three dimensional basis except for the maximum interturn and interdisc voltages which are two dimensional plots. All voltages are expressed as percentage of the amplitude of the excitation function at the end of the risetime, with such amplitude taken to be 100% .

The coil shown in fig 4.2 is a conventional disc type coil. Nevertheless and for an interleaved disc type coil, all the predictions and general definitions of the concepts mentioned above still stand.

4.3 COMPUTER RESOURCES AND ACCURACY

In any study involving computer work, it always has been the case of taking the benefit of obtaining the most accurate computational results. In our bid to calculate the coil responses to input voltage pulses impinging on its line-end and because of the huge computer resources required to obtain the most accurate results, an accuracy analysis has been performed in order to reach a compromise between computer resources and accuracy of the output results. In other words, the best economic way in terms of computer resources (most important is time consumption) of obtaining sufficiently accurate results has been monitored and later adopted during the whole of the computational studies. The accuracy analysis was carried out by separetely finding out the effects of two parameters, namely, number of discs in the coil and number of frequency samples.

4.3.1 NUMBER OF DISCS IN THE MODEL

As mentioned in section 3.3.2, single-section representation of the transformer coil would yield erroneous results in that it does not include the couplings between turns of different sections which is the most important feature of transformer windings. As a result, the multiple-section model concept was very important in order to take account of all couplings between turns not only of the same section but of different sections as well.

In the multiple-section model, the number of sections, or discs in our

case, included in the study has an effect on the accuracy of the computed results especially in the line-end region of the winding as well as on computer time and resources.

In order to observe the effect of the number of discs included in the model on both the accuracy of the output results and computer time consumption, we considered the following :

1) risetime of the excitation function = 60 nsec

2) Termination impedance to the model, $Z_T = Z_2$

3) Observation time T = 0.512 μsec

4) Number of frequency samples N = 256, i.e. sampling rate of 4 nsec

Under the conditions mentioned above, we monitered the output results of discs 1, 2 and 4 for number of discs in the model of 4, 6 and 8. These results are shown in fig 4.3 to fig 4.5, with the computer time consumed in each case illustrated in fig 4.6.

As it can be seen, by looking at the voltage distributions of the turns of disc 1 (fig 4.3) and disc 2 (fig 4.4), these voltage distributions vary considerably in the four-section and six-section models although it is obvious that less considerable variations occur at the end of the observation time when we go from a six-section model to an eight-section model. All this could be attributed to the fact that the more sections are included the longer it will take the travelling waves to reach the very end of the model in order to be reflected and reach the top sections again to cause any more sharp oscillations in the voltage waveshape of the turns of such sections. In fact, such sharp oscillations are in evidence in the turns of disc 4 in the six-section model (fig 4.5.b), with such oscillations almost non-existent in the case of eight-section model (fig 4.5.c). It should be noted that such oscillations occur with a certain time delay when more sections are included and that is due, as mentioned above, to the delay in travelling down and up the coil.

In addition, it is very important not to forget that wave reflections

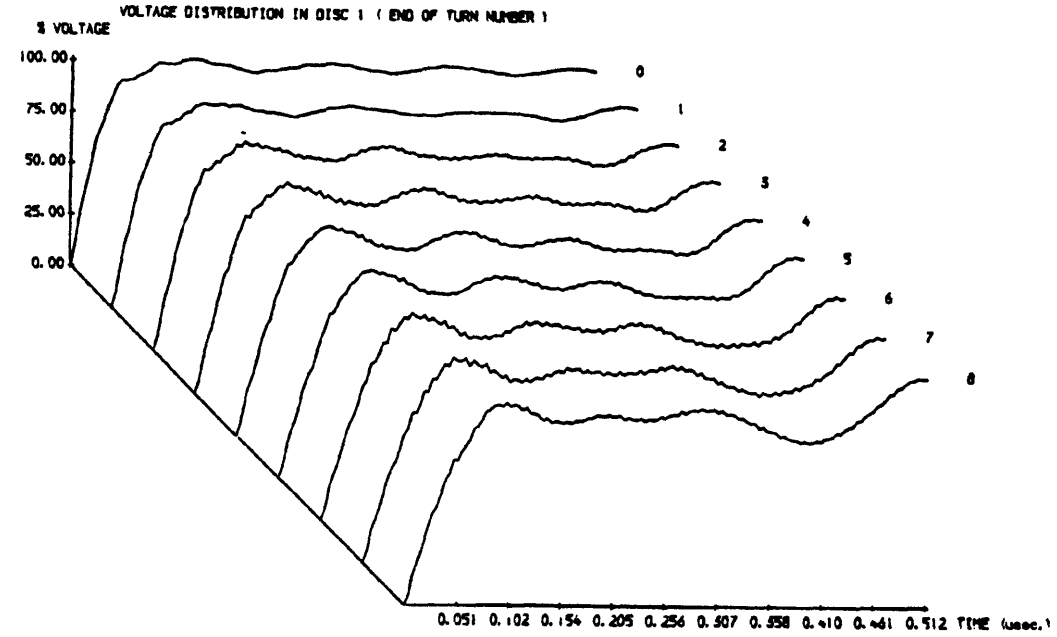

a)

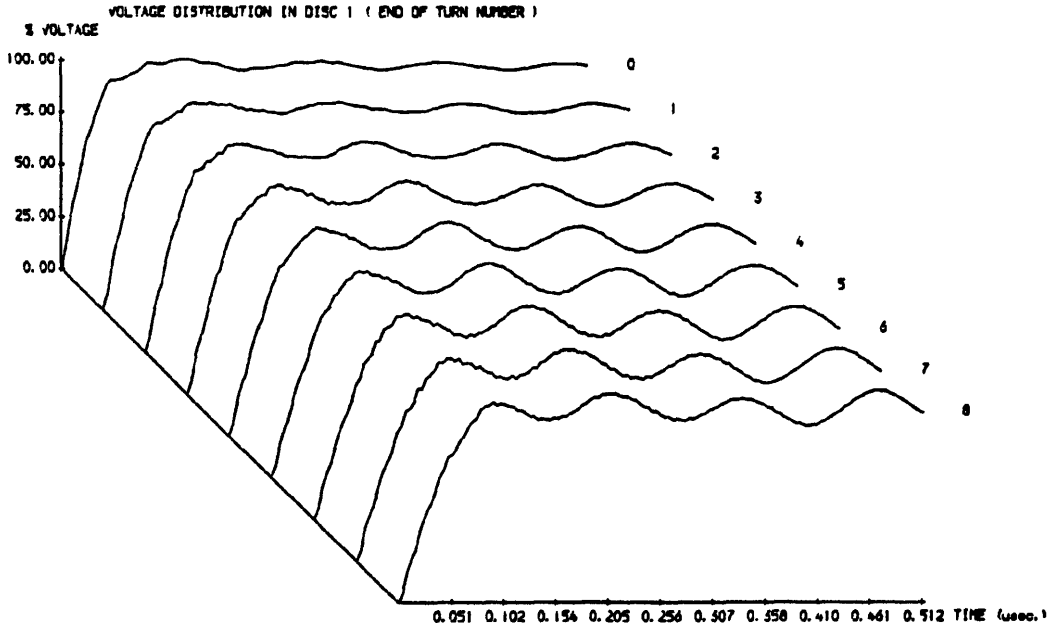

b)

Fig 4.3 Voltage distribution in disc 1 for different number of discs D in the model

a) D = 4

b) D = 6

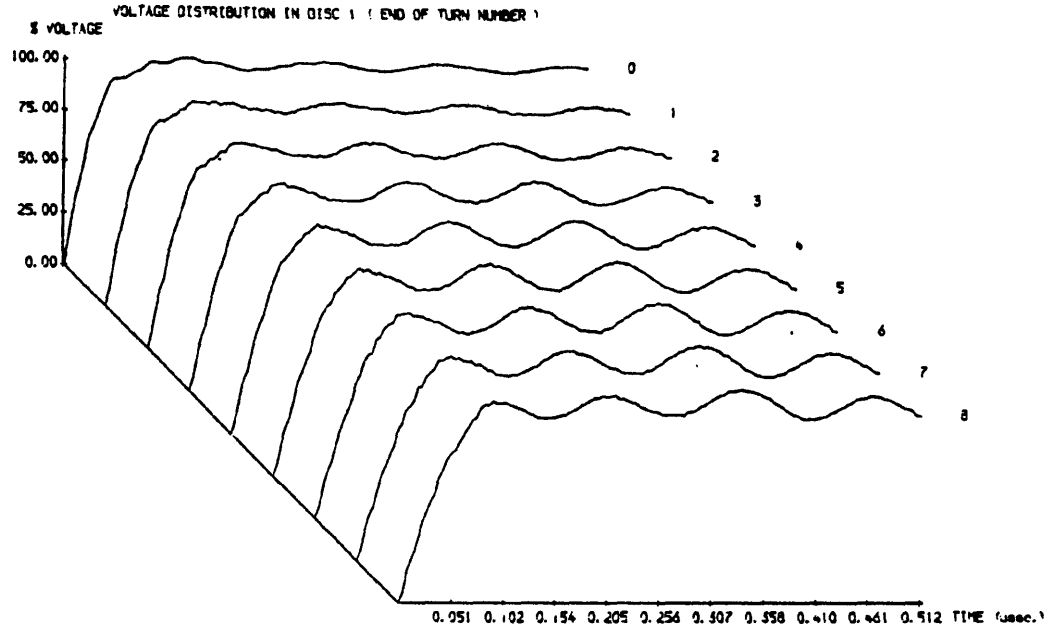

c)

Fig 4.3 Voltage distribution in disc 1 for different number of discs D in the model

c) D = 8

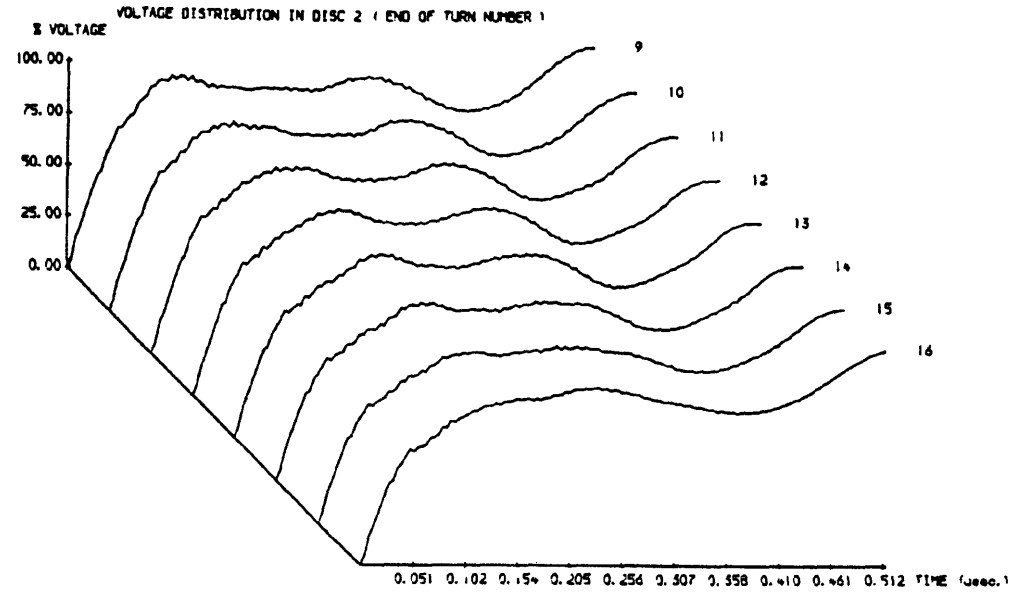

a)

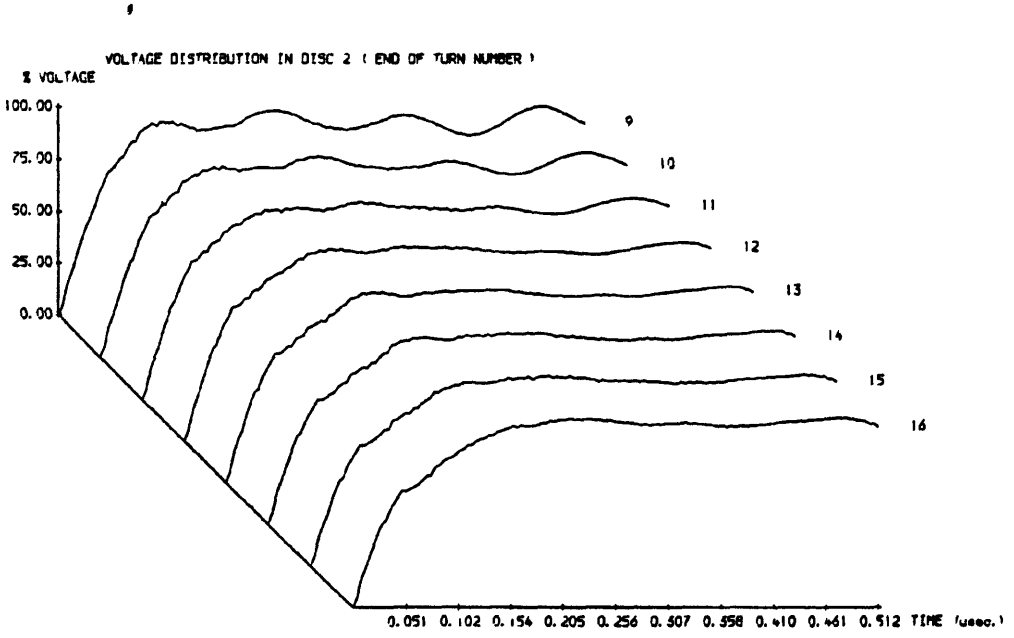

b)

Fig 4.4 Voltage distribution in disc 2 for different number of discs D in the model

a) D = 4

b) D = 6

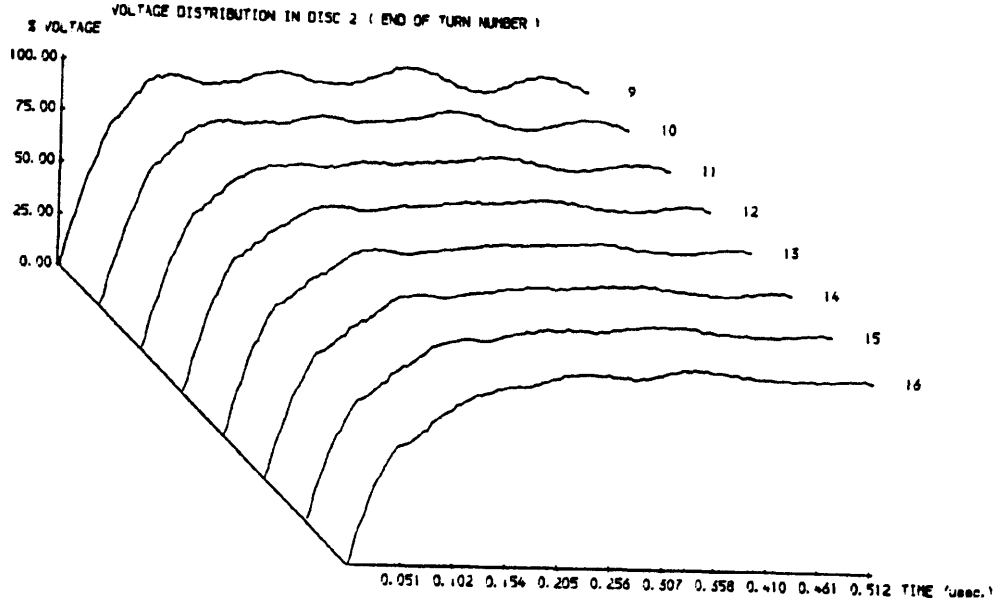

c)

Fig 4.4 Voltage distribution in disc 2 for different number of discs D in the model

c) D = 8

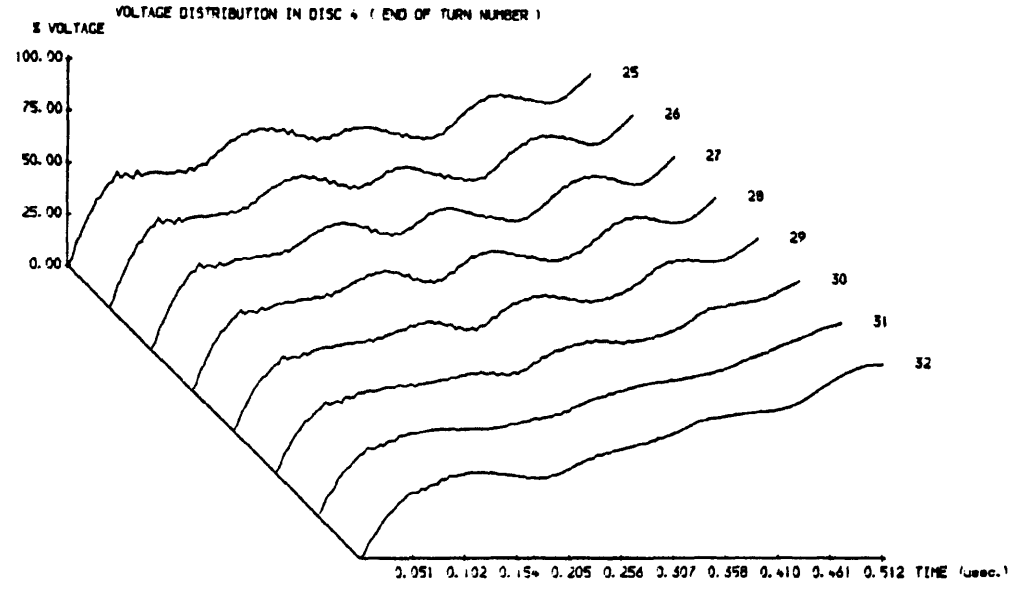

a)

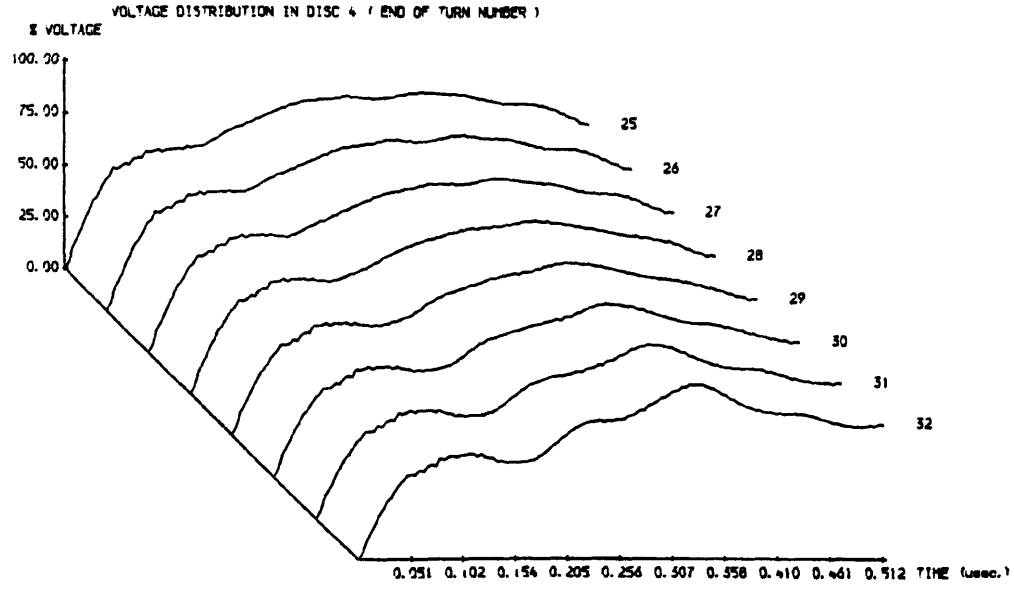

b)

Fig 4.5 Voltage distribution in disc 4 for different number of discs D in the model

a) D = 4

b) D = 6

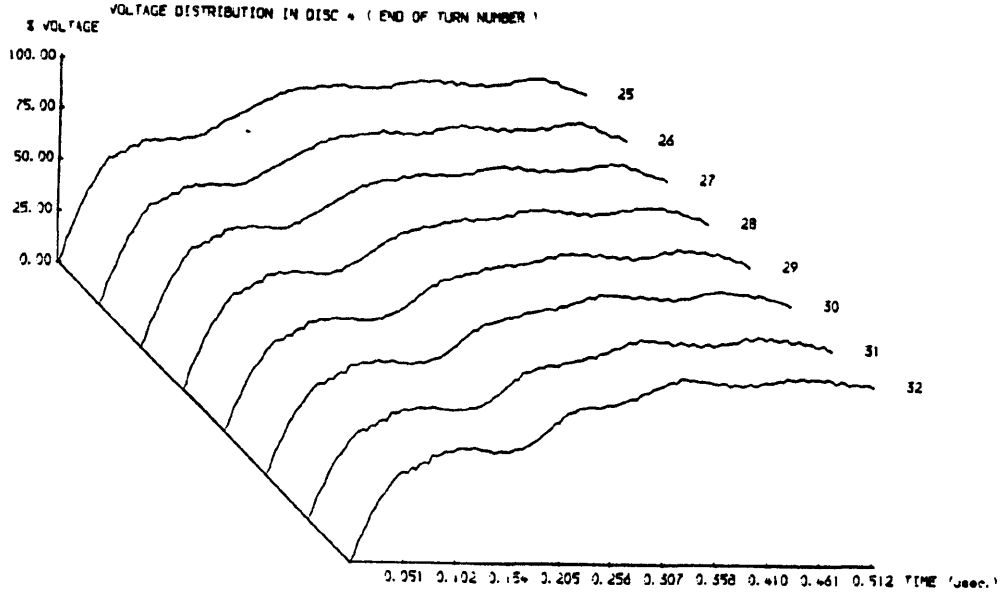

c)

Fig 4.5 Voltage distribution in disc 4 for different number of discs D in the model

c) D = 8

NUMBER OF DISCS	COMPUTER TIME CONSUMPTION (CPU SECONDS)		
	PART 1	PART 2 and PART 3	TOTAL
4	436	15	451
6	985	20	1005
8	2304	20	2324

Fig 4.6 Effect of number of discs in the model on computer time consumption

do occur not only at the very end of the model but at any point in the coil which represents a sudden change in impedance especially at the end of each section or, in other words, at the connections of the different sections. That explains the slight increase in the amplitude of the volatge of turn 16 towards the end of the observation time, when we move up from a six-section (fig 4.4.b) to an eight-section model (fig 4.4.c). Accordingly, a slight increase in the voltage of turns towards the end of the observation time of discs further down the winding is expected with the inclusion of more and more discs in the model.

Hence, the travelling wave phenomena inside the model is a very complex one and consequently it would be of great benefit to include more and more sections in the model to the point where it could be found that the inclusion of more discs would not affect to a certain acceptable limit the accuracy of the results of the sections of interest to us, and this also includes the capacitive distribution right at the begining of the obsevation time (initial period). For example, in our case, an eight-section model would be adequate as far as the top four discs are concerned. Moreover, the results up to the sixth disc were presented. However, with the eight-section model, a small computational instability was noticed towards the end of the observation time and this is entirely due to calculation instabilities related entirely to matrix size[47].

From above, it is clear that the observation time is closely related to the number of discs to be included in the study and the smaller the observation time the less the number of discs in the model is required.

Accordingly, an eight-section (eight single-section discs) was adopted for the following studies with accurate results over the observation time of 512 nsec.

4.3.2 NUMBER OF FREQUENCY SAMPLES

As mentioned in section 3.4, the computer model calculates the transfer fuction of the coil of the transformer winding to discrete frequencies. As

a result, a number N of frequency samples ($N = 2^m$) was taken which is also the number of time intervals T_0 into which twice the observation time 2T was divided i.e. $T_0 = \frac{2T}{N}$ [88]. By keeping the same obsevation time, increasing N means a smaller sampling time which in turn yields a higher frequency range in the study.

In order to observe the effect of the number of frequency samples on the accuracy of the output results, we considered the following :

1) Risetime of the excitation function = 60 nsec

2) A coil constituting of eight discs (conventionally wound) and terminated by a constant termination impedance $Z_T = Z_2$

3) Observation time T = 0.512 μsec

Under the conditions mentioned above, we monitored all the output results for a number of frequency samples of 256 and 1024 or, in other words, for sampling times of 4 nsec and 1 nsec (1 nsec being the sampling rate of the input excitaion function). These results are shown in fig 4.7 to fig 4.11.

As it can be seen, no noticeable difference could be spotted between the various results with 256 or 1024 samples, except in the maximum interturn voltages in the first few turns of the line-end disc . This is to be expected since the excitation function itself, no matter its sampling rate, has a faster rate of rise at the beginning of its wavefront than at the end of it, and of course, a sampling rate higher than that of the excitation function would not detect this faster rate of rise leading to slightly lower values for the maximum interturn voltages in the first few turns of the line-end disc. On the other hand, as far as computer time consumption is concerned, the running time for 1024 samples is four times that with 256 samples with, as said before, no noticeable difference between the results of the two cases. Moreover, storage of four times more is also required.

From what has been mentioned above, it is obvious that a number of

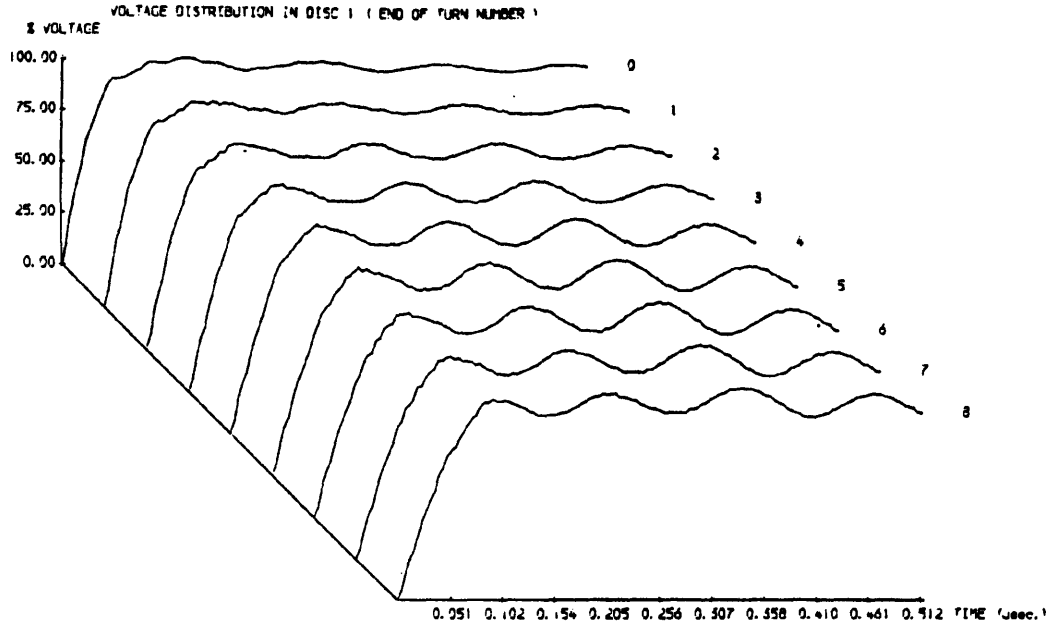

a)

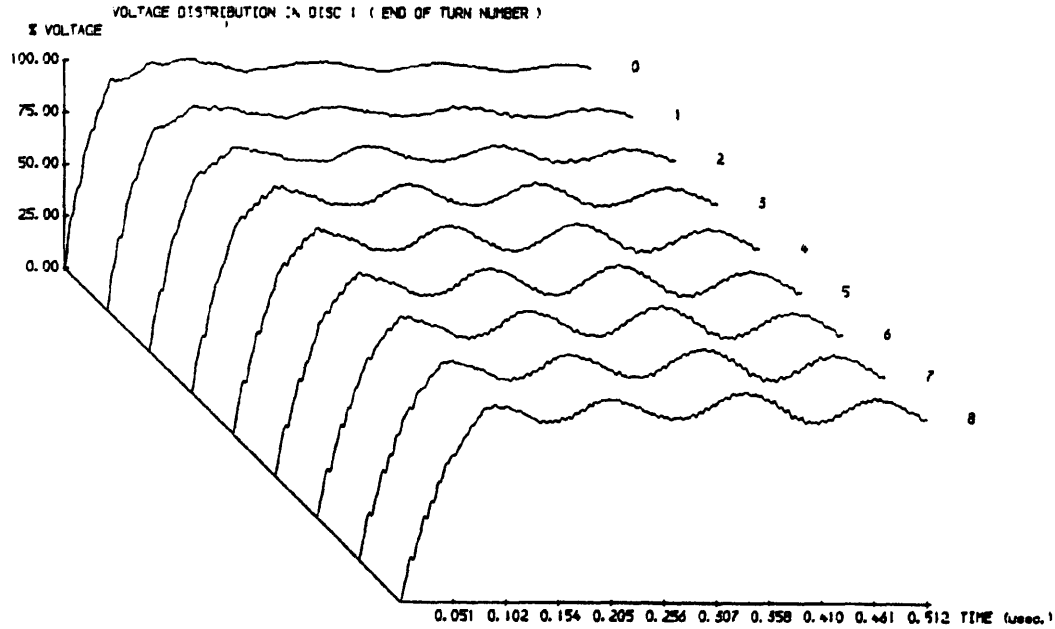

b)

Fig 4.7 Voltage distribution in disc 1 for different number N of frequency samples

a) N = 256

b) N = 1024

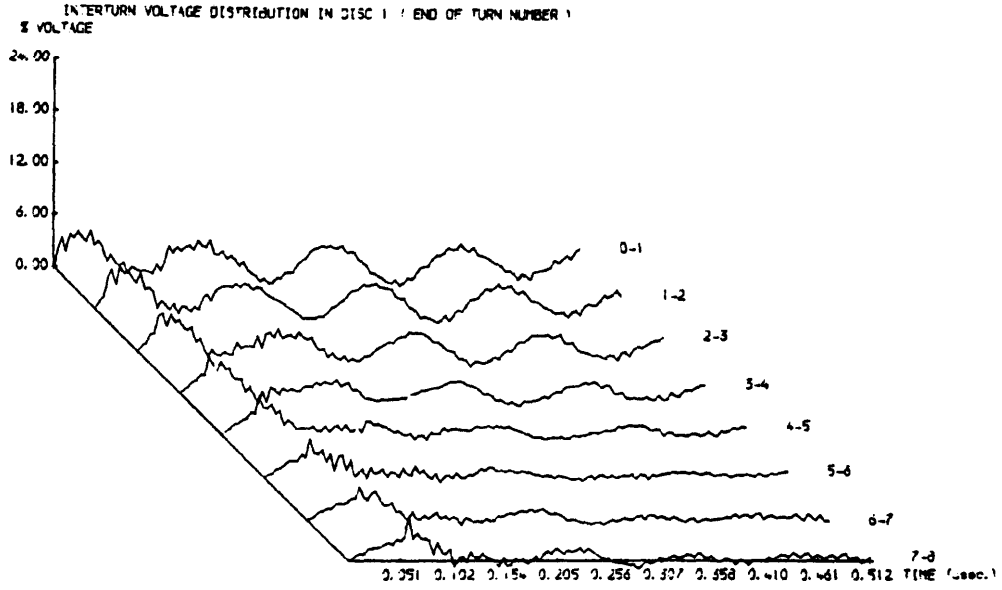

a)

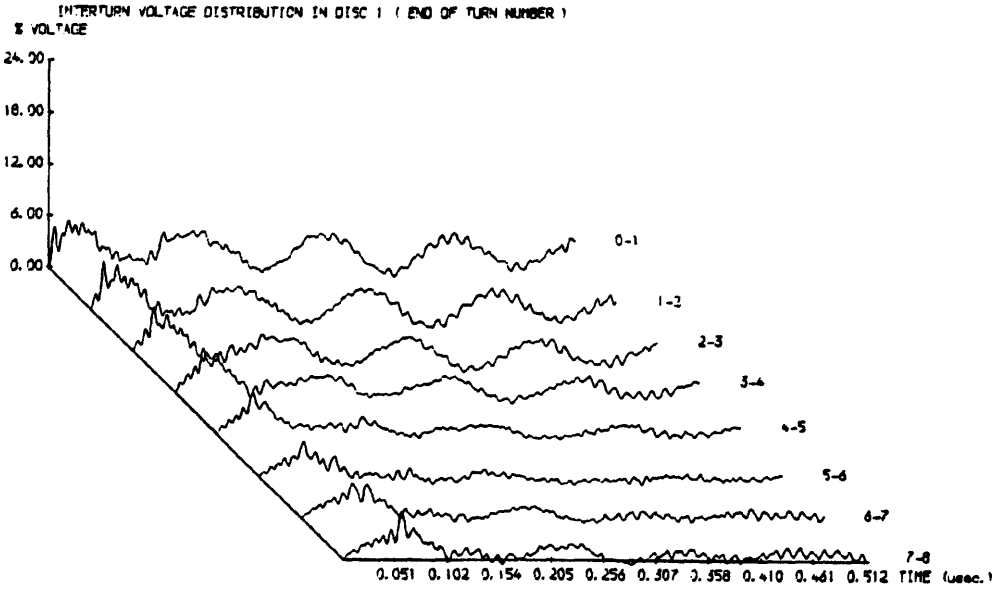

b)

Fig 4.8 Interturn voltage distribution in disc 1 for different number N of frequency samples

a) N = 256

b) N = 1024

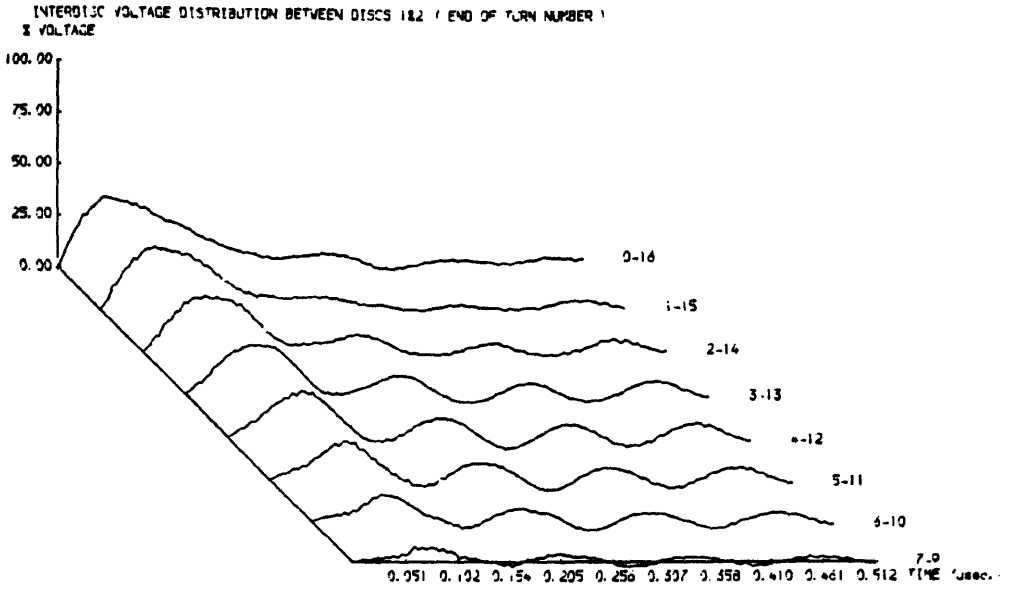

a)

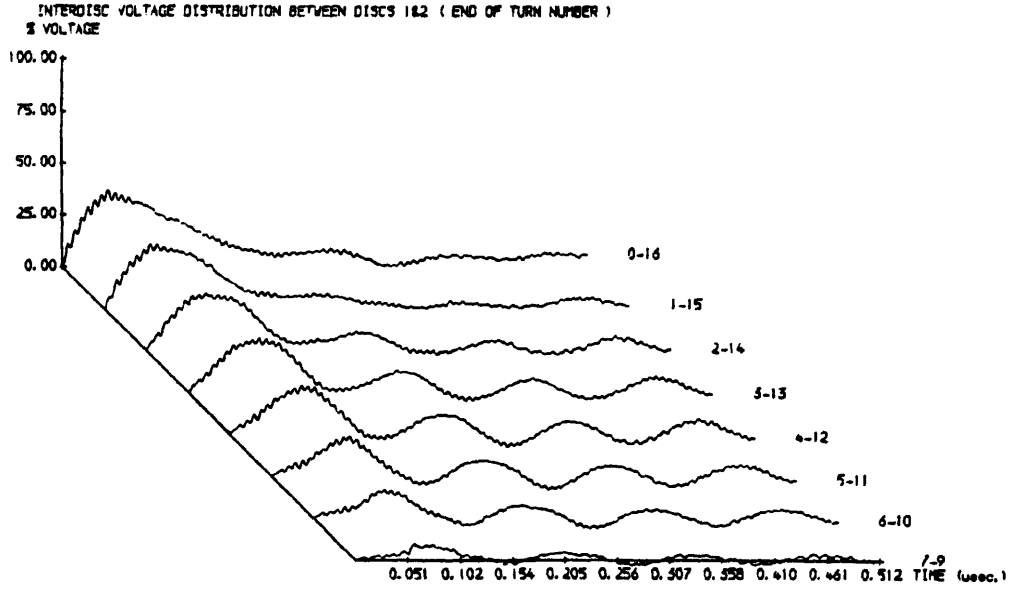

b)

Fig 4.9 Interdisc voltage distribution between discs 1 and 2 for different number N of frequency samples

a) N = 256

b) N = 1024

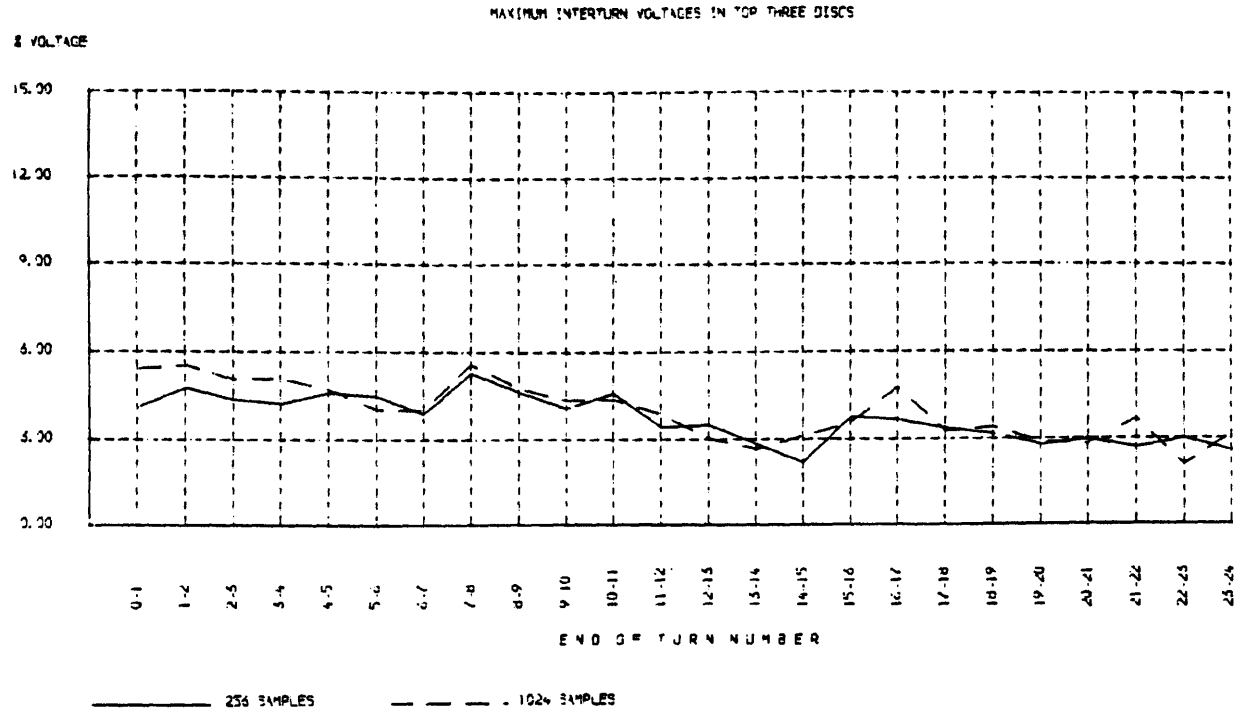

Fig 4.10 Effect of number of frequency samples on maximum interturn voltages

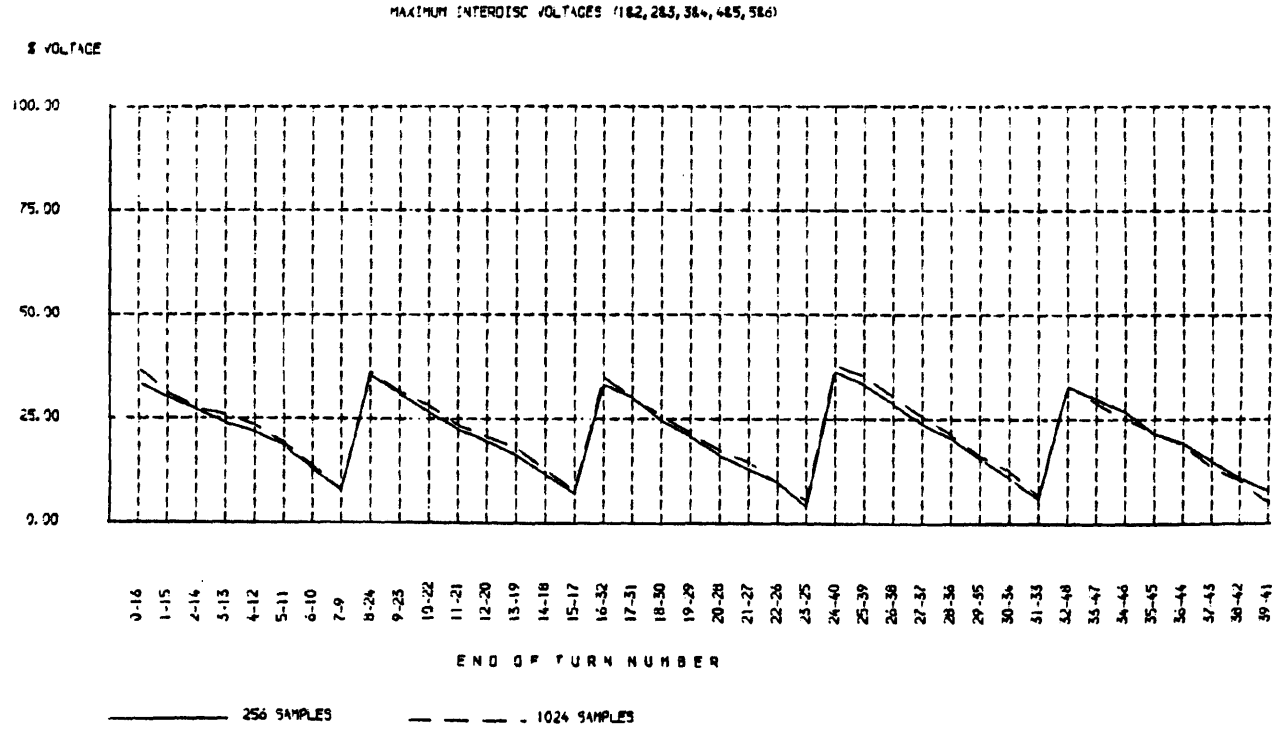

Fig 4.11 Effect of number of frequency samples on maximum interdisc voltages

frequency samples of N = 256 was very adequate for the accuracy of the model and computer resources and consequently N = 256 samples was adopted for all the computational studies.

4.4 ESTIMATION OF THE TEMINATION IMPEDANCE OF THE MODEL

Since it is impractical to include all sections of the transformer HV winding in the computer model which considers the turn itself as the basic element, it was decided to include a number D of discs in the model itself and terminate it by a termination impedance Z_T which is chosen to represent the characteristic impedance of the remaining cascade-connected sections further down the winding which have not been included in the study. In order to find a fairly good estimation of Z_T (function of frequency), the concept of coil impedance (element D(1,1) in equation 3.36) was used. The problem of finding the value of Z_T is an iterative one in nature in such that it always starts by finding the input impedance of the last section (connected to neutral) and then considers it as the termination impedance for the section before the one under study with such a process repeated until the impedance does not vary any more over all the frequency range from the one found in the iteration before, which would eventually represent the termination impedance of the model under study. However, due to the strong couplings between the cascade-connected sections in transformer windings, it was impossible to isolate any section in order to find its input impedance. As a result, by taking into consideration both the time for a travelling wave to travel down the winding and reach the input after being reflected and the obsevation time (512 nsec), it was decided to take a coil made of six sections of a conventional disc winding at once and find its input impedance. Hence , the procedure of finding Z_T, mentioned above, was repeated for coils made of six sections instead of one section as is the case for a.c.machine windings. In addition, there was the problem of couplings between the top and bottom sections of the coil and those of axially neighbouring coils, respectively. Such a problem could not

be solved easily and consequently two different approaches were made whose effects would be studied later.

First, it was assumed that since ground is axially too far away from the model under consideration, all capacitances to ground from the bottom and top sections of the model were neglected.

Second, the above approach was repeated but with a twelve sections coil with the input impedance being of the section in the middle or, in other words, the impedance as seen at the begining of section seven. Moreover, any signal applied to the middle of the coil would see two impedances in parallel up to the time where reflections arrive back from both ends. In accordance with what has been mentioned earlier on, during the observation time, the two parallel circuits were replaced by an equivalent one with its input impedance found.

For each of the two approaches explained above, a number of iterations have been made in order to find Z_T with the first approach taking four iterations and the second approach three iterations with the corresponding values of Z_T being Z_1 and Z_2 respectively as shown in fig 4.12 and fig 4.13.

4.5 ACCURACY OF THE COMPUTER MODEL

Before presenting the computational results of the transformer coil model, it is worthwhile illustrating the way in which the experimental work was carried out in order to validate the computer model.

4.5.1 EXPERIMENTAL SET-UP

In order to monitor the degree of accuracy and validity of the multiconductor transmission line model of the coil, we carried out a series of measurements on an actual HV conventional disc type winding whose coil was itself modelled on the computer. The winding under test was a single phase of a 1600 KVA, 6.6 Kv transformer winding whose details are given in appendix A.

The measurements were carried out using :

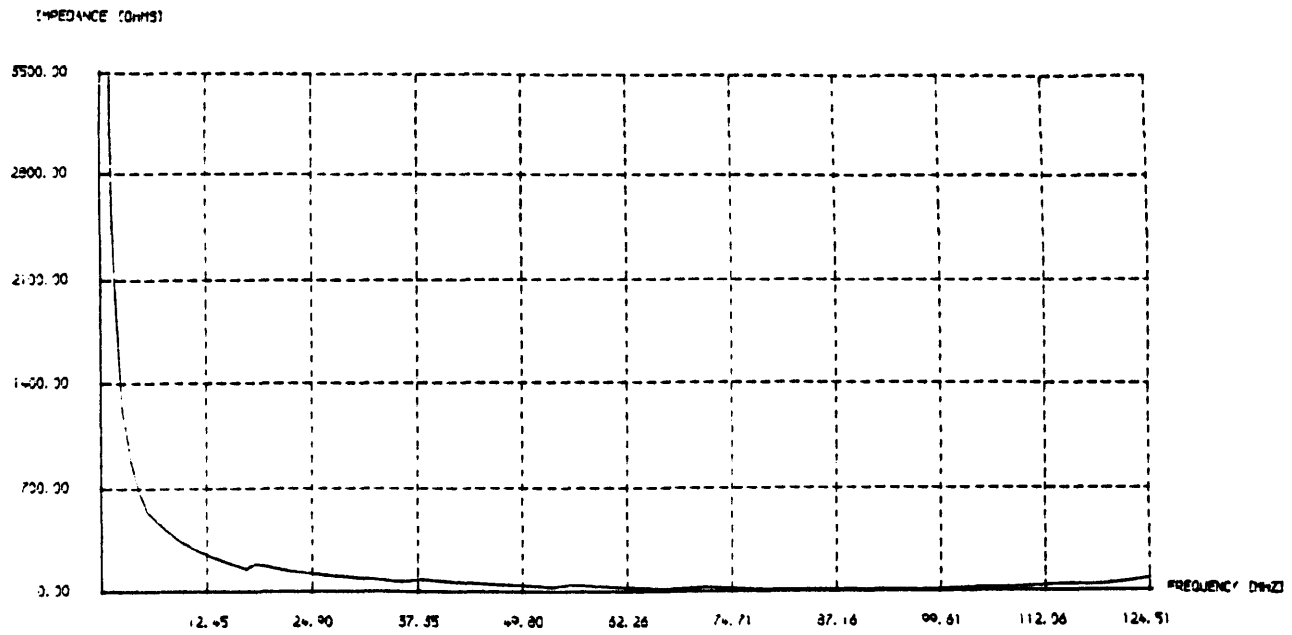

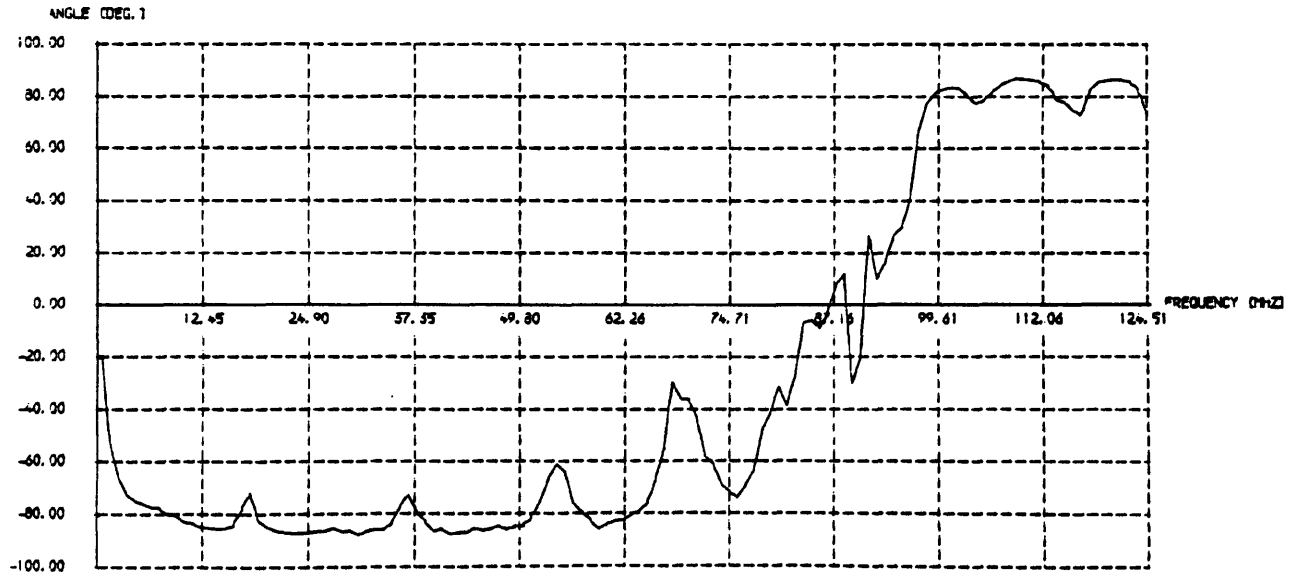

Fig 4.12 Termination impedance to the model, $Z_T = Z_1$ (first approach)

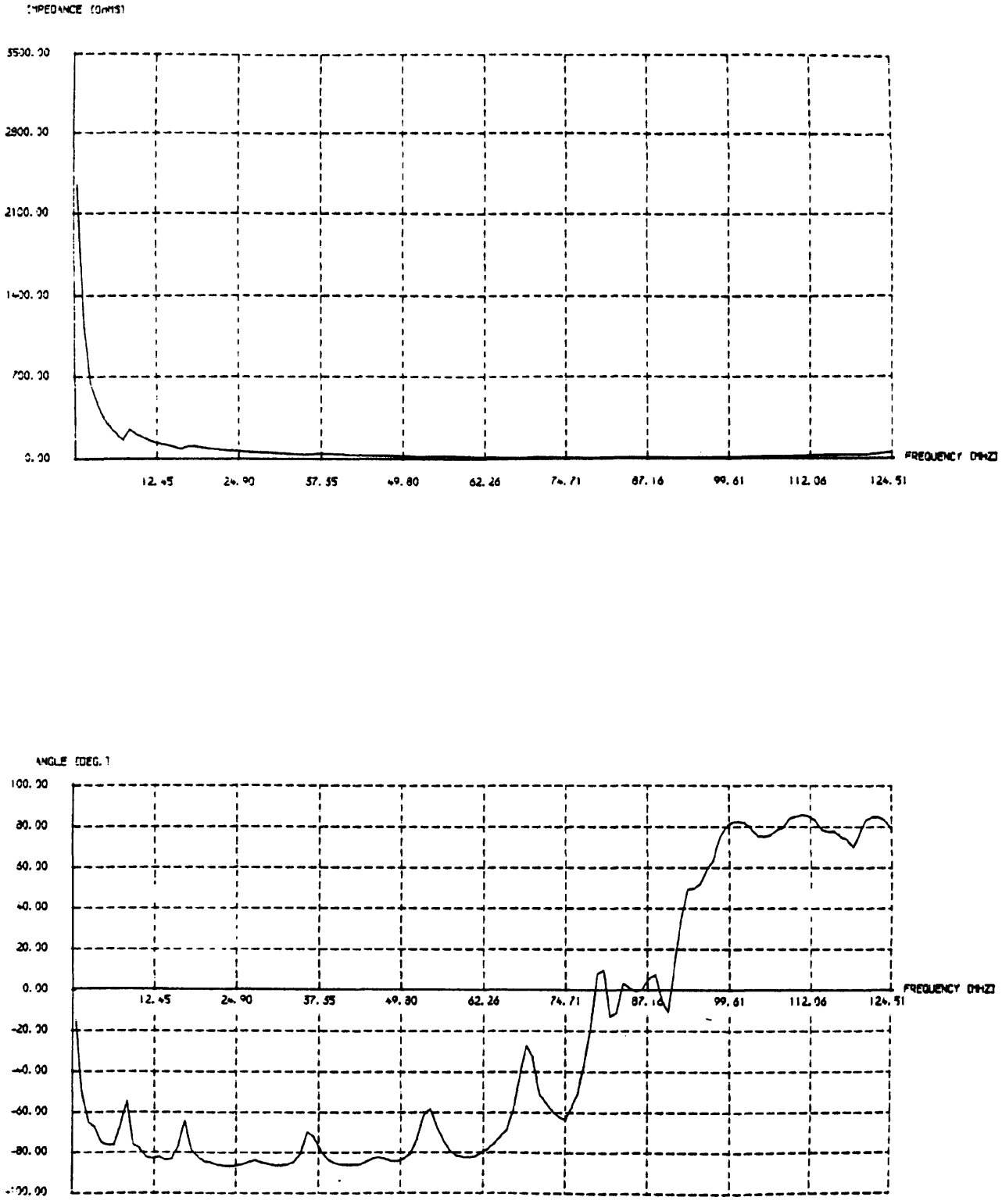

Fig 4.13 Termination impedance to the model, $Z_T = Z_2$ (second approach)

1) A Recurrent surge generator to produce very steep fronted waves similar to those obtained[5] on the power system, with the very steep fronted waves themselves being the excitation functions of the computer model as already mentioned in section 3.4.

2) A 300 MHz, 500 Ms/sec TEkTRONIX oscilloscope type 2440 and low capacitance probes with an attenuation of 10.

3) An AMSTRAD personal computer type 1512.

4) A HEWLETT PACKARD personal computer (Vectra QS/16).

5) A HEWLETT PACKARD Laser jet (series II) printer.

The Recurrent surge generator produced very fast fronted waves with different risetimes. Such waves were applied to the HV lead of the single phase disc type winding. The different measurements were made at each turn of the line-end disc and at the outer junctions of the other cacade-connected discs. The data for all measurements (waveform data) was stored on a floppy disk by using the AMSTRAD PC1512. Subsequently such data was read again by the HEWLETT PACKARD PC Vectra and then plotted (in three dimensions) on the laser jet printer by using the GWBASIC software. It is worthwhile mentioning that the waveform data of the surges produced by the recurrent surge generator was loaded onto the main frame (where the computer model was written) in order to have exactly the same input to both the actual and modelled transformer coils. In return, the computational results were loaded from the main frame onto the floppy disk in order for such results to be plotted on the laser jet printer for close and efficient comparison with the corresponding experimental results. The experimental set-up is shown in fig 4.14.

Computational studies were carried out on two types of transformer HV winding, namely, conventional disc type winding and interleaved (transposed) disc type winding. In the conventional disc type winding, each section in the coil model was equivalent to one disc whereas in the interleaved type winding, each section constituted of double-section discs

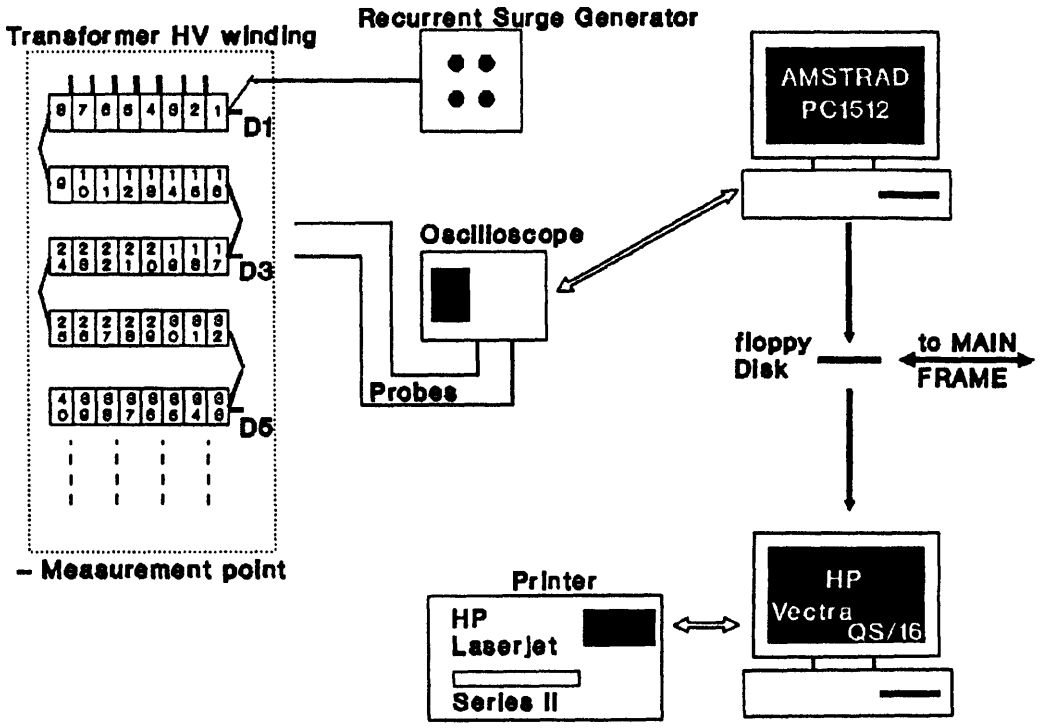

Fig 4.14 Experimental set-up

due to the transposing of turns inside the disc itself. However, because of the availability of only a conventional winding, comparison between computational and experimental results for the interleaved winding was not possible. Accordingly, the computational studies for the interleaved winding were carried out in order to investigate the effect of transposing on the surge response of transformer windings, which will be included in the sensitivity analysis.

4.5.2 COMPARISON BETWEEN COMPUTATIONAL AND EXPERIMENTAL RESULTS

An eight-section model of a conventional HV disc type winding made of eight single-section discs is shown in fig 4.15.a. The equivalent capacitance circuit of the coil is shown in fig 4.15.b. The values of the different capacitances were obtained as described in section 3.3.3. The termination impedance for the model was taken to be Z_2 as described in section 4.4. The excitation function to the model was the very steep fronted surge with a 60 nsec risetime, produced by the recurrent surge generator as described in section 3.4.

All the computational results for the coil under study, namely, voltage distribution at the end of all turns, interturn and interdisc voltages with their maximum values are shown in fig 4.16. A direct comparison between the computational and experimental results is illustrated in fig 4.17.

It is clear from both fig 4.16 and fig 4.17 that surge distribution in transformer windings is a complex phenomena and is mainly due to two modes, namely, parallel mode and series mode.

The parallel mode is clearly visible in the initial period of the observation time, directly after the very steep fronted wave reaches the transformer winding. This is evident from the simple fact that, in the first 50 nsec, the wavefront of the incoming wave is simply reproduced with a variant degree of attenuation at all the turns included in the study, as it could be seen from the voltage distribution in all discs of the coil (fig 4.16). Such instantaneous induced voltages in all the coil turns are

basically due to the strong axial and radial capacitive couplings which are the very important and dominant feature of the transformer winding in the initial period of the observation time. This is indeed the case since, for instance and as expected, the magnitude of the induced voltage at the end of turn 1 is higher than that at the end of turn 16 due to the fact that the radial capacitive coupling is by far stronger than the axial one. This is as well the cause for end of turn 8 (despite being separated from the line end radially by almost eight complete turns) managing an induced voltage higher than that of end of turn 16. However, this fact becomes less noticeable in the lower discs but still occuring. To summarize, in the initial period, the transformer winding is dominantly a capacitive network, with all the capacitive elements playing the only and prominent role in determining the magnitudes of the induced voltages at all the turns of the winding. This is what is known as the parallel mode of propagation.

The series mode of propagation is the travelling of the surge itself turn by turn throughout the winding. The arrival of the surge at each turn can be detected through a steeper rise in the rate of increase of the turn voltage. However, due to the fact that the risetime of the very steep fronted wave and its travel time through each disc of the winding are very close indeed, it is almost impossible to exactly predict the instant of time such wave would reach the turns of the first disc. Hence, in order to distinguish between the voltage resulting from series propagation of the surge and the induced voltage due to the capacitive coupling, it would be necessary to monitor the voltage distribution in the lower discs of the model where the travelling wave would be much delayed. In fact, the steeper rate of rise in the turn voltages becomes detectable in the voltage distributions in discs 4, 5 and 6 betwwen 160 nsec and 320 nsec. Moreover, when the travelling wave reaches the end of the coil, it is reflected back with a negative peak which is clearly illustrated in the sudden decrease in the voltage of turn 48 (in the sixth disc) towards the end of the

observation time. The only explanation for such negative peak is the sudden change in impedance at the end of the coil where in fact the termination impedance is connected. The effect of such reflection from the bottom end of the coil would not however be felt in the turns of the first five discs within the observation time considered in our case, due the travel time required for such negative reflection to reach the above mentioned discs which again stresses the series mode of propagation throughout the transformer winding. It is important to note that, due to the mutual couplings between all turns in the coil, any reflection would be automatically felt in all turns but with variant degrees. In addition, due to the impedance dicontinuites, not only at end of the coil, but at all section terminations (disc ends), the travelling wave would be reflected and refracted according to very well known rules thus causing variations in the voltage distributions of the turns at different instant of times. This is especially noticeable from the oscillatory behaviour of the voltage at the end of turn 8 (end of disc 1), with all the oscillations caused by the multiple reflections of the travelling wave from both ends of the section. To summarize, once the fast fronted surge reaches the transformer winding, it will propagate into the winding reaching the different turns at different instants of time with the travelling wave being reflected and refracted at all the impedance discontinuities, leading to variations with different magnitudes in the voltages of the different turns. This is what is known as the series mode of propagation.

Both parallel mode and series mode of propagation have a role in determining the interturn and interdisc voltges altough the series one is more dominant due to the fact that capacitive coupling only plays a significant role in the initial period of time. In relation to the interturn voltages, the series propagation of the travelling wave would cause the major peaks occuring in the interturn voltage distributions with the first two major peaks caused by the incident travelling wave and the

reflected wave, respectively. The separation of these peaks is proportional to the distance between the reflection point (impedance discontinuity) and the turn across which the voltage is being monitored. Accordingly, these two major peaks are expected to combine at the turn which is directly connected to the reflection point leading to a major peak with an even higher amplitude and this could be clearly seen from the interturn voltage distribution between turns 7-8 and 15-16 (as also illustrated in the maximum interturn voltages plot). It should be noticed, that the first major peak would occur delayed further and further in time as we go down the winding due to the time required by the travelling wave to travel through the winding itself. Furthermore, the amplitude of interturn voltages decreases towards the inside of the winding due to the attenuation in both magnitude and duration of the surge wavefront during propagation through the different turns. Hence, the general behaviour of the interturn voltages could be simply described from two simple facts, the decrease in magnitude and increase in time delay as the wave travels down the winding. It is very important to mention that the distribution of the interturn voltages is non-linear within each disc as it could be seen from the plot for the maximum interturn voltages.

As far as the interdisc voltages are concerned, their behaviour could be explained in the same way as the interturn voltages except that their magnitude is a lot higher (almost 35%) in comparison with the interturn voltages (almost 6%). In addition, no second major peak could be identified since the reflection of the bottom end of the coil would not reach the sections of interest within the scope of the observation time considered. Moreover, the highest interdisc voltage between consecutive discs is almost constant as we go down the winding as it could be seen from the maximum interdisc voltages plot which also shows that, in contrast to interturn volatges, the distribution in interdisc voltages is almost linear when dealing with two consecutive discs at once.

From what has been said so far, it is clear that the surge distribution is a very complex phenomena of series propagation, mutual and capacitive couplings.

From fig 4.17, the close agreement between computational and experimental results is clearly noticeable. The waveshapes of the different turn voltage distributions in the first disc and at the outer junctions of the adjacent discs have exactly the same trend in both the computational and experimental results although there exists a small difference in magnitude within acceptable limits of 10% of the incoming wave. This close agreement is also noticeable in both the interturn and interdisc voltages with the magnitude of the different corresponding major peaks, which could endanger insulation, within very much acceptable limits. However, in the case of inturturn voltge across the first turn of the line-end disc, an exceptionally high oscillation occuring only at the very begining of the observation time (first 10 nsec) was obtained in the experimental work, with a reasonably higher magnitude than the other peaks and whose reason could not be explained.

Furthermore, the accuracy of the computer model was confirmed for different risetimes of the wavefront of the excitation function. The comparison for risetimes of 30 nsec, 120 nsec and 240 nsec is represented in fig 4.18 to fig 4.20.

Having confirmed the accuracy of the computer model to represent the response of the top discs of the transformer high voltage winding to very steep fronted surges in the first 512 nsec after surge arrival, it would be appropriate to show the input impedance of such a model. Such input impedance could be connected to transformer terminals (one element representation of the transformer winding) when studying the nature of fast fronted switching transients in GIS systems. The input impedance of the model was calculated by using the concept of input admittance (element D(1,1) in equation 3.36) and is shown in fig 4.21.

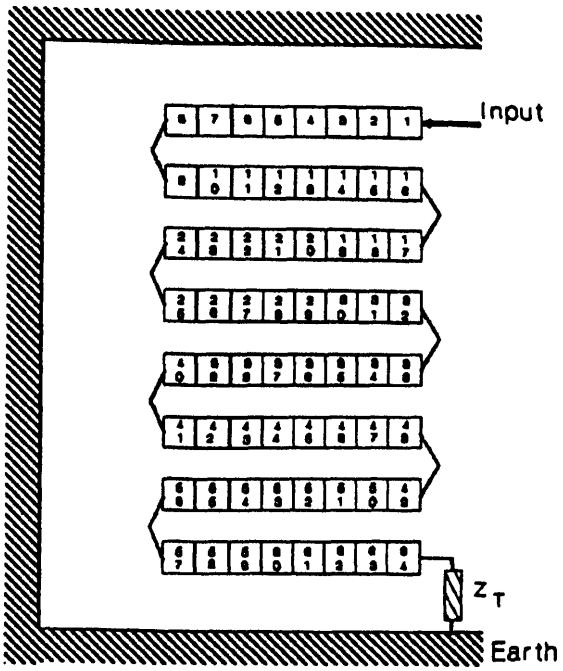

a)

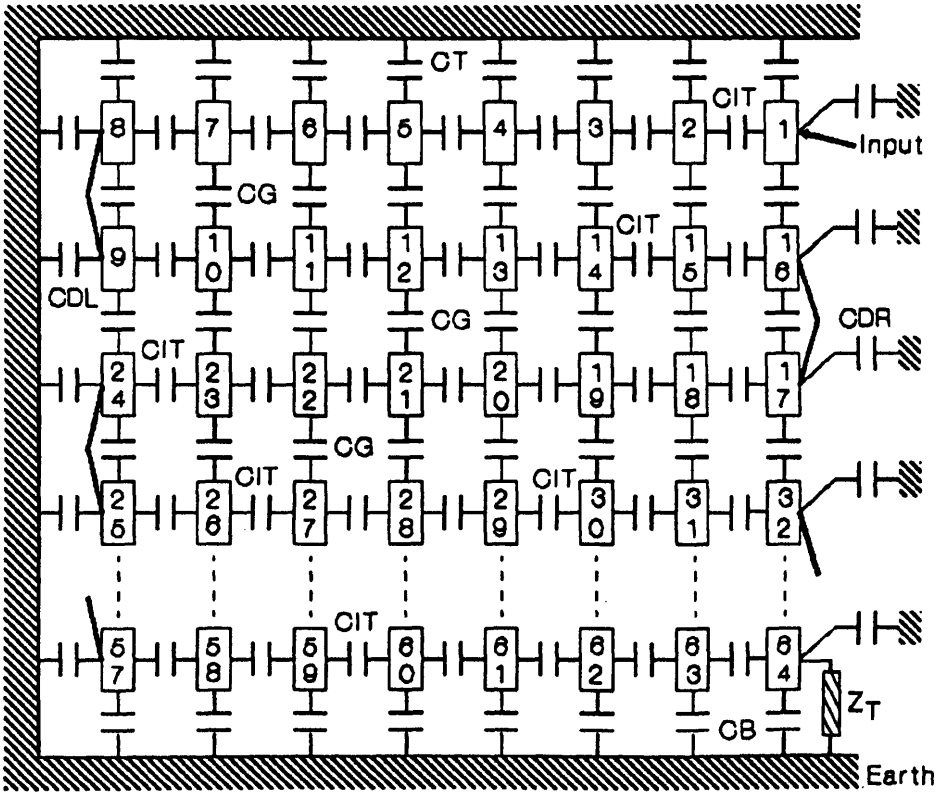

b)

Fig 4.15 Eight-section model of conventional winding

a) Configuration

b) Capacitance equivalent circuit

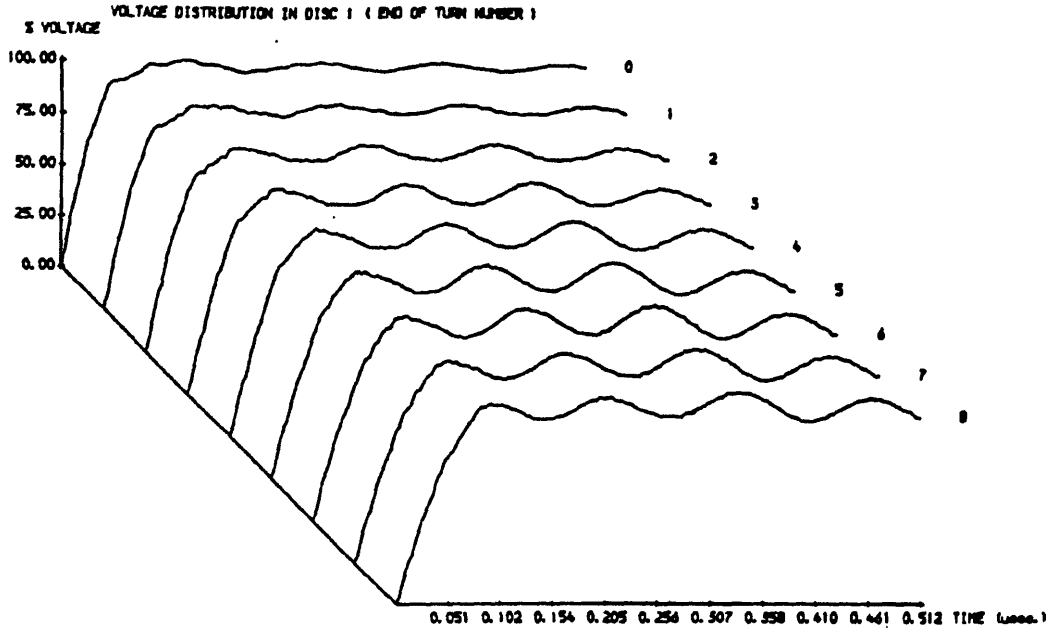

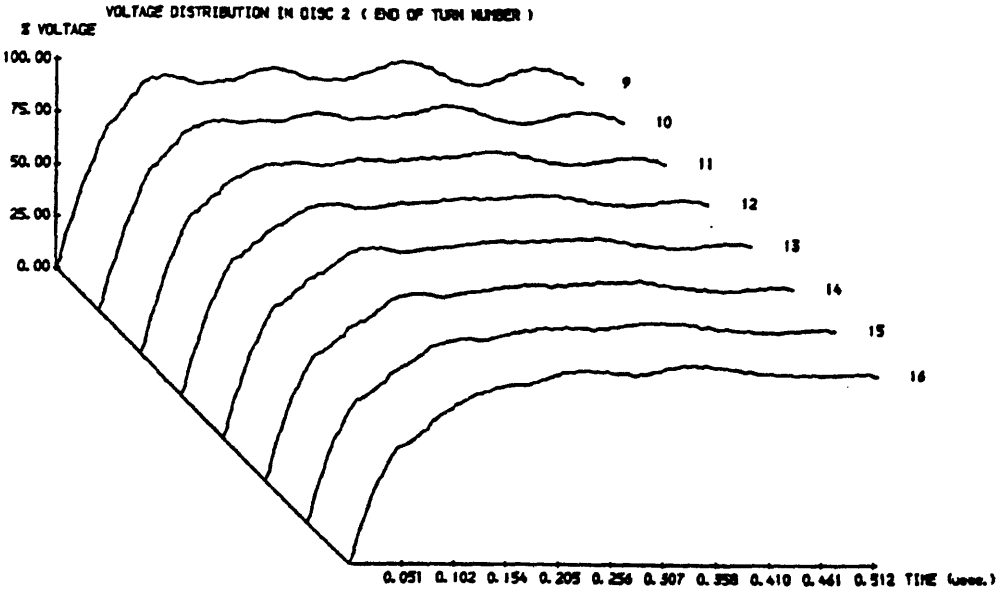

Fig 4.16 Computational results of eight-section model of conventional winding (risetime of the excitation function = 60 nsec) : turn to ground voltages

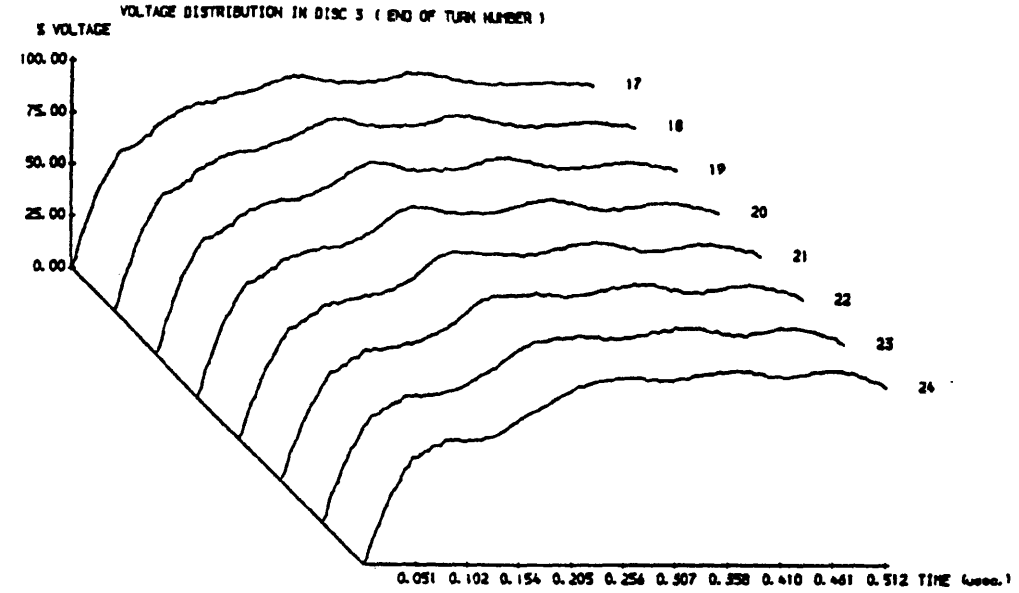

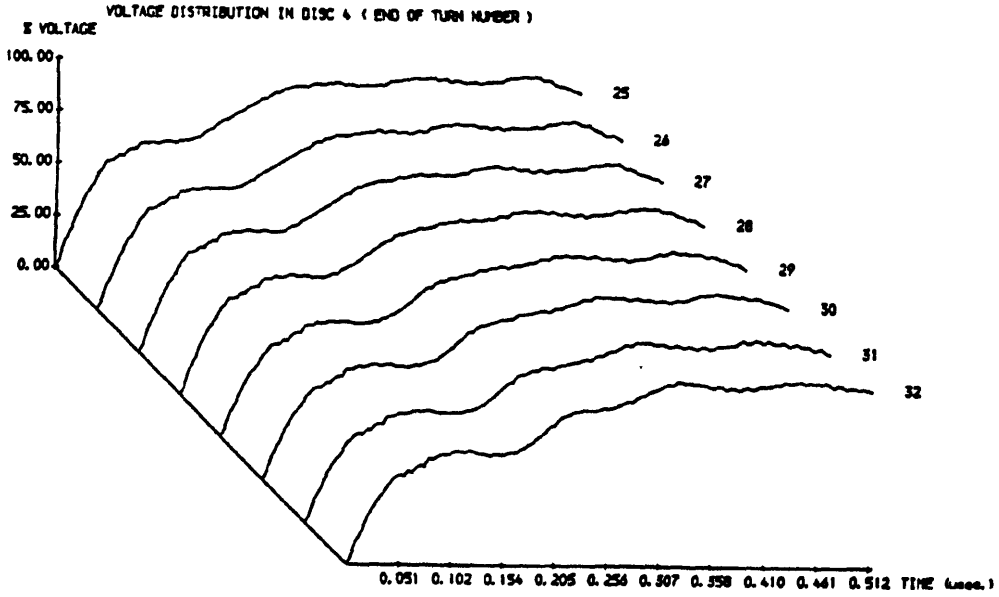

Fig 4.16 Computational results of eight-section model of conventional winding (risetime of the excitation function = 60 nsec) : turn to ground voltages

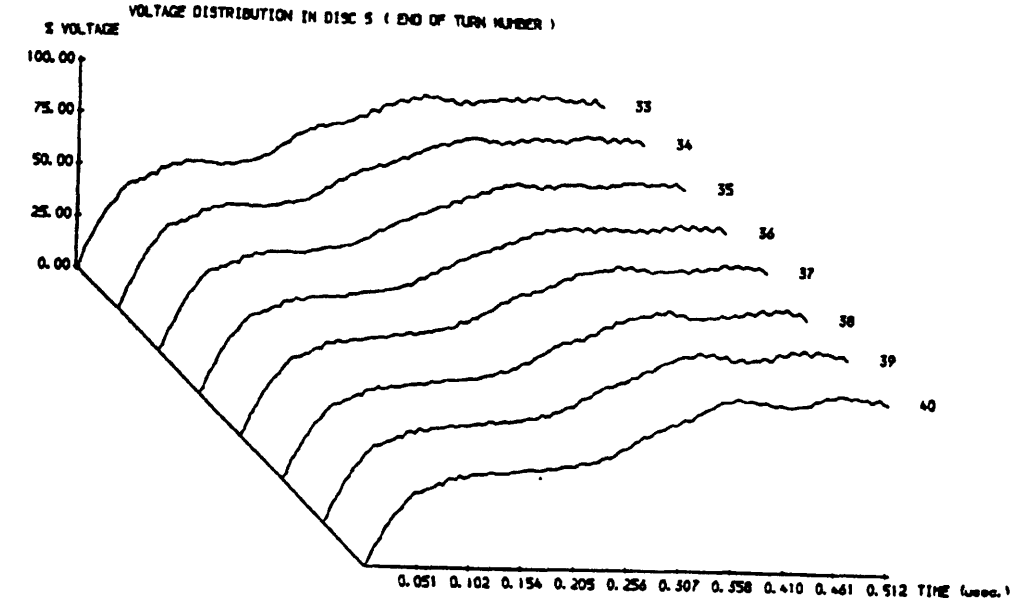

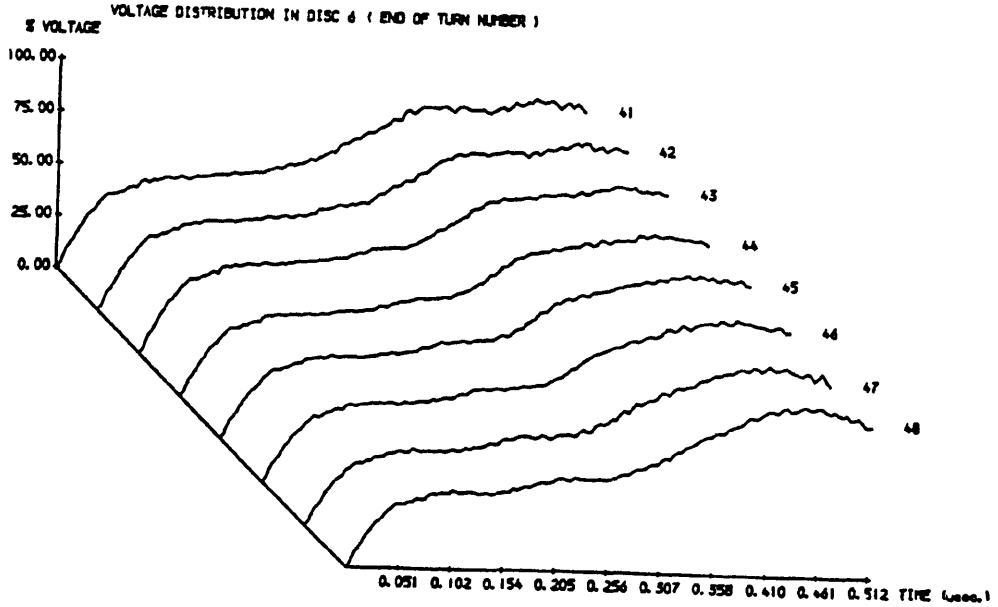

Fig 4.16 Computational results of eight-section model of conventional winding (risetime of the excitation function = 60 nsec) : turn to ground voltages

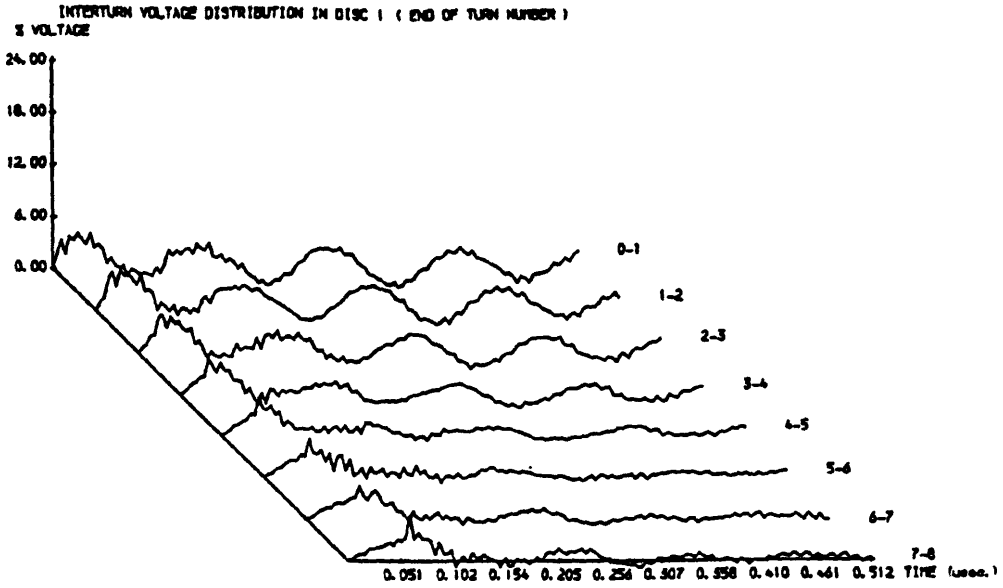

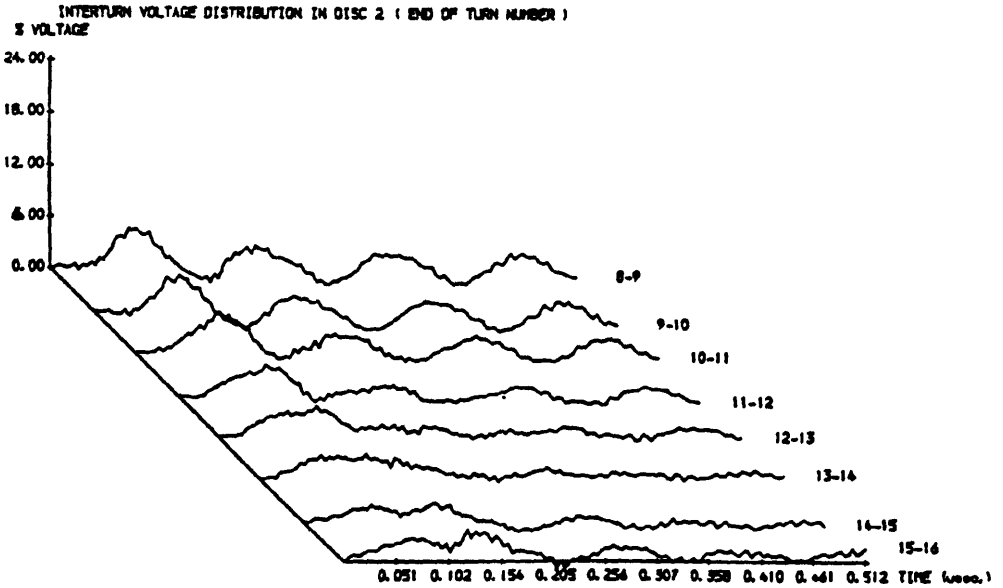

Fig 4.16 Computational results of eight-section model of conventional winding (risetime of the excitation function = 60 nsec) : voltages between turns

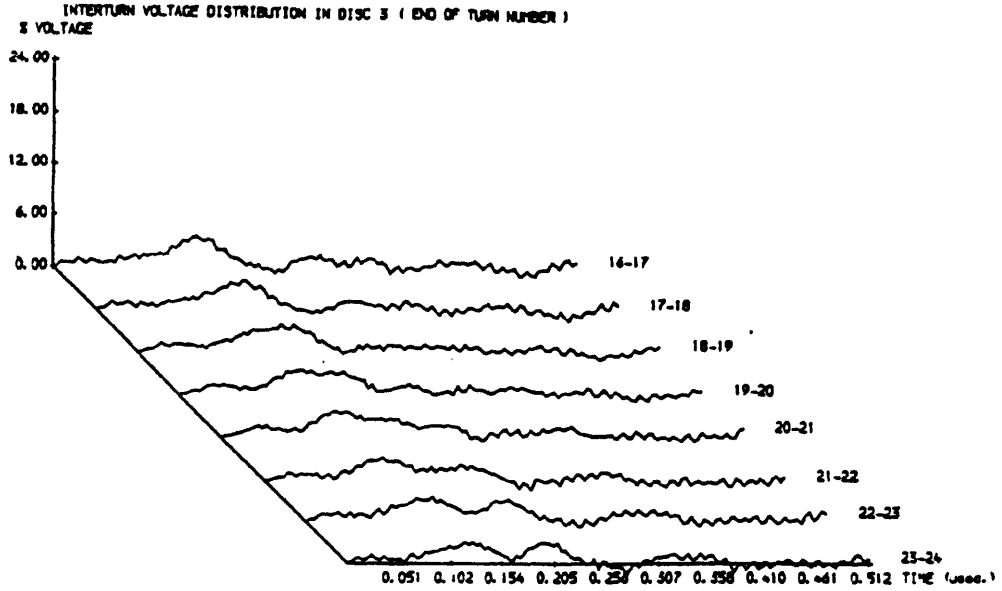

Fig 4.16 Computational results of eight-section model of conventional winding (risetime of the excitation function = 60 nsec) : voltages between turns

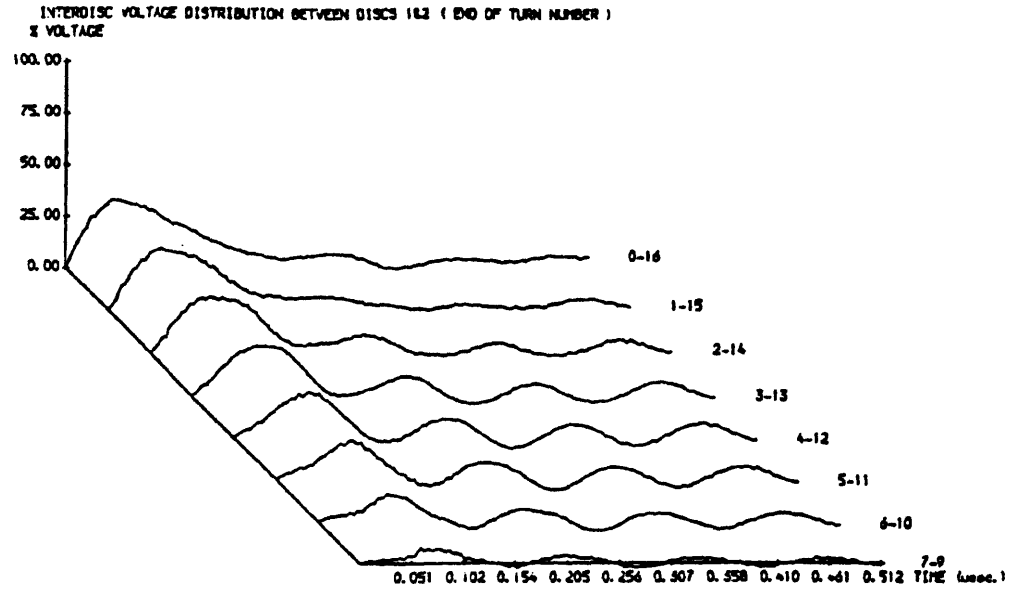

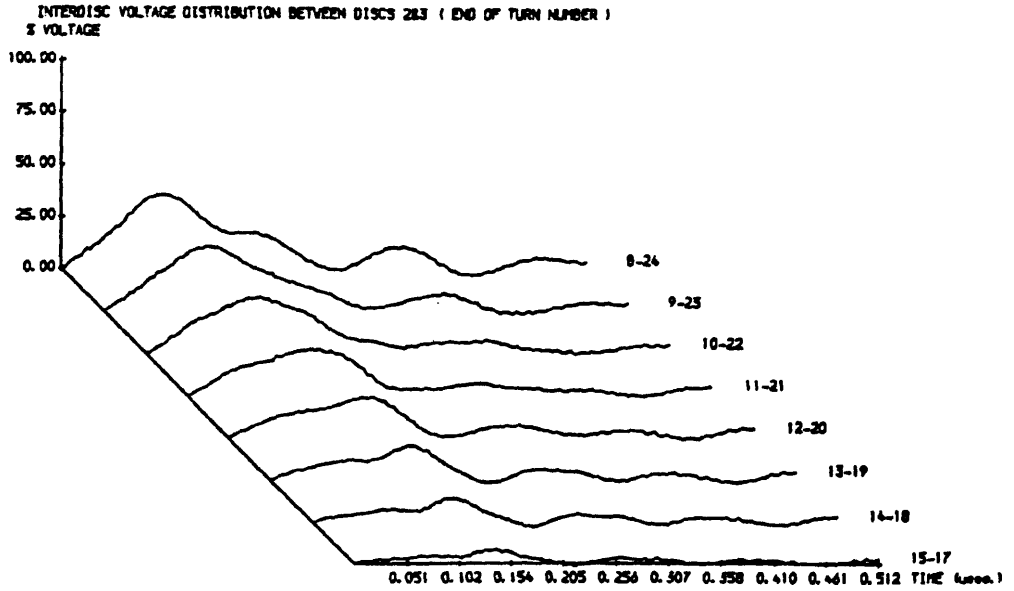

Fig 4.16 Computational results of eight-section model of conventional winding (risetime of the excitation function = 60 nsec) : voltages between turns

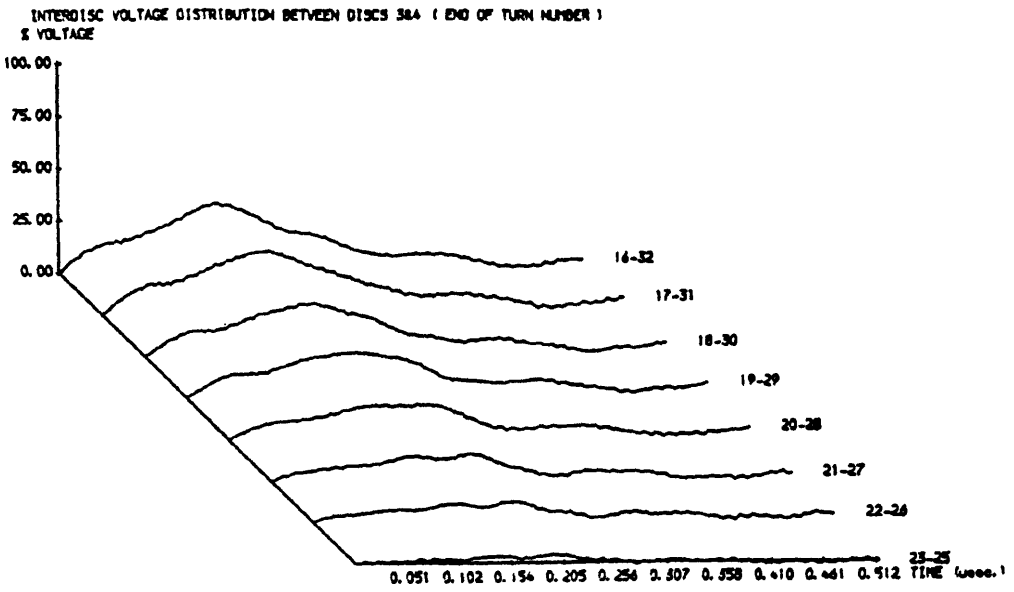

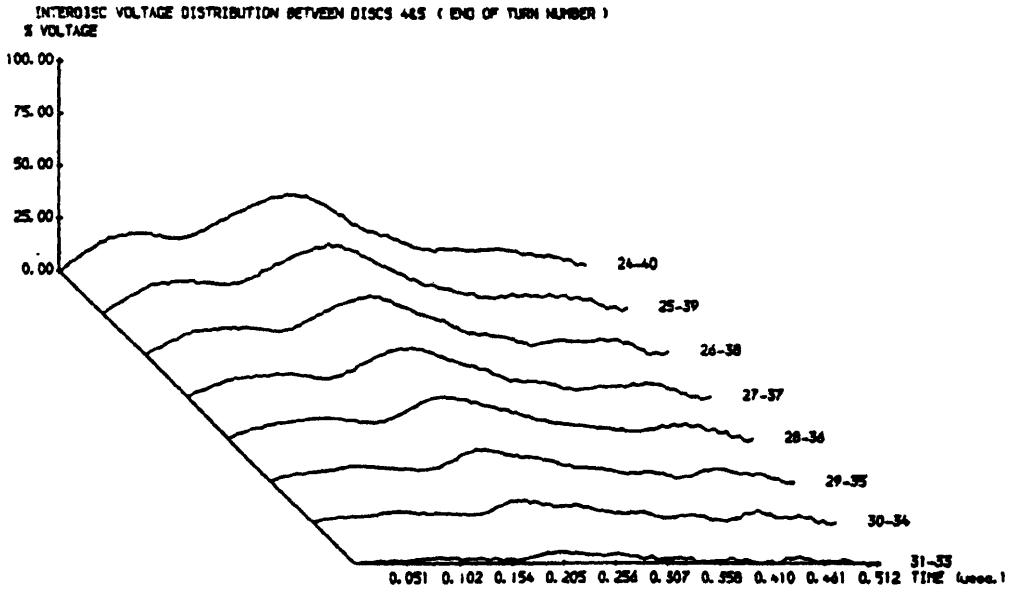

Fig 4.16 Computational results of eight-section model of conventional winding (risetime of the excitation function = 60 nsec) : voltages between turns

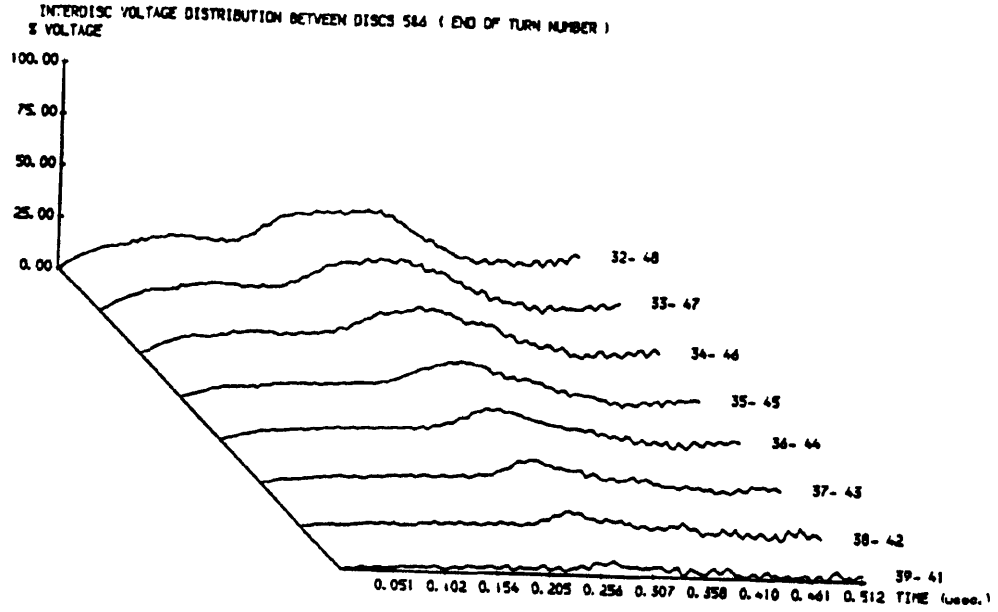

Fig 4.16 Computational results of eight-section model of conventional winding (risetime of the excitation function = 60 nsec) : voltages between turns

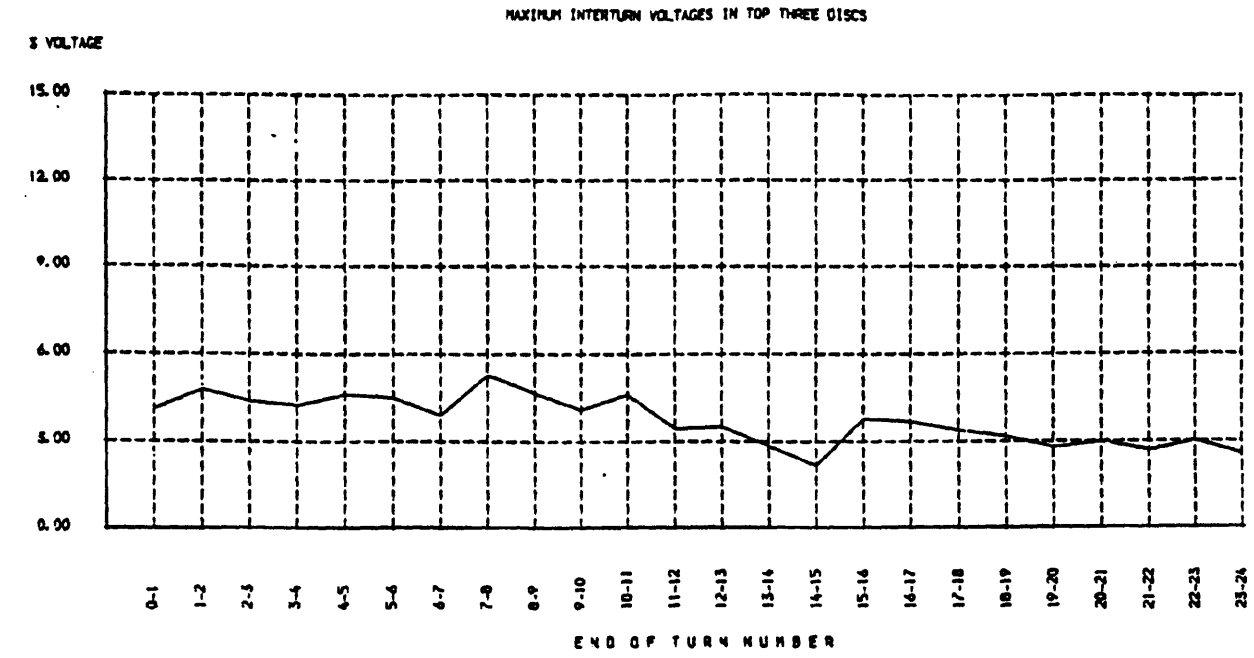

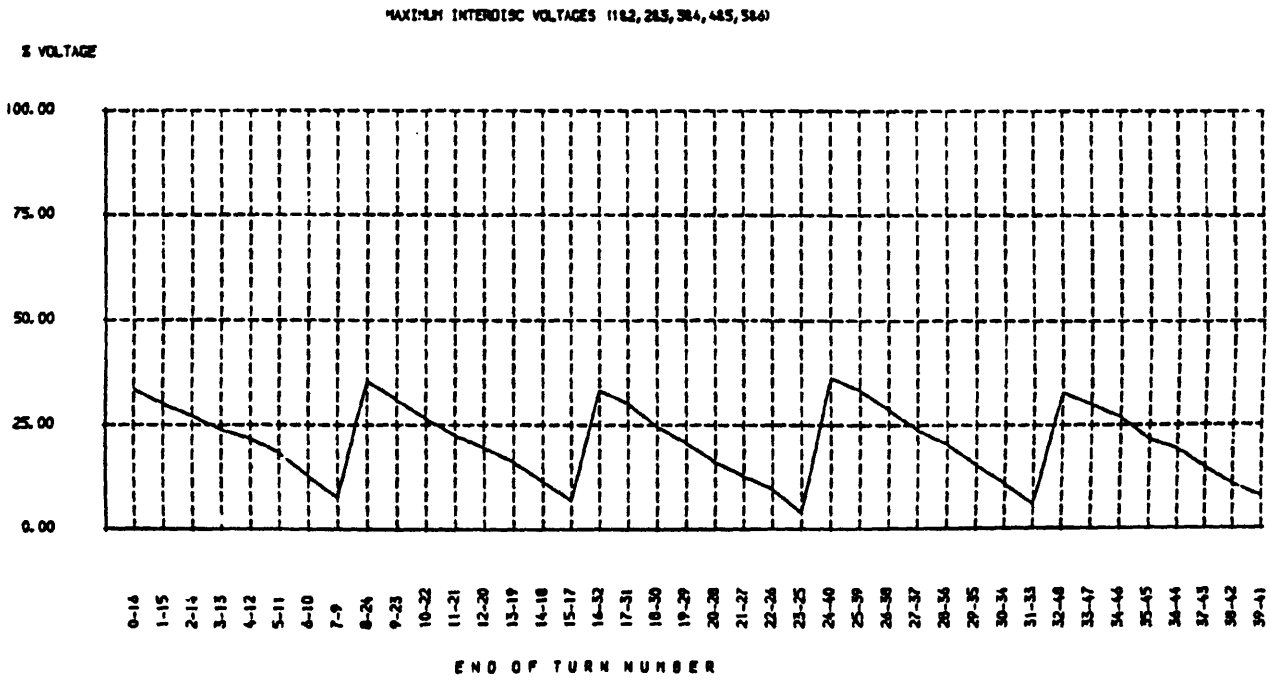

Fig 4.16 Computational results of eight-section model of conventional winding (risetime of the excitation function = 60 nsec) : maximum voltages between turns

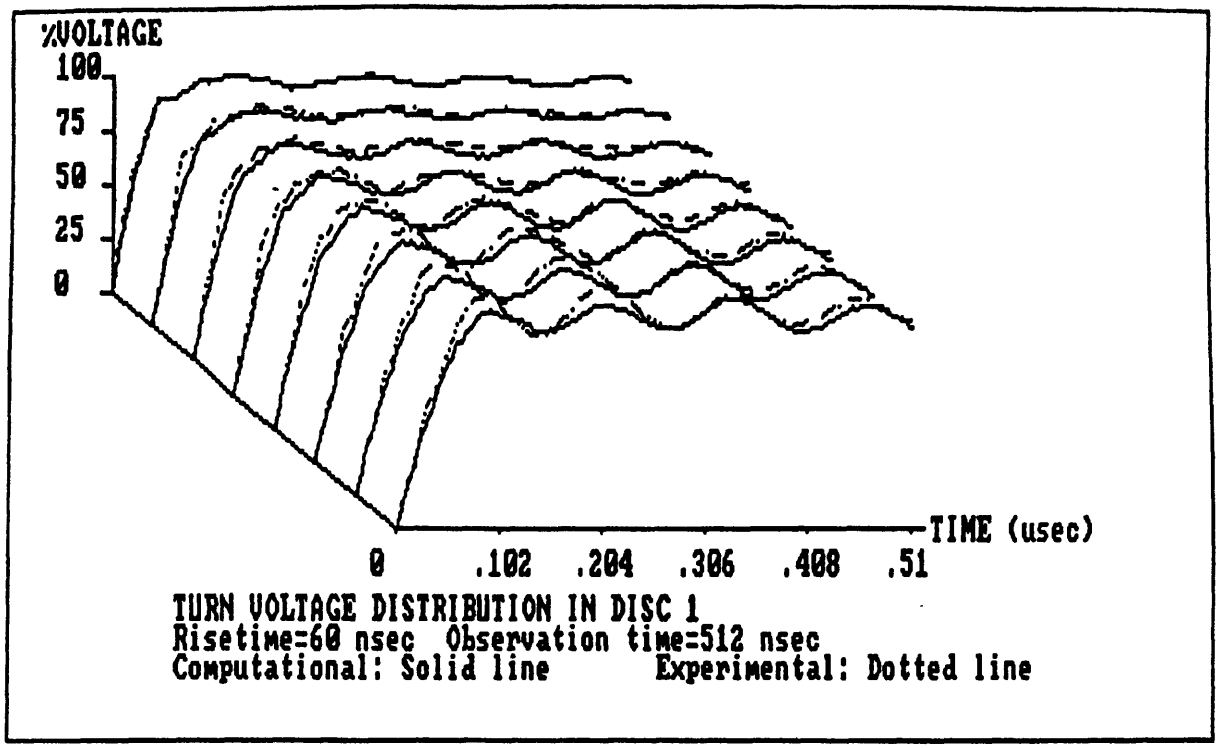

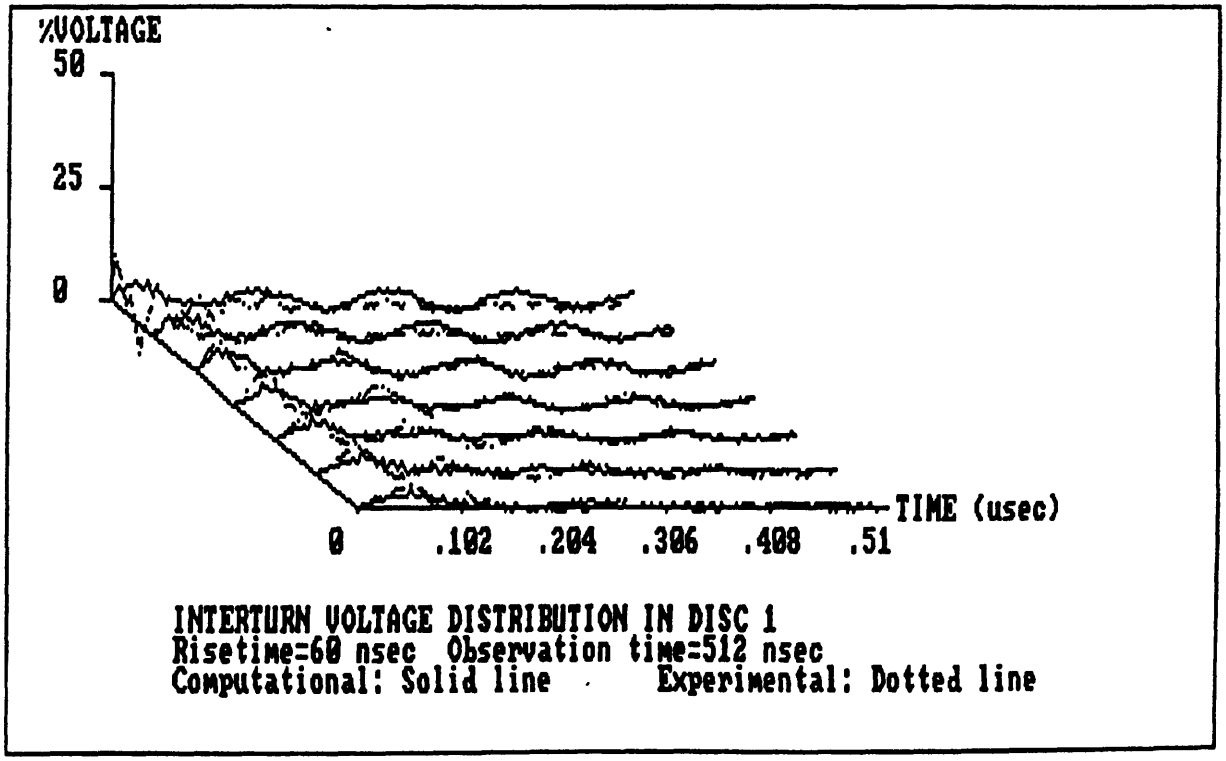

Fig 4.17 Comparison between computational and experimental results
Risetime of the excitation function = 60 nsec

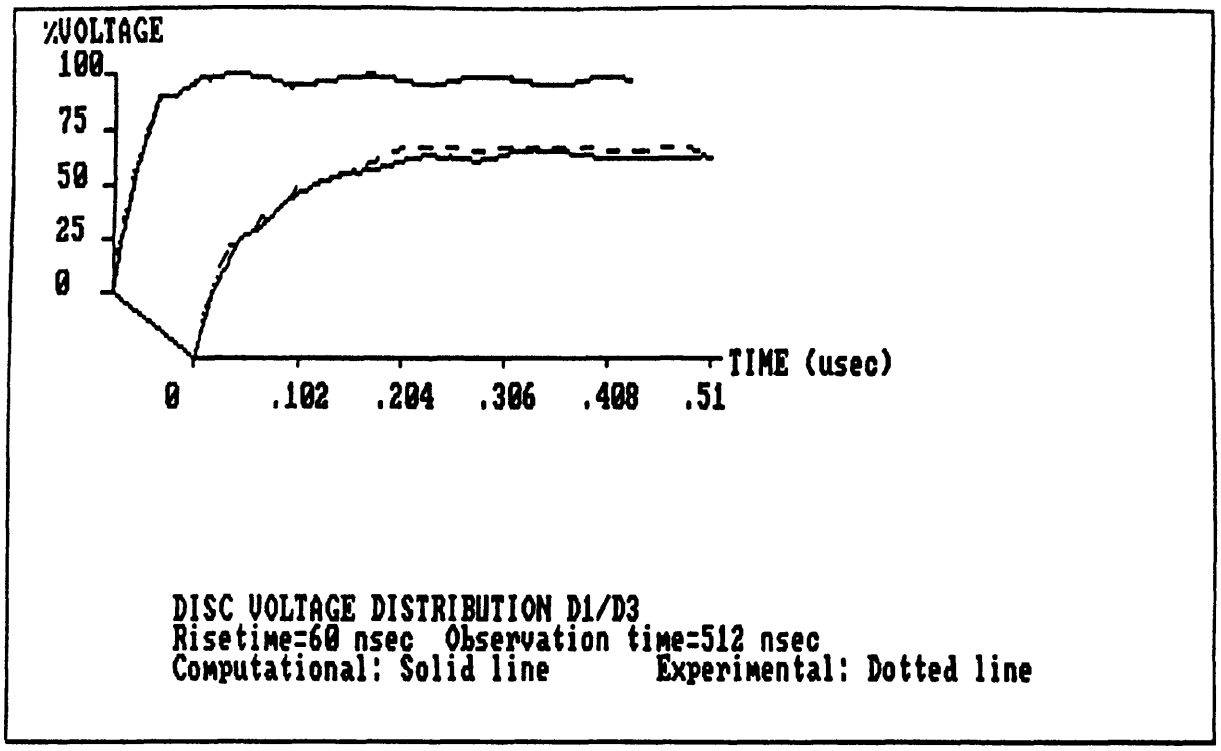

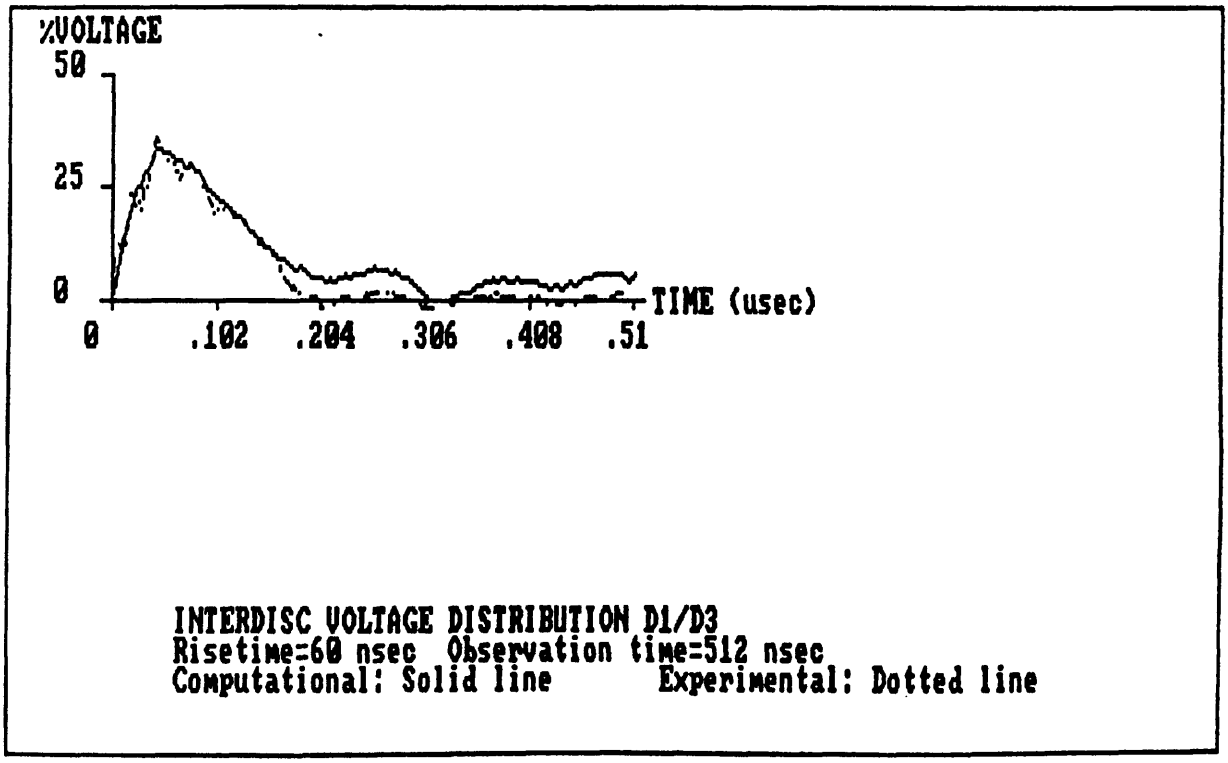

Fig 4.17 Comparison between computational and experimental results
Risetime of the excitation function = 60 nsec

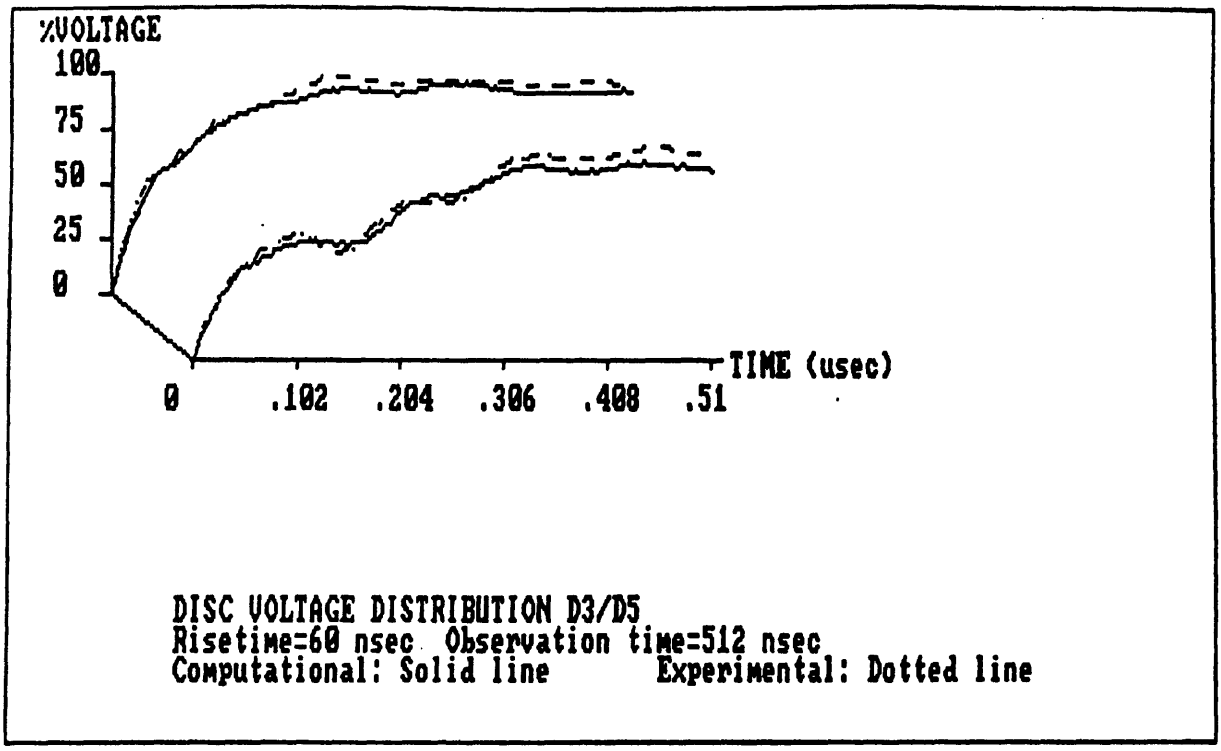

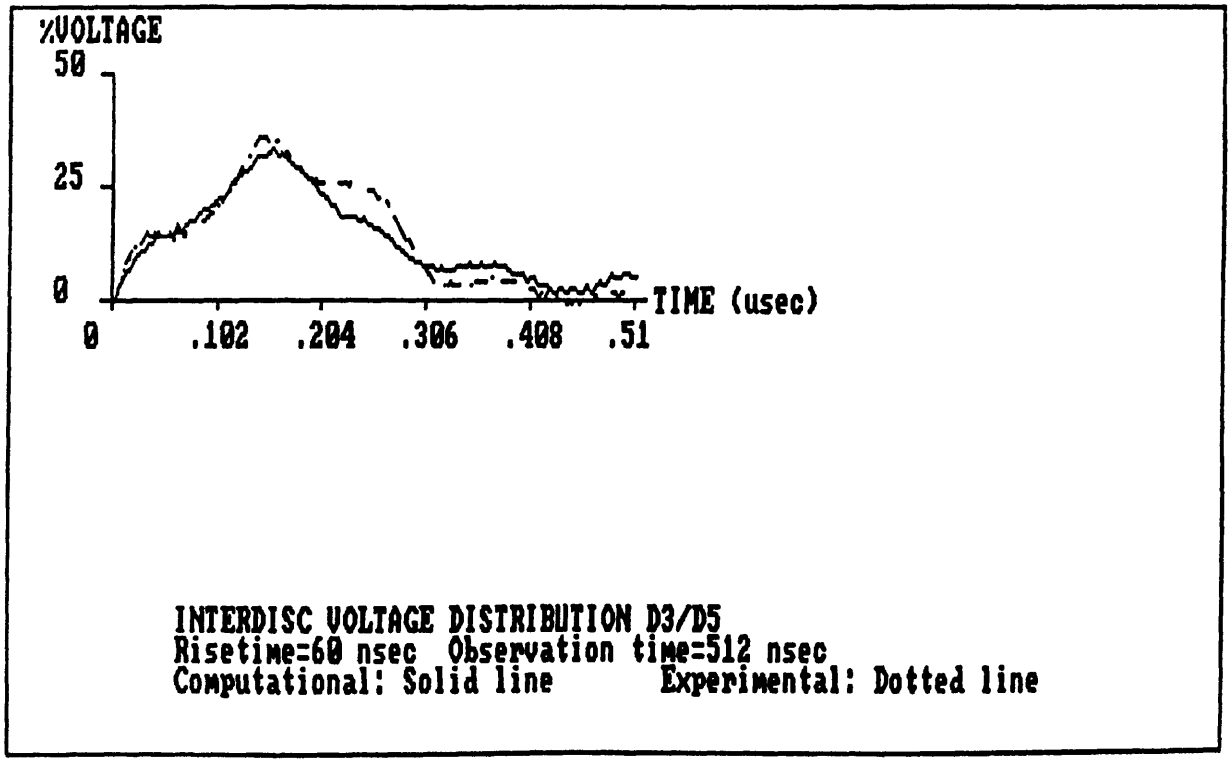

Fig 4.17 Comparison between computational and experimental results
Risetime of the excitation function = 60 nsec

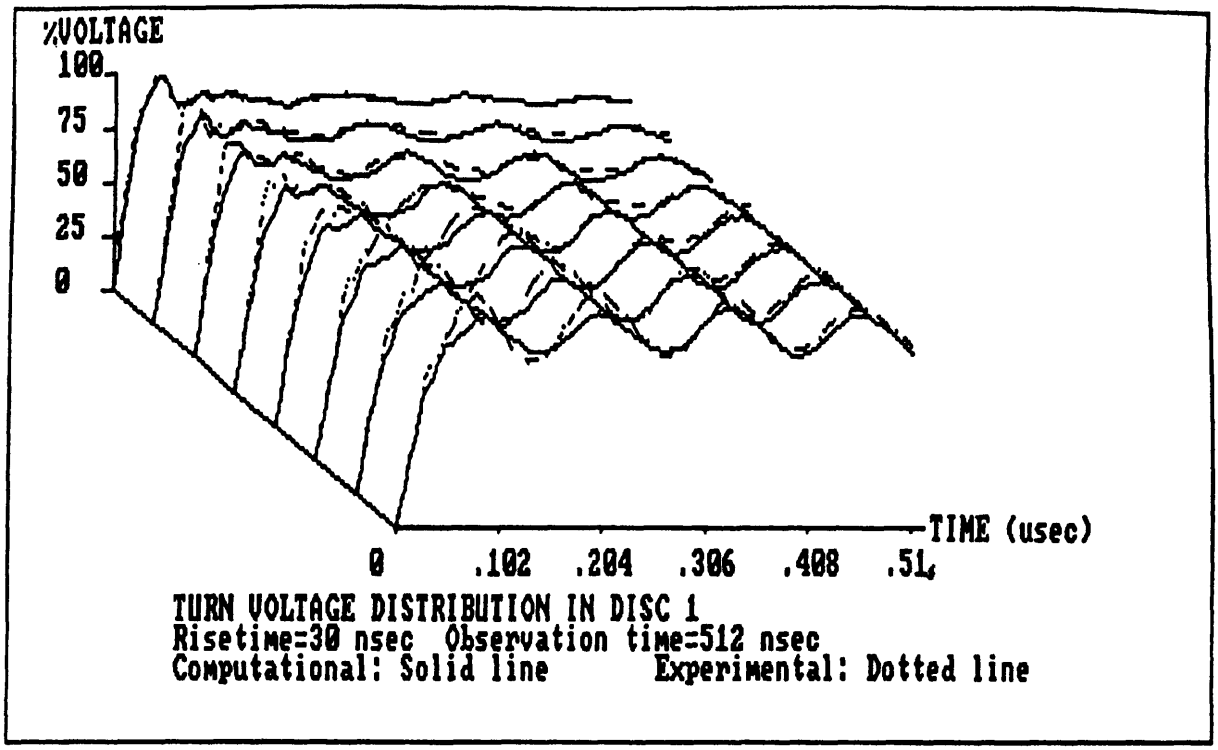

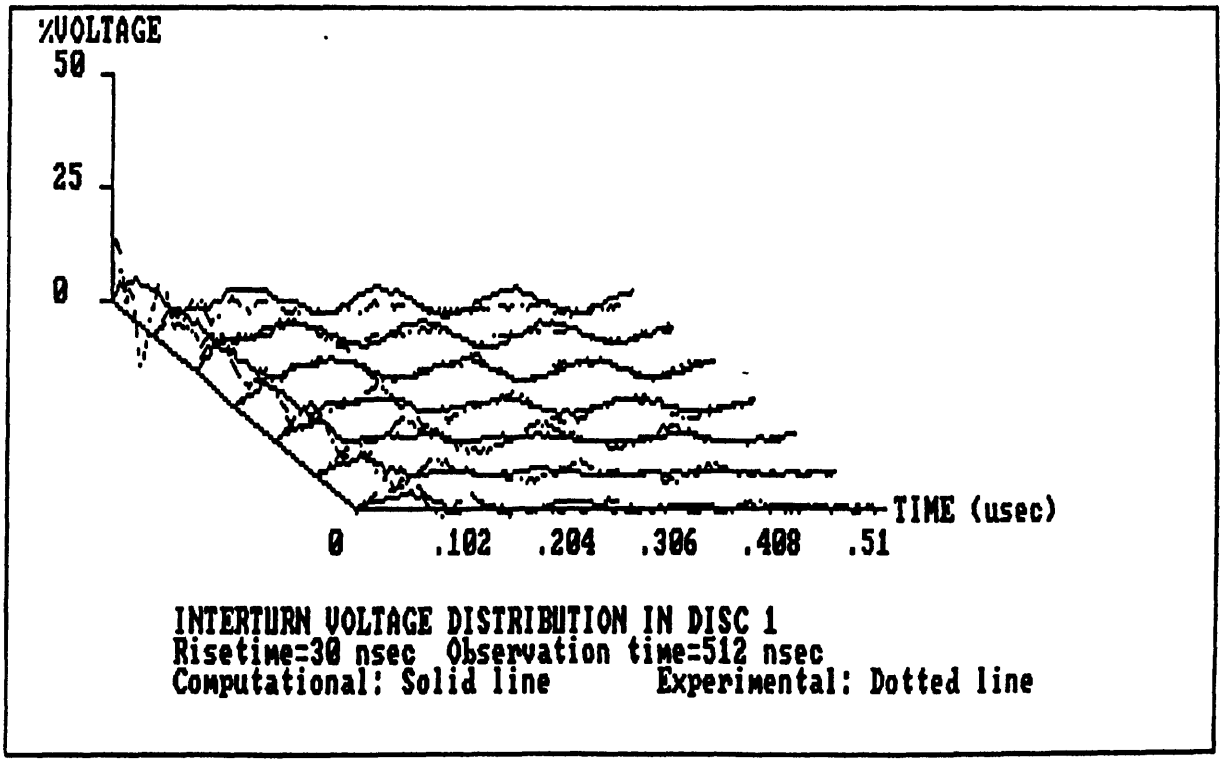

Fig 4.18 Comparison between computational and experimental results
Risetime of the excitation function = 30 nsec

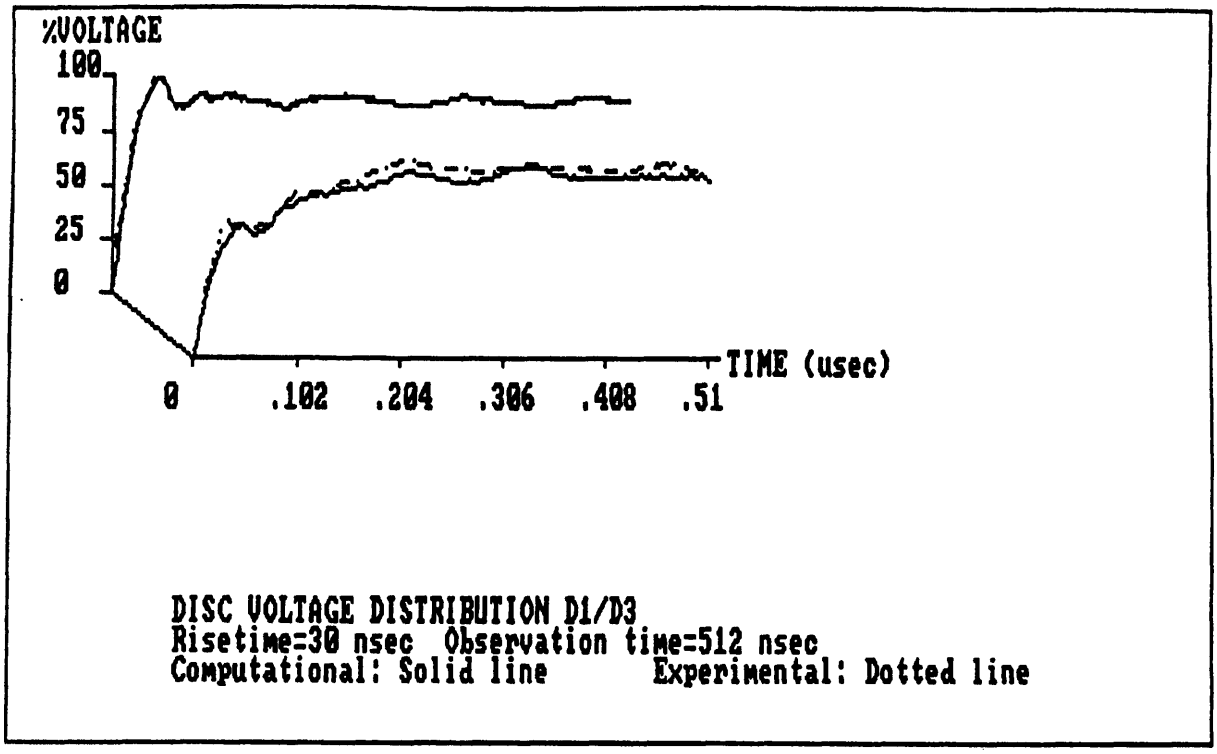

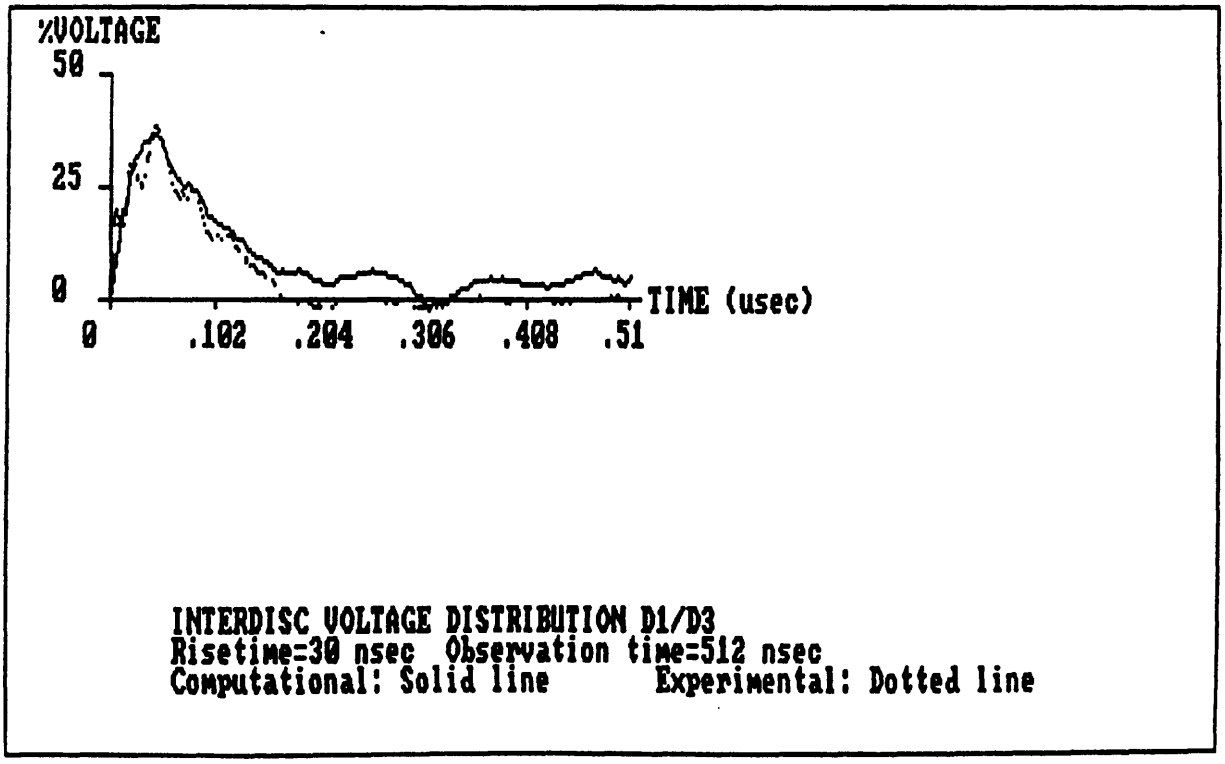

Fig 4.18 Comparison between computational and experimental results
Risetime of the excitation function = 30 nsec

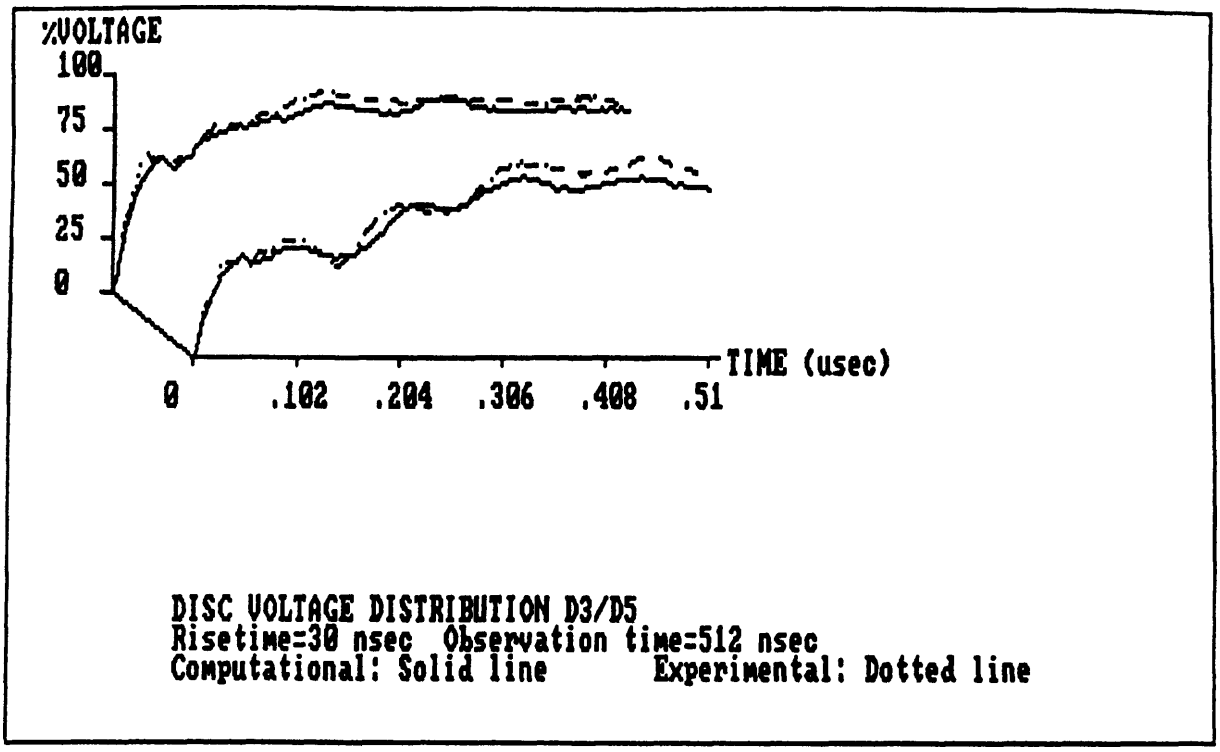

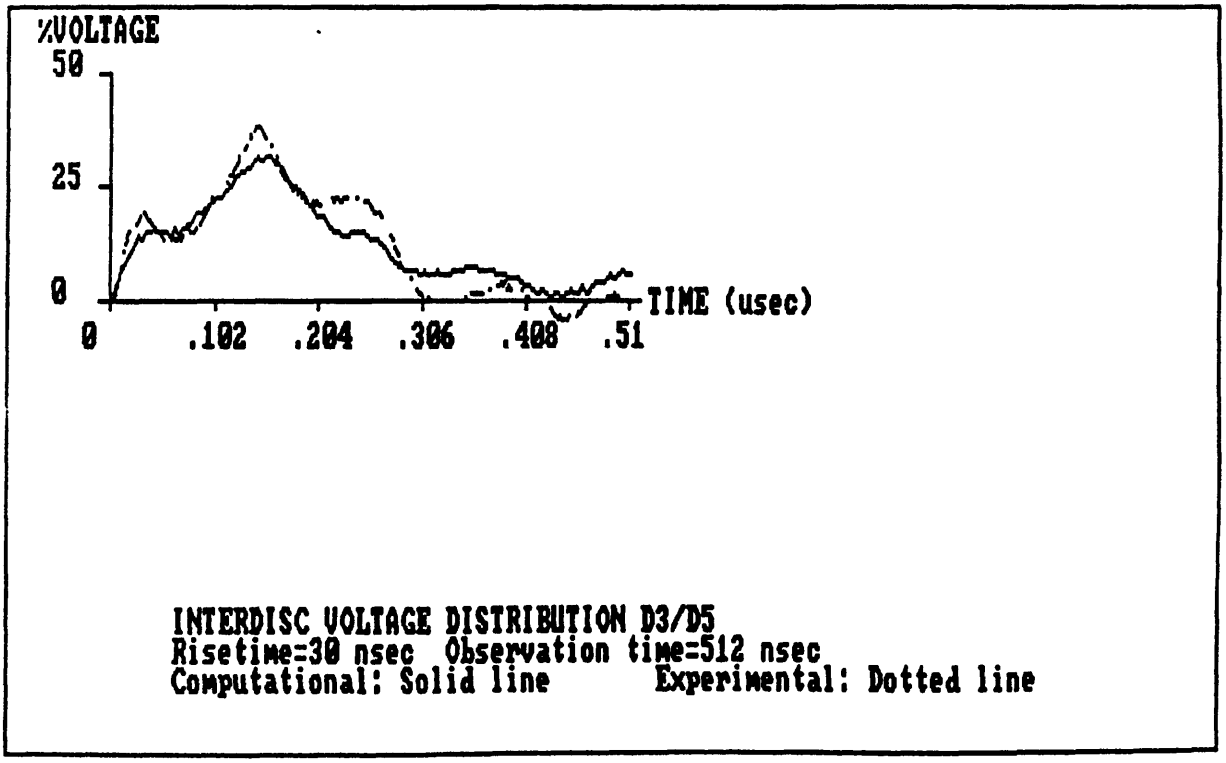

Fig 4.18 Comparison between computational and experimental results
Risetime of the excitation function = 30 nsec

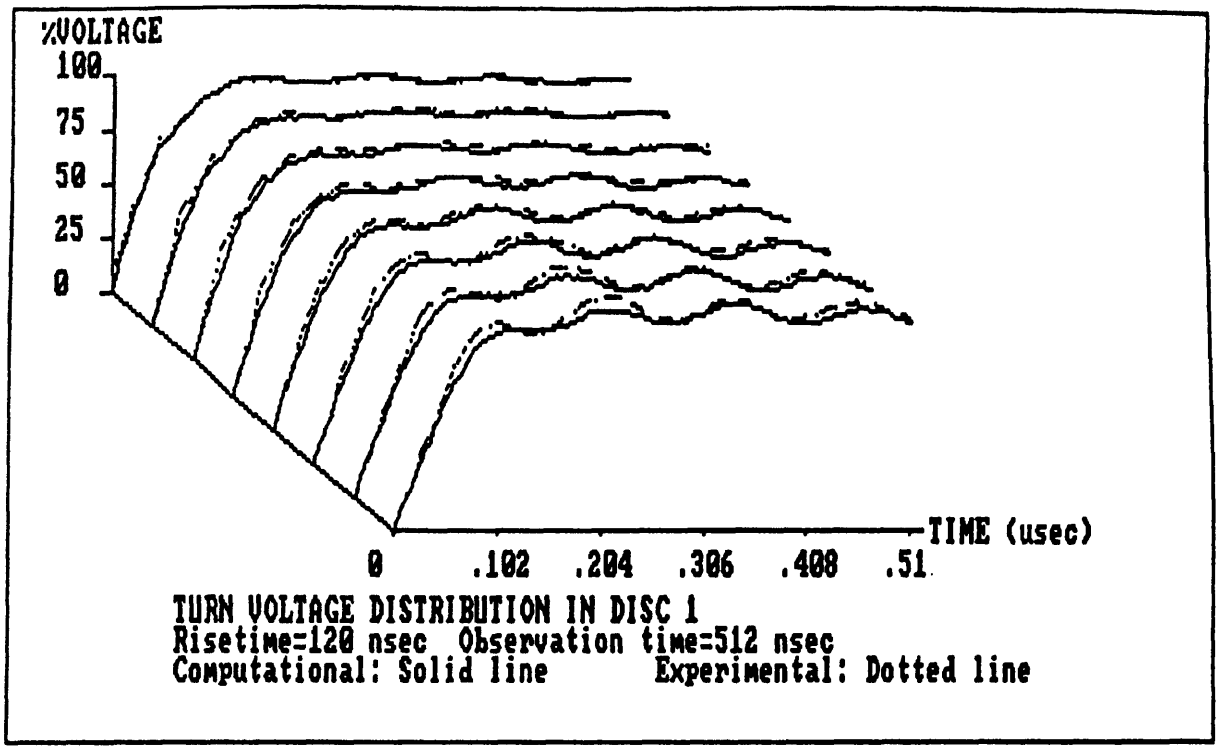

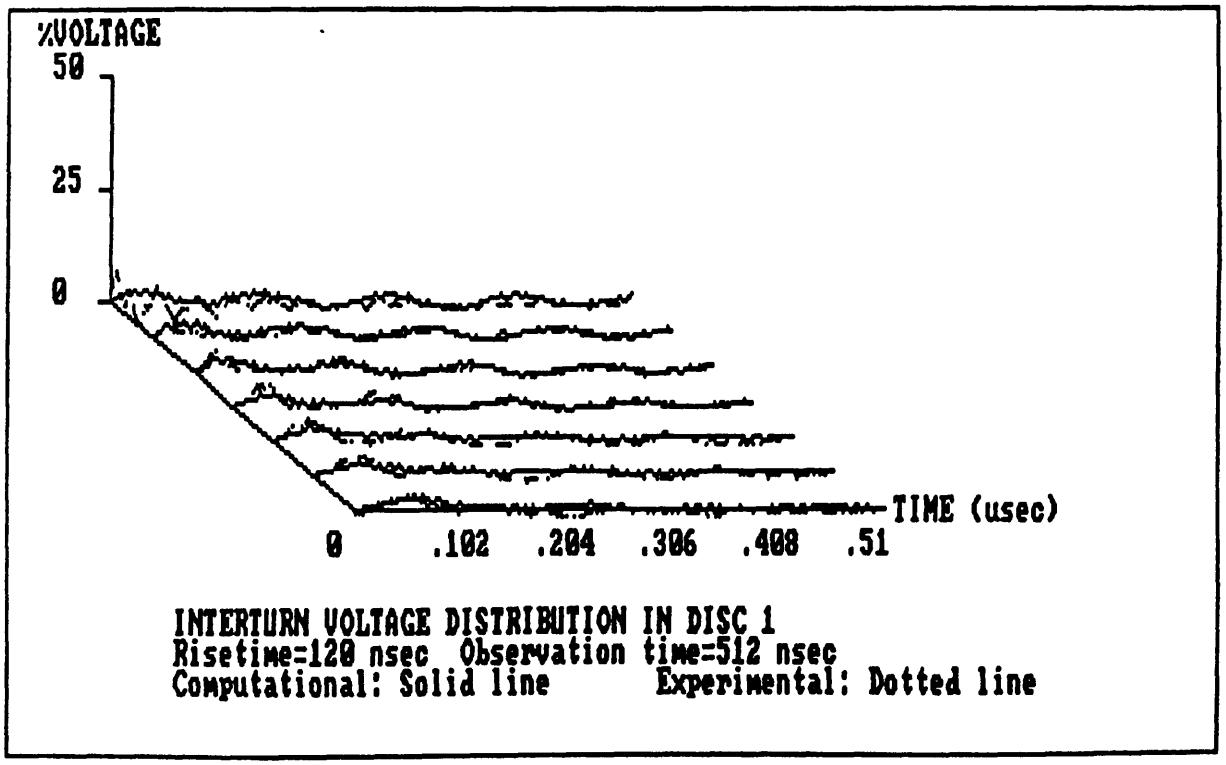

Fig 4.19 Comparison between computational and experimental results
Risetime of the excitation function = 120 nsec

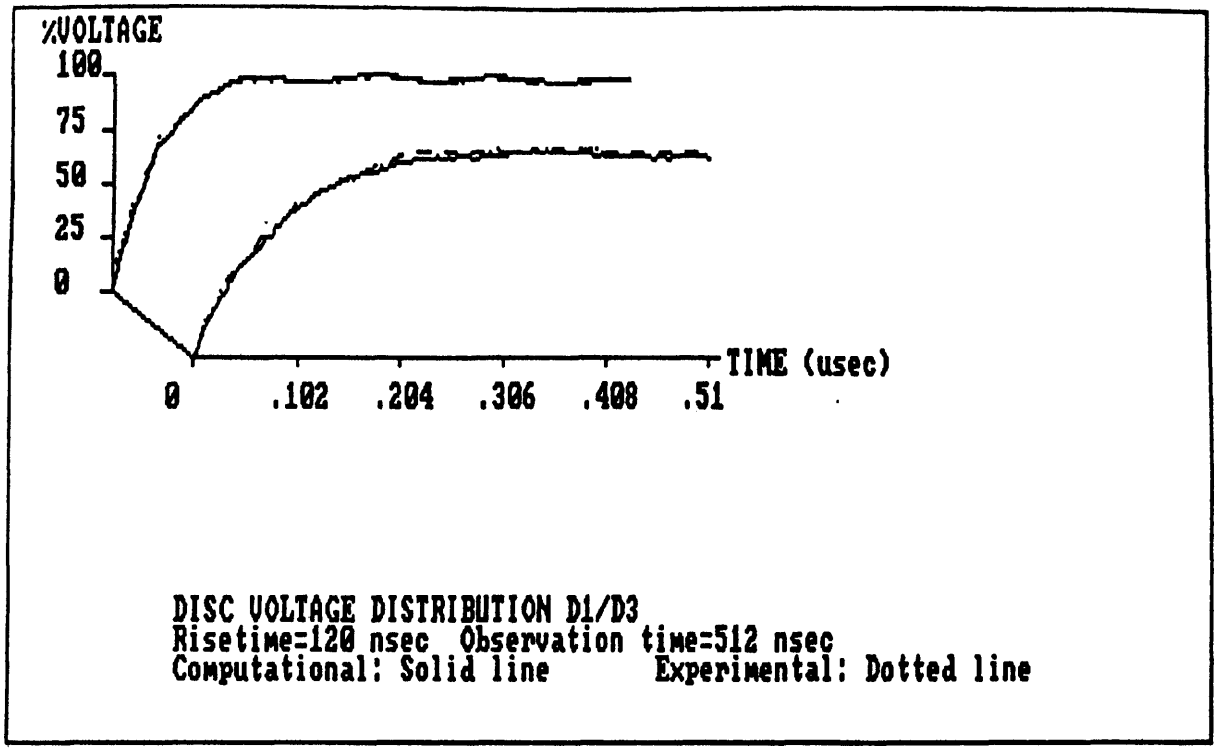

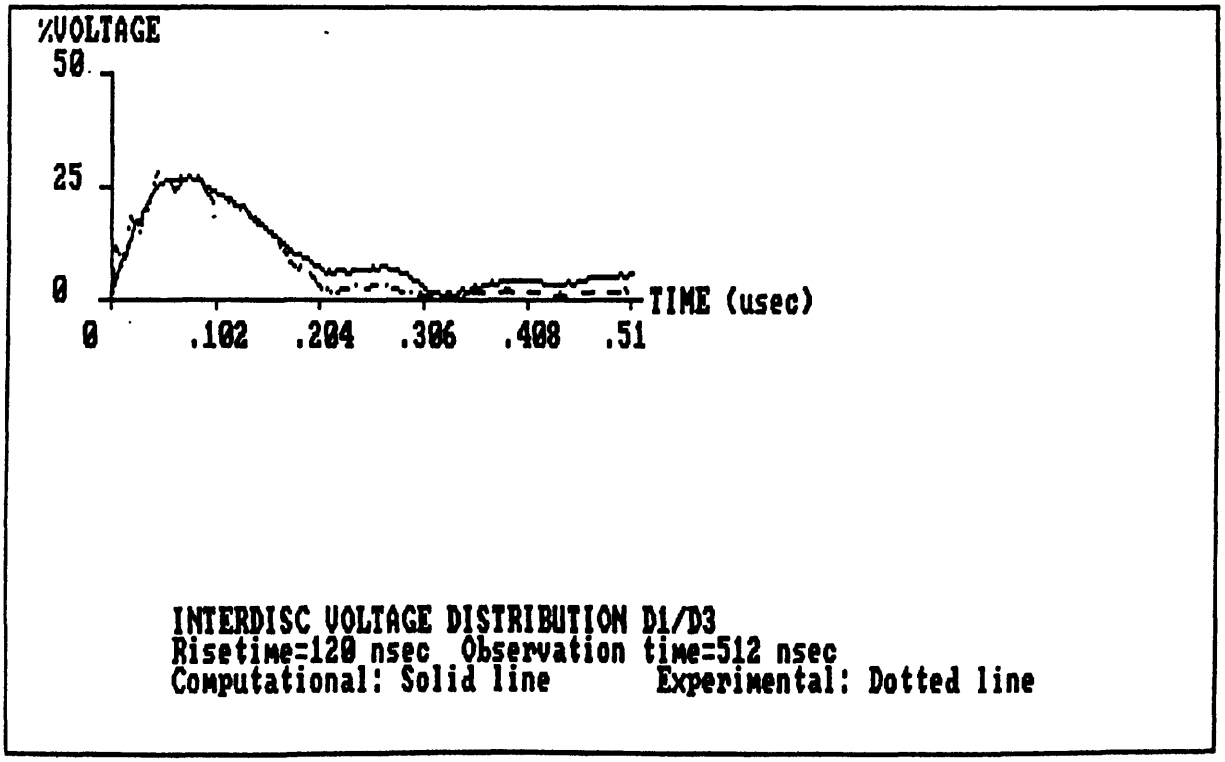

Fig 4.19 Comparison between computational and experimental results
Risetime of the excitation function = 120 nsec

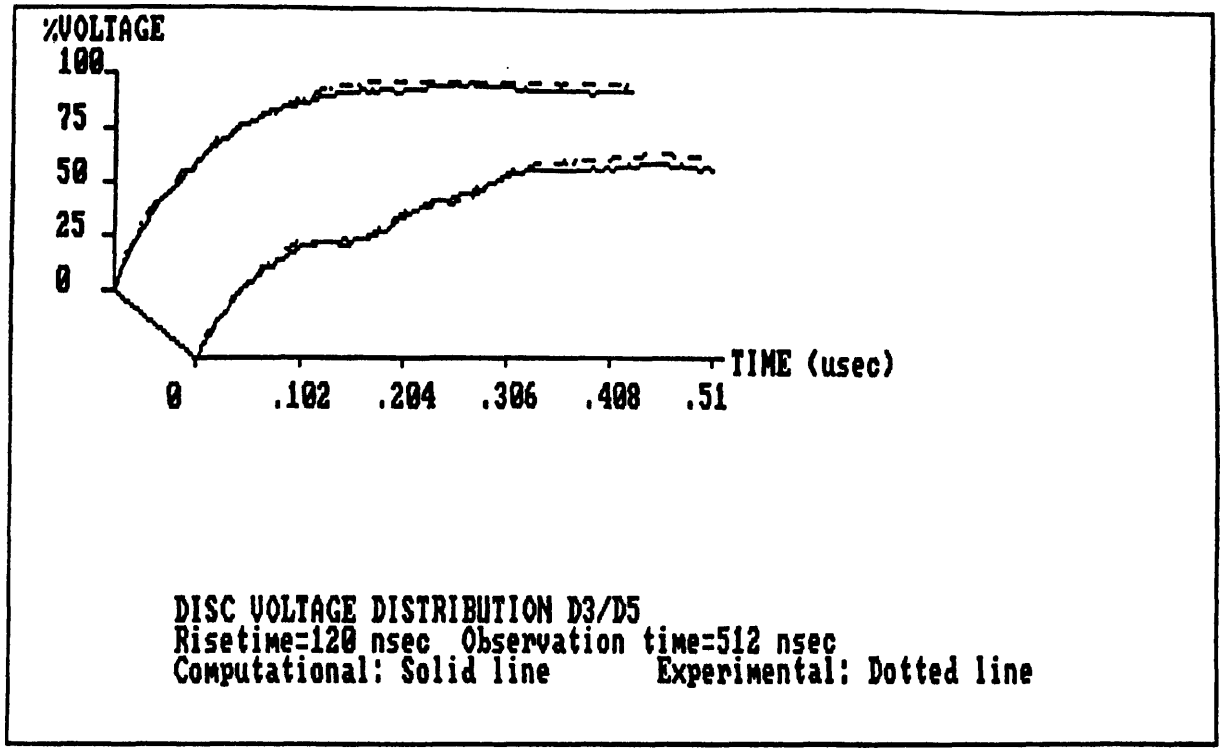

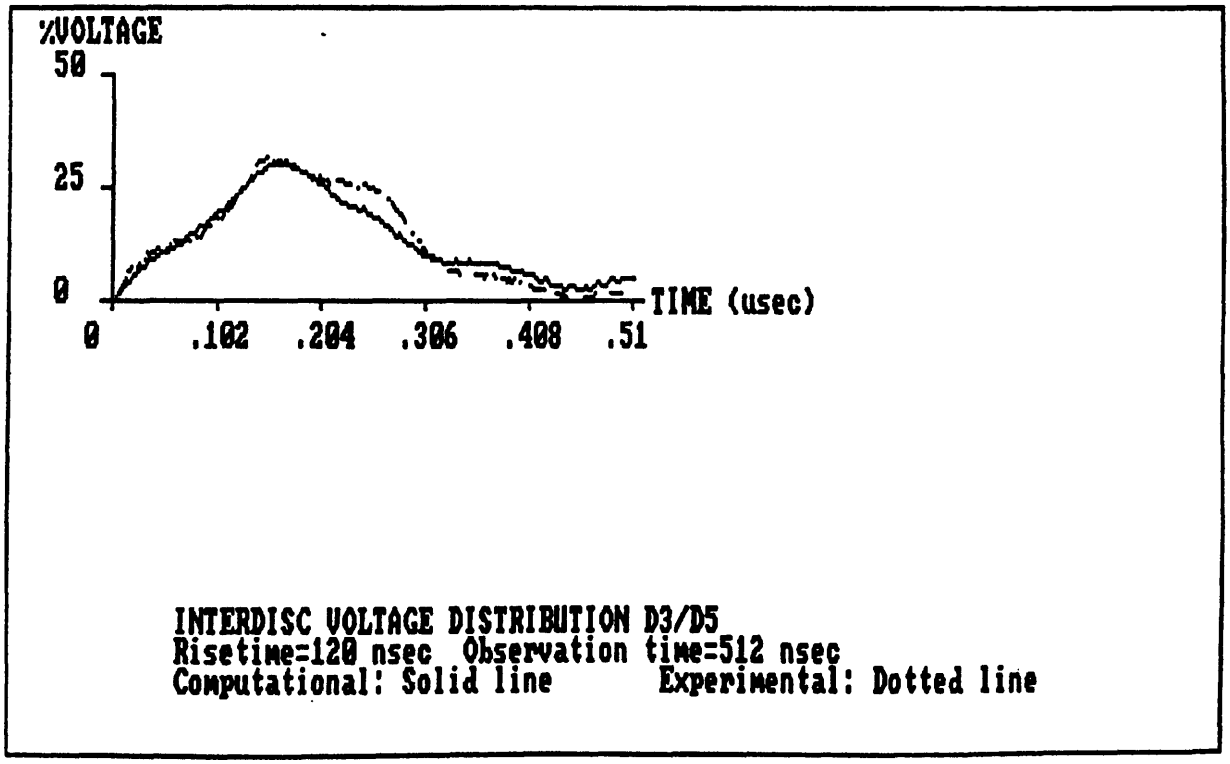

Fig 4.19 Comparison between computational and experimental results
Risetime of the excitation function = 120 nsec

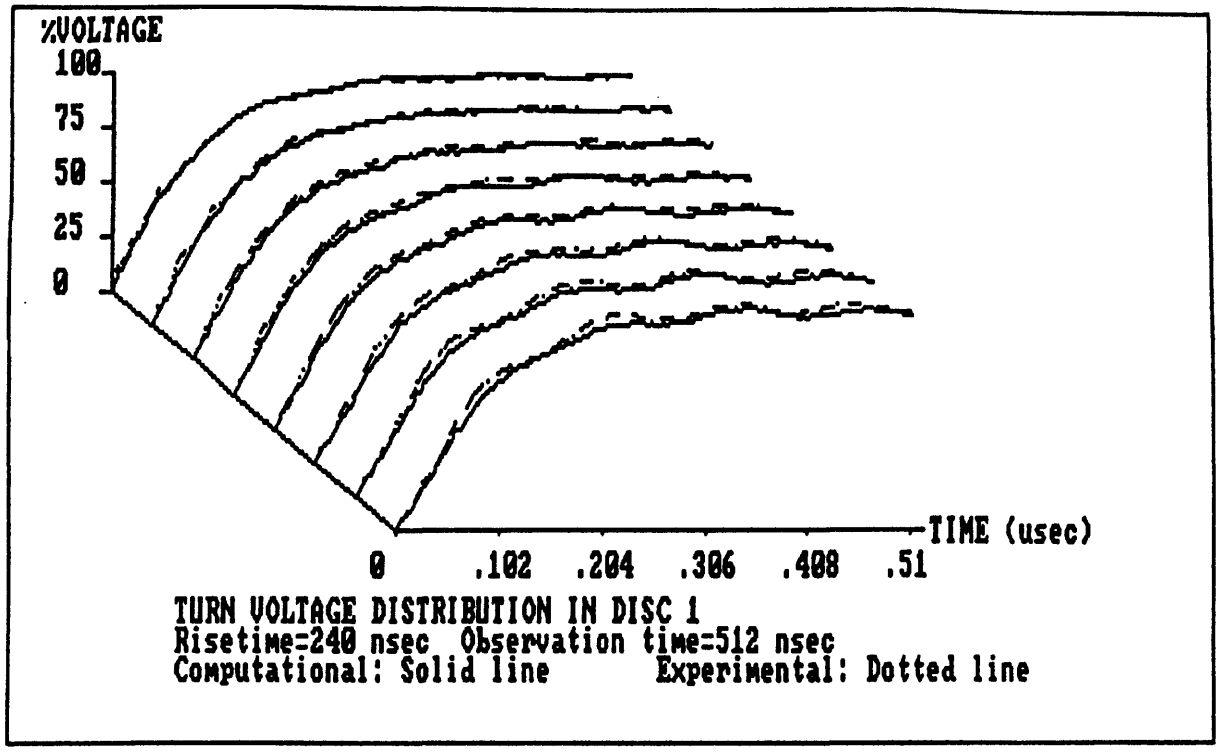

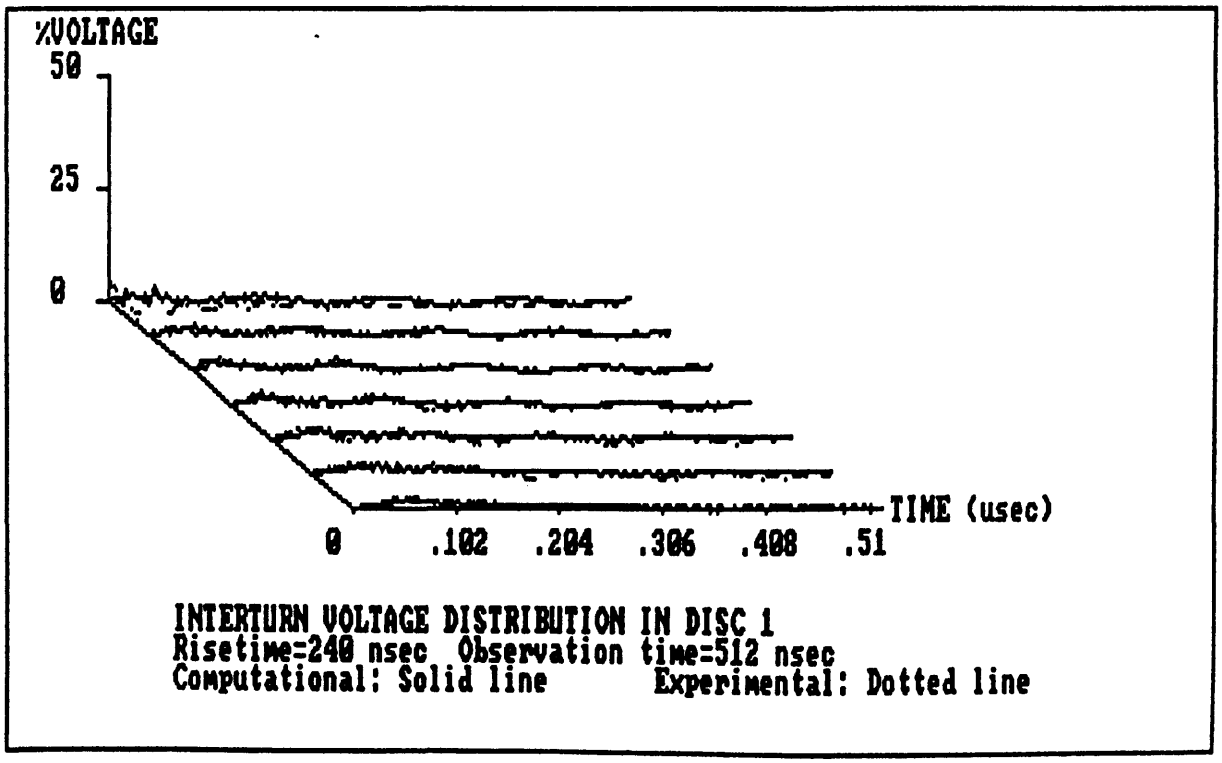

Fig 4.20 Comparison between computational and experimental results
Risetime of the excitation function = 240 nsec

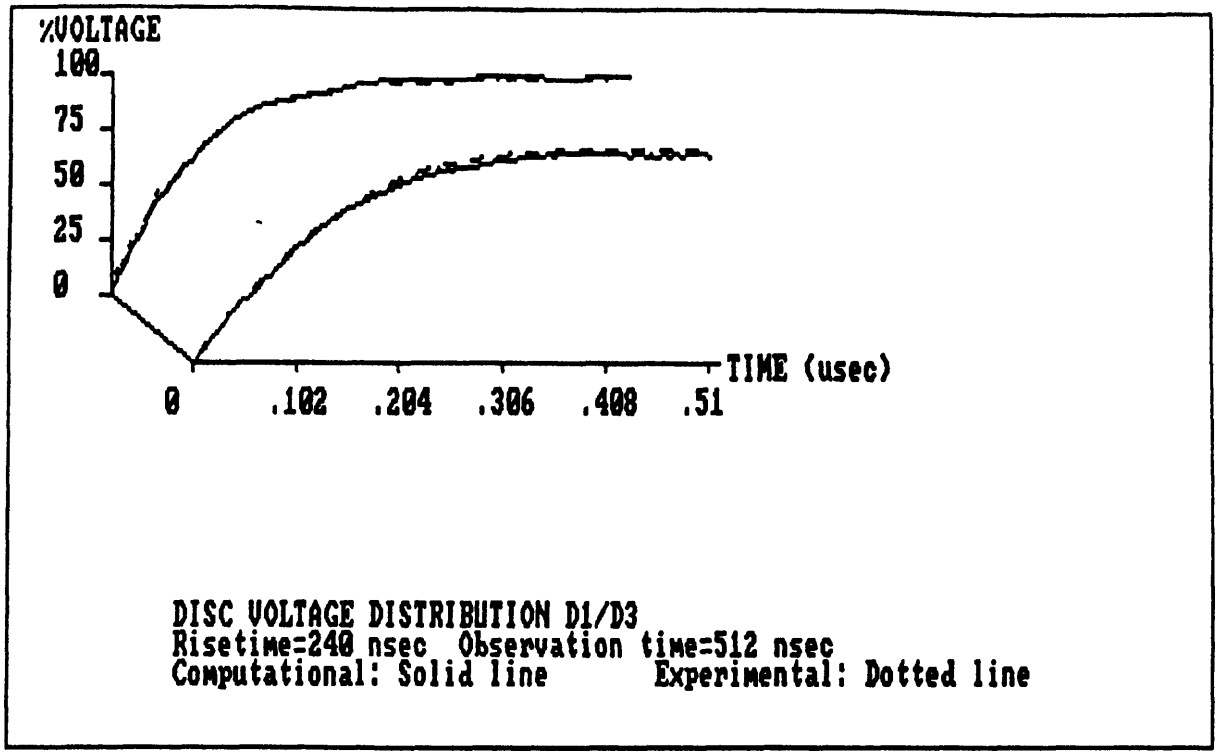

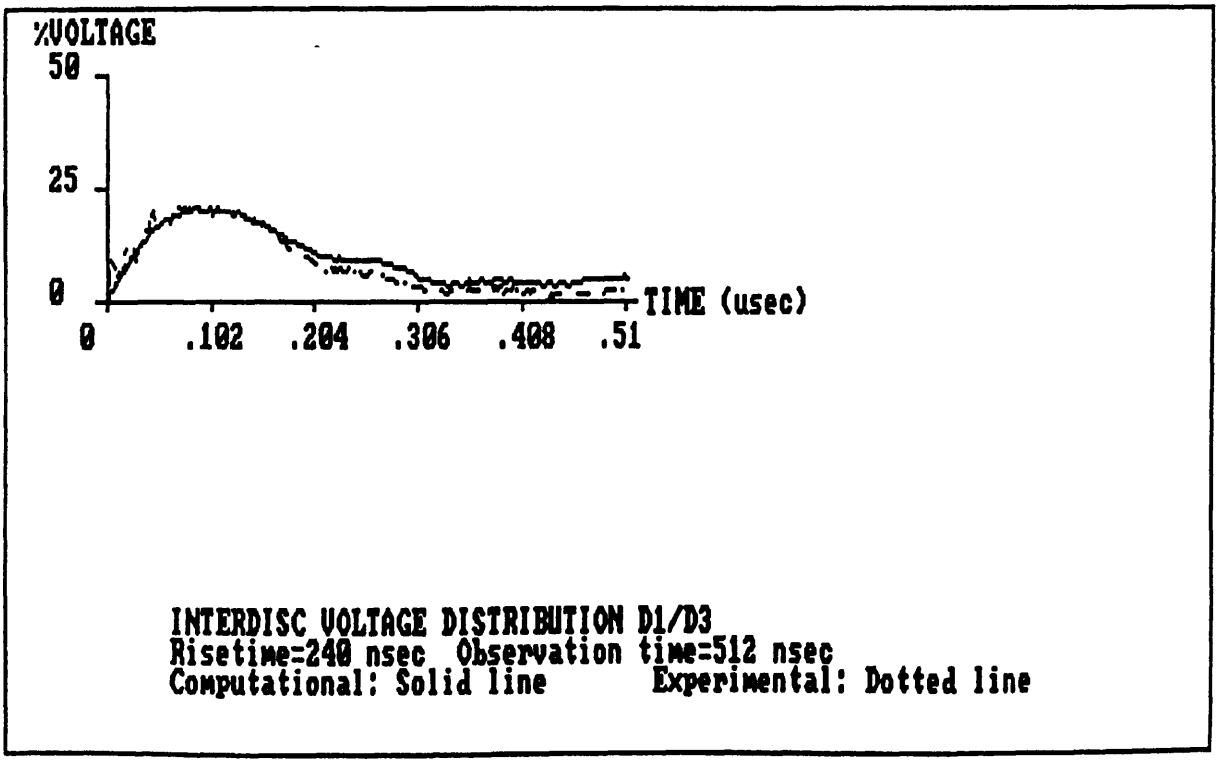

Fig 4.20 Comparison between computational and experimental results
Risetime of the excitation function = 240 nsec

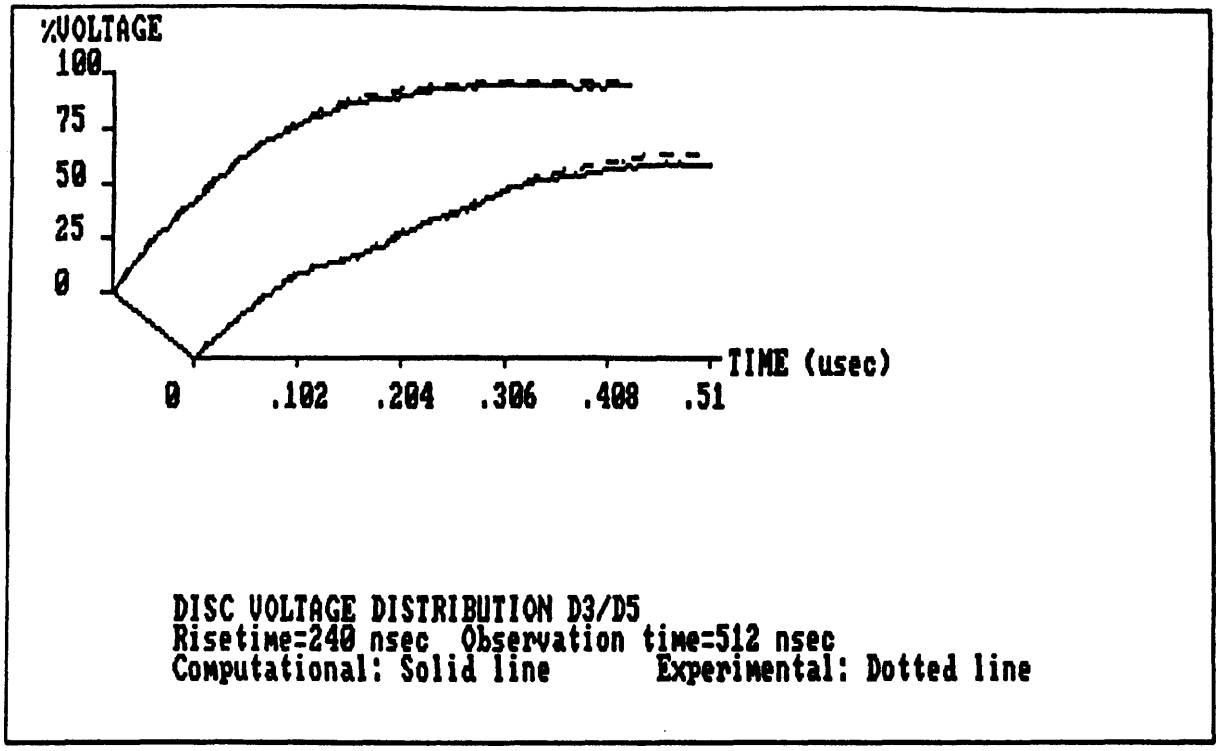

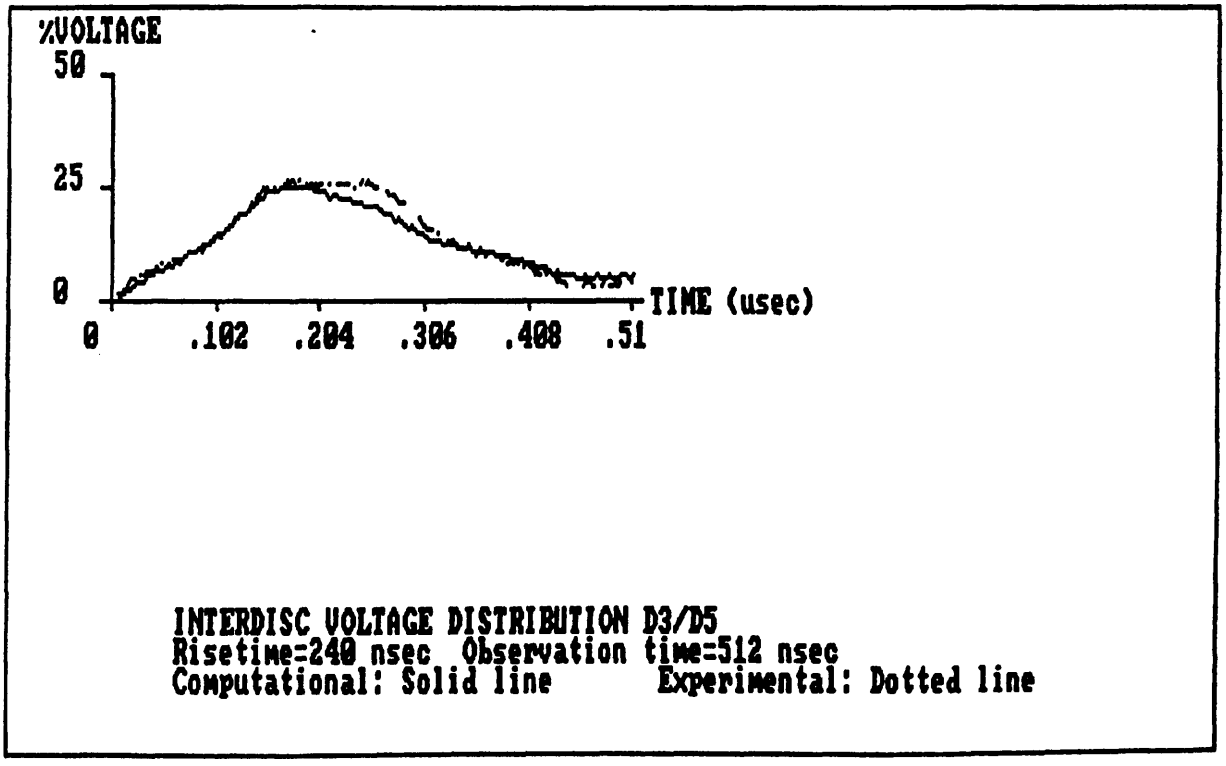

Fig 4.20 Comparison between computational and experimental results
Risetime of the excitation function = 240 nsec

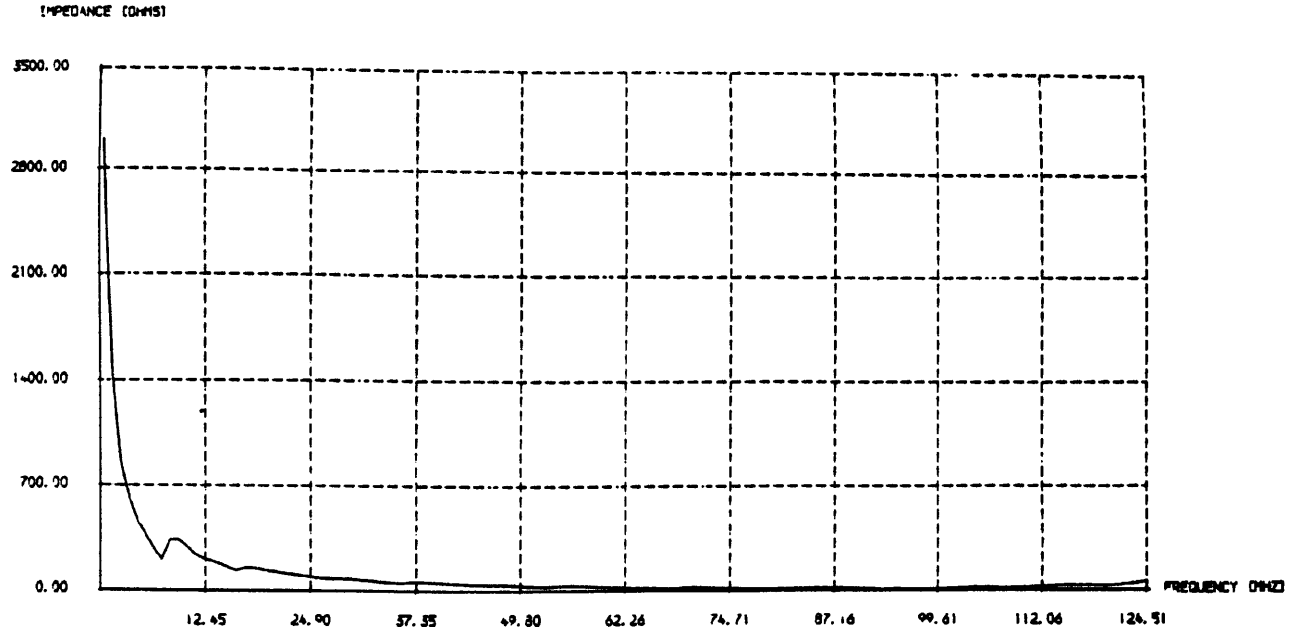

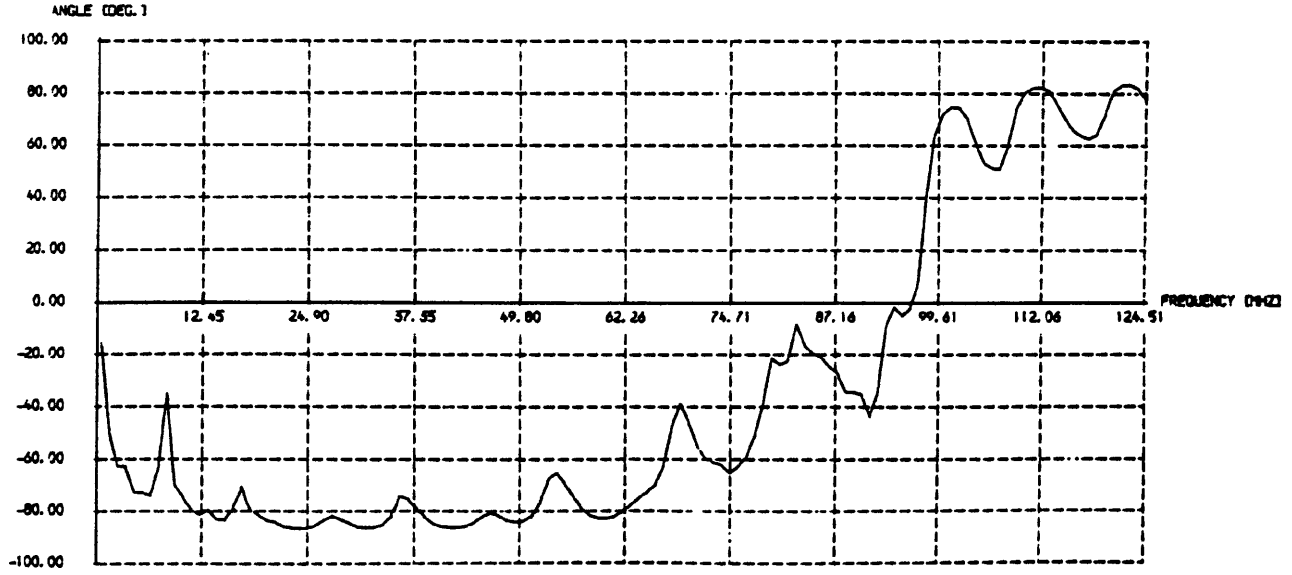

fig 4.21 Input impedance of the model

4.6 DISCUSSION

The model successfully incorporated the two modes of propagation inside the winding, namely, the parallel mode due to the capacitive transfer in the initial period of time and the series mode of propagation turn by turn throughout the winding.

The parallel mode of propagation was evident through the instantaneous reproduction of the wavefront of the incoming wave at all turns with different degrees of attenuation dictated solely by the strong axial and radial capacitive couplings. This parallel mode of propagation is a direct result of the fact that in the initial period of time directly after surge arrival, the transformer winding is indeed dominantly a capacitive network.

The series mode of propagation was detectable through a steep rise in the rate of increase of the turn voltages especially in the lower discs of the model where the travelling wave would be much delayed. The series mode of propagation was also evident from the variations in the different turn voltages due to the multiple reflections and refractions of the travelling wave at impedance discontinuities within the coil. This was especially noticeable from the oscillatory behaviour of the voltage of the last turn of the line-end disc with all the oscillations caused by the multiple reflections of the travelling wave from both ends of the disc.

Both modes of propagation contributed to the interurn and interdisc voltages although the series mode of propagation had a major role in such contribution since the parallel mode is only dominant in the initial period of time after surge arrival. The series mode of propagation caused the major peaks in the interturn voltage distributions with first two major peaks caused by the incident travelling wave and the reflected wave respectively. Such major peaks occured delayed further and further as we went down the winding with a decrease in their magnitudes due to the time required by the fast fronted surge to travel down the winding and the flattening of its wavefront during such propagation. The behaviour of the interdisc voltages

is similar to the interturn voltages except that their magnitude was a lot higher and no major second peak could be identified within the scope of the observation time. Finally, in contrast to the non-linear distribution of the interturn voltages in each disc, the distribution of interdisc voltages was almost linear when dealing with two consecutive discs at once.

This feature of the model in representing both modes together resulted in the model being capable of predicting the distribution of very steep fronted surges impinging on the line-end coil during the first 512 nsec after surge arrival with a reasonable degree of accuracy. In fact, the accuracy of the model extended to the first four discs in the line-end region of the transformer winding where most of the insulation failure could occur as a consequence of the very fast fronted surges reaching the winding.

The validity of the computer model was demonstrated through the close agreement between the computational results and the corresponding experimental results obtained from measurements on the transformer winding which already existed in the HV laboratory. The different measurements were performed at each turn of the line end disc and the outer junctions of the other cascade-connected discs. Such measurements were repeated for very steep fronted surges with different risetimes, namely, 30 nsec, 60 nsec, 120 nsec and 240 nsec. The various differences between the corresponding computational and experimental results were estimated as percentages of the applied voltage.

As far as the turn to ground voltages were concerned, a slight difference in the rate of rise of the voltages of the turns in the line-end disc was noticed. The order of such difference increased with wavefront duration up to 6% for the case of the 240 nsec wavefront. In contrast, no such difference was detected in the voltages of the turns at the outer junctions. Moreover, in relation to the magnitudes of the various voltages, the maximum discrepancy of 11% occured with the steepest wave (30 nsec duration), with such error reduced to 10% , 7% and 5% for wavefront

durations of 60 nsec, 120 nsec and 240 nsec respectively. Furthermore, the same trend in the different waveshapes was obtained.

With regard to the interturn voltages in the line-end disc, no noticeable differences in the magnitudes was observed with wavefront durations of 120 nsec and 240 nsec. However, an error of 2% was seen in the maximum interturn voltages for the steeper waves. Furthermore, the same trend in the corresponding waveshapes was noticed, with the highest interturn voltages occuring at the very begining of the observation time. However, it should be mentioned that in the first 10 nsec after surge arrival and across the turn directly connected to the line-end terminal,an exceptionally high oscillation with reasonably higher magnitudes than the other major peaks was obtained in the experimental work, and whose reason could not be explained. Such oscillation was evident with all the different surges but especially noticeable in the 30 nsec and 60 nsec wavefront cases.

In the case of interdisc voltages, the discrepancy in the magnitude of the major peak between the first two discs in the line-end region was almost 2% for all surges. In addition, the same trend in their waveshapes was also in evidence although a difference in their magnitudes of up to 6% for the steepest wave (30 nsec) was spotted within the scope of the observation time. On the other hand, the biggest difference in the magnitude of the major peak between the third and fourth disc was 6% in the case of the 30 nsec surge, with such difference decreasing to 3% for the 60 nsec wave and no noticeable discrepancy for the slower waves. Again, the same trend in the waveshapes was noticed with the margin of error being 6% for all cases. Furthermore, it is important to mention that, all the major peaks in the corresponding computational and experimental results occured at almost the same instant in time.

However, in order to extend the accuracy of the model to these top four discs, eight discs had to be included in the model in order to minimize the effect of the termination impedance whose value as function of frequency

could only be fairly estimated. It should be stressed that in the scope of the observation time of 512 nsec, eight discs were enough to ensure the above mentioned accuracy. The surge voltage distribution in the discs further down the winding could be predicted by including more discs in the model but it should be stressed that calculation instabilities entirely related to matrix size might occur. In addition, it was found that reducing the sampling time from 4 nsec to 1 nsec (by quadrupling the number of frequency samples) would not yield any noticeable difference between the various computational results with huge computer resources in both time consumption and storage required.

The termination impedance of the model was found by using the concept of coil impedance (element D(1,1) in equation 3.36). Such termination impedance represented the characteristic impedance of the remaining cascade-connected sections further down the winding which have not been included in the model. The problem of finding the termination impedance as a function of frequency was an iterative one in nature. By taking six sections of the transformer winding at once, the input impedance of the coil was found and subsequently used as a termination impedance for the coil above, with such process repeated until the value of the impedance did not vary over the whole frequency range of the studies. Moreover, The problem of couplings between the top and bottom sections of the coil under consideration and the sections of axially neighbouring coils was solved by repeating the above iterative procedure but with twelve sections and the termination impedance being the impedance seen at the middle of the coil. Hence, the value of the termination impedance found in the latter (second) approach was adopted through the whole studies.

The accuracy of the computer model also confirmed the exactness of the way the electrical parameters of the coil were obtained and the assumptions made in their evaluation.

CHAPTER 5

SENSITIVITY ANALYSIS

This chapter deals with the sensitivity analysis of the computer model of the transformer coil. It describes the effects of various parameters on the surge distribution, interturn and interdisc voltages. Those parameters are, namely, risetime of the impinging surge, termination impedance of the model, insulation permittivities of the insulating media, capacitance to ground and inductance of the coil. The effect of transposing of turns is also illustrated. Throughout the chapter, the different effects are analysed and discussed. Finally, a discussion on the sensitivity of the transformer coil is provided.

5.1 EFFECT OF SURGE RISETIME

Since the purpose of the present studies is to investigate the distribution of very fast fronted surges impinging on transformer windings as a result of switching operations in GIS, it would be appropriate to consider surges with different risetimes which could reach transformers[5] directly or indirectly connected to GIS. Accordingly, the different risetimes which have been considered were 30 nsec, 60 nsec, 120 nsec and 240 nsec. The effects of the different risetimes are shown in fig 5.1 to fig 5.5.

From fig 5.1 it is clear that the less the wavefront duration is, the smaller the magnitudes of oscillations in the voltage distribution of the line-end disc. In other words, an increase in the risetime of the incoming surge results in a flattening of the voltage distribution. This could be explained by the simple fact that when a wave with a steeper front strikes the winding, a higher proportion of the wave arrives at the line-end disc (end of turn 8) where it is reflected back, according to very well known rules, creating a reflected wave with higher amplitude which causes bigger

oscillations in the turn voltage distribution with the decrease in wavefront duration.

The above mentioned fact also explains the increase in magnitude of all peaks of both interturn and interdisc voltages with the decrease in the surge risetime, as shown in fig 5.2 to fig 5.5. More, their general trend is also preserved, i.e, non-linearity of interturn voltage distribution within each disc (fig 5.4) and the almost linear interdisc voltage distribution between the corresponding turns of two consecutive discs (fig 5.5). It is important to mention that with a risetime of 30 nsec, the highest interturn voltage occured between the first two turns connected to the line-end whereas in all other cases the highest interturn voltage occured across the turn at the remote end of the line-end disc.

Hence, we can conclude that the risetime of the incoming very fast fronted surge is a major parameter in determining the interturn and interdisc voltages and accordingly the resulting insulation stresses.

Having studied the effect of surge risetime, all remaining sensitivity analysis studies were carried out by using the very fast fronted surge with a 60 nsec risetime.

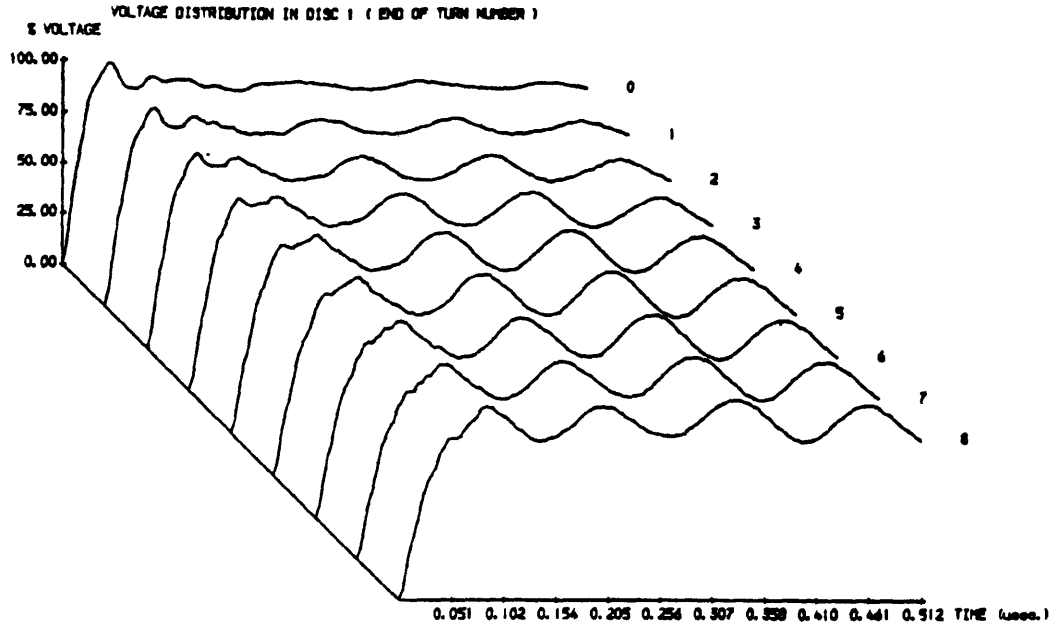

a)

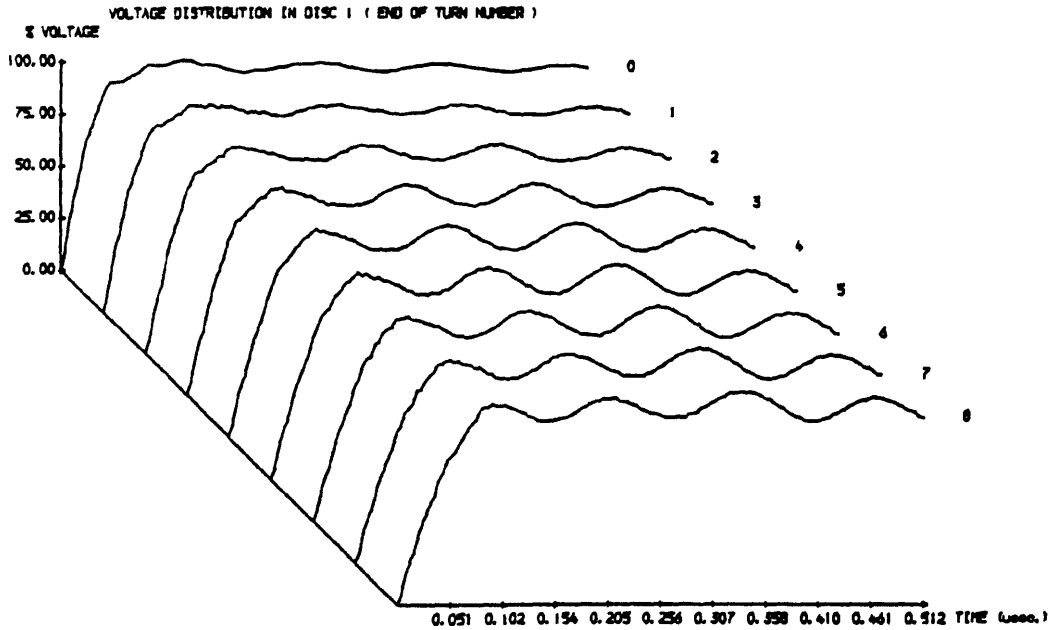

b)

Fig 5.1 Voltage distribution in disc 1 for different risetimes

a) 30 nsec

b) 60 nsec

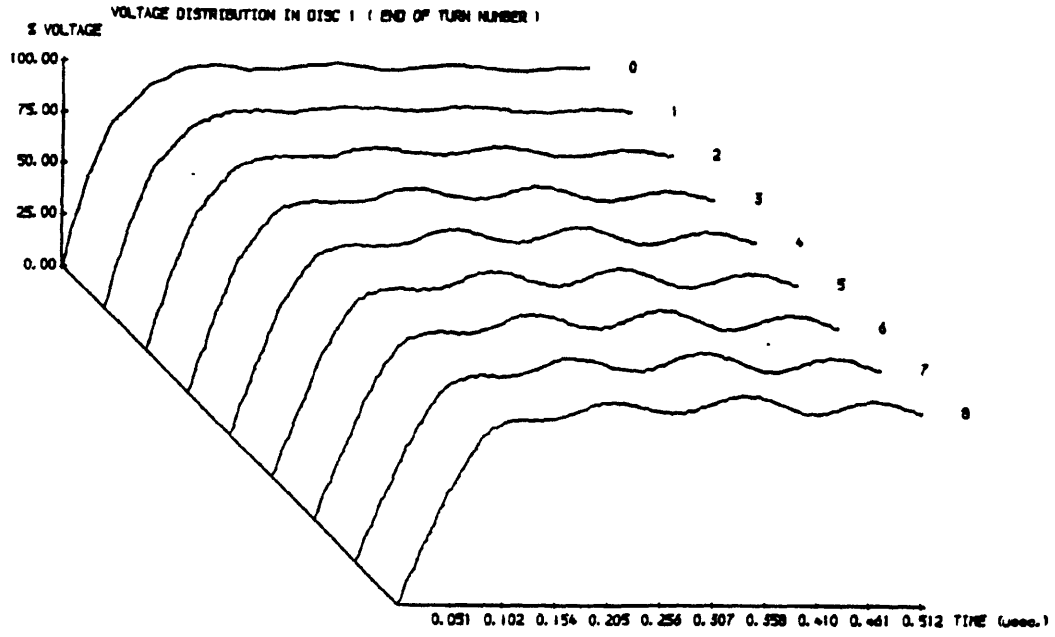

c)

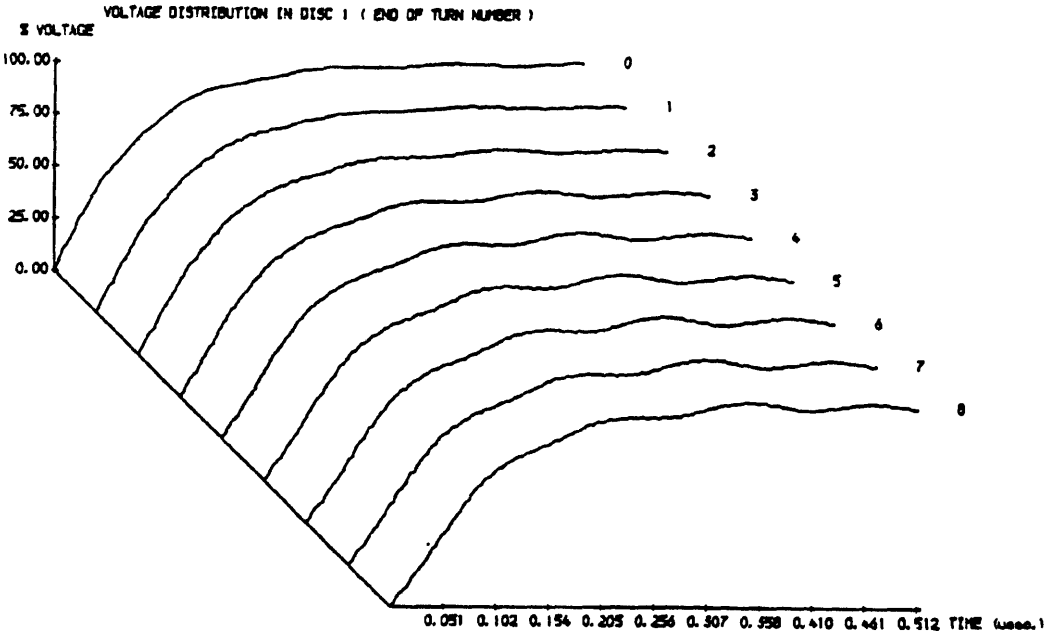

d)

Fig 5.1 Voltage distribution in disc 1 for different risetimes

c) 120 nsec

d) 240 nsec

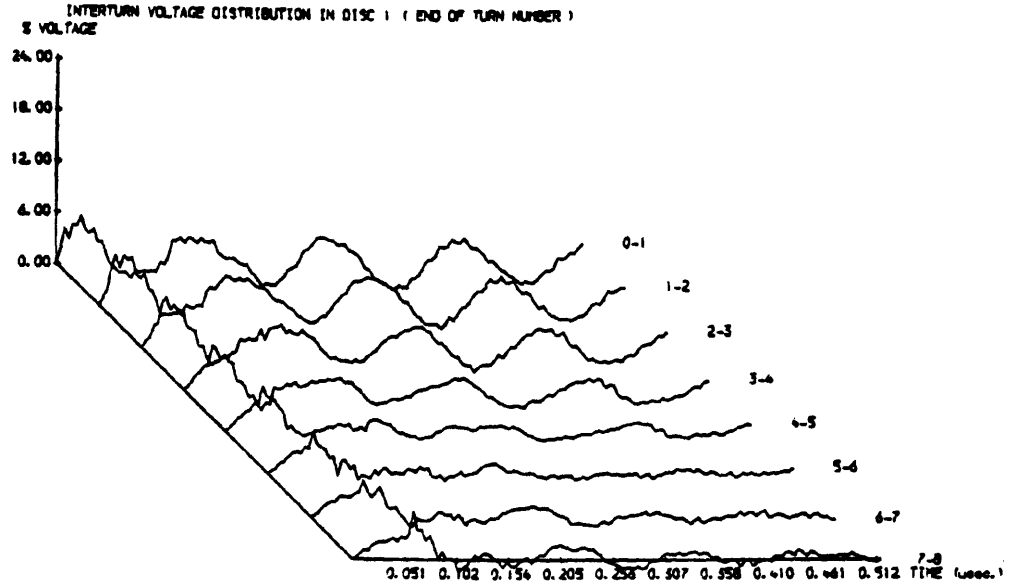

a)

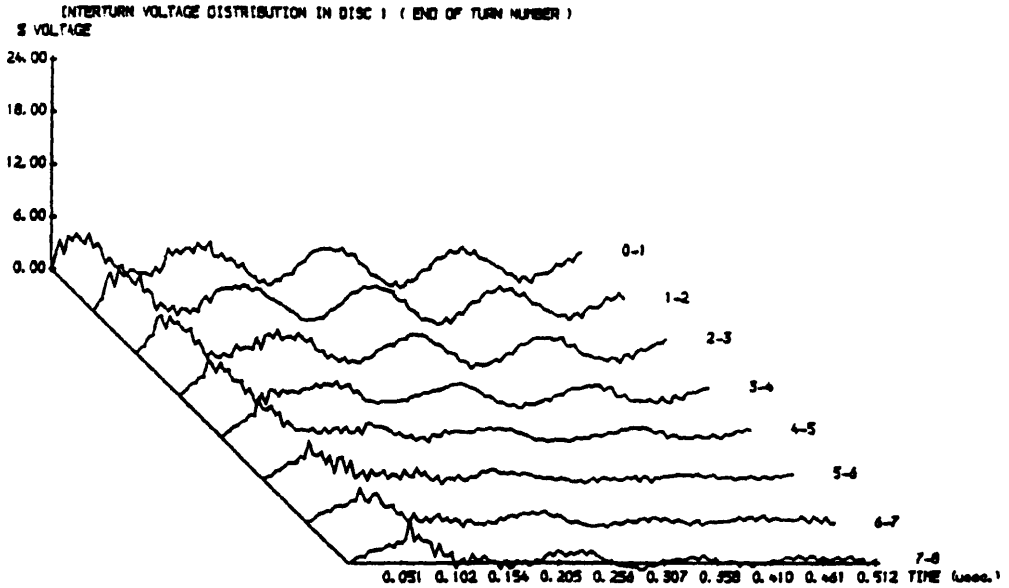

b)

Fig 5.2 Interturn voltage distribution in disc 1 for different risetimes

a) 30 nsec

b) 60 nsec

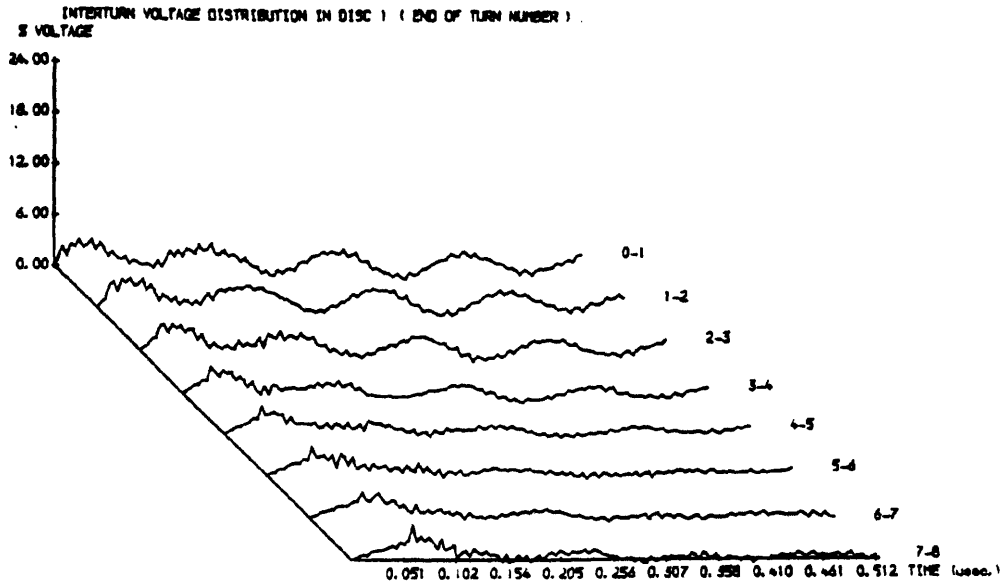

c)

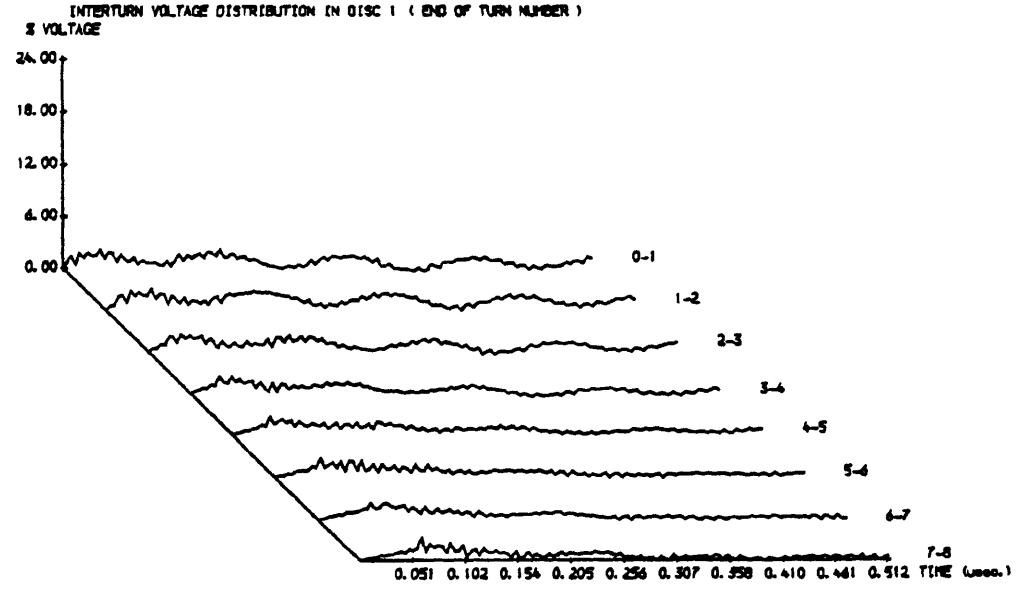

d)

Fig 5.2 Interturn voltage distribution in disc 1 for different risetimes

c) 120 nsec

d) 240 nsec

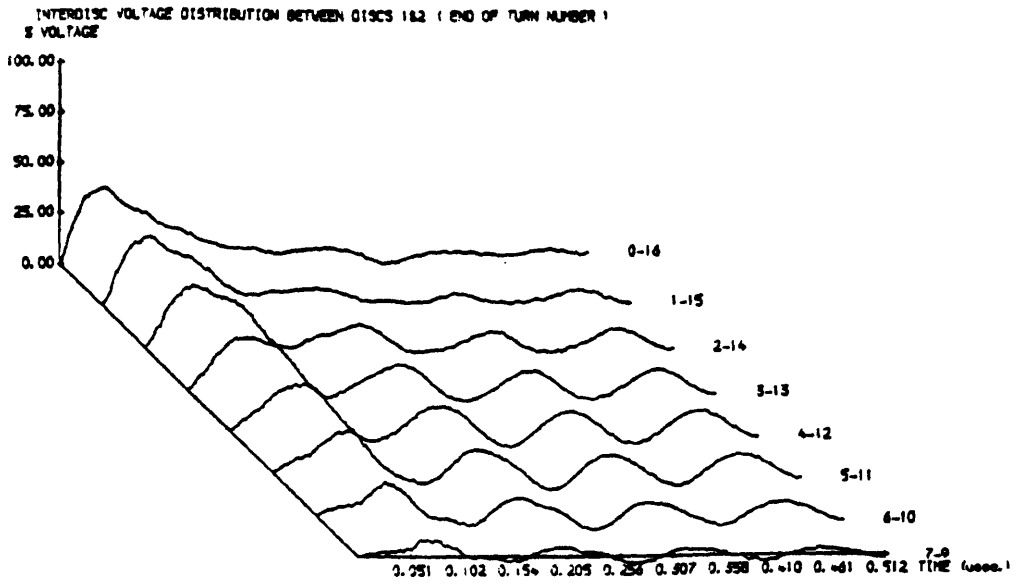

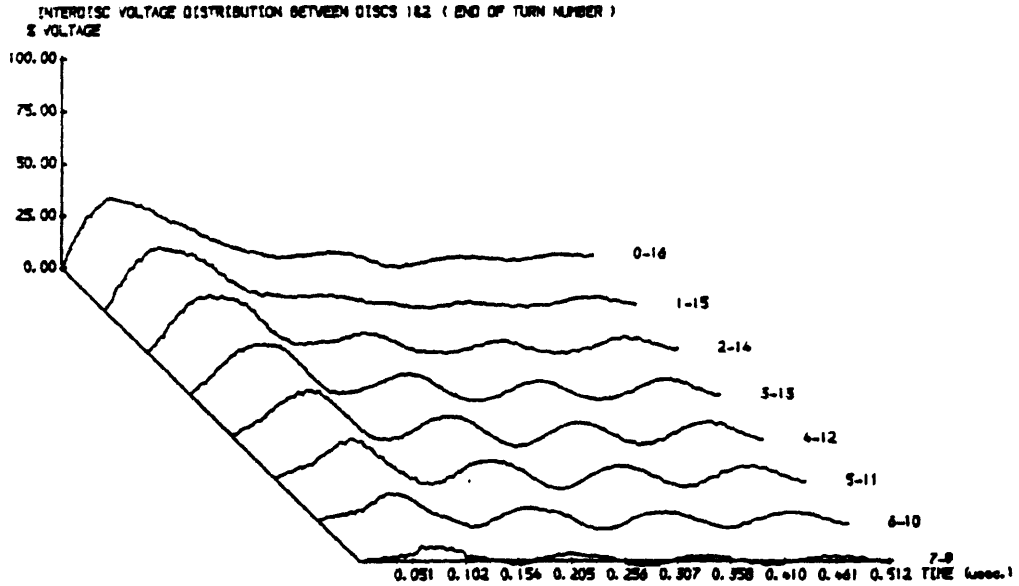

Fig 5.3 Interdisc voltage distribution between discs 1 and 2 for different risetimes

a) 30 nsec

b) 60 nsec

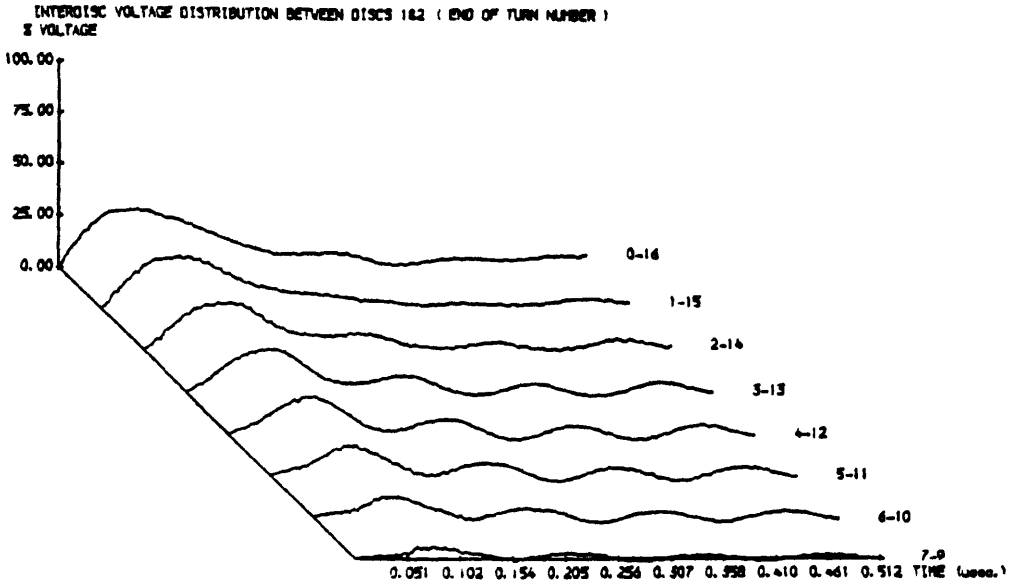

c)

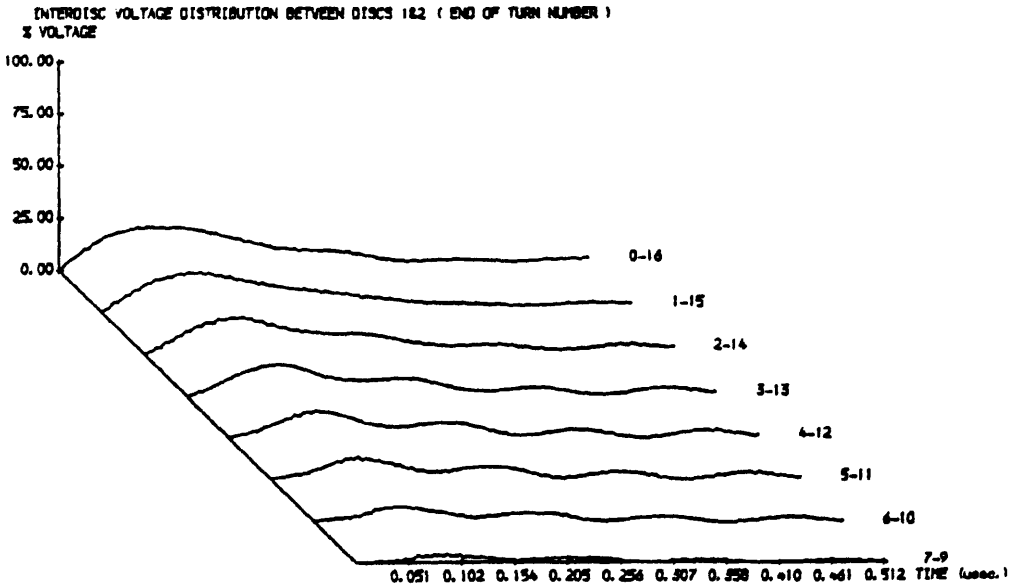

d)

Fig 5.3 Interdisc voltage distribution between discs 1 and 2 for different risetimes

c) 120 nsec

d) 240 nsec

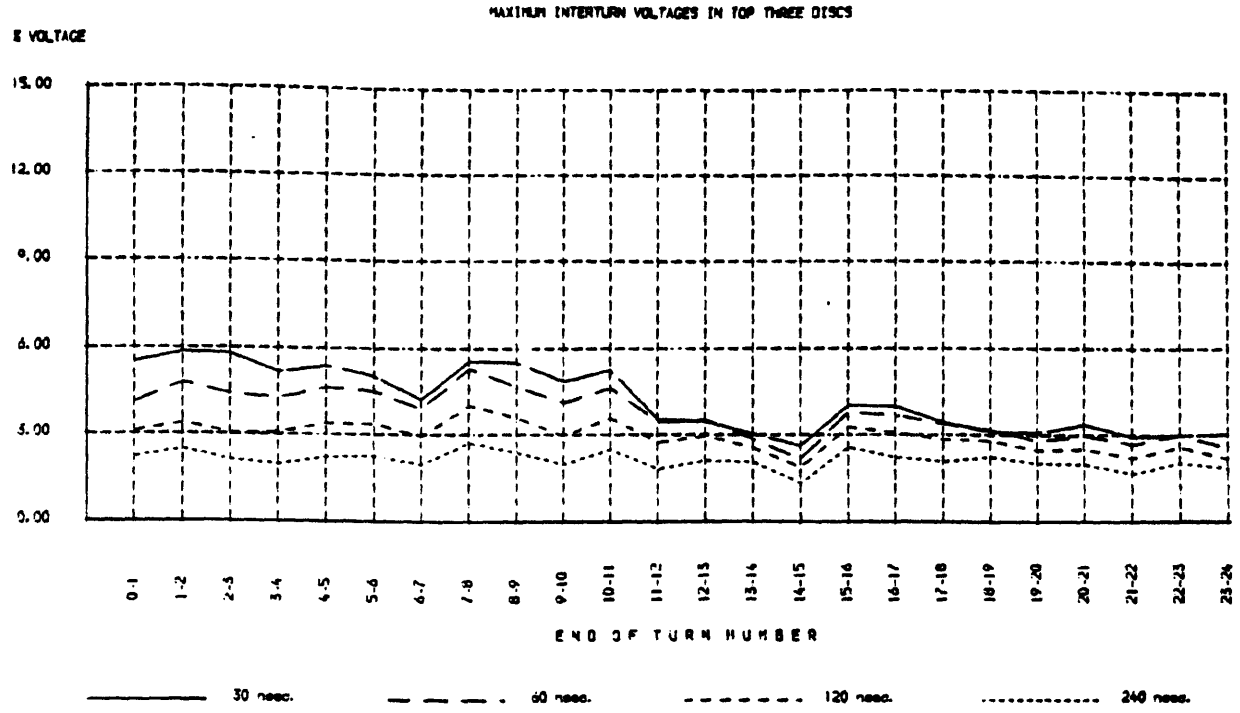

Fig 5.4 Maximum interturn voltages for different risetimes

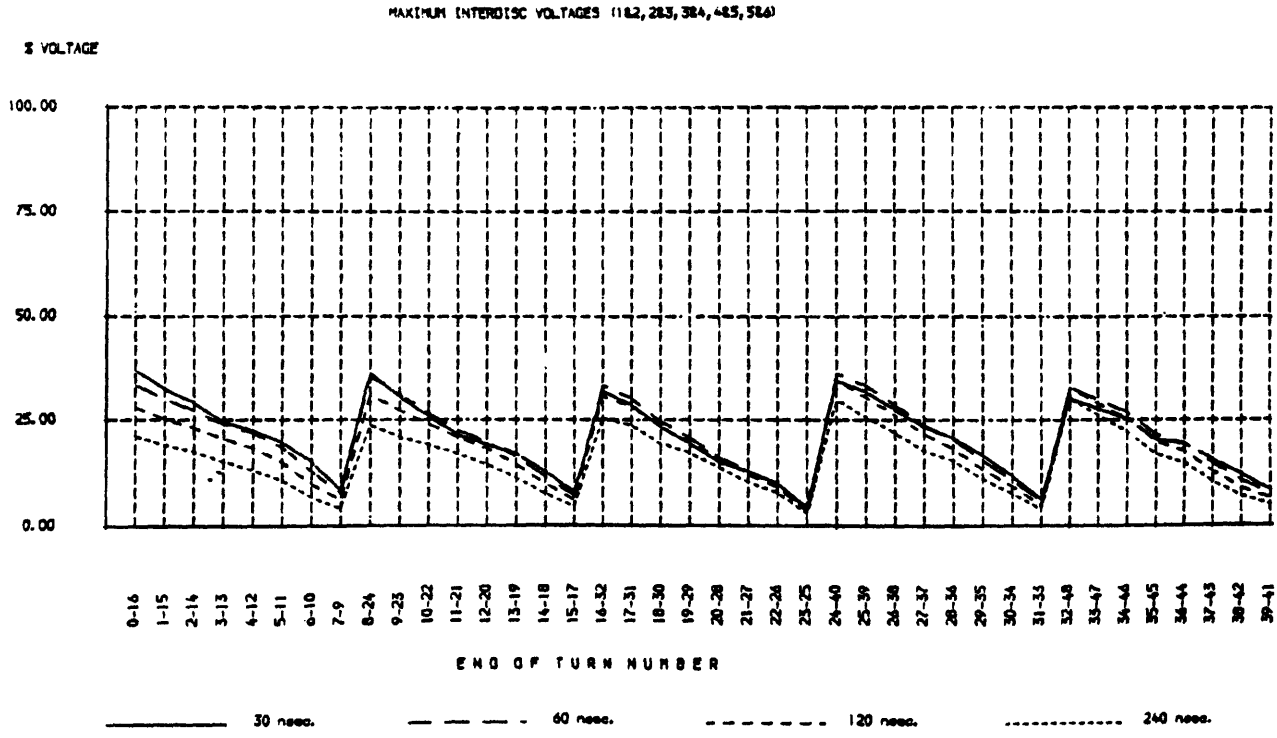

Fig 5.5 Maximum interdisc voltages for different risetimes

5.2 EFFECT OF TERMINATION IMPEDANCE

The studies on the conventional disc type coil were repeated using the two estimations for the termination impedance found using the first and second approaches explained in section 4.4, namely, Z_1 and Z_2, with $Z_1 > Z_2$. The effects on the output results are shown in fig 5.6 to fig 5.9.

As it can be seen from fig 5.6, the termination impedance has a negligible effect on the voltage distribution in the line-end disc. This is to be expected since the location of the termination impedance is too far down the winding at the end of th eighth section and, moreover, no reflection from the bottom end of the coil would reach the line-end disc within the scope of the observation time considered.

The effect of the termination impedance becomes more and more apparent on the lower sections of the coil. In fact, a higher termination impedance leads to further isolation of the turns of the lower sections from ground leading to an increase in their potential. This is evident from fig 5.7.b which shows a higher potential for turn 32 using the first approach ($Z_T = Z_1$) in comparison with the second approach ($Z_T = Z_2$) shown in fig 5.7.a.

Furthermore, terminating the model with a higher impedance means lower interturn and interdisc voltages as shown in fig 5.8 and fig 5.9 which again stress the fact the termination impedance would have more effect on the lower sections of the coil.

However, in relation to interturn and interdisc voltages, the peaks obtained from the computational studies (performed with the second approach) were slightly lower from the corresponding peaks obtained from the experimental work. As a result, terminating the model with the impedance found from the first approach would cause more divergence from the experimental results and the accuracy of the computer model would then be affected. Consequently, the termination impedance obtained from the second approach was used throughout the computational studies.

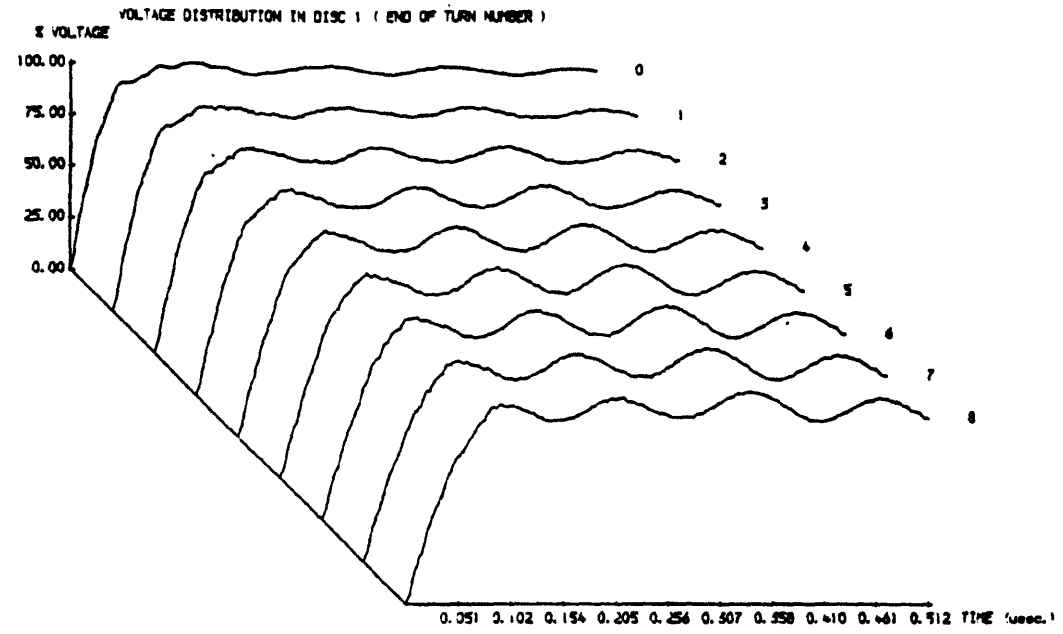

a)

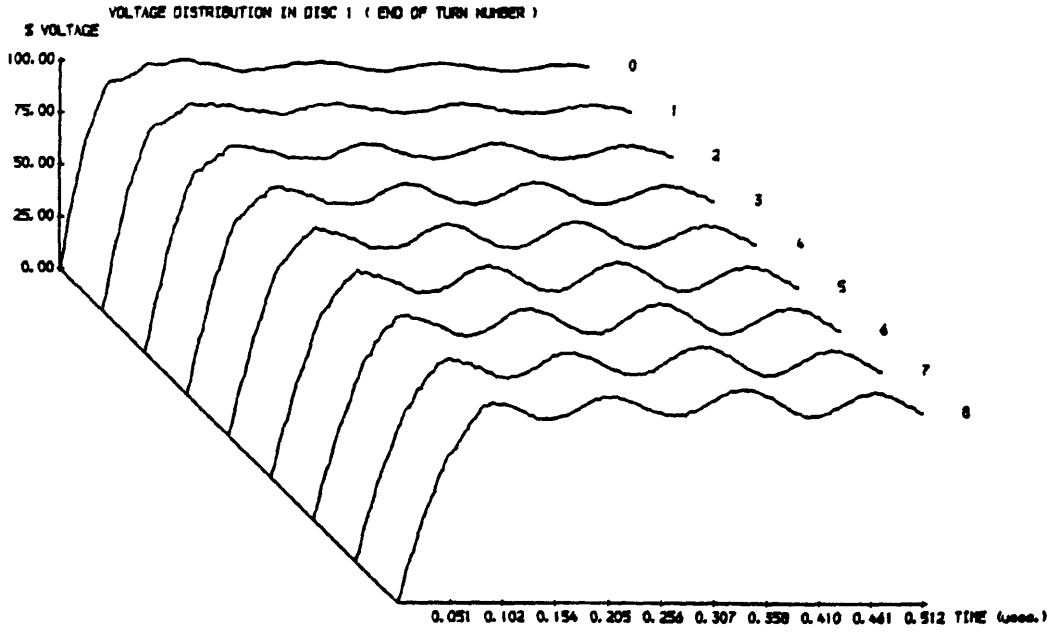

b)

Fig 5.6 Voltage distribution in disc 1 for different termination impedances

a) Second approach

b) First approach

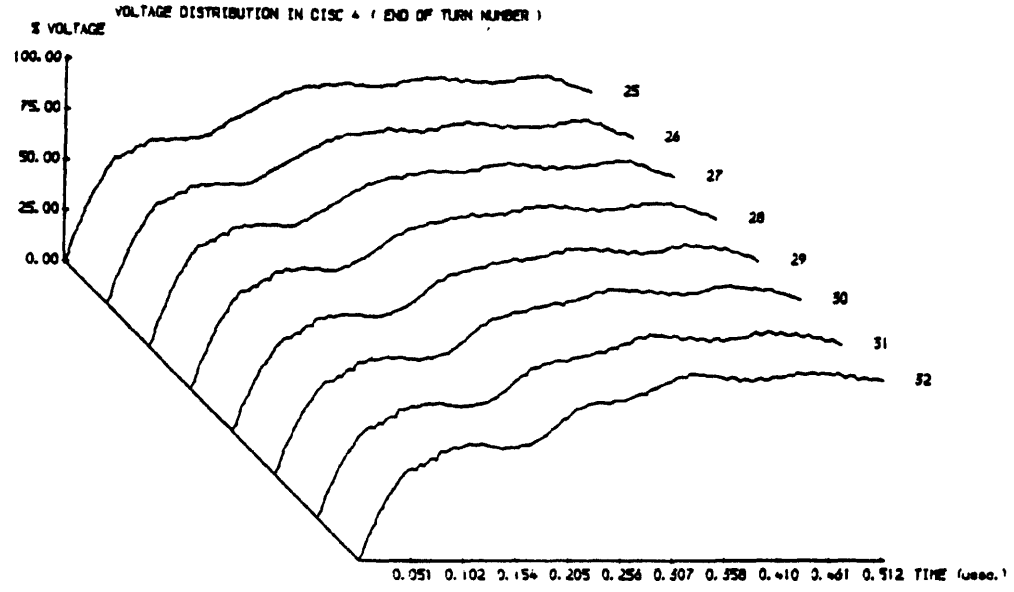

a)

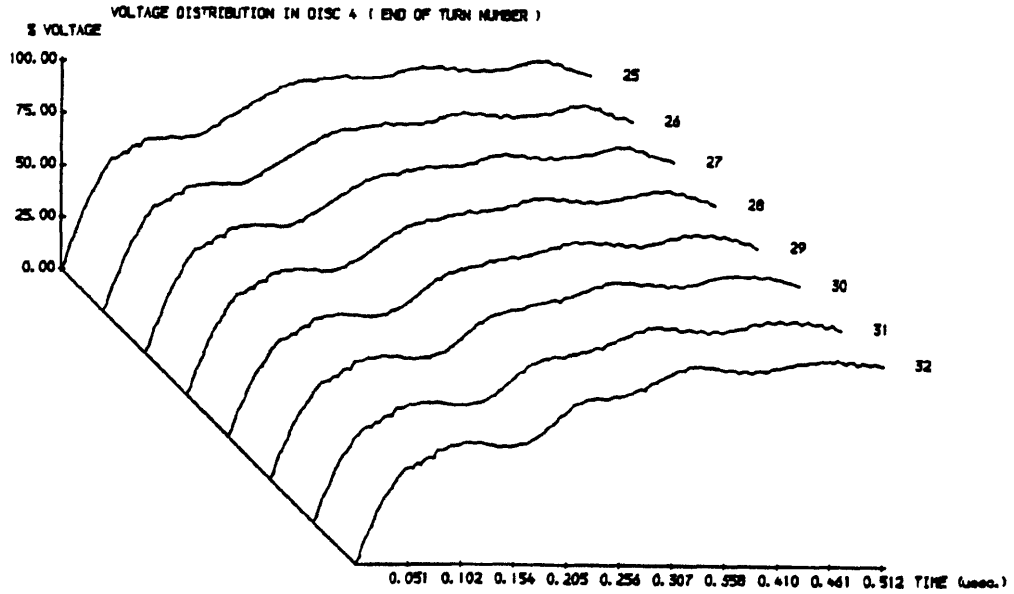

b)

Fig 5.7 Voltage distribution in disc 4 for different termination impedances

a) Second approach

b) First approach

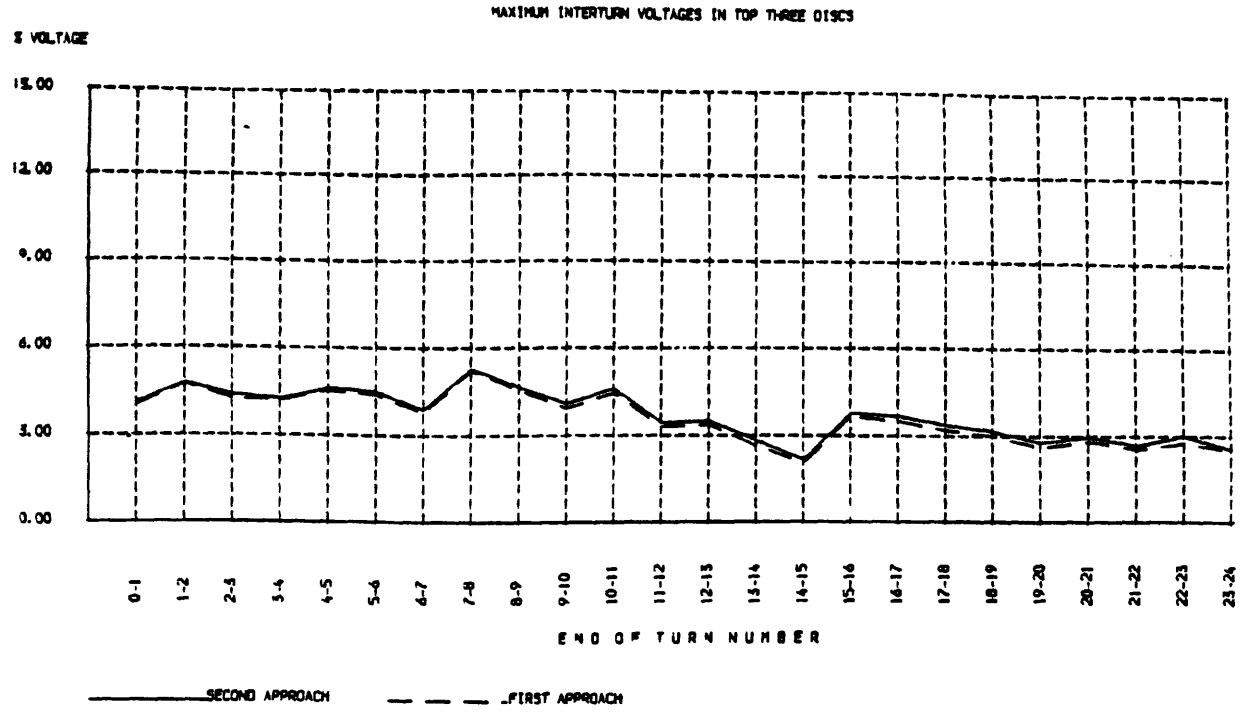

Fig 5.8 Maximum interturn voltages for different termination impedances

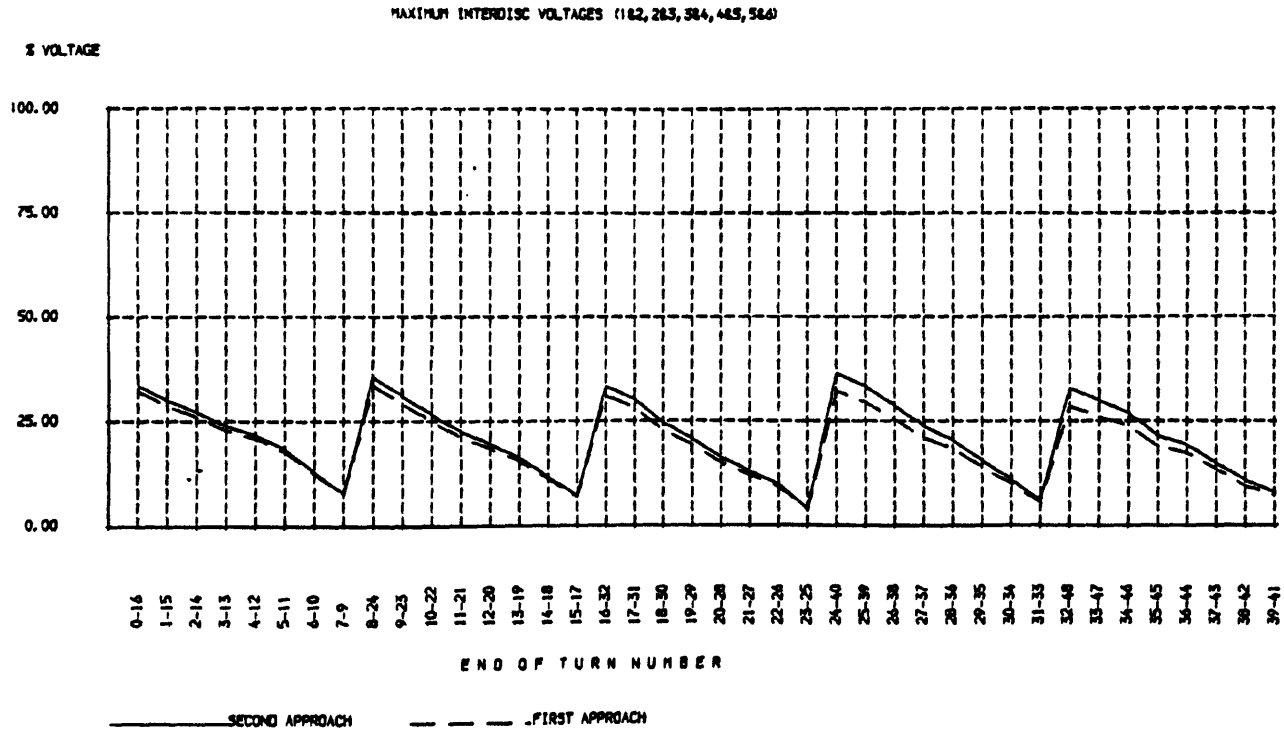

Fig 5.9 Maximum interdisc voltages for different termination impedances

5.3 EFFECT OF TRANSPOSING OF WINDINGS

In order to study the effect of interleaving of turns on the surge distribution behaviour in transformer windings, computational studies were performed for an interleaved disc type coil which has the same dimensions as the conventional disc type winding. The interleaved type coil and its equivalent capacitance circuit are shown in fig 5.10. Its electrical parameters were calculated similarly to those of the conventional type coil (section 3.3.3). The results for the interleaved disc type coil are shown in fig 5.11.

By comparing fig 5.11 and fig 4.16, it is clear that transposing the winding leads to a more linear voltage distribution during the initial period of time, i.e, a better initial voltage distribution. This could be clearly detected from the higher induced voltage at all turns of the interleaved coil during the initial period of time after surge arrival. This in turn is due to the better capacitive distribution obtained from interleaving the winding which increases the series capacitance of the coil. Furthermore, interleaving of the winding leads to the wave reaching the impedance discontinuities in almost half the time in comparison with the interleaved winding, which explains the increasing number of oscillations in the voltage distribution of the different turns.

However, the interturn voltages in some parts of the interleaved coil are higher than in the conventional winding, but the interdisc voltages are considerably lower. Hence, the ratio of interdisc to interturn voltages is a lot more favourable in an interleaved winding than in a conventional winding. In our studies, in fact, this ratio is of the order of 2 in the transposed coil whereas in the other type the same ratio is in the order of 6. It should be mentioned, however, that in an interleaved winding, both the interturn and interdisc voltage distributions are non-linear.

To summarize, transposing the turns improves the surge distribution and solves the problem of correlating interturn and interdisc insulation.

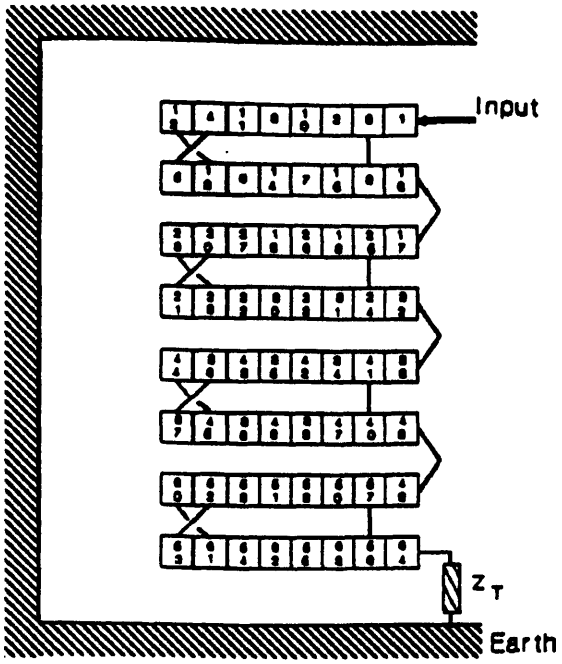

a)

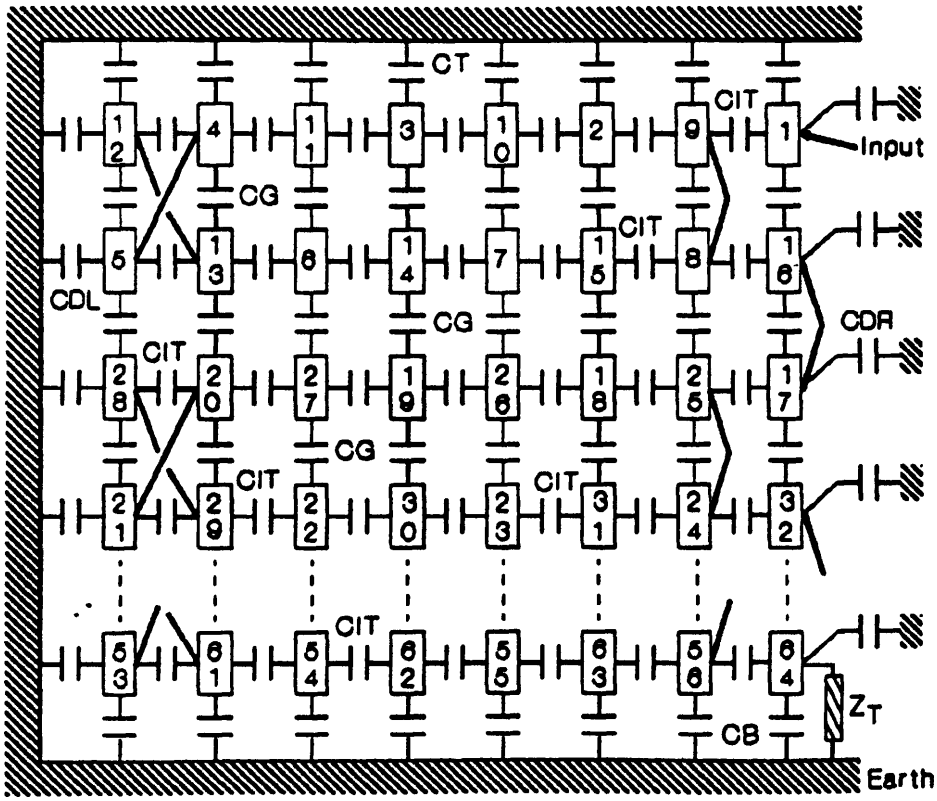

b)

Fig 5.10 Four-section model of interleaved winding

a) Configuration

b) Capacitance equivalent circuit

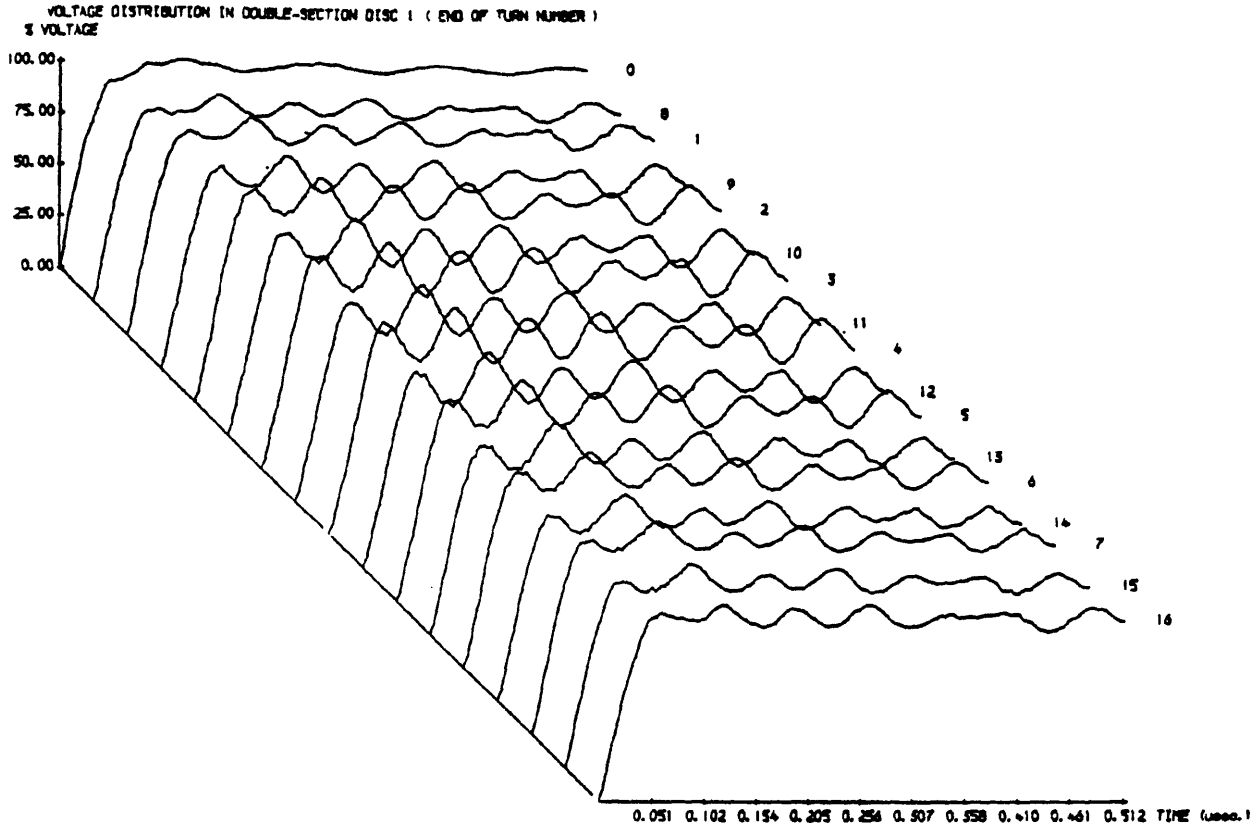

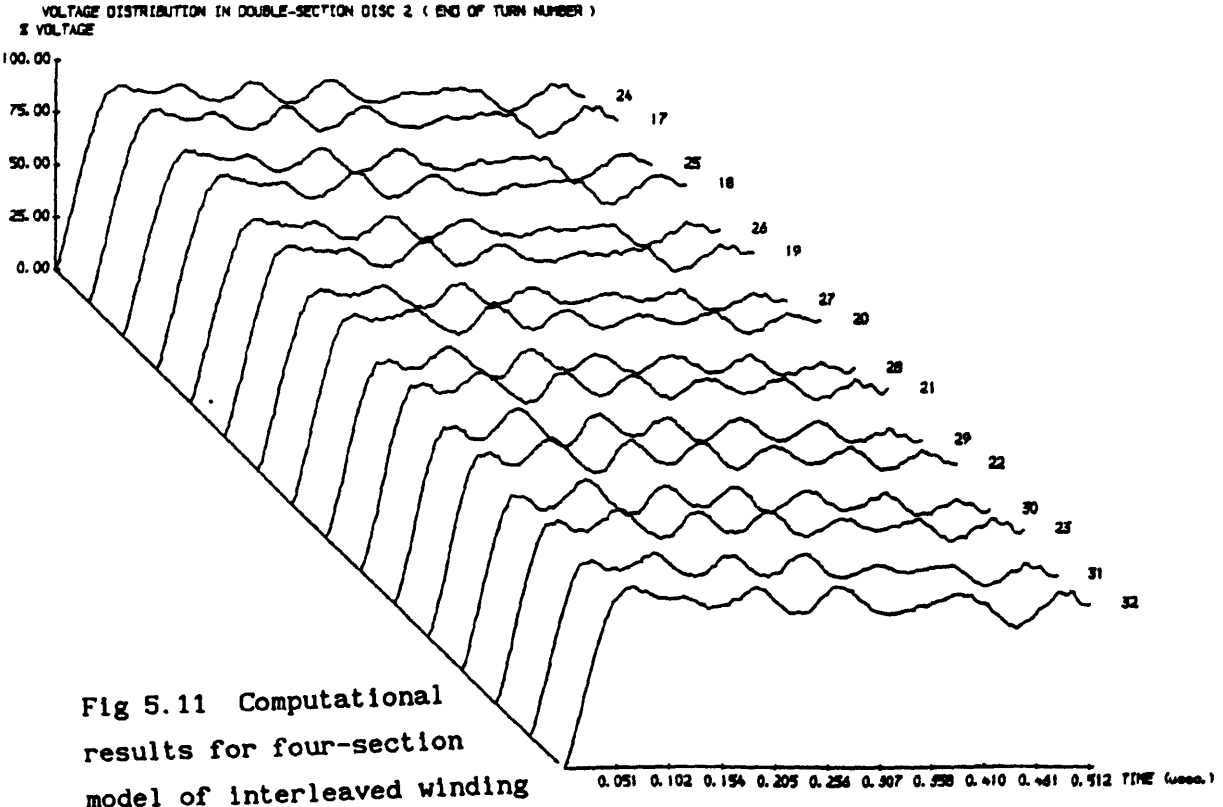

Fig 5.11 Computational results for four-section model of interleaved winding (Risetime of the excitation function = 60 nsec)

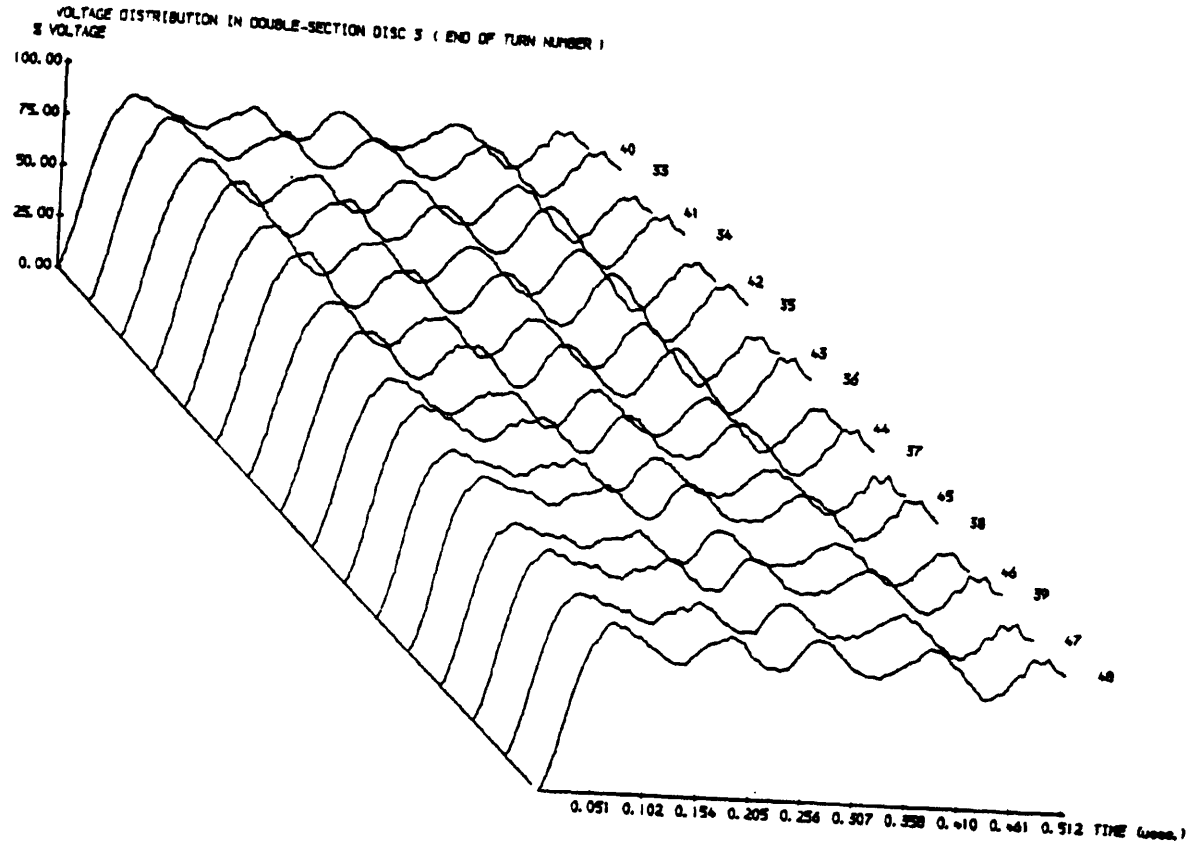

Fig 5.11 Computational results for four-section model of interleaved winding (Risetime of the excitation function = 60 nsec)

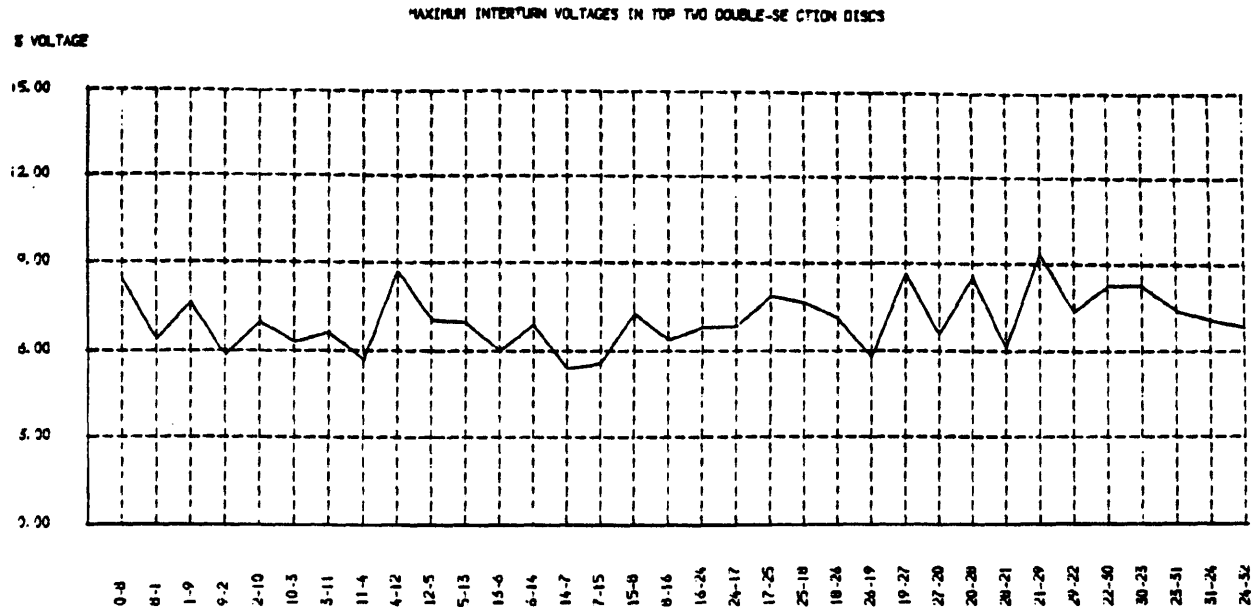

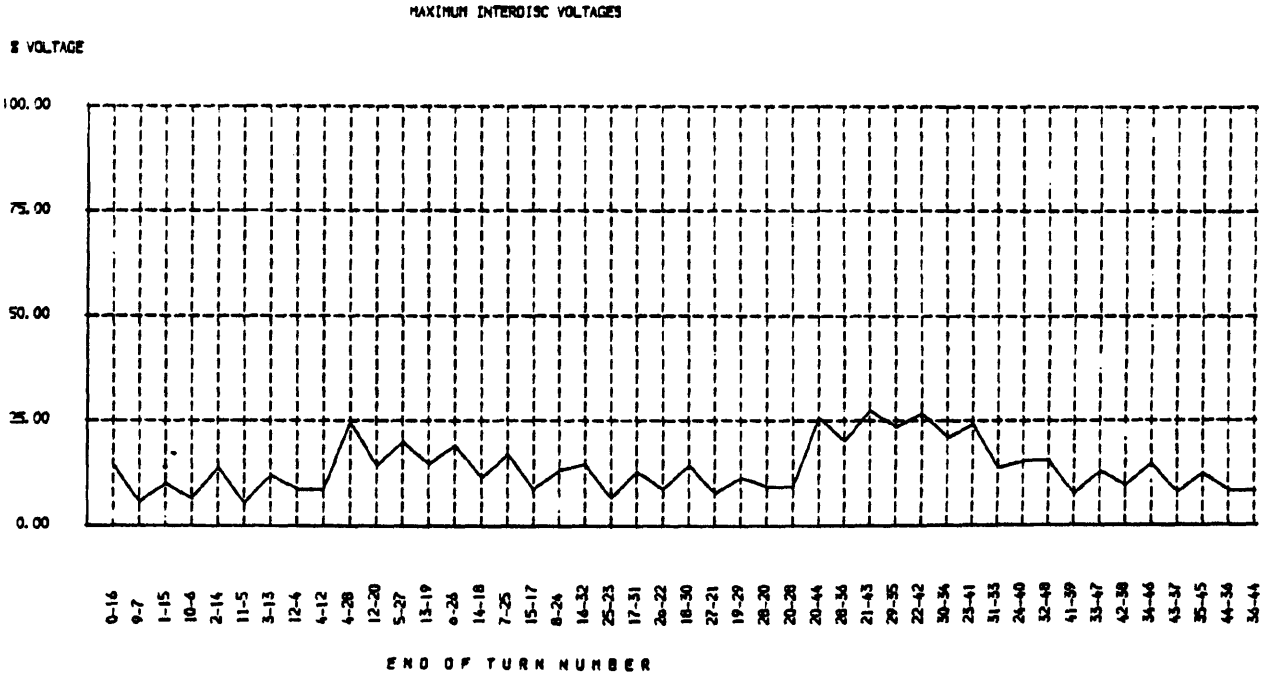

Fig 5.11 Computational results for four-section model of interleaved winding (Risetime of the excitation function = 60 nsec)

5.4 EFFECT OF INSULATION PERMITTIVITY

Insulation permittivities have an important effect on surge distribution in transformer windings. This importance arises from the fact that such parameters play a dominant role in determining the values of the various ground and series capacitances of the coil (equation (3.40)). Moreover, such capacitances are dominant in the initial period of time after surge arrival and posess an important role in determining the coil propagation characteristics as well.

In order to assess the effect of insulation permittivities, the values of the permittivities of two insulating media, namely, the interturn insulation and the main insulation (cooling medium), were changed once at a time.

In the first case, the cooling medium permittivity was considered to be K1 = 3.5. In other words, the coil with the same paper insulation was placed in oil. This case was referred to as condition 2.

In the other case, the interturn insulation permittivity was taken to be K2 = 2.5. In other words, the coil was still placed in air but with a different paper insulation between the turns. This case was referred to as condition 3.

The case in which the coil kept its original parameters, i.e. K1 = 1.0 and K2 = 3.5, was referred to as condition 1.

The effects of the above mentioned changes are illustrated in fig 5.12 to fig 5.14.

A close examination of fig 5.12 shows that a change in the insulation permittivity will modify the pattern of reflections and refractions in the coil. This is apparent from the variation in oscillations amplitudes of turn voltages in the line-end disc. Such amplitude variations could be explained by the simple fact that a change in insulation permittivity leads to a change in capacitive couplings resulting in a different impedance encountered by the travelling wave at impedance discontinuities. As a

result, waves with different amplitudes are reflected back which causes the variation in oscillation magnitudes referred to above. An increase in the insulation permittivity of the cooling medium results in bigger oscillation magnitudes which is also the case for a decrease in the interurn insulation permittivity, as shown in fig 5.12.

Furthermore, an increase in the permittivity of the cooling medium causes a forward shifting of the voltage distribution along the time axis (fig 5.12), resulting from a lower velocity of propagation. On the other hand, a decrease in the interturn insulation permittivity forces a backward shifting of the voltage profile in the time axis due to higher velocity of propagation of the incoming wave through the coil. Such changes in the velocity of propagation are a direct consequence of the considerable variations in the various capacitive couplings.

Similar shifting is also obtained in the interturn and interdisc voltages. More, changes in the insulation permittivity not only shift the interturn and interdisc voltages but also modify their magnitude as it could be seen from fig 5.13 and fig 5.14. This could be explained as follows :

1) A decrease in the interturn insulation permittivity decreases the interturn capacitive couplings in both radial and axial directions, although the radial capacitive coupling is by far the most affected. Such decrease in interturn capacitive couplings tends to increase the interturn voltage due to the lower induced voltage in the initial period of time after surge arrival. Hence, when the surge reaches turn " n-1 ", a higher interturn voltage occurs due to the lower induced voltage in turn " n ". Similar explanation applies to interdisc voltages although they are affected not only by the axial capacitive coupling but also to a lesser extent by the radial capacitive coupling. The increases in interturn and interdisc voltages throughout the coil as a result of smaller interturn insulation permittivity (condition 2) in comparison with the original

parameter (condition 1) are shown in fig 5.13 and fig 5.14 respectively.

2) An increase in the cooling medium insulation permittivity increases both the capacitive coupling to ground and the axial interturn capacitive coupling. The increase in the coupling to ground increases the interturn voltages because all turns are less isolated from ground and their potential remains low until surge arrival. However, despite the increase in axial interturn capacitive coupling which should improve the performance of the coil, the effect of capacitive coupling to ground is dominant. This is clearly illustrated in the increase in both interturn and interdisc voltages due to the increase in cooling medium permittivity (condition 3) in comparison with the original parameter as shown in fig 5.13 and 5.14 respectively.

From fig 5.13 and fig 5.14, it is clear that a variation in insulation permittivity preserves the same trend in the both the interturn and interdisc voltages. However, when the coil is placed in oil (condition 3), the highest interturn voltage occurs across turn 10 in the second disc instead of turn 8 as in the other two conditions.

From what has been said so far, we can conclude that the insulation permittivity plays an important role in the surge distribution and hence is a major factor in determining the interturn and interdisc voltages. Accordingly, such a parameter should be carefully studied when examining insulation stresses resulting from very fast fronted surges reaching the transformer winding.

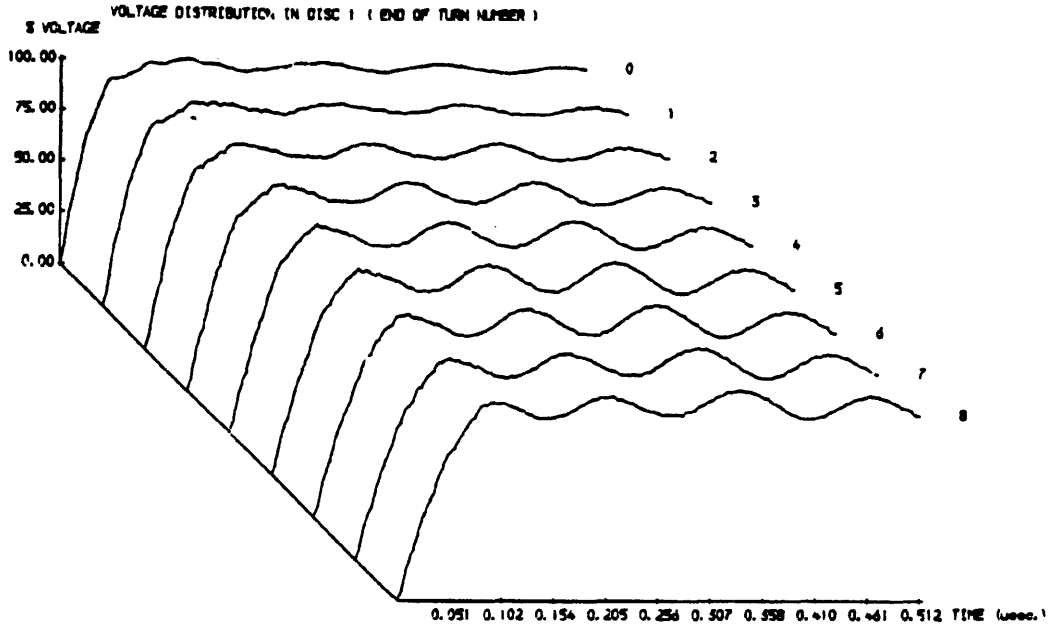

a)

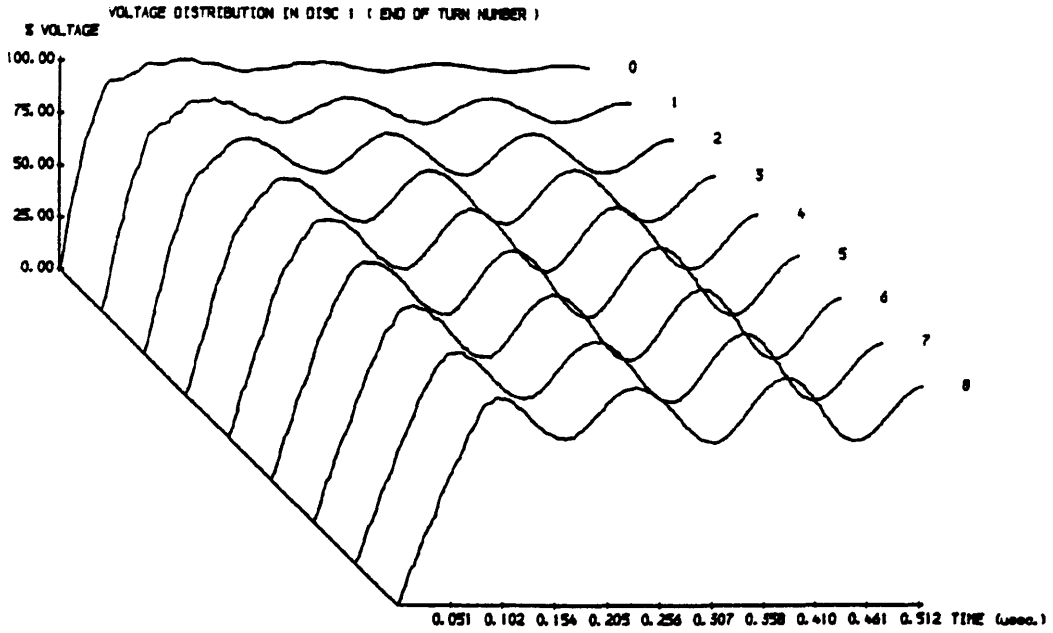

b)

Fig 5.12 Voltage distribution in disc 1 for different insulation permittivities (K1 : Cooling medium, K2 : Conductor covering)
a) Condition 1 : K1 = 1.0, K2 = 3.5
b) Condition 2 : K1 = 3.5, K2 = 3.5

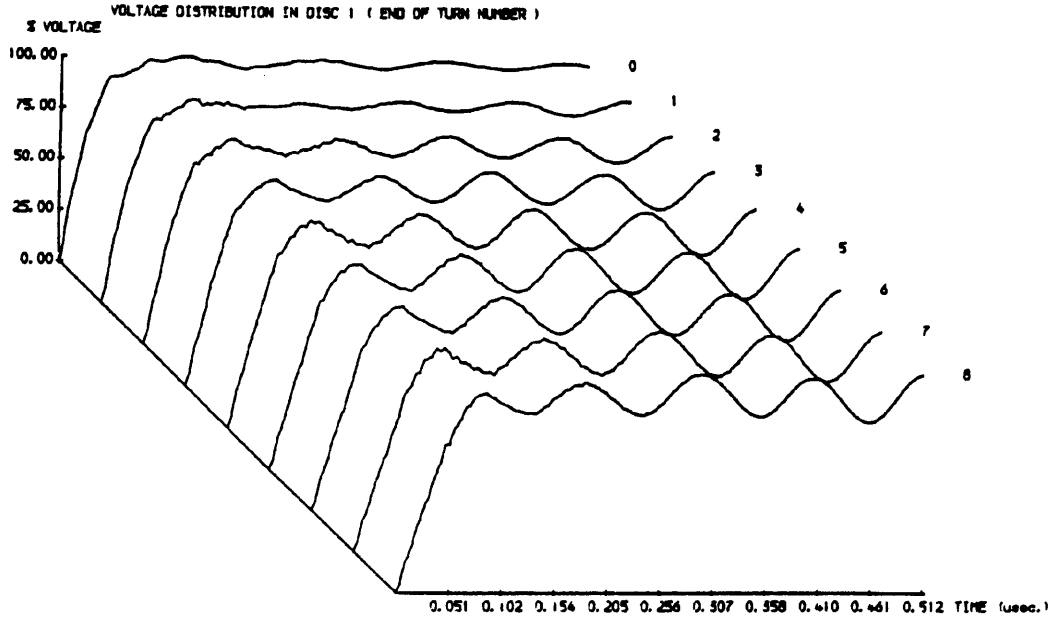

c)

Fig 5.12 Voltage distribution in disc 1 for different insulation permittivities (K1 : Cooling medium, K2 : Conductor covering)
c) Condition 3 : K1 = 1.0, K2 = 2.5

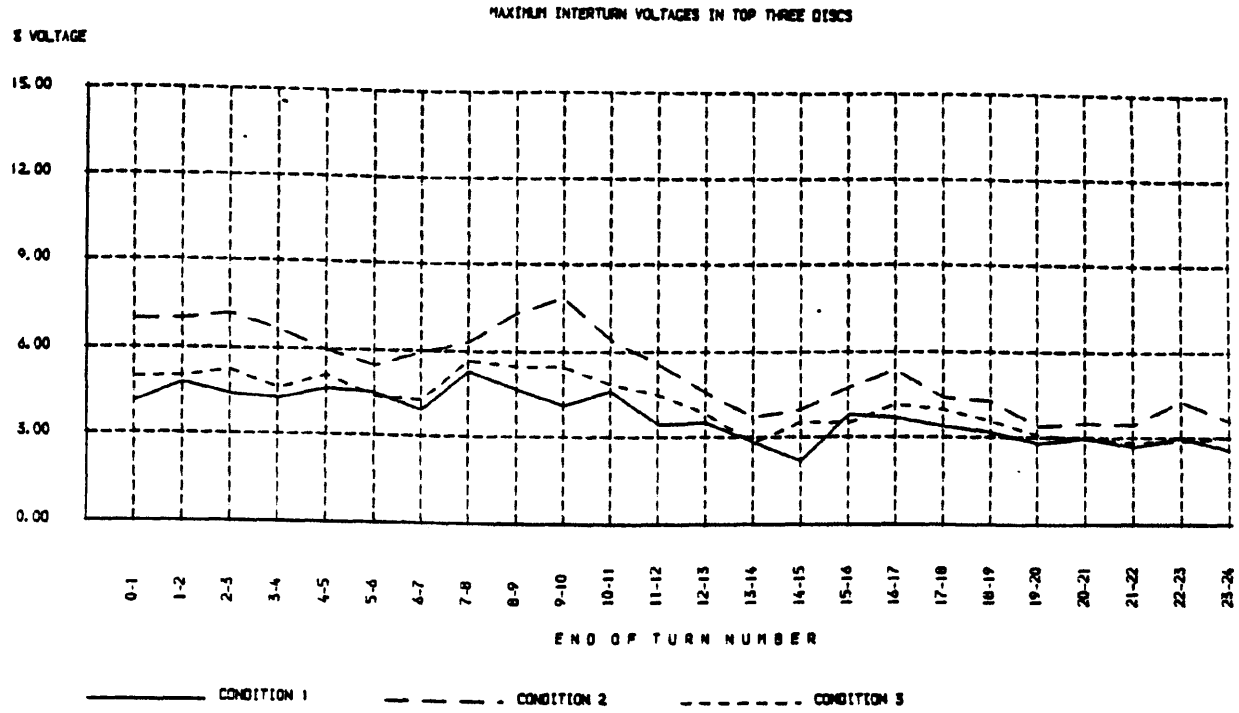

Fig 5.13 Maximum interturn voltages for different insulation permittivities (K1 : Cooling medium, K2 : Conductor covering)
Condition 1 : K1 = 1.0, K2 = 3.5 ; Condition 2 : K1 = 3.5, K2 = 3.5
Condition 3 : K1 = 1.0, K2 = 2.5

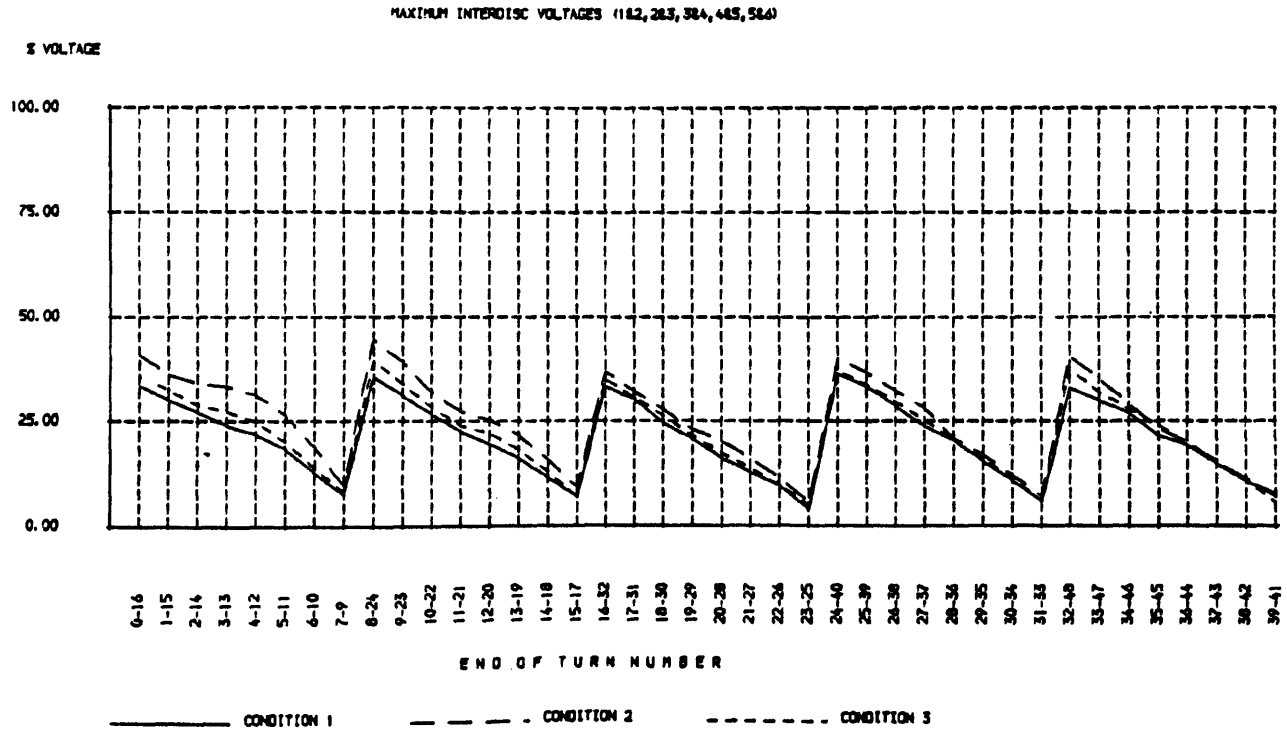

Fig 5.14 Maximum interdisc voltages for different insulation permittivities (K1 : Cooling medium, K2 : Conductor covering)
Condition 1 : K1 = 1.0, K2 = 3.5 ; Condition 2 : K1 = 3.5, K2 = 3.5
Condition 3 : K1 = 1.0, K2 = 2.5

5.5 EFFECT OF CAPACITANCE TO GROUND

It is well known that the capacitance to ground plays a prominent role in the initial volatge distribution[8-13,15,41] in transformer windings. In order to study the effect of capacitance to ground on the surge voltage distribution in transformer windings, the values of two ground capacitances, namely, capacitance of each disc to core (CDL) and capacitance of each turn of the line-end disc to ground (CT), were varied once at a time.

In the first case, CT was given double its original value. This case was referred to as condition 2.

In the other case, the ground capacitance to core of each disc was increased by 100% from its original value. This case was referred to as condition 3.

The case in which the coil kept its original parameters was referred as condition 1.

The effect of the above parameters are shown in fig 5.15 to fig 5.18.

Any noticeable increase in the value of a ground capacitance would be quickly reflected in a less linear voltage distribution in the initial period after surge arrival with sharper oscillations in the tail of the waveshapes. This is to be expected because of the increase in the capacitive coupling to ground which leads to a lower induced voltage at all different turns in the initial period of time. This could be clearly illustrated by comparing the voltage distribution of turn 32 in condition 1 (fig 5.16.a) and in condition 3 (fig 5.16.c). Moreover, the increase in capacitance to ground affects the reflections and refractions patterns due to the change in impedance encountered at all impedance discontinuities, leading to variation in oscillation amplitudes in the wavetail of the surges as shown in fig 5.15. This effect is also visilble from the sharper oscillations in the voltages of disc 4 (fig 5.16)and the amplitudes of such voltages towards the end of the observation time. It is important to

mention that no shifting of the voltage distribution in the time axis could be detected, or in other words, no noticeable variation in the velocity of propagation occured as a result of changes in the ground capacitance.

As mentioned in the preceding section, an increase in capacitive coupling to ground increases the interturn and interdisc voltages as shown in fig 5.17 and fig 5.18.

To summarize, the capacitances to ground play a prominent role in determining the interturn and interdisc voltages. However, their effect on surge propagation velocity is negligible.

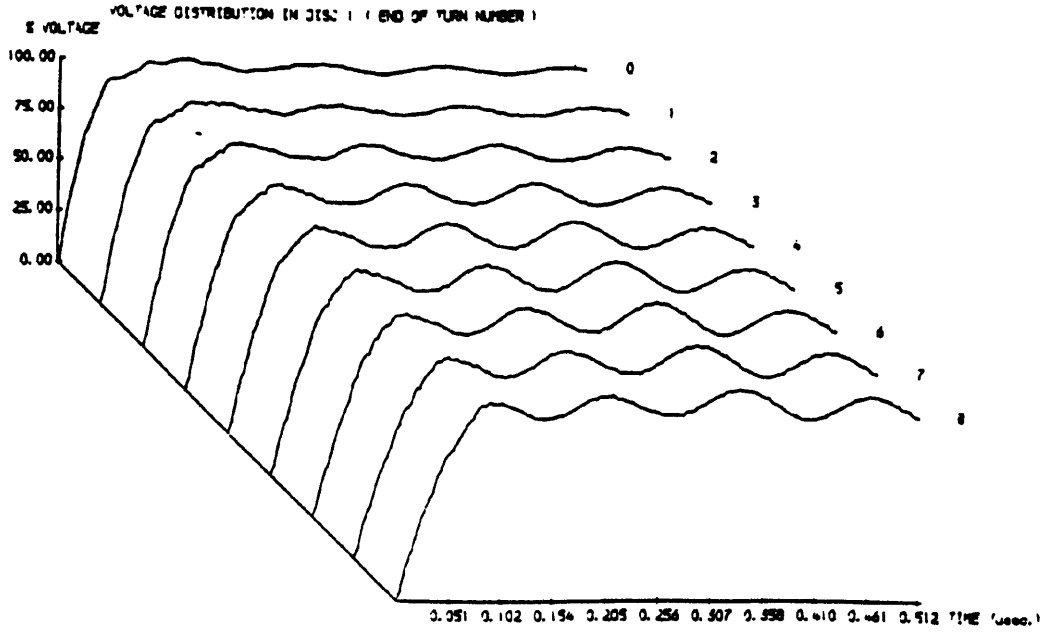

a)

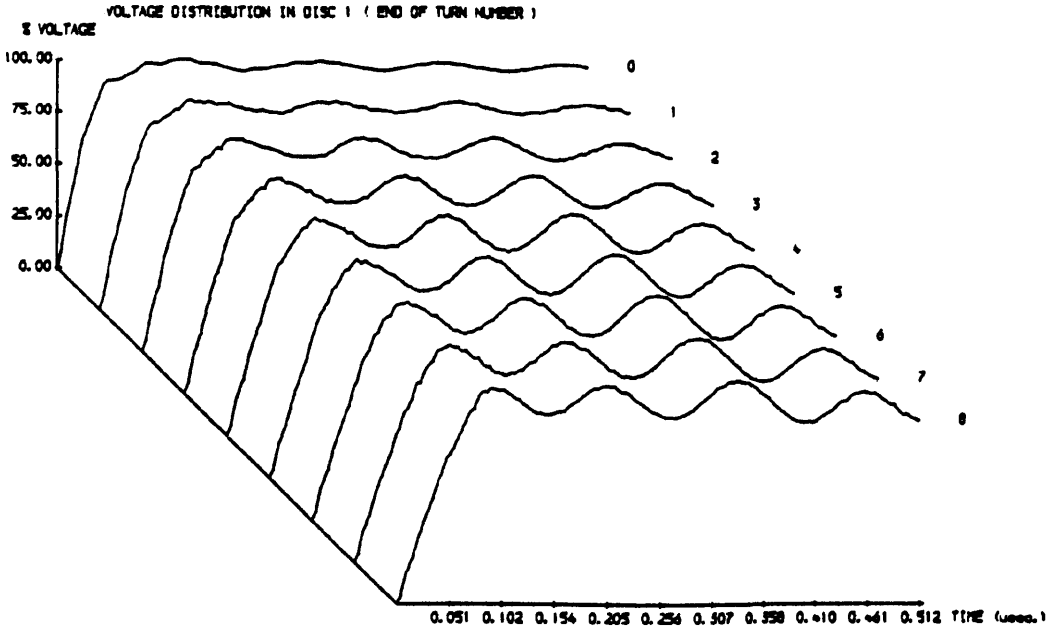

b)

Fig 5.15 Voltage distribution in disc 1 for different capacitances to ground (CT : Capacitance on top, CDL : Capacitance to core)
a) Condition 1 : CT = 2.2 pF, CDL = 4.06 pF
b) Condition 2 : CT = 4.4 pF, CDL = 4.06 pF

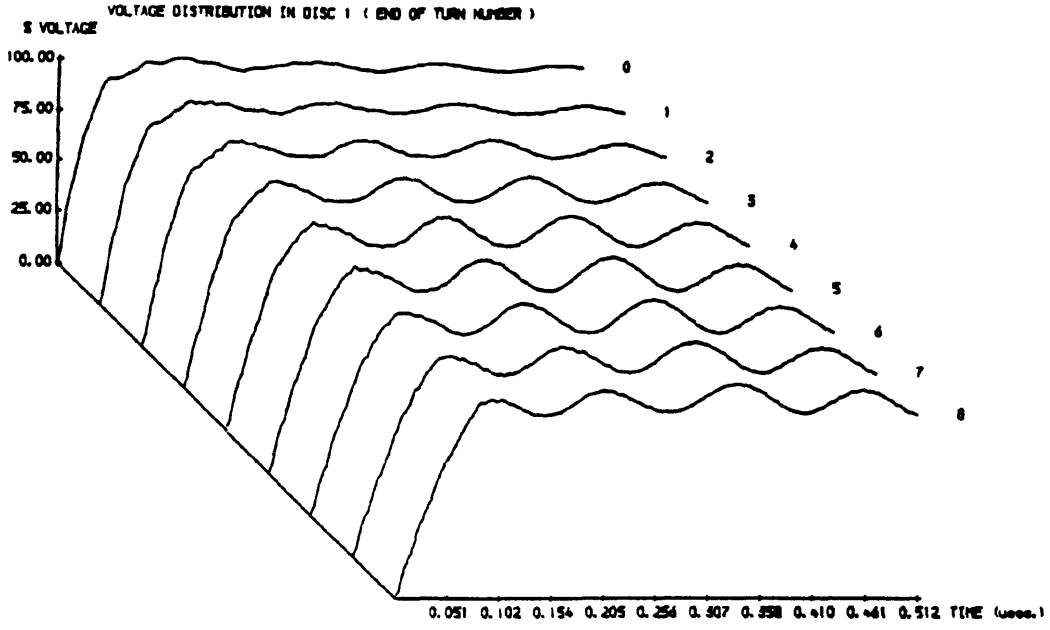

c)

Fig 5.15 Voltage distribution in disc 1 for different capacitances to ground (CT : Capacitance on top, CDL : Capacitance to core)
c) Condition 3 : CT = 2.2 pF, CDL = 8.12 pF

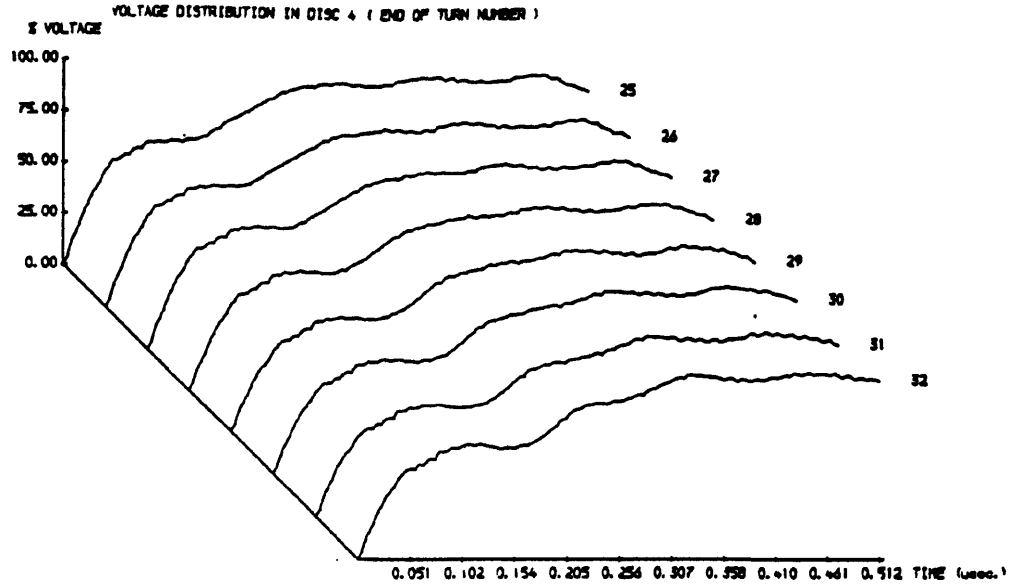

a)

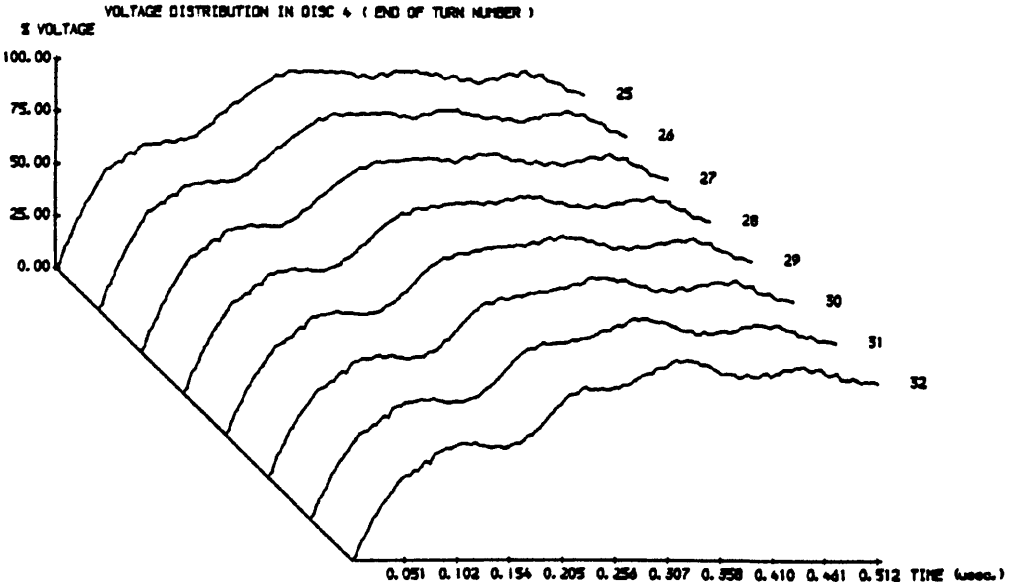

b)

Fig 5.16 Voltage distribution in disc 4 for different capacitances to ground (CT : Capacitance on top, CDL : Capacitance to core)
a) Condition 1 : CT = 2.2 pF, CDL = 4.06 pF
b) Condition 2 : CT = 4.4 pF, CDL = 4.06 pF

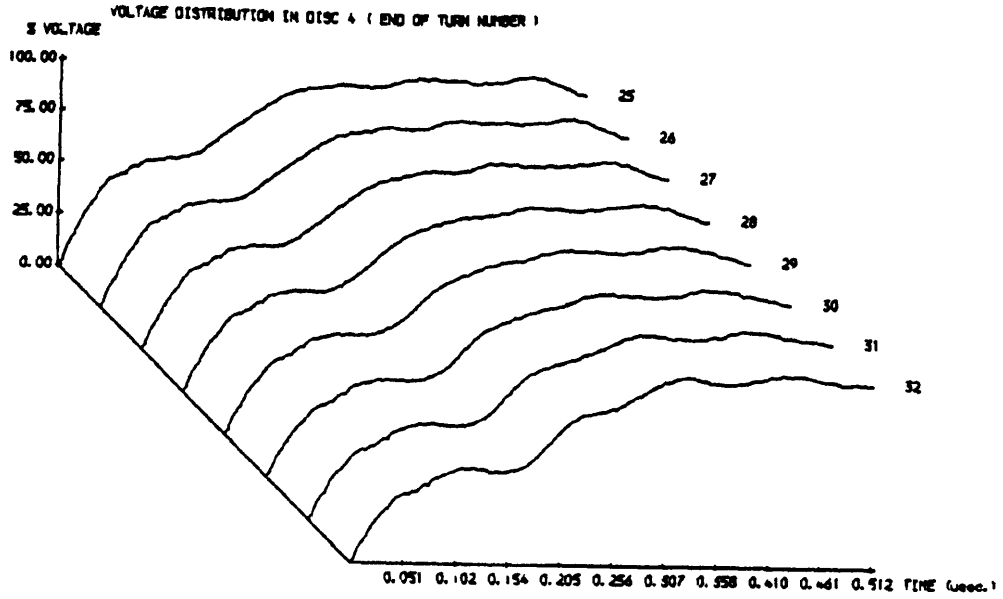

c)

Fig 5.16 Voltage distribution in disc 4 for different capacitances to ground (CT : Capacitance on top, CDL : Capacitance to core)
c) Condition 3 : CT = 2.2 pF, CDL = 8.12 pF

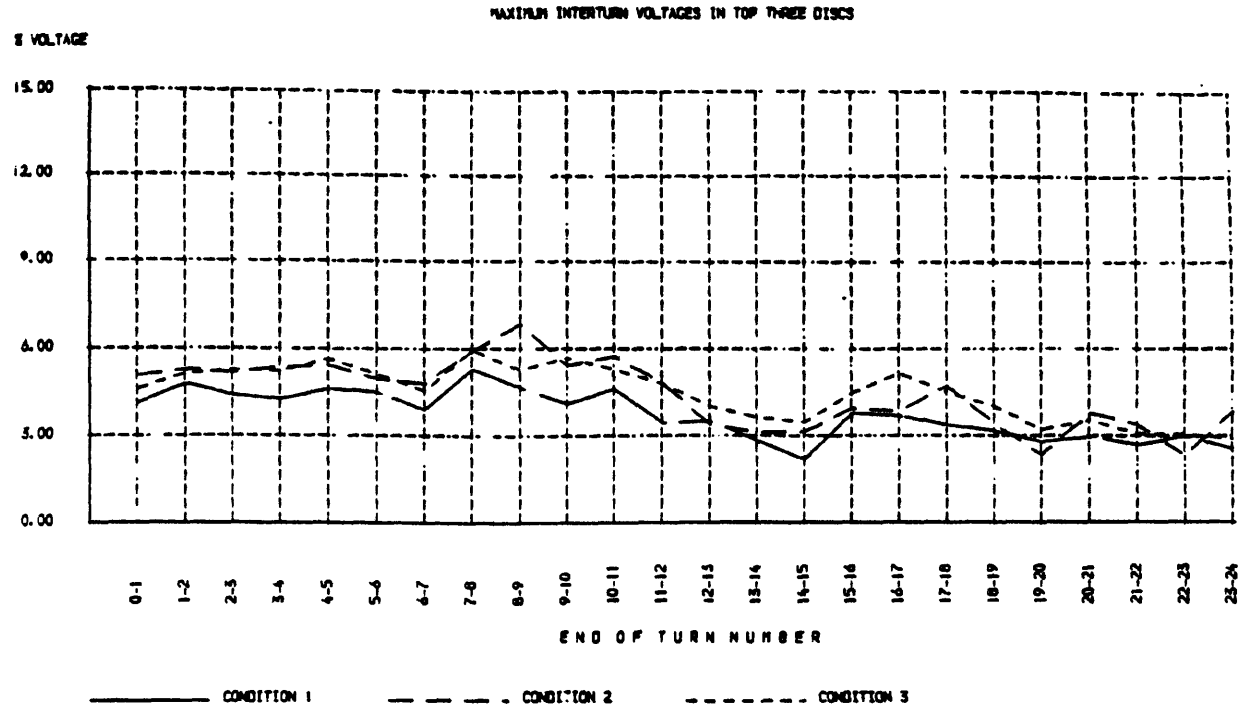

Fig 5.17 Maximum interturn voltages for different capacitances to ground

Condition 1 : CT = 2.2 pF, CDL = 4.06 pF

Condition 2 : CT = 4.4 pF, CDL = 4.06 pF

Condition 3 : CT = 2.2 pF, CDL = 8.12 pF

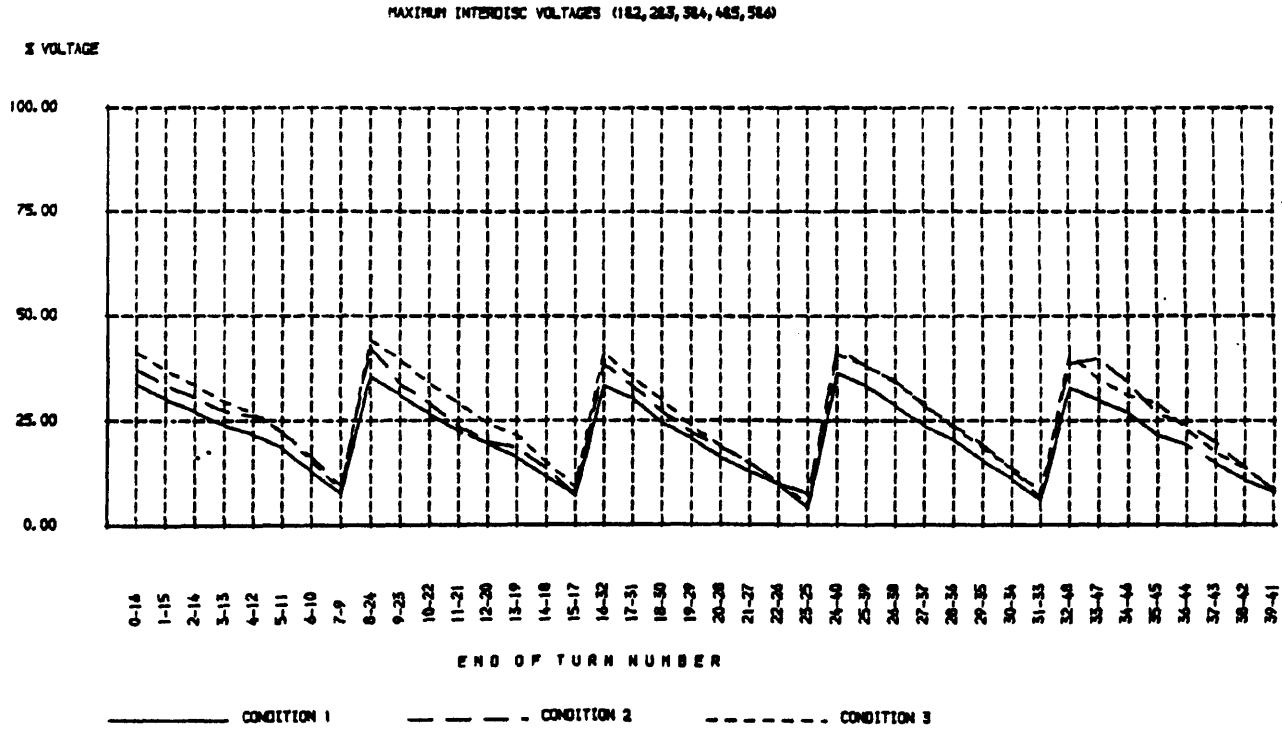

Fig 5.18 Maximum interdisc voltages for different capacitances to ground

Condition 1 : CT = 2.2 pF, CDL = 4.06 pF

Condition 2 : CT = 4.4 pF, CDL = 4.06 pF

Condition 3 : CT = 2.2 pF, CDL = 8.12 pF

5.6 EFFECT OF INDUCTANCE

At the very high frequencies (> 0.5 MHz) involved in our studies, the inductance of the coil was obtained by multiplying the inductance in air by a loss factor K_{loss} in order to take account of the unknown losses[62,63] which do occur at such very high frequencies. This fact has already been justified by the close agreement between the corresponding computational and experimental results for surge distribution in the transformer winding. However, the effect of considering the inductance in air (condition 2) was studied and is shown in fig 5.19 to fig 5.21. condition 1 represents the coil with the original parameters.

As it can be seen from fig 5.19, the clear effect of increasing the coil inductance is a shifting of the voltage profile in the forward direction along the time axis, due to a smaller velocity of propagation, as in the case of insulation permittivity. Moreover, the change in inductance changes the reflection and refraction patterns due to the change in impedance encountered by the travelling waves at impedance discontinuities. This could again be clearly detected from the increase in the oscillations magnitudes in the voltage distributions of the different turns due to the increase in inductance.

Similarly to insulation permittivity changes, an increase in the inductance would not only shift the interturn and interdisc voltages in the forward direction along the time axis, but also increases their magnitudes as it could be seen from fig 5.20 and fig 5.21.

From the effect of inductance on surge voltage distribution in transformers, assuming that the inductance at the very high frequencies is that of an air core would give erroneous results as the computational results would diverge in both frequency and magnitude from the actual experimental results.

To conclude, the inductance is a major factor in determining the surge voltage distribution and subsequently the interturn and interdisc voltages.

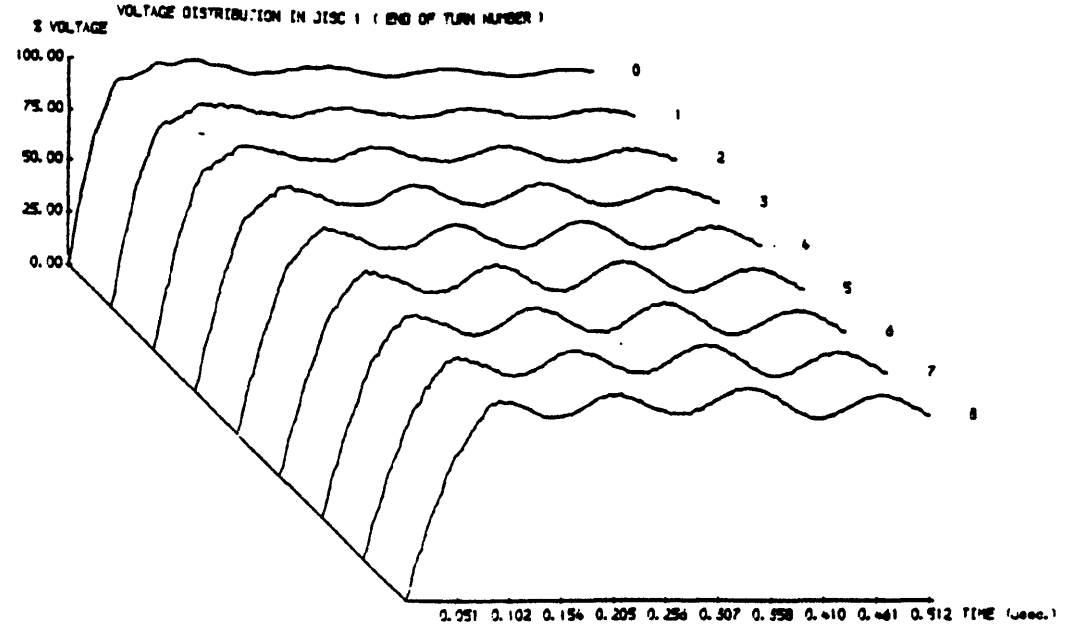

a)

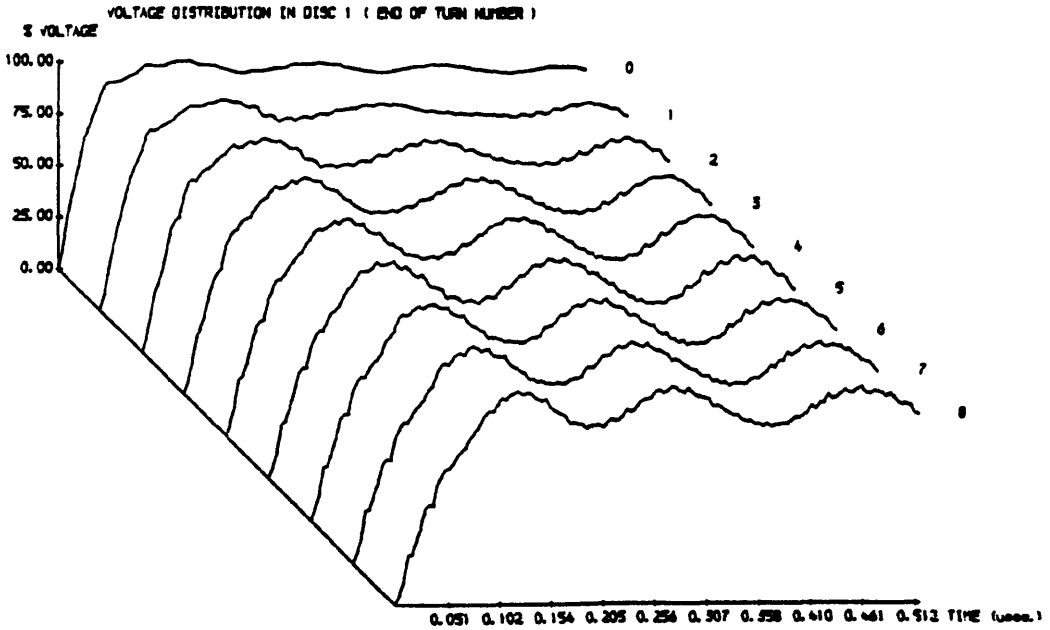

b)

Fig 5.19 Voltage distribution in disc 1 for different inductances

a) Condition 1 : 50% of air core inductance

b) Condition 2 : Air core inductance

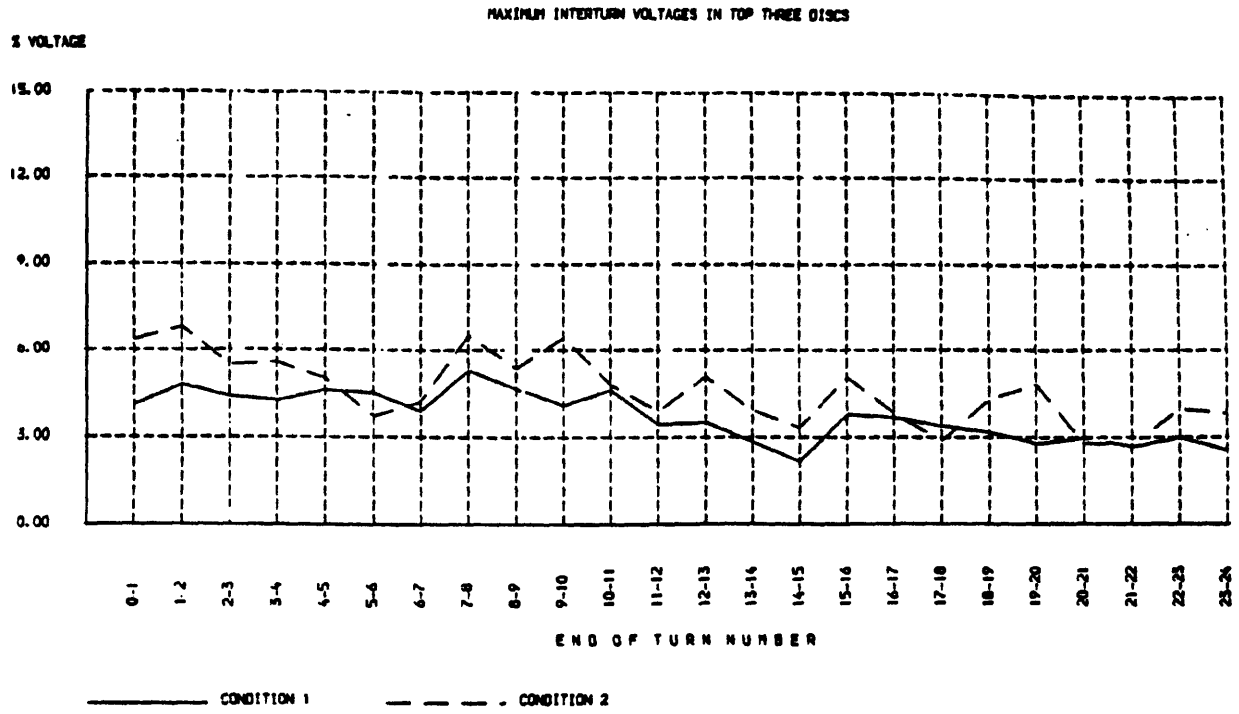

Fig 5.20 Maximum interturn voltages for different inductances
Condition 1 : 50% of air core inductance ; Condition 2 : Air core inductance

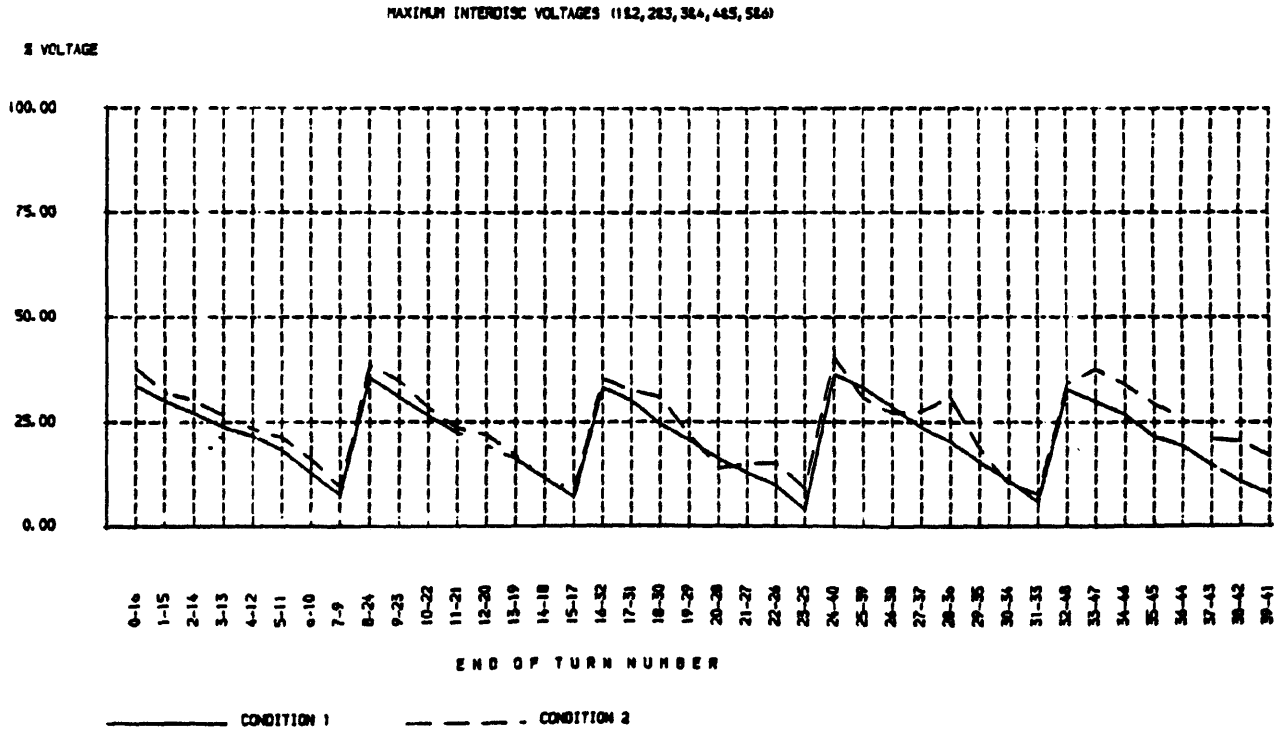

Fig 5.21 Maximum interdisc voltages for different inductances
Condition 1 : 50% of air core inductance ; Condition 2 : Air core inductance

5.7 DISCUSSION

The sensitivity analysis carried out in order to study the effects of various parameters on transformer response to very fast fronted surges has led to the following assesments :

An increase in the risetime of the incoming surge resulted in a flattening of the voltage distributions of the various turns. This was attributed to the simple fact that a smaller proportion of the slower front of the incoming wave reached the impedance discontinuities where it was reflected leading to the creation of reflected waves with smaller magnitudes which in turn caused smaller oscillations in turn voltage distributions. Consequently, such fact was also responsible for the decrease in the magnitudes of all peaks of both interturn and interdisc voltages with the increase in wavefront duration. However, it was noticed that the steepest surge caused the highest interturn voltage to occur across the turns connected directly to the line-end terminal instead of the turns at the remote end of the line-end disc.

Transposing of turns inside the winding led to a better initial voltage distribution. This was detected from the higher induced voltages at all turns upon surge arrival, which was a direct consequence of the better capacitive distribution resulting from the increased series capacitance of the interleaved winding. Furthermore, the different turn voltages exhibited higher frequencies of oscillation as the travelling wave reached the various impedance discontinuities in almost half the time required in case of the conventional winding. Moreover, the problem of correlation between radial and axial insulation was solved due to the smaller ratio between interturn and interdisc voltages since the the interturn voltages in some parts of the interleaved coil were higher than those in the conventional winding with the interdisc voltages considerably lower. However, both the interturn and interdisc voltage distributions were non-linear.

A change in the insulation permittivity modified the pattern of

reflections and refractions in the coil leading to variation in the oscillations amplitudes of the turn voltages especially in the line-end disc. Such variation was caused by the travelling wave encountering changed impedances at the various discontinuities as a consequence of the changes in the capacitive couplings brought about by alterations in the insulation permittivity. Such modifications in the capacitive couplings also yielded changes in the velocity of propagation, which was detected through the shifting of the turn to ground, interturn and interdisc voltage distributions along the time axis. Moreover, a change in the insulation permittivity caused an alteration in the amplitudes of the interturn and interdisc voltages again as a direct result of the variations in axial and radial interturn capacitive couplings and capacitive coupling to ground.

A change in the inductance of the coil also modified the reflection and refraction patterns due to the changes in in impedances met by the travelling waves at the various discontinuities as a result of the variations in the inductive couplings. This also led to a change in the velocity of propagation of the incoming wave and variations in the amplitudes of both interturn and interdisc voltages, as in case of insulation permittivity.

Any increase in the capacitance to ground led to a less linear initial voltage distribution due to the lower induced voltages at all different turns directly after surge arrival. This was attributed to the fact that with a higher capacitive coupling to ground, the turns were less isolated from earth and their potential remained low until surge arrival. This in turn yielded higher interturn and interdisc voltages. However, no variation in the velocity of propagation was noticed. Again, due to the changes in the capacitances, the reflection and refraction patterns were affected leading to variations in the oscillation amplitudes in the wavetail of the turn to ground voltage distributions.

The effect of the termination impedance to the model became more and

more apparent on the voltage distributions in the lower sections of the model. This was to be expected since with the location of the termination impedance at the end of the eighth disc, no reflection from the bottom end of the coil would reach the top discs within the scope of the observation time considered and, furthermore, the termination impedance would not influence the voltage distributions in the top discs through the capacitive network (parallel mode). In fact, a higher termination impedance led to further isolation of the turns of the lower sections from ground, therefore leading to an increase in their potential and hence lower interturn and interdisc voltages. Consequently, it was found that the best estimation for the termination impedance would be the input impedance of the two coils seen by the travelling wave as being in parallel within the scope of the observation time.

Any variation in the series losses did not have any impact on the various results as it was thought that the importance of such parameter would only show later on outside the scope of the observation time. In other words, in the first half microsecond after surge arrival, the capacitive and inductive distributions were the main features in predicting very fast fronted surge distributions.

From above, we can conclude that the computer model of the transformer winding correctly predicted the effects of the different parameters. Accordingly, the developed model could be applied to different transformers operating under different conditions, leading to a better and clear assessment of the insulation condition for any individual application.

CHAPTER 6

CONCLUSIONS

With the increasing usage of Gas Insulated Substations during the last two decades, the propability of very fast fronted surges reaching transformer windings has become greater. On reaching transformer windings, such very fast fronted surges will propagate into the windings and subsequently create severe insulation stresses. Hence, the problem of predicting surge volatge distribution in transformer windings has since attracted more and more interest. In this thesis, a computer model has been developed in order to predict the surge voltage distribution in the line-end region of the transformer winding together with the resulting interturn and interdisc voltages, due to very steep fronted reaching such windings as a consequence of switching operations performed within GIS.

The computer model is based on multiconductor transmission line theory together with modal analysis. It represents the transformer coil as a two-port network in which the individual turn constitutes the basic element. As a result, all couplings between the individual turns of the same and different sections were taken into consideration. The capacitance matrices used in the model were calculated by approximating the walls of the turns to parallel plate capacitors. The inductance matrices, due to the non-homogeneity of the insulating medium, were calculated from the simple relation between the inverse capacitance matrices in air and velocity of light since the inductive elements are invariant parameters of dielectric permittivity. Further, due to unknown losses which occur at the very high frequencies involved in the studies, the inductance matrix of the coil was found to be 50% less than the air core inductance. On the other hand, the model was terminated by an impedance which represented the cascade-connected discs not included in the studies since it is impractical

and unnecessary to include all the winding in the model.

The computer model accurately predicted the very fast fronted surge distribution in the top four discs in the line-end region, where most insulation failures are likely to occur, within the considered observation time of 512 nsec after surge arrival. The accuracy of the model was demonstrated through the close agreement between the computational and experimental results obtained from measurements on the actual HV transformer winding, and for surges with different risetimes.

The accuracy of the model is a direct result of its feature to represent both the capacitive transfer (parallel mode) and series mode of propagation of the incoming surge inside the winding. The parallel mode of propagation is dominant in the initial period of time after surge arrival, leading to instantaneous induced voltages at all turns with their amplitudes dictated by the axial and radial capacitive couplings. The series mode of propagation is the propagation of the surge itself turn by turn through the winding , resulting in steeper rates of rise in the voltages of the different turns upon surge arrival (at those turns) and variations in such voltages due to the multiple reflections and refractions at the different impedance discontinuities, which are transmitted throughout the winding by the various mutual couplings. Both modes of propagation together with the mutual couplings contribute to the interturn and interdisc voltages although the series mode is the dominant factor due to its flattening effect on the surge wavefront inside the winding and its role throughout the observation time. The maximum interturn voltages decrease in magnitude away from the line-end terminal, with a delay in their occurence due to the travel time of the surge, and they posess a non-linear trend within each disc. In contrast, The maximum interdisc voltages between the turns of two consecutive discs are almost linear with the largest peaks (between non-connected ends of consecutive discs) having almost constant magnitudes in the line-end region of the winding (

all peaks occur with time delay due to the travel time of the surge).

However, in order to extend the accuracy of the model to the top four discs in the scope of the observation time, an eight-disc model was used in order to minimize the effect of the termination impedance at the end of the model whose value over the whole frequency spectrum could only be fairly estimated. Hence, the surge voltage distribution in the discs further down the winding could be predicted by including more discs in the model but with calculation instabilities related to matrix size likely to occur.

Moreover, the accuracy of the computer model confirmed the exactness of the evaluation of the electrical parameters of the coil under study, whose input impedance over the whole frequency spectrum was also presented.

A sensitivity analysis was carried out in order to study the effects of various parameters on transformer surge distribution and, consequently, monitor the applicability of the developed model to different transformers operating under different conditions. Those parameters included the wavefront duration of the incoming wave, interleaving of the turns, insulation permittivities of the insulating media, capacitance to ground, inductance of the coil and termination impedance to the model. The study of different risetimes has shown that a faster surge causes an increase in both interturn and interdisc volatges with a shift in the location of the highest interturn from the inside of the line-end disc to the first two turns connected to the line-end terminal in the case of the steepest surge (30 nsec). A change in either insulation permittivity or inductance affects the velocity of propagation of the surge inside the coil and changes the amplitudes of the interturn and interdisc voltages. An increase in any capacitance to ground leads to less initial voltage distribution and higher differential voltages. In contrast, transposing of the turns leads to a better initial voltage distribution and lower interdisc voltages but higher interturn voltages and , as a result, a much improved correlation between axial and radial insulation. Finally, the study of the effect of

different termination impedances has revealed that an increase in its value leads to lower interturn and interdisc volatges especially in the lower sections of the winding. Thus, the input impedance of two coils in parallel, in the scope of the considered observation time, is the best obtainable estimation for the termination impedance of the model.

The model developed in the Ph.D research could be implemented in larger models of GIS in order to adequately represent the transformer winding when investigating the characteristics of the wavefronts of very steep surges created by switching operations in GIS, which is of utmost importance in the first few hundred nanoseconds. Such future studies would accurately predict the characteristics of the surge impinging on the transformer terminals and, at the same time, assess the insulation stresses inside the winding.

REFERENCES

(1) " Very Fast Transients Phenomena Associated with Gas Insulated Substations ", in " Monograph 35 on GIS Very Fast Transients ", CE / SC, 33 / 13, GT / WG 09, 1989.

(2) K. FESER, W. PFAFF, J. MEPELLINK and K. DIDERICH, " Very Fast Transients in GIS ", CIGRE 33-87 (WG 09).

(3) W. BOECK and R. WITZMANN, " Main Influences on the Fast Transient Development in GIS ", Fifth International Symposium on High Voltage Engineering, Braunschweig, 1987, paper 12-01.

(4) S. A. BOGGS, F. Y. CHU, N.FUJIMOTO, A. KRENICKY, A. PLESSL and D. SCHLICHT, " Disconnect Switch Induced Transients and Trapped Charge in Gas Insulated Substations ", IEEE Trans.,PAS Vol. 101, No. 10, 1982, pp. 3539.

(5) N. FUJIMOTO and S. A. BOGGS, " Characteristics of GIS Disconnector-Induced Short Risetime Transients Incident on Externally Connected Power System Components ", IEEE PES Winter Meeting, 1987, Paper 87 WM 1185-2.

(6) G. ECKLIN, D. SCHLICHT and A. PLESSL, " Overvoltages in GIS Caused by the Operation of Isolators ", Surges in High-Voltage Networks, K. RAGALLER, ed. Plenum, 1980.

(7) F. REISINGER, A. DIESSNER, M. MUHR and H. SCHENNER, " Field Measurements of Fast Transient Voltages in 420 Kv GIS WIEN SUED ", CIGRE Symposium, Vienna, 1987.

(8) K. J. CORNICK, " Surge Voltages in Transformers and Reactors ", Lecture Notes, UMIST.

(9) A.T. CHADWICK, J. M. FERGUSON, D. H. RYDER and G. F. STEARN, " Design of Power Transformers to Withstand Surges Due to Lightning with Special Reference to A New Type of Winding ", Proceedings, Institution of Electrical Engineers, London, England, Vol. 97, Pt. II, 1950, pp. 737.

(10) R. KUCHLER, " Die Transformatoren ", Springer-Verlag, Berlin / Heidlberg / New York, 1966.

(11) L. F. BLUME and A. BOYAJIAN, " Transient Voltage Characteristics of Transformers ", Transformer Engineering (Book), 1951 Edition.

(12) B. HELLER and A. VEVERKA, " Surge Phenomena in Electrical Machines ", Iliffe, London, 1968.

(13) L. M. BURRAGE, E. F. VEVERKA and B.W.McCONNELL, " Steep Front Short Duration Low Voltage Impulse Performance of Distribution Transformers ", IEEE WM126-6, 1987.

(14) D. MACDONALD, " Power Transformers for High Voltage Transmission ", Bruce Peebles & Co. Ltd, Edinburgh.

(15) G. M. STEIN, " A Study of the Initial Voltage Distribution of Concentric Transformer Windings ",IEEE Trans., Pas Vol. 83, 1964,pp.877-893

(16) A. T. CHADWICK, J. M. FERGUSON, D. H. RYDER and G.F. STEARN, " A New Type of Transformer winding Giving Improved Impulse Voltage Distribution ", Report No. 107, CIGRE, Paris, France, 1950.

(17) E. J. GRIMMER and W. L. TEAGUE, " Improved Core Form Transformer Windings ", AIEE Trans., Vol. 70, Pt 1, 1951, pp. 962-967.

(18) W. MULLER and W. STEIN, " Behaviour of High Voltage Transformer Windings on Steep Fronted Input Waves of Nanosecond Duration ", Siemens Power Engineering V, No. 5, 1983, pp.259-262.

(19) A. PEDERSEN, " On the Response of Interleaved Transformer Windings to Surge Voltages ", IEEE Trans., PAS Vol.82, 1963, pp.349-356.

(20) W. J. McNUTT, T. J. BLALOCK and R. A. HINTON, " Response of Transformer Windings to System Transient Voltages ", IEEE Trans., PAS Vol. 93, NO. 1, 1974, pp. 457-467.

(21) A. J. McELROY, " On the Significance of Recent EHV Transformer Failures Involving Winding Resonnance ", IEEE Trans., PAS Vol. 94, No. 4, 1975, pp.1301-1316.

(22) H. B. MARGOLIS, J. D. M. PHELPS, A. A. CARLOMANGO and A. J. MCELROY, " Experience with Part Winding Resonnance in EHV Auto-Transformers : Diagnostics and Corrective Measures ", IEEE Trans., PAS Vol. 94, NO. 4, 1975, pp.1294-1300.

(23) R. C. DEGENEFF, W. J. McCNUTT, W. NEUGBAUER, J. PANEK, M. E. McCALLUM and C. C. HONEY, " Transformer Response to System Switching Voltages ", IEEE Trans., PAS Vol. 101, 1982, pp.1457-1470.

(24) R. J. MUSIL, G. PREININGER, E. SCHOPPER and S. WENGER, " Voltage Stresses Produced by Aperiodic and Oscillatory System Overvoltages in Transformer Windings ",IEEE Trans., PAS Vol. 100, No. 1, 1981, pp. 431-438.

(25) T. ADIELSON, A. CARLSON, H. B. MARGOLIS and J. A. HALLADAY, " Resonnant Overvolatges in EHV Transformers ", IEEE Trans., PAS Vol. 100, 1981, pp.3536-3571.

(26) J. SCHMIDT and H. WITT, " Response of a Transformer Winding on Excitation at Frequencies Higher than 200 KHz ", Contribution to Discussion of Group 12, CIGRE 1984, to Question 20 of the Special Report 12-00.

(27) " Experiences regarding Transformer Failures Due to Very Fast Transients (VFT) and Results of Investigations of the Oscillation Behaviour of Windings Stressed by VFT ", Presented by VEB Transformatorenwek " Karl Liebknecht " to CIGRE WG 12-11 on 07.12.1987.

(28) O. BOSOTTI, W. MOSCA, G. RIZZI, L. HASKOFF, E. KYNASI and H. LUHRMANN, " Phenomena Associated with Switching Capacitive Currents by Disconnectors in Metal Enclosed SF6-Insulated Switchgear ", CIGRE 13-06, 1982.

(29) A. EDLINGER, G. MAUTHE, F. PINNEKAMP, D. SCHLICHT and W. SCHMIDT, " Disconnector Switching of Charging Currents in Metal Enclosed SF6-Gas Insulated Switchgear at EHV ", CIGRE 13-14,1984.

(30) J. LALOT, A. SABOT and J. KIEFFER, " Dielectric Behaviour of GIS Switching Disconnectors, Comparison of Possible phase Opposition Tests ", IEEE Trans. on Power Delivery, Vol. 3, NO. 1, 1988.

(31) W. BOECK, W. TASCHNER, J. GORABLENKOW, G. F. LUXA and L. MENTEN, " Insulating Behaviour of SF6 with and without Solid Insulation in Case of Fast Transients ", CIGRE 15-07, 1986.

(32) W. TASCHNER, " Voltage-Time Curves of SF6 Insulation for Steep Fronted Impulse Voltages Below 1 μs ", 8th International Conference on Gas Discharges and their Application, Oxford, 1985, pp. 259.

(33) W. PFEIFFER
" IMPULSTECKNICK ", Carl Hansa Verlag Munchen Wien, 1976, pp. 44.

(34) W. PFEIFFER, " Gesetzmaβigkeit Beim Durchschlag Von Funkenstrecken in Komprimiertem Schwefelhexafluorid ", ETZ-A, Vol. 95, 1974, pp.405.

(35) J. LALOT, A. SABOT, J. KIEFFER and S. W. ROWE, " Preventing Earth Fault During Switching of Disconnectors in GIS Including Voltage Transformer ", IEEE Trans., Vol. PWRD-1, 1986, pp.203.

(36) S. A. BOGGS, M. FUJIMOTO, M. COLLOD and E THURIES, " The Modelling of Statistical Operating Parameters and the Computation of Operation-Induced Surge Waveforms for GIS disconnectors ", CIGRE 13-15, 1984.

(37) R. WITZMANN, " Fast Transients in Gas Insulated Substations (GIS). Modelling of Different GIS Components ", 5th ISH, Braunschweig, FRG, 1987, Paper 12-06.

(38) S. OGAWA, E. HAGINOMORI, S. NISHIWAKI, T. YOSHIDA and K. TERASAKA, " Estimation of Restriking Transient Overvoltage on Disconnecting Switch for GIS ", IEEE Trans., Vol PWRD-1, 1986, pp.95.

(39) N. FUJIMOTO, H. A. STUCKLESS and S. A. BOGGS, " Calculation of Disconnector Induced Overvoltages in Gas-Insulated Substations ", in L. G. CHRISTOPHOROU and M. O. PACE (Eds), Gaseous Dielectrics IV, Pergamon Press, New York, 1984.

(40) N. FUJIMOTO, E. P. DICK, S. A. BOGGS and G. L. FORD, " Transient Ground-Potential Rise in Gas Insulated Substations - experimental Studies ", IEEE Trans., PAS Vol 101, No. 10, 1982.

(41) A. GREENWOOD, " Electrical Transients in Power Systems ", John Whiley & Sons, USA ,1971.

(42) R. RUDENBERG, " Performance of Travelling Waves in Coils and Windings ", Trans. AIEE, Vol 59, 1940, pp.1031-1045.

(43) T. J. LEWIS, " The Transient Behaviour of Ladder Network of the type Representing Transformer and Machine Windings ", Proc. IEE, 1954, Vol. 101, Pt 2, pp. 541-553.

(44) B. M. DENT and E. R. HARTILL, " A Method of Analysis of Transformer Impulse Voltage Distribution Using A digital Computer ", Proc. IEE, Vol. 105, 1958.

(45) M. KRONDL and A. SCHLEICH, " Predetermination of the Transient Voltages in Transformers Subject to Impulse Voltage ", Bulletin Oerlikon, 1965, pp. 114-133.

(46) R. C. DUGAN, R. GABRICK, J. C. WRIGHT and K. W. PATTEN, " Validated Techniques for Modelling Shell-form type EHV Transformers ", IEEE Trans. on Power Delivery, Vol. 4, No. 2, 1989.

(47) P. I. FEREGESTAD and T. HENRIKSEN, " Transient Oscillations in Multi-Winding Transformers ", IEEE Trans., PAS Vol. 93, 1974, pp.500-509.

(48) A. MIKI, T. HOSOYA and K. OKUYAMA, " A Calculation Method for Impulse Voltage Distribution and Transferred Voltage in Transformer Windings ", IEEE Trans., PAS Vol. 97, 1978, pp. 930-939.

(49) L. M. BURRAGE et AL, " Assess of the Impact of Steep Front Short Duration Impulse on Electric Power System Insulation-Phase I, Final Report ", ORNL/Sub/85-28611, 10/14/86.

(50) D. KONIG, Contribution to CIGRE WG 33, Preferential Subject 3, Question 11, CIGRE Meeting Discussion, 1988.

(51) G. PREININGER, Contribution to CIGRE WG 33, Preferential Subject 3, Question 11, CIGRE Meeting Discussion, 1988.

(52) M. T. WRIGHT, S.J.YANG and K. McCLAY, " General Theory of Fast-Fronted Interturn Voltage Distribution in Electrical Machine Windings ", IEE Proc., Vol. 130, Pt. B, No. 4, 1983.

(53) P. G. MACLAREN and H. ORAEE, " Multiconductor Transmission-Line Model for Line-end Coil of Large A.C. Machines ", IEE Proc., Vol. 132, Pt. B, No. 3, 1985.

(54) J. L. GUARDADO and K. J. CORNICK, " A Computer model for Calculating Steep-Fronted Surge Distribution in Machine Windings ", IEEE PES, Summer Meeting 1988, Paper No. WM88 SM 609-0.

(55) J.L. GUARDADO, " Computer Models for Representing Electrical Machines during Switching Transients ", Ph.D thesis, UMIST,1989.

(56) J. P. BICKFORD, " Multiconductor Line Analysis ", Lecture Notes, 1983, UMIST.

(57) G.W. CARTER, " The Electromagnetic Field in its Engineering Aspects ", Longmans, Second Edition, London, 1967.

(58) S. SADULLAH, " Field Analysis of a Transformer Winding with Applications ", M.Sc Dissertation, UMIST, 1987.

(59) R. K. MOORE, " Travelling Wave Engineering ", McGraw Hill, Electronic and Electrical Series, 1960.

(60) J. AVILA ROSALES and F.L. ALVARADO, " Non-linear Frequency Dependent Transformer Model for Electromagnetic Transient Studies in Power Systems ", IEEE Trans., PAS Vol. 101, No. 11, 1982.

(61) F. W. CHANG, " Transient Analysis of Lossless Coupled Transmission Lines in a Nonhomogeneous Dielectric Medium ", IEEE Trans. on Microwave Theory and Techniques, Vol. MTT-18, No. 9, 1970.

(62) K. K. LI, " The Parameters of Transformer Windings for Surge Distribution Calculations ", M.Sc Dissertation, 1971, UMIST.

(63) M. J. PIRENNE, " Theorie Generale des Phenomenes Oscillatoires dans les Enroulements de Transformateurs ", Revue Generale de l'Electricite, 1940, p.19.

(64) D.K.CHENG, " Analysis of Linear Systems ", Addison Wasley series in Elect. Eng., 1959.

(65) E.R. ZEINER, W.H. TRANTER and D.R.FANNIN, " Signals and Systems Contineous and Discrete ", Macmillan Publishing co., New York, 1983.

(66) H.NAKANISHI and A AMETANI, " Transient Calculation of a Transmission Line using Superposition Law ", IEE Proc., Vol. 133, Pt. c, No. 5, 1986.

(67) E.O. BRIGHAM, " Fast Fourier Transform ", Prentice-Hall, 1974.

(68) A.N.D. TLEIS, " Prestriking Transients in Industrial Distribution Systems ", M.Sc Dissertation, UMIST, 1986.

(69) T.A. THEODOSSIOU, " Distribution of Very Fast Fronted Surges in Transformer Windings ", M.Sc Dissertation, UMIST, 1987.

APPENDIX A

ELECTRICAL CHARACTERISTICS OF TRANSFORMER WINDING

The transformer winding simulated in the computer program has the electrical characteristics given below :

Number of discs per winding (D)	72
Number of turns per disc (T)	8
Length of mean turn (LMT)	1709 mm
Axial length of disc (ALD)	6.5 mm
Interturn insulation thickness (IIT)	0.5 mm
Physical length of coil axially (ALC)	949 mm
Number of spacers per circle (NS)	12
Width of spacers (WS)	38 mm
Thickness of spacers (TS)	6.35 mm
Outside diameter of LV winding (RO)	417 mm
Radial depth of disc (RDD)	41 mm
Number of LV-WRAP duct sticks per circle (N1)	24
Width of LV-WRAP duct sticks (W1)	13 mm
Radial thickness of LV-WRAP duct sticks (T1)	10 mm
Thickness of Wrap number 1 (TW1)	3.2 mm
Number of WRAP-WRAP duct sticks per circle (N2)	12
Width of WRAP-WRAP duct sticks (W2)	16 mm
Radial thickness of WRAP-WRAP duct sticks (T2)	13 mm
Thickness of Wrap number two (TW2)	3.2 mm
Number of WRAP-HV duct sticks per circle (N3)	12
Width of WRAP-HV duct sticks (W3)	19 mm
Radial thickness of WRAP-HV duct (T3)	13 mm
Permittivity of cooling medium (K1)	1.0

Permittivity of conductor covering (K2)	3.5
Permittivity of disc spacers (K3)	6.0
Permittivity of HV-LV duct sticks (K4)	4.0

APPENDIX B (COURTESEY : GEC DISTRIBUTION TRANSFORMERS LTD)

CALCULATIONS AND EQUATIONS FOR IMPULSED DISC COILS

$$\text{Interturn Capacitance} = \frac{0.225 * LMT * ALD * K2}{25.4 * ITT}$$

Interdisc Capacitance =

$$\frac{0.225 * RDD}{25.4} * \left[\frac{NS * WS}{(TS / K3) + (IIT / K2)} + \frac{LMT - (NS * WS)}{(TS / K1) + (IIT / K2)} \right]$$

$$\text{Ground Capacitance} = \frac{0.615 * ALC / 25.4}{\frac{1}{C1} + \frac{1}{C2} + \frac{1}{C3} + \frac{1}{C4} + \frac{1}{C5}}$$

Where

$$C1 = \frac{(K4 * N1 * W1 / 25.4) + (K1 * (\pi * (R1 + R2) - N1 * W1 / 25.4))}{\pi * (R2 + R1) * LOG (R2 / R1)}$$

$$C2 = \frac{K2}{LOG (R3 / R2)}$$

$$C3 = \frac{(K4 * N2 * W2 / 25.4) + (K1 * (\pi * (R3 + R4) - N2 * W2 / 25.4))}{\pi * (R3 + R4) * LOG (R4 / R3)}$$

$$C4 = \frac{K2}{LOG (R5 / R4)}$$

$$C5 = \frac{(K4 * N3 * W3 / 25.4) + (K1 * (\pi * (R5 + R6) - N3 * W3 / 25.4))}{\pi * (R5 + R6) * LOG (R6 / R5)}$$

$$R1 = \frac{RO}{2 * 25.4} \quad ; \quad R2 = R1 + \frac{T1}{25.4} \quad ; \quad R3 = R2 + \frac{TW1}{25.4}$$

$$R4 = R3 + \frac{T2}{25.4} \quad ; \quad R5 = R4 + \frac{TW2}{25.4} \quad ; \quad R6 = R5 + \frac{T3}{25.4}$$

All symbols are defined in appendix A.

APPENDIX C

CONVOLUTION[64]

The convolution of two functions in the time domain is based on a very important theorem known as the convolution theorem. This theorem states that :

If $L[f_1(t)] = F_1(s)$ and $L[f_2(t)] = F_2(s)$ then

$$f_1 * f_2 = L\left[\int_0^t f_1(t-\tau)\, f_2(\tau)\, d\tau\right] = L\left[\int_0^t f_1(\tau)\, f_2(t-\tau)\, d\tau = F_1(s)\, F_2(s)\right] \quad \ldots(C.1)$$

where $F_1(s)$ and $F_2(s)$ are the laplace transforms of the functions $f_1(t)$ and $f_2(t)$ respectively.

To illustrate the graphical interpretation of the convolution integral of two functions $f_1(t)$ and $f_2(t)$, let

$$f_1(t) = \exp(-a\tau)\, U(\tau)$$

$$f_2(t) = \tau\, U(\tau)$$

then

$$f_1 * f_2 = L\left[\int_0^t f_1(t-\tau)\, f_2(\tau)\, d\tau\right] = L\left[\int_0^t \exp[-a(t-\tau)]\, U(t-\tau)\, \tau\, U(\tau)\, d\tau\right] \quad \ldots(C.2)$$

Fig C.1.a, C.1.b and C.1.c are the graphs of the functions $f_1(\tau)$, $f_1(\tau-t)$ and $f_1(t_1-\tau)$ where t is an arbitrary value of t. $f_2(t)$ is shown in fig C.1.d and the product of $f_1(t_1-\tau)\, f_2(\tau)$ in fig C.1.e. If we put $t = t_1$ in (C.2), then the value of the definite integral

$$\int_0^{t_1} \exp[-a(t_1-\tau)]\, U(t_1-\tau)\, \tau\, U(\tau)\, d\tau = \exp(-at_1) \int_0^{t_1} \tau \exp(a\tau)\, d\tau \quad \ldots(C.3)$$

is the area under the product curve in fig C.1.e. This area corresponds to the point at $t = t_1$ on the curve in fig C.1.f which, hence, represents the convolution of the two functions $f_2 * f_1$.

Note here that the same result will be obtained if the convolution is

done the other way, i.e, $f_1 * f_2$.

In our case, and in order to obtain the convolution of the excitation function and the turn voltage (to ground) at time $t = T_n = nT_0$, both functions were approxiamted by a series of regular pulses of duration T_0 each. The convolution integral at time $t = T_n$ was then given by,

$$C(t) = \sum_{t=0}^{T_n} e(\tau)\, T_0\, V_t(T_n-\tau) \qquad \ldots(C.4)$$

or $$C(t) = \sum_{t=0}^{T_n} V_t(\tau)\, T_0\, e(T_n-\tau) \qquad \ldots(C.5)$$

where $e(\tau)$ is the value of the ecitation function at $t = \tau$

V_t is the turn voltage

In our program, the convolution was found by successfully using equations (C.4) and (C.5), i.e. :

$$\begin{aligned} C(t) = {} & e(T_0)\, T_0\, V_t(T_n-T_0) + V_t(T_1)\, T_0\, e(T_n-T_1) \\ & + e(T_2)\, T_0\, V_t(T_n-T_2) + V_t(T_3)\, T_0\, e(T_n-T_3) \\ & + \ldots\ldots\ldots\ldots \end{aligned} \qquad \ldots(C.6)$$

This convolution function represented the turn-to-ground voltage in the time domain as a response to the input excitation function.

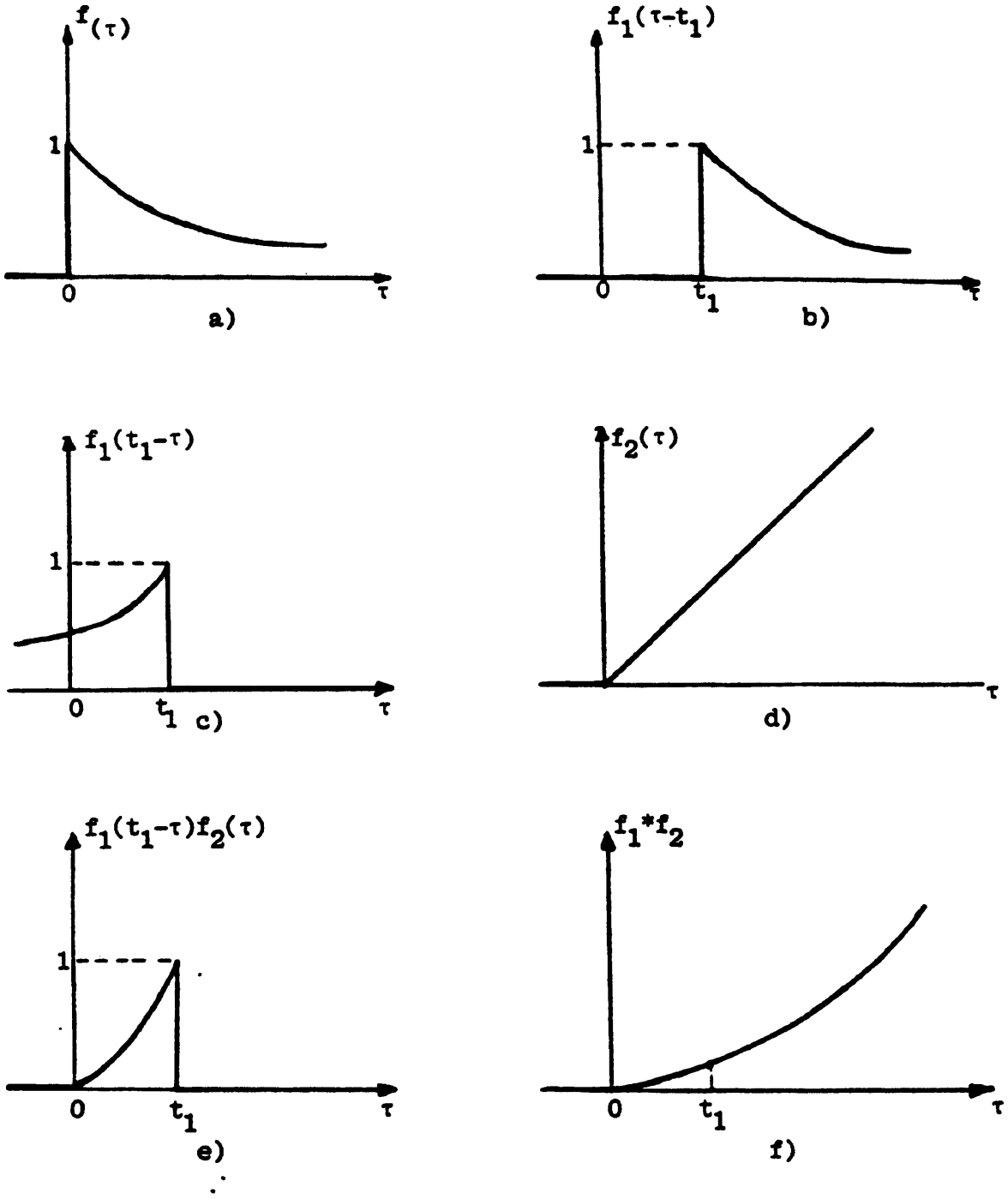

Fig C.1 Graphical interpretation of convolution